D 2022

U.PORTO
FEUP FACULDADE DE ENGENHARIA
UNIVERSIDADE DO PORTO

DEVELOPMENT AND OPTIMIZATION OF RETINOIC ACID CONTROLLED DELIVERY NANO- AND MICROSYSTEMS FOR THERAPEUTIC APPLICATIONS

ANTÓNIA REGINA SALES MACHADO GONÇALVES

TESE DE DOUTORAMENTO APRESENTADA
À FACULDADE DE ENGENHARIA DA UNIVERSIDADE DO PORTO EM
PROGRAMA DOUTORAL EM ENGENHARIA QUÍMICA E BIOLÓGICA

U.PORTO
FEUP FACULDADE DE ENGENHARIA
UNIVERSIDADE DO PORTO

Development and optimization of retinoic acid controlled delivery nano- and microsystems for therapeutic applications

by

Antónia Regina Sales Machado Gonçalves

A dissertation submitted in partial fulfilment of the requirements for the degree of Doctor of Philosophy in Chemical and Biological Engineering

Supervisors

Doctor Berta Maria Abreu Nogueiro Estevinho

Professor Fernando Alberto Nogueira da Rocha

Laboratory for Process Engineering, Environment, Biotechnology and Energy (LEPABE)

Porto, November 2022

lepabe
Laboratory for Process Engineering,
Environment, Biotechnology and Energy

Antónia Gonçalves acknowledges Fundação para a Ciência e a Tecnologia (FCT) for the award of doctoral research grant (SFRH/BD/129207/2017), co-financed by the European Social Fund (ESF) through North Portugal Regional Operational Programme (NORTE 2020) and by national founds from the Ministry of Science, Technology and Higher Education (MCTES). Antónia Gonçalves also acknowledges Fundação para a Ciência e a Tecnologia (FCT) for the research grant (COVID/BD/152371/2022), co-financed by national founds from the Ministry of Science, Technology and Higher Education (MCTES) and by the European Social Fund (ESF) and Por_Norte Programme.

This work was financially supported by:

I. Project POCI-01-0145-FEDER-006939 (Laboratory for Process Engineering, Environment, Biotechnology and Energy – UID/EQU/00511/2013);
II. Project "LEPABE-2-ECO-INNOVATION" – NORTE-01-0145-FEDER-000005, funded by Norte Portugal Regional Operational Programme (NORTE 2020), under PORTUGAL 2020 Partnership Agreement, through the European Regional Development Fund (ERDF);
III. Base Funding – UIDB/00511/2020 of the Laboratory for Process Engineering, Environment, Biotechnology and Energy – LEPABE – funded by national funds through the FCT/MCTES (PIDDAC);
IV. Project POCI-01-0145-FEDER-028715 (MicroDelivery – Development of controlled delivery functional systems by microencapsulation of natural and active compounds with therapeutic, nutritional and technological interest), funded by FEDER funds through COMPETE2020 – Programa Operacional Competitividade e Internacionalização (POCI) and by national funds (PIDDAC) through FCT/MCTES;
V. LA/P/0045/2020 (AliCE), UIDB/00511/2020 and UIDP/00511/2020 (LEPABE), funded by national funds through FCT/MCTES (PIDDAC);
VI. Project UIDB/50006/2020.

Acknowledgments

First of all, I would like to thank my supervisors Doctor Berta Estevinho and Professor Fernando Rocha. Thank you for the opportunity to work in a research area that fascinated me from the beginning and that I believe can contribute to building a better world for the generations to come. Thank you also for your guidance, support and for teaching me more than I could have imagined over the last years.

I am sincerely grateful to Professor Isabel Ferreira, Doctor Olga Viegas and Professor Miguel Faria from the Faculty of Pharmacy of the University of Porto. Thank you for the invaluable collaboration. Thank you for the opportunity to learn from your knowledge and experience. Thank you for the availability and support. I also would like to thank to Doctor Susana Casal, Anabela Costa and Anabela Borges for the technical support and all the help that was provided when I needed.

I would like to thank my colleagues and friends from laboratory E204B at the Faculty of Engineering of the University of Porto: Anabela Veiga, António Ferreira, Carolina Silva, Cecília Rodrigues, Filipa Castro, Filipe Almeida, Ioana Carlan, Joana Ferreira, Marisa Ribeiro, Patrícia Cruz and Sílvia Coelho. Thank you for all the good moments we shared, the mutual help and the great working environment. Also, I thank to Stéphanie Andrade from laboratory E204A for all academic sharing over these years. At last, I thank Professor Madalena Dias and Yaidelin Manrique for granting the usage of zetasizer and all the help provided.

I also would like to thank to all those I met in the Faculty of Pharmacy of the University of Porto: professors, researchers and students. Thank you to be kind and for all the help and availability. You became my life better and easier in the last year of my PhD. To Madalena Sobral I also would like to thank for all the knowledge and time shared before I start my experiments.

I am deeply grateful to my friends: Ana Cristina, Ana Sofia Pereira, Ângela Mota, Cristiana Faria, Joana Azevedo, Joana Rodrigues, Maria Antónia Silva, Patrícia Ferreira, Sofia Romano, Tânia Santos and Tiago Dias. Thank you for encouraging me in the most difficult times and for celebrating my achievements. Overall, thank you for being there for me even in the most ordinary days. It was priceless.

At last, I thank to my family for all the support and attempts to understand this challenging career I have chosen for myself so far. Particularly, I thank those who even far away are always with me in my heart. Thank you for all the love.

"*Para ser grande, sê inteiro:*
Nada teu exagera ou exclui."
Ricardo Reis

Abstract

Retinoic acid (RA) is a fat-soluble vitamin and a naturally occurring endogenous retinoid. This signalling molecule plays a key role as chemopreventive and/or chemotherapeutic against several types of cancer, namely acute promyelocytic leukemia (APL). All-trans RA greatly improved the treatment of APL, being referred as the only effective strategy. However, the efficiency of RA as pharmaceutical agent is hampered by poor aqueous solubility, high sensitivity to air, UV light and oxidizing compounds, short half-life and severe side-effects. This work proposes the development and optimization of RA controlled delivery systems, based in microparticle formulations obtained by spray-drying, to be used in the treatment of APL. The ultimate goal is to obtain a controlled delivery system for RA oral administration capable to provide a slow release of this bioactive compound in the intestinal lumen. This approach might improve the bioavailability of RA in the human body as thus its efficiency as anticancer compound. Spray-drying of solutions composed by RA (dissolved in ethanol) and the encapsulating agent (alginic acid sodium, modified chitosan and arabic gum, individually prepared in ultra-pure water) resulted in biopolymer-based microparticles that mostly presented high loss of RA over time. Moreover, alginic acid sodium-based microparticles enabled the slower RA release in octanol (> 7 h). Among the RA-loaded microparticles obtained from oil-in-water emulsions individually composed by modified chitosan, alginic acid sodium, arabic gum, xanthan gum and gelatin, the highest encapsulation efficiency was registered for modified chitosan- and alginic acid sodium-based microparticles (65 ± 6 and 62 ± 5%, respectively). This parameter showed to be significantly influenced by the inlet air temperature (studies performed for modified chitosan-based microparticles). The slower controlled release of RA in octanol was also achieved for the microparticles composed by alginic acid sodium as encapsulating agent (almost 8 h). Binary and ternary blends of alginic acid sodium, modified chitosan and xanthan gum were proposed to produce RA-loaded microparticles from oil-in-water emulsions, and the most prolonged RA release in octanol was registered for most of microparticles composed by alginic acid sodium (almost 7 h). Moreover, the highest encapsulation efficiency was observed for the xanthan gum + alginic acid sodium-based microparticles (76 ± 4%). Ethyl cellulose (EC)- and EC + polyethylene glycol (PEG)-based solutions increased at least 250-fold the mass of RA added to the system to be fed to the spray-dryer, when compared to the biopolymer-based systems proposed. EC- and EC + PEG-based microparticles showed an encapsulation efficiency of around 100% and enabled the stabilization of RA controlled release in octanol in 40 min. Intestinal bioaccessibility of RA was significantly higher when EC- and EC + PEG-based microparticles were digested without a reference diet (84 ± 1 and 54 ± 4%, respectively) and similar among EC- and EC + PEG-based microparticles co-ingested with diet. The highest RA bioaccessibility at gastric level was 3 ± 2% for all the tested conditions. RA intestinal transport was highly affected by the samples used in the experiment, with determination of a higher amount of RA that reached the basolateral compartment for the blank digesta spiked with RA (7.8 ± 0.6%). Co-encapsulation of RA, curcumin and/or resveratrol into alginic acid sodium-based microparticles and microparticles composed by the EC + PEG blend registered an encapsulation efficiency that ranged from 26 ± 3 to 34 ± 1% and 91 ± 6 to 97 ± 8%, respectively. Controlled release profiles in octanol were very similar among

the co-encapsulated bioactive compounds. Co-release of bioactive compounds prolonged between 48 min and more than 6 h from alginic acid-based microparticles and stabilized between 60 and 80 min from EC + PEG-based microparticles.

Keywords: Biopolymers, Controlled release, Encapsulation, *In vitro* digestion, Intestinal transport, Retinoic acid, Spray-drying, Synthetic polymers.

Resumo

O ácido retinóico é uma vitamina lipossolúvel e um retinóide endógeno de ocorrência natural. Esta molécula sinalizadora desempenha um papel fundamental como quimio preventivo e/ou quimio terapêutico contra vários tipos de cancro, nomeadamente a leucemia promielocítica aguda. O ácido all-trans retinóico melhorou consideravelmente o tratamento da leucemia promielocítica aguda, sendo referido como a única estratégia eficaz. No entanto, a eficiência do ácido retinóico como agente farmacêutico é prejudicada pela sua baixa solubilidade aquosa, elevada sensibilidade ao ar, radiação UV e compostos oxidantes, tempo de meia-vida curto e efeitos secundários graves. Este trabalho propõe o desenvolvimento e otimização de sistemas de libertação controlada para o ácido retinóico, baseados em formulações de micropartículas obtidas por spray-drying, para serem utilizados no tratamento da leucemia promielocítica aguda. O objetivo final é obtenção um sistema de libertação controlada para administração oral do ácido retinóico capaz de proporcionar a libertação lenta deste composto bioativo no lúmen intestinal. Esta abordagem pode melhorar a biodisponibilidade do ácido retinóico no corpo humano, bem como a sua eficiência como composto anticancerígeno. O spray-drying de soluções compostas por ácido retinóico (dissolvido em etanol) e agente encapsulante (ácido algínico de sódio, quitosano modificado e goma arábica, preparadas individualmente em água ultrapura) resultou em micropartículas à base de biopolímeros que, na sua maioria, apresentaram uma elevada perda de ácido retinóico ao longo do tempo. Além disso, micropartículas à base de ácido algínico de sódio permitiram uma libertação mais lenta do ácido retinoico em octanol (> 7 h). Entre as micropartículas carregadas com ácido retinóico obtidas a partir de emulsões óleo em água compostas individualmente por quitosano modificado, ácido algínico de sódio, goma arábica, goma xantana e gelatina, a maior eficiência de encapsulação foi registada para micropartículas à base de quitosano modificado e ácido algínico de sódio (65 ± 6 e 62 ± 5%, respetivamente). Este parâmetro mostrou ser significativamente influenciado pela temperatura de entrada ar no spray-dryer (estudos realizados para micropartículas à base de quitosano modificado). A libertação controlada mais lenta de ácido retinóico em octanol foi também alcançada para as micropartículas compostas por ácido algínico de sódio como agente encapsulante (quase 8 h). Misturas binárias e ternárias de ácido algínico de sódio, quitosano modificado e goma xantana foram propostas para a produção de micropartículas carregadas com ácido retinóico a partir de emulsões óleo em água, para as quais a libertação mais longa de ácido retinóico em octanol foi registada para a maioria das micropartículas compostas por ácido algínico de sódio (quase 7 h). Além disso, a maior eficiência de encapsulação foi observada para as micropartículas à base de goma xantana + ácido algínico de sódio (76 ± 4%). As soluções à base de etilcelulose e etilcelulose + polietilenoglicol aumentaram pelo menos 250 vezes a massa de ácido retinóico adicionada ao sistema a ser alimentado ao spray-dryer, quando comparado aos sistemas à base de biopolímeros propostos. As micropartículas à base de etilcelulose e etilcelulose + polietilenoglicol mostraram uma eficiência de encapsulação em torno de 100% e permitiram a estabilização da libertação controlada do ácido retinóico em octanol em 40 min. A bioacessibilidade intestinal do ácido retinóico foi significativamente maior quando micropartículas à base de etilcelulose e etilcelulose + polietilenoglicol foram digeridas sem uma dieta de referência (84 ± 1 e 54 ± 4%, respetivamente) e similar entre micropartículas à base

de etilcelulose e etilcelulose + polietilenoglicol co-ingeridas com a dieta. A maior bioacessibilidade de ácido retinóico a nível gástrico foi de 3 ± 2%, para todas as condições testadas. O transporte intestinal de ácido retinóico foi altamente afetado pelas amostras utilizadas no ensaio, tendo sido determinada uma quantidade maior de ácido retinóico que alcançou o compartimento basolateral para o branco da digestão enriquecido com ácido retinóico (7,8 ± 0,6%). A co-encapsulação de RA, curcumina e/ou resveratrol em micropartículas à base de ácido algínico de sódio e micropartículas compostas por etilcelulose + polietilenoglicol registou uma eficiência de encapsulação que variou de 26 ± 3 a 34 ± 1% e 91 ± 6 a 97 ± 8%, respetivamente. Os perfis de libertação controlada em octanol foram muito semelhantes entre os compostos bioativos co-encapsulados. A co-libertação dos compostos bioativos prolongou-se entre 48 min e mais de 6 h para as micropartículas à base de ácido algínico de sódio e foi estabilizada entre 60 e 80 min para as micropartículas à base de etilcelulose + polietilenoglicol.

Palavras-chave: Biopolímeros, Libertação controlada, Encapsulação, Digestão *in vitro*, Transporte intestinal, Ácido retinoico, Spray-drying, Polímeros sintéticos.

List of contributions

Publications

- Gonçalves, A; Rocha, F, Estevinho, B. N. Pharmaceutical/Clinical strategies in the treatment of acute promyelocytic leukaemia – Comprehensive overview. Submitted for publication.
- Gonçalves, A; Rocha, F, Estevinho, B. N. Co-encapsulation of retinoic acid, curcumin and resveratrol by spray-drying of alginic acid sodium-based emulsions and ethyl cellulose-based solutions: Impact on the co-delivery profiles. International Journal of Biological Macromolecules. Accepted for publication. https://doi.org/10.1016/j.ijbiomac.2022.10.207.
- Gonçalves, A; Viegas, O; Faria, M; Ferreira, I; Rocha, F; Estevinho, B N. *In vitro* bioaccessibility and intestinal transport of retinoic acid in ethyl cellulose-based microparticles and impact of meal co-ingestion. Submitted for publication.
- Gonçalves, A; Rocha, F; Estevinho, B N. Application of ethyl cellulose and ethyl cellulose + polyethylene glycol for the development of polymer-based formulations by spray-drying technology for retinoic acid encapsulation. Foods. 2022, 11, 2533, https://doi.org/10.3390/foods11162533.
- Gonçalves, A; Estevinho, B N; Rocha, F. Microencapsulation of retinoic acid by atomization into biopolymeric matrices: Binary and ternary blends of alginic acid sodium, xanthan gum and modified chitosan. Food Hydrocolloids. 2022, 124, Part B, 107310, https://doi.org/10.1016/j.foodhyd.2021.107310.
- Gonçalves, A; Estevinho, B N; Rocha, F. Spray-drying of oil-in-water emulsions for encapsulation of retinoic acid: Polysaccharide- and protein-based microparticles characterization and controlled release studies. Food Hydrocolloids. 2022, 124, Part A, 107193, https://doi.org/10.1016/j.foodhyd.2021.107193.
- Gonçalves, A; Estevinho, B N; Rocha, F. Methodologies for simulation of gastrointestinal digestion of different controlled delivery systems and further uptake of encapsulated bioactive compounds. Trends in Food Science & Technology. 2021, 114, 510-520, https://doi.org/10.1016/j.tifs.2021.06.007.
- Gonçalves, A; Estevinho, B N; Rocha, F. Formulation approaches for improved retinoids delivery in the treatment of several pathologies. European Journal of Pharmaceutics and Biopharmaceutics. 2019, 143, 80-90, https://doi.org/10.1016/j.ejpb.2019.08.014.
- Gonçalves, A; Estevinho, B N; Rocha, F. Characterization of biopolymer-based systems obtained by spray-drying for retinoic acid controlled delivery, Powder Technology. 2019 345, 758-765, https://doi.org/10.1016/j.powtec.2019.01.062.

Oral communications

- Gonçalves, A; Rocha, F, Estevinho, B. N. Co-encapsulation of retinoic acid, curcumin and resveratrol with the evaluation of the co-delivery profiles and of the potential benefits in the treatment of acute promyelocytic leukemia. 11th World Congress of Chemical Engineering, 4-8 June, 2023.
- Gonçalves, A.; Estevinho, B N; Rocha, F. Biopolymer-based delivery systems for controlled release of retinoic acid using spray-drying technology. CHISA 2021 Virtually – International Congress of Chemical and Process Engineering, Prague, Czech Republic, 15-18 March, 2021.
- Gonçalves, A.; Estevinho, B N; Rocha, F. Design and characterization of retinoic acid-loaded biopolymers obtained using microencapsulation by spray-drying. 5th International ISEKI_Food Conference, Stuttgart, Germany, July 2018.

Poster communications

- Gonçalves, A.; Estevinho, B N; Rocha, F. Binary and ternary blends of biopolymers for encapsulation of retinoic acid using spray-drying technology. DCE21 – Doctoral Congress in Engineering, Porto, Portugal, June 2021.

List of Figures

Figure 1.1 – Schematic representation of spray-drying process. 4

Figure 1.2 – Doctoral project overview: iterative process for RA-loaded microparticles improvement. 5

Figure 2.1 – General structure of retinoids (adapted from [39]). Retinoids with the end groups CH_2OH, CHO and COOH correspond to retinol, retinal and retinoic acid, respectively. 11

Figure 2.2 – Retinoids of first, second, third and fourth generation (adapted from [39]). 12

Figure 2.3 – Metabolic interconversion between vitamin A (retinol) natural structures (adapted from [35,37,44,96]). Abbreviations: CRABP: cellular RA-binding protein; CRBP II: cellular retinol-binding protein type II; LRAT: lecithin retinol acyl transferase; RALDH: retinaldehyde dehydrogenase; RBP: retinol binding protein; RDH: retinol dehydrogenase; TTR: transthyretin. 15

Figure 3.1 – Delivery systems designed for encapsulation of bioactive compounds in food sector (adapted from [101,174]). 31

Figure 4.1 – SEM images of empty (A, B and C) and RA-loaded polymeric-based microcapsules (D, E and F) using arabic gum (A and D), modified chitosan (B and E) and alginic acid sodium (C and F) as encapsulating agents. Magnification =10,000 times, beam intensity (HV) 15.00 kV, distance between the sample and the lens (WD) around 10 mm. 57

Figure 4.2 – Global uncertainty considering the uncertainties associated to the standard preparation (U1), calibration curve (U2), precision (U3) and accuracy (U4). (A) Variation of global uncertainty for all the standard solutions concentrations. (B) Relative weight of each individual source of uncertainty for all the standard solutions concentration. 58

Figure 4.3 – RA release profiles obtained from different biopolymers-based systems using arabic gum (●), modified chitosan (▲) and alginic acid sodium (■) as encapsulating agents. Results are presented as the average and standard deviation of three independent assays. 60

Figure 5.1 – Relation between shear stress and shear rate for the emulsions prepared with modified chitosan (■), arabic gum (▲), alginic acid sodium (●), gelatin (♦). Results are presented as the average and standard deviation of three independent assays 73

Figure 5.2 – Viscosity curve of the emulsion prepared with xanthan gum. Results are presented as the average and standard deviation of three independent assays. 73

Figure 5.3 – Surface morphology of RA-loaded-modified chitosan-based microparticles produced at 115 ℃ (A and D), 130 ℃ (B and E) and 150 ℃ (C and F) of inlet air temperature. Magnification =10,000 (A, B and C) and 20,000 (D, E and F) times, beam intensity (HV) 15.00 kV, distance between the sample and the lens (WD) around 10 mm. 78

Figure 5.4 – Cumulative RA release from modified chitosan-based microparticles produced at 115 ℃ (●), 130 ℃ (■) and 150 ℃ (▲) of inlet air temperature. Results are presented as the average and standard deviation of three independent assays. Weibull model was fitted to the obtained controlled release profiles: 115 ℃ (●), 130 ℃ (■) and 150 ℃ (▲). 79

Figure 5.5 – Surface morphology of MpE (A, B, C, D and E), MpOT (F, G, H, I and J) and MpRA (K, L, M, N and O) microparticles composed by modified chitosan (A, F and K), arabic gum (B, G and L), alginic acid sodium (C, H and M), gelatin (D, I and N) and xanthan gum (E, J and O). Magnification = 20,000 times, beam intensity (HV) 15.00 kV, distance between the sample and the lens (WD) around 10 mm. 82

Figure 5.6 – Cumulative RA release from biopolymer-microparticles individually composed by modified chitosan (■), arabic gum (▲), alginic acid sodium (×), gelatin (♦) and xanthan gum (●). Results are presented as the average and standard deviation of three independent assays. Weibull model was fitted to the obtained controlled release profiles: modified chitosan (■), arabic gum (▲), alginic acid sodium (×), gelatin (♦) and xanthan gum (●).....84

Figure 6.1 – Increase between shear stress and shear rate for the emulsion composed by the modified chitosan + alginic acid sodium blend. Results are presented as the average and standard deviation of three independent assays.....96

Figure 6.2 – Viscosity curves of the emulsions prepared with different biopolymers blends (xanthan gum + alginic acid sodium (●), modified chitosan + xanthan gum (■) and modified chitosan + xanthan gum + alginic acid sodium (▲)). Results are presented as the average and standard deviation of three independent assays ..96

Figure 6.3 – Surface morphology of BBMpE (A, B, C and D), BBMpOT (E, F, G and H) and BBMpRA (I, J, K and L) microparticles composed by xanthan gum + alginic acid sodium blend (A, E and I), modified chitosan + alginic acid sodium blend (B, F and J), modified chitosan + xanthan gum blend (C, G and K) and modified chitosan + xanthan gum + alginic acid sodium blend (D, H and L). Magnification = 20,000 times, beam intensity (HV) 15.00 kV, distance between the sample and the lens (WD) around 10 mm.....102

Figure 6.4 – Response surfaces of encapsulating efficiency (A) and loading capacity (B) based on a simplex centroid design.....103

Figure 6.5 – Cumulative RA release from microparticles composed by modified chitosan + alginic acid sodium blend (pink triangles), modified chitosan + xanthan gum blend (green filled crosses), modified chitosan + xanthan gum + alginic acid sodium blend (blue circles) and xanthan gum + alginic acid sodium blend (orange squares). Results are presented as the average and standard deviation of three independent assays. Weibull model was fitted to the obtained controlled release profiles: modified chitosan + alginic acid sodium blend (black triangles), modified chitosan + xanthan gum blend (black filled crosses), modified chitosan + xanthan gum + alginic acid sodium blend (black circles) and xanthan gum + alginic acid sodium blend (black squares). 106

Figure 6.6 – Response surface of RA release times based on a simplex centroid design. 107

Figure 7.1 – Surface morphology of MpPE (A and B) and MpPRA (C and D) microparticles composed by EC (A and C) and EC + PEG blend (B and D). Magnification = 20,000 times, beam intensity (HV) 15.00 kV, distance between the sample and the lens (WD) around 10 mm. 119

Figure 7.2 – Particle size distribution of microparticles MpPE composed by EC + PEG blend, considering differential volume distribution: replicate 1 - grey circles, replicate 2 - dark grey circles, replicate 3 – black circles.....119

Figure 7.3 – Cumulative RA release from polymer-microparticles composed by EC (pink circles) and by the EC + PEG blend (blue triangles). Results are presented as the average and standard deviation of three independent assays.....121

Figure 8.1 – *In vitro* digestion of RA-loaded EC- and ECP-based microparticles, with and without diet, and intestinal transport of RA. 131

Figure 8.2 – Surface morphology of microparticles EC (A) and microparticles ECP (B). Magnification = 50,000 times, beam intensity (HV) 15.00 kV, distance between the sample and the lens (WD) around 10 mm.....134

Figure 8.3 – Gastric and intestinal bioaccessibility (%) of RA after the *in vitro* digestion of RA-loaded microparticles with and without diet. **** $p < 0.0001$, *** $p < 0.001$.....135

Figure 8.4 – Apical retention and intestinal transport of RA after 2 h of transport. ** $p < 0.01$, * $p < 0.05$. ..137

Figure 9.1 – Relation between shear stress and shear rate for the alginic acid sodium-based emulsions composed by RA (circles), RA + curcumin (diamonds), RA + resveratrol (squares) and RA + curcumin + resveratrol (triangles). Results are presented as the average and standard deviation of two independent assays. 147

Figure 9.2 – Surface morphology of MpB (A, B, C and D) and MpP (E, F, G and H) microparticles loaded with RA (A and E), RA + curcumin (B and F), RA + resveratrol (C and G) and RA + curcumin + resveratrol (D and H). Magnification = 20,000 times, beam intensity (HV) 15.00 kV, distance between the sample and the lens (WD) around 10 mm. 151

Figure 9.3 – Cumulative release of RA (squares), curcumin (triangles) and resveratrol (circles) from MpB (light grey) and MpP (dark grey) microparticles loaded with RA (A), RA + curcumin (B), RA + resveratrol (C) and RA + curcumin + resveratrol (D). Results are presented as the average and standard deviation of two independent assays. Weibull model was fitted to the obtained controlled release profiles from MpB microparticles: RA (black squares), curcumin (black triangles) and resveratrol (black circles).....155

List of Tables

Table 2.1 – The most recent RA controlled delivery systems developed for the treatment of several pathologies. 23

Table 3.1 – Overview of methodologies used to determine bioaccessibility and bioavailability of bioactive compounds.....36

Table 3.2 – Studies on the behaviour of different bioactive compound-loaded controlled delivery systems when submitted to various *in vitro* static digestion models (continuation).....40

Table 4.1 – Product yield of empty and RA-loaded microcapsules obtained by spray-drying technology using different biopolymers as encapsulating agents.....55

Table 4.2 – Average size of all microcapsules formulations produced considering a differential volume distribution and a differential number distribution.....56

Table 4.3 – Accuracy of RA at different concentration level.....58

Table 4.4 – Parameters and correlation coefficients of the kinetics of zero-order, Higuchi, Korsmeyer-Peppas and Weibull applied to the experimental RA release profiles. 63

Table 5.1 – Rheological parameters, apparent viscosity, zeta potential and droplet size of emulsions prepared with different biopolymers. 74

Table 5.2 – Product yield and physical properties of RA loaded-modified chitosan-based microparticles produced at different inlet air temperatures.....76

Table 5.3 – Product yield, emulsion volume and particle diameter of microparticles produced using different formulations.....80

Table 5.4 – Encapsulation efficiency and loading capacity of RA-loaded microparticles obtained using different encapsulating agents.....83

Table 5.5 – Parameters and correlation coefficients of the models of zero-order, Higuchi, Korsmeyer-Peppas and Weibull applied to the experimental RA release profiles. 86

Table 6.1 – Rheological parameters, apparent viscosity, zeta potential and droplet size of emulsions prepared with different blends of alginic acid sodium, xanthan gum and modified chitosan. 98

Table 6.2 – Product yield, RA encapsulation efficiency, RA loading capacity and particle diameter of microparticles produced using different formulations.....100

Table 6.3 – Application of the models of zero-order, Higuchi, Korsmeyer-Peppas and Weibull to the experimental RA release profiles. 108

Table 7.1 – Characterization of polymer-based microparticles for RA encapsulation: product yield, particle diameter, encapsulation efficiency and loading capacity. 118

Table 7.2 – Parameters and correlation coefficients of zero-order, Higuchi, Korsmeyer-Peppas and Weibull models fitted to the experimental RA release profiles.....122

Table 8.1 – Proximal composition of the meal used in *in vitro* digestion experiments following a western diet. 130

Table 8.2 – Product yield, encapsulation efficiency and loading capacity of RA-loaded microparticles composed by different synthetic polymer formulations. 134

Table 9.1 – Concentration range, LOD and LOQ and correlation coefficients related to the calibration curves of RA, curcumin and resveratrol.....145

Table 9.2 – Rheological parameters, apparent viscosity, zeta potential and droplet size of alginic acid sodium based-emulsions composed by RA, RA + curcumin, RA + resveratrol and RA + curcumin + resveratrol. 148

Table 9.3 – Characterization of MpB and MpP microparticles: product yield, particle diameter, encapsulation efficiency and loading capacity. 150

Table 9.4 – Parameters and correlation coefficients of the models of zero-order, Higuchi, Korsmeyer-Peppas and Weibull applied to the experimental RA, curcumin and resveratrol release profiles from MpB microparticles. 156

Table 9.5 – Parameters and correlation coefficients of the models of zero-order, Higuchi, Korsmeyer-Peppas and Weibull applied to the experimental RA, curcumin and resveratrol release profiles from MpP microparticles. 157

Table of Contents

CHAPTER 1 - INTRODUCTION 1

1.1. Scope and motivation 3
1.2. Research goals 5
1.3. Thesis outline 6

CHAPTER 2 - FORMULATION APPROACHES FOR IMPROVED RETINOIDS DELIVERY IN THE TREATMENT OF SEVERAL PATHOLOGIES 9

2.1. Introduction 11
2.2. Retinoids metabolism 14
2.3. Mechanisms of action of retinoids 15
2.4. Carrier-based formulations used for controlled delivery of retinoids 17
2.4.1. Most important methods implemented for RA encapsulation 17
2.4.1.1. Emulsions 17
2.4.1.2. SLN 18
2.4.1.3. NLC 18
2.4.1.4. Liposomes 18
2.4.1.5. Niosomes 19
2.4.1.6. Ethosomes 19
2.4.1.7. Transethosomes 19
2.4.1.8. Polymers 20
2.4.2. RA controlled delivery systems for therapeutic applications 20
2.5. Concluding remarks 26

CHAPTER 3 - METHODOLOGIES FOR SIMULATION OF GASTROINTESTINAL DIGESTION OF DIFFERENT CONTROLLED DELIVERY SYSTEMS AND FURTHER UPTAKE OF ENCAPSULATED BIOACTIVE COMPOUNDS .27

3.1. Introduction 29
3.2. Delivery systems for encapsulation of nutraceuticals 30
3.2.1. Carrier-based systems 31
3.2.1.1. Particles and capsules 31
3.2.1.2. Hydrogels 31
3.2.1.3. Emulsions 32
3.2.1.4. Solid lipid nanoparticles (SLN) 32
3.2.1.5. Nanostructured lipid carriers (NLC) 32
3.2.1.6. Liposomes 32

3.2.2. Encapsulating methods used in food sector....32
3.2.2.1. Spray-drying....33
3.2.2.2. Freeze-drying....33
3.2.2.3. Coacervation....33
3.2.2.4. Fluidized bed coating....33
3.2.2.5. Emulsification....34
3.2.2.6. Liposome entrapment....34
3.2.2.7. Inclusion complexation....34
3.3. Behaviour of carrier-based systems under simulated gastrointestinal conditions....34
3.3.1. *In vitro* digestion models....36
3.3.1.1. Static models....36
3.3.1.2. Dynamic models....38
3.3.1.2.1. DGM....39
3.3.1.2.2. HGS....44
3.3.1.2.3. TIM....44
3.3.1.2.4. SHIME....45
3.3.2. Intestinal absorption and presystemic metabolism evaluation....45
3.3.3. Incorporation of gut microflora....47
3.3.4. *In vivo* methodologies....47
3.4. Conclusion....48

CHAPTER 4 – CHARACTERIZATION OF BIOPOLYMER-BASED SYSTEMS OBTAINED BY SPRAY-DRYING FOR RETINOIC ACID CONTROLLED DELIVERY....49

4.1. Introduction....51
4.2. Material and Methods....52
4.2.1. Materials....52
4.2.2. Preparation of solutions to be fed to the spray-dryer....52
4.2.3. Spray-drying conditions....53
4.2.4. Particle size distribution....53
4.2.5. Scanning electron microscopy (SEM)....54
4.2.6. Analytical method validation....54
4.2.7. Controlled release experiments....54
4.3. Results and discussion....54
4.3.1. Microcapsules analysis....56
4.3.2. RA controlled release....57
4.3.2.1. Analytical method validation....57
4.3.2.2. Controlled release profiles....59

4.3.2.3. Kinetic models 61
4.4. Conclusion 64

CHAPTER 5 – SPRAY-DRYING OF OIL-IN-WATER EMULSIONS FOR ENCAPSULATION OF RETINOIC ACID: POLYSACCHARIDE- AND PROTEIN-BASED MICROPARTICLES CHARACTERIZATION AND CONTROLLED RELEASE STUDIES 65

5.1. Introduction 67
5.2. Material and Methods 68
5.2.1. Materials 68
5.2.2. Emulsions preparation 68
5.2.3. Spray-drying technology 69
5.2.4. Emulsions viscosity 69
5.2.5. Emulsions zeta potential 69
5.2.6. Droplet and particle size distribution 70
5.2.7. Microparticle morphology 70
5.2.8. Encapsulation efficiency and loading capacity 70
5.2.9. Controlled release experiments 70
5.2.10. Statistical analysis 71
5.3. Results and discussion 71
5.3.1. Emulsions characterization 71
5.3.1.1. Viscosity 72
5.3.1.2. Stability of colloidal systems 75
5.3.1.3. Droplet size distribution 75
5.3.2. Optimization of the spray-drying inlet air temperature 76
5.3.2.1. Product yield 76
5.3.2.2. RA retained in the microparticles 77
5.3.2.3. Morphology 77
5.3.2.4. Particle size 78
5.3.3. Biopolymer-based microparticles characterization 79
5.3.4. Surface morphology of microparticles 81
5.3.5. Microparticle particle size measurement 81
5.3.6. Encapsulation efficiency and loading capacity 83
5.3.7. Drug controlled release assay 83
5.3.8. Kinetic models 85
5.4. Conclusion 87

CHAPTER 6 – MICROENCAPSULATION OF RETINOIC ACID BY ATOMIZATION INTO BIOPOLYMERIC MATRICES: BINARY AND TERNARY BLENDS OF ALGINIC ACID SODIUM, XANTHAN GUM AND MODIFIED CHITOSAN 89

6.1. Introduction 91
6.2. Material and Methods 92
6.2.1. Materials 92
6.2.2. Preparation of emulsions 92
6.2.3. Spray-drying technique 93
6.2.4. Emulsions viscosity 93
6.2.5. Emulsions zeta potential 93
6.2.6. Emulsions droplet size and microparticle size 93
6.2.7. Morphology of microparticles 93
6.2.8. Encapsulation efficiency and loading capacity 94
6.2.9. Controlled release assays 94
6.2.10. Statistical analysis 95
6.3. Results and discussion 95
6.3.1. Emulsions characterization 95
6.3.1.1. Viscosity 95
6.3.1.2. Stability of colloids 97
6.3.1.3. Droplet size distribution 97
6.3.2. Biopolymers blends-based microparticles production 99
6.3.3. Particle size distribution 99
6.3.4. Microparticles morphology 101
6.3.5. Encapsulation efficiency and loading capacity 104
6.3.6. Controlled release 104
6.3.7. Kinetic models 107
6.4. Conclusions 109

CHAPTER 7 - APPLICATION OF ETHYL CELLULOSE AND ETHYL CELLULOSE + POLYETHYLENE GLYCOL FOR THE DEVELOPMENT OF POLYMER-BASED FORMULATIONS BY SPRAY-DRYING TECHNOLOGY FOR RETINOIC ACID ENCAPSULATION 111

7.1. Introduction 113
7.2. Material and Methods 114
7.2.1. Materials 114
7.2.2. Formulation of RA loaded-polymer-based microparticles by spray-drying technology 114
7.2.3. Microparticle morphology 115

7.2.4. Particle size distribution 115
7.2.5. Encapsulation efficiency and loading capacity 115
7.2.6. Controlled release experiments 116
7.2.7. Statistical analysis 116
7.3. Results and discussion 116
7.3.1. Surface morphology of microparticles 117
7.3.2. Microparticle particle size 120
7.3.3. Encapsulation efficiency and loading capacity 120
7.3.4. Drug controlled release 120
7.3.5. Kinetic models 122
7.4. Conclusion 123

CHAPTER 8 - *IN VITRO* BIOACCESSIBILITY AND INTESTINAL TRANSPORT OF RETINOIC ACID IN ETHYL CELLULOSE-BASED MICROPARTICLES AND IMPACT OF MEAL CO-INGESTION 125

8.1. Introduction 127
8.2. Material and Methods 128
8.2.1. Materials 128
8.2.2. RA encapsulation into microparticles composed by EC and the EC+PEG blend by spray-drying 129
8.2.3. Encapsulation efficiency and loading capacity 129
8.2.4. Characterization of RA-loaded microparticles 129
8.2.5. Preparation of meal 129
8.2.6. INFOGEST *in vitro* digestion 131
8.2.7. Cell culture and intestinal transport 132
8.2.8. RA extraction and HPLC analyses 132
8.2.9. Statistical analysis 133
8.3. Results and discussion 133
8.3.1. Production and characterization of EC- and ECP-based microparticles loaded with RA 133
8.3.2. RA bioaccessibility at gastric and intestinal levels 135
8.3.3. Intestinal transport of RA 136
8.4. Conclusion 138

CHAPTER 9 - (BIO)POLYMER-BASED MICROPARTICLES OBTAINED BY SPRAY DRYING AS CO-ENCAPSULATION SYSTEMS FOR CO DELIVERY OF RETINOIC ACID, CURCUMIN AND/OR RESVERATROL 139

9.1. Introduction 141
9.2. Material and Methods 143
9.2.1. Materials 143
9.2.2. Preparation of systems to be fed to the spray-dryer 143

9.2.3. Spray-drying technology 144
9.2.4. Emulsions viscosity 144
9.2.5. Emulsions zeta potential 144
9.2.6. Droplet and particle size distribution 144
9.2.7. Microparticle morphology 145
9.2.8. Encapsulation efficiency and loading capacity 145
9.2.9. Controlled release experiments 146
9.2.10. Statistical analysis 146
9.3. Results and discussion 147
9.3.1. Emulsions characterization 147
9.3.1.1. Viscosity 147
9.3.1.2. Stability of colloidal systems 149
9.3.1.3. Droplet size distribution 149
9.3.2. Characterization of carrier-based loaded microparticles 149
9.3.3. Surface morphology of microparticles 151
9.3.4. Particle size 152
9.3.5. Encapsulation efficiency and loading capacity 152
9.3.6. Drug controlled release assay 152
9.3.7. Kinetic models 155
9.4. Conclusion 158

CHAPTER 10 - CONCLUSIONS AND FUTURE PERSPECTIVES 159

10.1. Conclusions 161
10.2. Future perspectives 163

Nomenclature

Roman symbols

K_0 – Zero-order release constant

K_1 – First-order release constant

K_H – Higuchi constant

K_K – Korsmeyer constant.

M_t – Dissolution/release (%) of the active compound at time t

M_∞ – Dissolution/release (%) of the active compound at infinite time,

n – Release exponent

Q_0 – Initial amount of the drug/active compound in solution

Q_t – Cumulative amount of the drug/active compound released at the time t

Q_t/Q_∞ – Fraction of active compound released until time t

t_0 – Lag-time of the dissolution

U1 – Uncertainty associated to the standard preparation

U2 – Uncertainty associated to the calibration curve

U3 – Uncertainty associated to precision

U4 – Uncertainty associated to accuracy

Greek symbols

β – Indicates the shape parameter of the curve

τ_d – Time when 63.2% of M has been dissolved/released

Acronyms

APL – Acute promyelocytic leukemia

BBMpE – Unloaded microparticles (only composed by the xanthan gum + alginic acid sodium, modified chitosan + alginic acid sodium, modified chitosan + xanthan gum or modified chitosan + xanthan gum + alginic acid sodium blend as encapsulating agents)

BBMpOT – Microparticles loaded with coconut oil and tween 80 (Tween 80 was added to coconut oil and the final mixture was dispersed with xanthan gum + alginic acid sodium, modified chitosan + alginic acid sodium, modified chitosan + xanthan gum or modified chitosan + xanthan gum + alginic acid sodium solutions)

BBMpRA – Microparticles loaded with RA dissolved in coconut oil and mixed with tween 80 (Tween 80 was added to RA dissolved in coconut oil and the final mixture was dispersed with with xanthan gum + alginic acid

sodium, modified chitosan + alginic acid sodium, modified chitosan + xanthan gum or modified chitosan + xanthan gum + alginic acid sodium solutions)

CRABP – Cellular RA-binding protein

CRBP – Cellular retinol-binding protein

CRBP II – Cellular retinol-binding protein type II

DGM – Dynamic gastric model

DHIS – Dynamic human stomach-intestine system

DMEM – High glucose Dulbecco's modified Eagle's medium

DMSO – Dimethyl sulfoxide

DRSD – Dynamic rat stomach-duodenum system

EC – Ethyl cellulose

ECP – Ethyl cellulose + polyethylene glycol

FDA – Food and Drug Administration

GDS – Gastric digestion simulator

GRAS - Generally Recognized as Safe

HBSS – Hanks balanced salt solution

HGS – Human gastric simulator

HPLC – High performance liquid chromatography

IMGS – *In vitro* mechanical gastric system

LOD – Detection limit

LOQ – Quantification limit

LRAT – Lecithin retinol acyl transferase

Mc1 – Empty microcapsules (only composed by arabic gum, modified chitosan or alginic acid sodium as encapsulating agents)

Mc2 – RA-loaded microcapsules (RA dissolved in ethanol was mixed with arabic gum, modified chitosan or alginic acid sodium solutions)

MpB – Loaded microparticles for co-encapsulation of RA, curcumin and/or resveratrol (Tween 80 was added to RA, RA + curcumin, RA + resveratrol or RA + curcumin + resveratrol dissolved in coconut oil and the final mixture was dispersed with alginic acid sodium solution)

MpE – Unloaded microparticles (only composed by alginic acid sodium, modified chitosan, arabic gum, xanthan gum or gelatin as encapsulating agents)

MpOT – Microparticles loaded with coconut oil and tween 80 (Tween 80 was added to coconut oil and the final mixture was dispersed with alginic acid sodium, modified chitosan, arabic gum, xanthan gum or gelatin solutions)

MpPE – Unloaded microparticles (only composed by EC or EC + PEG as encapsulating agents)

MpP – Loaded microparticles for co-encapsulation of RA, curcumin and/or resveratrol (RA, RA + curcumin, RA + resveratrol or RA + curcumin + resveratrol dissolved with EC + PEG solution)

MpPRA – RA-loaded microparticles (RA dissolved with EC or EC + PEG solution)

MpRA – Microparticles loaded with RA dissolved in coconut oil and mixed with tween 80 (Tween 80 was added to RA dissolved in coconut oil and the final mixture was dispersed with alginic acid sodium, modified chitosan, arabic gum, xanthan gum or gelatin solutions)

MTT – (3-(4,5-dimethylthiazol-2-yl)-2,5- diphenyltetrazolium bromide)

N-CoR – Nuclear receptor co-repressor

NLC – Nanostructured lipid carriers

O/W – Oil-in-water

O/W/O – Oil-in-water-in-oil

PEG - Polyethylene glycol

PLGA – Poly(lactic-co-glycolic acid)

PVA – Polyvinyl alcohol

RA – Retinoic acid

RALDH – Retinaldehyde dehydrogenase

RARs – RA receptors

RAREs – RA response elements

RBP – Retinol binding protein

RDH – Retinol dehydrogenase

RXRs – Retinoid X receptors

SEDDS – Self-emulsifying drug delivery systems

SGF – Simulated gastric fluid

SHIME – Simulator of the human intestinal microbial ecosystem

SIF – Simulated intestinal fluid

SLN – Solid lipid nanoparticles

STRA6 – Stimulated by retinoic acid 6

TEER – Transepithelial electric resistance

TIM – TNO's gastrointestinal model

TTR – Transthyretin

W/O – Water-in-oil

W/O/O – Water-in-oil-in-oil

W/O/O/W – Water-in-oil-in-oil-in-water

W/O/W – Water-in-oil-in-water

Chapter 1- Introduction

The first chapter starts with the scope and motivation behind the subject of research of this thesis. The main goal and the overall tasks performed in this study are then presented. At last, the thesis outline is revealed.

1.1. Scope and motivation

Encapsulation arises as an emerging technology capable to promote the innovation and the development of new products with industrial interest. Incorporation of bioactive compounds into carrier-based systems at a nano and micro scale has been widely described in food [1,2] and pharmaceutical [3,4] sectors, providing scientific, technological and commercial opportunities to these industries. Most of these compounds are very sensitive and unstable under specific conditions (light, heat and oxygen, among others), as well as during processing and storage [5]. Accordingly, the direct integration of food- and pharmaceutical-grade bioactive compounds and ingredients to produce functional foods, medical foods and excipient foods can be a challenge for the industry. This challenge increases with the highly lipophilic properties and low and/or variable bioaccessibility and bioavailability of the bioactive compounds intended to be used in products for oral ingestion [6–9]. The development of nano- and microstructures capable to protect the bioactive compounds against adverse outside surrounding environment, to promote its dispersion, to increase the solubility and to beneficiate the controlled release and absorption of lipophilic molecules at desired locations within the gastrointestinal tract is of major importance to increase the bioavailability and ultimately to improve the efficacy of target bioactive compounds in the human body [9–11]. Addressing these formulations for the addition of bioactive compounds into food and pharmaceutical products may promote the preservation, safety, quality and ability of final product to fulfil the purpose for which it was designed.

Most of the carrier-based systems proposed in food and pharmaceutical sectors include particles and capsules, nanostructured lipid carriers (NLC), solid lipid nanoparticles (SLN), hydrogels, liposomes, emulsions and self-emulsifying drug delivery systems (SEDDS). In some studies, the combination of encapsulating methods is considered to obtain a structure with specific characteristics according to its final application. Particles and capsules can be produced by several materials (*e.g.* biopolymers and synthetic polymers) using different encapsulation techniques, namely spray-drying technology. Microencapsulation by spray-drying is one of the oldest encapsulation methods [12] and recognized to be simple and economically advantageous. Spray-drying is based on the atomization of a liquid system (a solution, suspension or emulsion containing the bioactive compound(s) to be encapsulated and the encapsulating agent(s)) with the formation of a dry powder (Figure 1.1) [13]. This process is very fast (a few seconds), whereby the obtained nano- and/or microparticles are suitable for the encapsulation of heat-sensitive bioactive compounds [14]. Accordingly, spray-drying is widely used in the food industry and a common method applied in the pharmaceutical industry [15,16].

The development of a bio-friendly carrier-based system for retinoic acid (RA) encapsulation emerges as an alternative approach for oral administration of this bioactive compound. This type of formulations might increase the therapeutic action of RA by increasing its bioavailability in patients. RA is a natural derivative of vitamin A (retinol) recognized as a most successful example of antitumor agent for the treatment of several malignancies [17], being the only effective in the treatment of acute promyelocytic leukemia (APL) [18]. APL is a distinct M3 subtype of acute myeloid leukaemia and it has origin in the PML/RARA fusion protein due to the translocation between PML and RARα genes located on chromosome 15 and 17 [19–21]. APL was reported

as a rapidly fatal disease until the late 1980s [22]. Currently, it is considered the most curable subtype of acute myeloid leukemia with survival rates of 80 to 90%, with the combination of all-trans-RA and arsenic trioxide (non-chemotherapy regimen) [23]. Eventually, the combination of these compounds and chemotherapy is also considered in the treatment of APL [22]. The usage of new retinoids and the combination of different compounds with all-trans RA or arsenic trioxide has been investigated to activate alternative mechanisms of action and, consequently, lead to a synergistic effect on growth control and apoptosis of malignant cells in APL [24]. Herein, curcumin and resveratrol are promising molecules to treat APL.

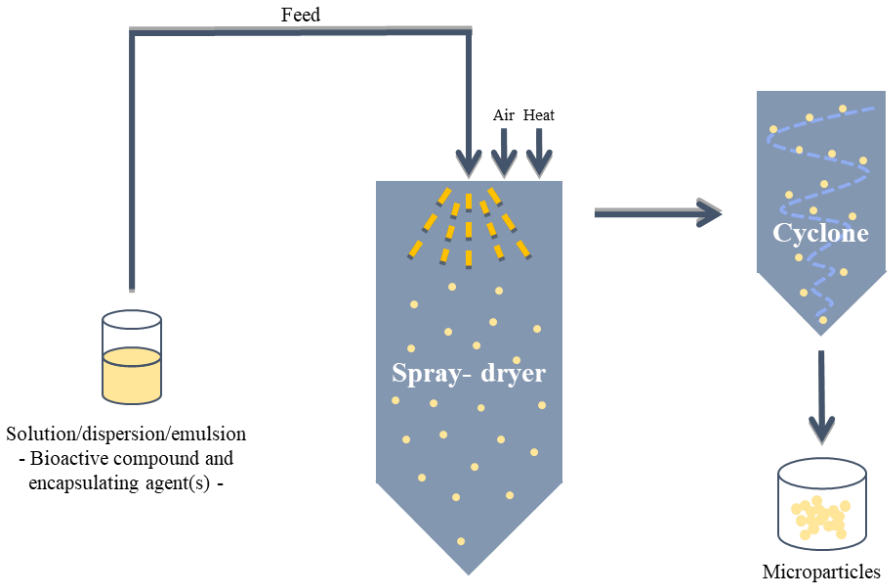


Figure 1.1 – Schematic representation of spray-drying process.

Despite of RA efficacy, the efficiency of this medical agent is highly hampered by its short half-life in the blood [25,26] due to continuous oral administration, as well as sensitivity to ambient conditions, low solubility and short gastrointestinal absorption [27]. Furthermore, RA administration deals with severe side-effects [28]. Encapsulation by spray-drying is a suitable technology to produce biocompatible particles to deliver RA to treat patients with APL in a direct and efficient mode. For the best of our knowledge, the current number of studies focused on RA encapsulation for the treatment of APL is scarce. They include the incorporation of RA into liposomes to evaluate the effect of these systems on the cellular metabolism of this bioactive compound [29,30]. Moreover, RA-loaded copolymer nanoparticles based on polyethylene glycol (PEG)-poly(L-lactide) and PEG-poly(e-caprolactone) were proposed to compare the differentiation induction potential of HL-60 cells with free RA [31]. Cholesteryl butyrate SLN were also investigated for the assessment of cell viability and distribution of cell cycle phases for HL-60, Jurkat, and THP-1 cell lines [32]. The most recent study is related to development a poly(lactic-co-glycolic acid) (PLGA) microspheres to direct RA delivery to immune structures of the gut and reduce systemic exposure [33]. A single study describes the encapsulation of RA by spray-drying into modified polyvinylalcohol (PVA) polymeric micelles [34]. The work herein presented provide an approach based on the proposal of different types of systems – solutions and emulsions – composed by biopolymers and

synthetic polymers as encapsulating agents (individually used and as a blend) for controlled release of RA in the intestine (oral administration).

1.2. Research goals

The ultimate goal of this thesis was the development of an appropriate RA controlled delivery system based on spray-drying encapsulation technology to be used in therapeutic treatments, particularly in the treatment of APL. To accomplish this goal, different natural and synthetic polymers known to have adequate biocompatibility towards human cells were used as encapsulating agents. Several formulations (solutions and emulsions) composed by polymers used individually and as a blend of materials were considered to produced RA-loaded microparticles. Moreover, the operational conditions to be used in the spray-dryer for RA were optimized. The obtained carrier-based systems were characterized in terms of encapsulation efficiency, size and surface morphology. RA controlled release was also evaluated considering an appropriate environment simulating the phospholipids membrane characteristics and the RA kinetics release considering the fundamental equations governing the controlled release of active compounds were stablished. The most promising RA-loaded systems were subjected to the simulation *in vitro* digestion coupled to intestinal (Caco-2 cells) absorption models. Herein, RA bioavailability and transepithelial transport efficiency was estimated. Furthermore, cytotoxicity and cell viability of this cellular model was evaluated in respect to RA controlled release. An overview of this doctoral project is shown in Figure 1.2.

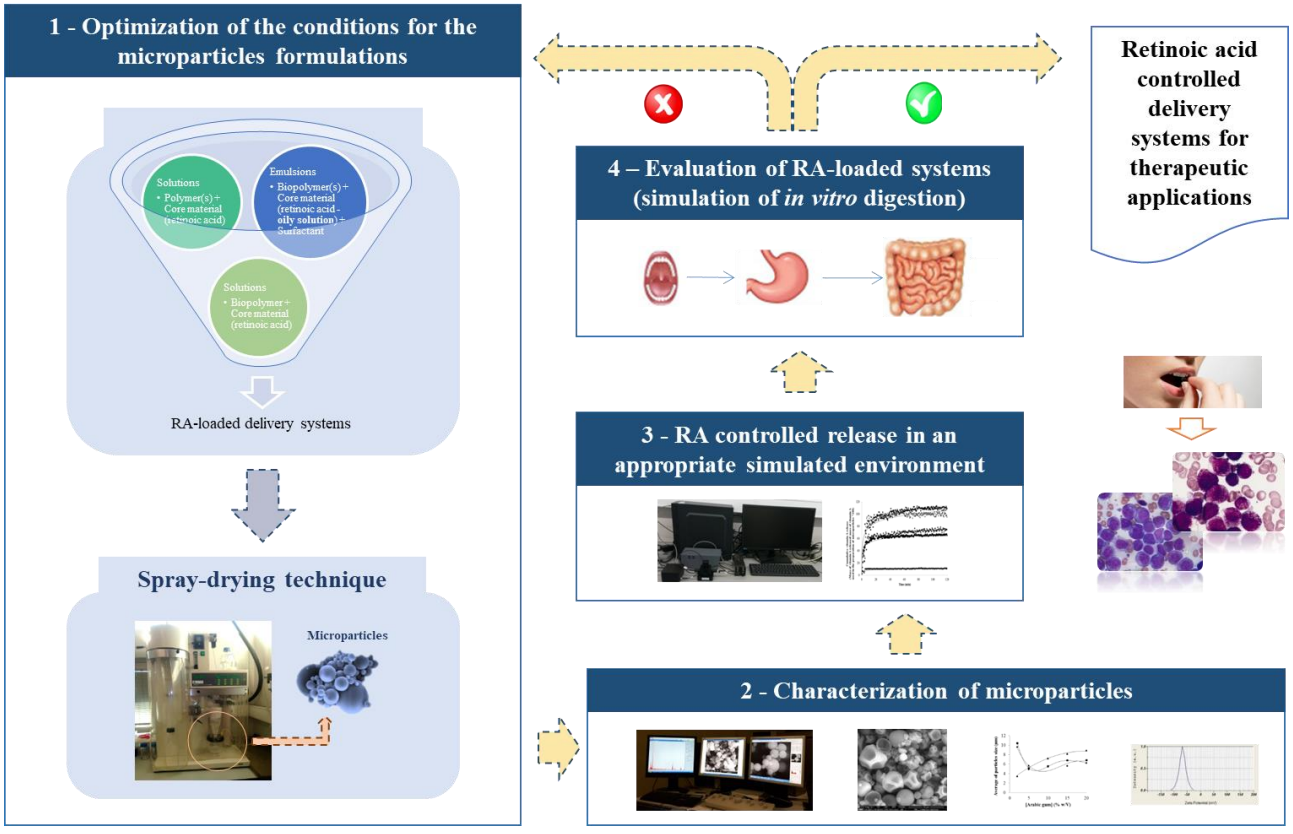


Figure 1.2 – Doctoral project overview: iterative process for RA-loaded microparticles improvement**.**

1.3. Thesis outline

This thesis is divided into 10 chapters.

Chapter 1 describes the thesis scope and motivation, research goals and the thesis outline.

Chapter 2 explores the concept of retinoid. The structure and metabolism, the mechanisms of action and the therapeutic value of retinoids and its side-effects are presented in this chapter.

Chapter 3 provides a comprehensive overview about the simulated methods used to evaluate the behaviour of carrier-based systems within the human gastrointestinal tract. An approach based on *in vitro* (static and dynamic) digestion models, methodologies to evaluate the intestinal absorption and presystemic metabolism, *in vitro* simulation of microbial fermentation and *in vivo* methodologies was considered and discussed. The main delivery systems and encapsulating methods with importance in the food field are also herein described.

Chapter 4 presents formulations composed by RA (dissolved in ethanol) and different biopolymeric solutions (alginic acid sodium, modified chitosan and arabic gum, individually used) to be fed to the spray-dryer for RA encapsulation. The obtained microparticles were evaluated in terms of morphology, particle size and RA controlled release profiles.

Chapter 5 presents oil-in-water emulsions composed by RA (dissolved in coconut oil), a biopolymer (alginic acid sodium, modified chitosan, arabic gum, gelatin and xanthan gum) and the surfactant Tween 80. They were characterized (rheological properties, stability and droplet size distribution) and further spray-dried under optimized conditions. The impact of microparticles formulation in the encapsulation efficiency, morphology, particle size and RA controlled release behaviour was evaluated.

Chapter 6 presents oil-in-water emulsions with an overall similar composition of the emulsions proposed in Chapter 5, but considering binary and ternary blends of the biopolymers that individually enabled the production of RA-loaded microparticles with the most advantageous characteristics (xanthan gum + alginic acid sodium (50%–50%), modified chitosan + alginic acid sodium (50%–50%), modified chitosan + xanthan gum (50%–50%) and modified chitosan + xanthan gum + alginic acid sodium (33.3%-33.3%–33.3%)). The emulsions produced and the microparticles obtained by spray-drying were characterized considering the parameters presented in Chapter 5. Moreover, it was stablished a comparation among the main characteristics of microparticles herein obtained and the microparticles individually composed by alginic acid sodium, modified chitosan and xanthan gum (Chapter 5).

Chapter 7 presents two synthetic polymers – ethyl cellulose (EC) and polyethylene glycol (PEG) – for the development of carrier-based systems for RA encapsulation using spray-drying technology. Herein, RA was mixed in EC and EC + PEG solutions (both dissolved in absolute ethanol). The obtained microparticles were analysed regarding the size, surface structure, RA controlled release profiles, encapsulation efficiency and the

ability to incorporate a higher amount of RA in the formulation to be spray-dried when compared to the other formulations proposed (Chapters 4, 5 and 6).

Chapter 8 presents the bioaccessibility (gastric and intestinal) and intestinal transport of RA encapsulated into EC and EC + PEG-based microparticles (microparticles proposed in Chapter 7). RA-loaded microparticles were subjected to the INFOGEST *in vitro* digestion method with and without a meal (western diet).

Chapter 9 presents co-encapsulation of RA, curcumin and/or resveratrol into alginic acid sodium-based microparticles obtained from dried oil-in-water emulsions and EC + PEG-based microparticles (carrier-based microparticles proposed in Chapters 5 and 7, respectively). Microparticles loaded with RA, RA + curcumin, RA + resveratrol and RA + curcumin + resveratrol were produced. The emulsions and microparticles were characterized according to the parameters presented in Chapter 5 and 7. Biopolymer and synthetic polymers-based microparticles were compared regarding surface morphology, size, encapsulation efficiency and co-delivery of selected bioactive compounds.

Chapter 10 gathers the final remarks of the thesis, indicating the most relevant conclusions of this research and perspectives for future work.

Chapter 2 - Formulation approaches for improved retinoids delivery in the treatment of several pathologies

---

The second chapter starts exploring the competences and the difficulties of using retinoids in health care. The metabolism and the main considerations about the mechanism of action of retinoids are also discussed. The final sections are focused on the most recent studies about RA controlled delivery systems to be used in the medical field.

This chapter is published in:

Gonçalves, A; Estevinho, B N; Rocha, F. Formulation approaches for improved retinoids delivery in the treatment of several pathologies. European Journal of Pharmaceutics and Biopharmaceutics. 2019, 143, 80-90, https://doi.org/10.1016/j.ejpb.2019.08.014.

2.1. Introduction

Retinoids are a set of bioactive molecules which includes vitamin A (retinol) and its natural and synthetic derivatives. They are signalling molecules involved in reproduction, embryogenesis, cellular proliferation and differentiation, immunological activity, vision and epithelial cellular integrity [35].

Vitamin A was first described in 1913 [36]. It is a fat-soluble vitamin composed of a cyclohexenyl ring, a polyene side chain and a polar end-group (Figure 2.1) [37,38].

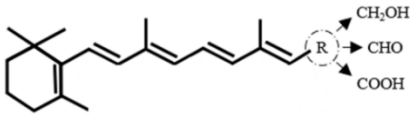


Figure 2.1 – General structure of retinoids (adapted from [39]). Retinoids with the end groups CH_2OH, CHO and COOH correspond to retinol, retinal and retinoic acid, respectively.

Vitamin A (retinol), retinal and retinoic acid (RA) are naturally occurring endogenous retinoids (the interconversion between these non-aromatic compounds is described in detail in section 2.2.) and belong to the first generation of retinoids [38]. RA exists as different isomers and the most common RA isomers include all-trans RA (recognized as the vitamin A metabolite with the highest biological activity [40]), 9-cis RA and 13-cis RA [41] (Figure 2.2). The synthetic analogues of these isomers are tretinoin, alitretinoin and isotretinoin, respectively, and they are also included in this group of retinoids [37,42,43]. These compounds are oral and topically administrated. Other synthetic retinoids (RA analogues) were pharmaceutically developed and categorized as retinoids of second (mono-aromatic retinoids), third (polyaromatic retinoids) and fourth (pyranone retinoids) generation [37,44] (Figure 2.2). Mono-aromatic retinoids include acitretin and etretinate (orally administrated), while polyaromatic retinoids comprise bexarotene (oral and topically administrated), tazarotene (topically administrated), adalapene (topically administrated) and fenretinide (orally administrated) [37,42,45]. At last, seletinoid G (topically administrated) fits in pyranone retinoids [37].

One of the major focuses of retinoids action is related to its anticancer activity. Retinoids regulate tumor-cell growth through the inhibition of cellular proliferation and induction of differentiation, apoptosis and cellular cycle arrest in pre-cancerous and cancerous cells [39,42,46,47]. Particularly, RA plays an important key role as chemopreventive and/or chemotherapeutic. It is an antitumor agent used to treat acute promyelocytic leukemia (APL) [18], skin [42], lymphoma [43], breast [48], ovarian [49], head and neck [50], cervical [51], lung [52], neuroblastoma [53], glioblastoma [54], glioma [55], and melanoma [56] cancer, among others. In fact, this strategy is the only effective treatment for APL [18]. Food and Drug Administration (FDA) approved the usage of all-trans RA in the treatment of APL since 1995 [57]. However, cancer patients can handle several side-effects due to RA administration. In the treatment of APL many patients became resistant to all-trans RA despite continued treatment [58]. Continuous oral administration or intravenous injection are related to a fast reduction of RA half-life in the blood [25,26]. Accordingly, the brief remissions period observed can be explained through

the decrease of concentration of RA in the plasma of patients with cancer [58]. Furthermore, patients treated with all-trans RA may present headache, abdominal pain, nausea, and hypertriglyceridemia, among others [28,58–60]. Also, patients may suffer of retinoid acute resistance [28], which is characterized by the appearance

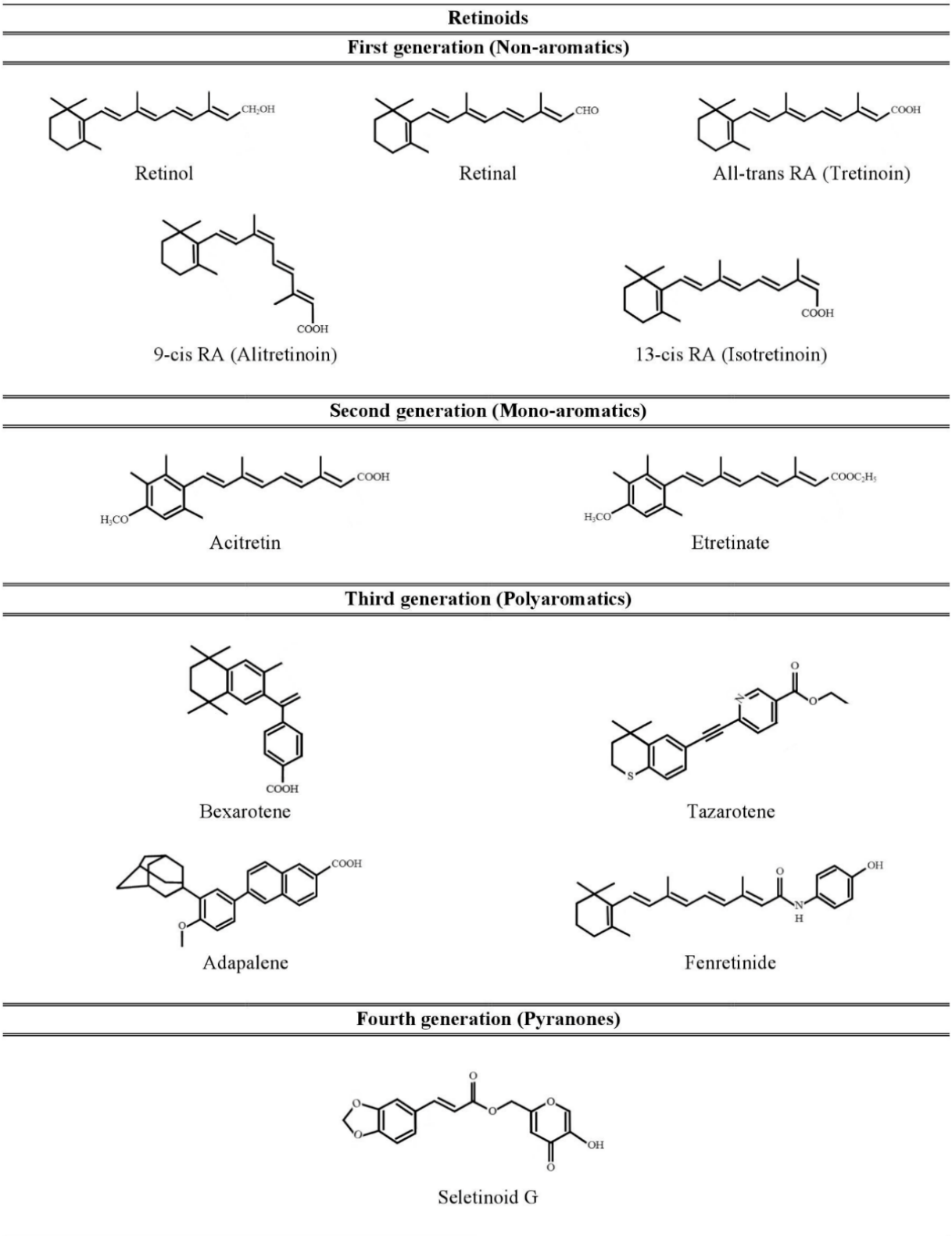


Figure 2.2 – Retinoids of first, second, third and fourth generation (adapted from [39]).

of fever, dyspnea, pulmonary infiltrates, respiratory distress interstitial, hypotension, pleural and pericardial effusion, high number of white blood cells and acute renal failure [59,61]. Dexamethasone administration can be used to treat this condition [61]. 9-cis RA and 13-cis RA also showed to be effective against some malignancies. 9-cis RA was approved for the cutaneous lesions of Kaposi's sarcoma (topical treatment) [62], while 13-cis RA has been investigated to be used in thyroid cancer treatment [63]. In respect to synthetic retinoids, bexarotene and fenretinide were produced to be used in cutaneous T-cell lymphoma [64] and breast cancer chemoprevention [65], respectively. The development of novel synthetic retinoids was promoted considering the efficiency of natural retinoids, but also as a strategy to decrease the toxicity related to the natural retinoids [45,66].

Retinoids have been also widely used for treatment of some dermatological disorders, namely acne vulgaris, psoriasis and photo damaged skin, among others [67–69]. Herein, tretinoin and isotretinoin are the main compounds to be used in the treatment of acne [42]. Moreover, tretinoin is the most explored retinoid in photoaging therapy [37], as well as seletinoid G [37]. Also, this compound is used to accelerate the skin healing process and to enhance skin appearance [57,70]. At last, it was observed the successful usage of tretinoin in the treatment of pigmentary abnormalities [71,72]. In turn, isotretinoin has been also implemented to treat rosacea, particularly for the subtypes phymatous, granulomatous, steroid-induced rosacea or rosacea fulminans and Morbihan disease [42]. In addition to tretinoin and isotretinoin, adapalene [42] and tazarotene [37] are also used to treat acne. The advantage of adapalene when compared to tretinoin and isotretinoin is the ability to provide higher photostability [42]. The psoriasis treatment have been successfully carried out by the usage of acitretin and etretinate [42] and tazarotene [37]. Most of these retinoids addressed to solve skin problems are topically applied and high doses might be administrated. The side-effects related to this kind of administration include skin irritation (*e.g.* erythema, dryness, peeling, dermatitis and burning at the application site) and high vulnerability to the sunlight which limits retinoids therapy acceptance by patients [42,69,73,74]. These problems are more commonly observed with tretinoin and tazarotene [37]. In turn, the systemic use of retinoids leads to hair loss, conjunctivitis, mucocutaneous xerosis and the increase of transaminases and triglyceride amount [42].

In line with the topics above, retinoids delivery to the patients has been a challenge. In addition to the severe side-effects related to retinoids administration, retinoids may not reach the target cells/tissues in the desired concentrations, which arise as a major constraint for the therapeutic treatment efficiency [75]. It can be explained by the variable retinoid concentration in the plasma (as referred previously), the poor retinoids gastrointestinal absorption and rapid metabolism [27] and the poor solubility in water and highly instability of retinoids in the presence of oxidants, heat and light, among others [35,76]. Accordingly, the routine use of retinoids may not constitute by itself, on its current approach, a competent strategy for the treatment of certain cancers and skin pathologies, as described above. Encapsulation of retinoids into different delivery systems has been explored and projected to improve the conventional methods of administration of these bioactive compounds. The ultimate goal is to increase the bioavailability of these molecules in the human body and, subsequently, become retinoids more efficient as medical agent. Currently, a significant growth in the global encapsulation market is

predicted. Particularly, pharmaceutical application dominated the industry, being expected a compound annual growth rate of 11% from 2016 to 2025 [77].

The article provides a general discussion about the metabolism and the mechanisms of action of retinoids and the most recent carrier-based formulations developed for controlled delivery of RA.

2.2. Retinoids metabolism

The human body cannot produce vitamin A, whereby the practice of a balanced diet is mandatory in order to certify the intake of the recommend supply of this essential nutrient [48]. Dietary sources of vitamin A include carotenoid-rich plants (*i.e.* such as carrots and plants with green leaves [78]) and liver, eggs and milk, which contain retinyl esters, the storage form of retinol [35,38,79]. Among these, the major source of vitamin A is provided in the form of retinyl esters [79]. When ingested and in the first phase of digestion, carotenoids and retinyl esters are dissolved in the food fat phase, forming emulsions in the gastric environment as well as in the duodenum (small intestine) [79]. β-carotene, α-carotene and β-cryptoxanthin might be absorbed by small intestine and taken up by enterocytes. Herein, these molecules are transformed into retinal [80–82]), which is further reduced to retinol. In turn, retinyl esters are first hydrolysed to retinol by pancreatic and intestinal enzymes and then absorbed by the small intestinal lumen [79,83]. Retinol enters the enterocytes and bind to cellular retinol-binding protein type II (CRBP II). It is a specific binding protein with an important key role promoting the re-esterification of retinol with long chain fatty acids through lecithin retinol acyl transferase (LRAT) [82,84]. Nevertheless, a significant amount of retinol remains on its unesterified form, being secreted into portal circulation [85]. The higher amount of formed retinyl esters is afterwards assimilated by chylomicrons which are released from enterocytes to the intestinal lymphatic circulation and then enters into blood circulation [86,87]. The chylomicrons remnants obtained by the hydrolysis of triacylglycerol and the exchange of apolipoprotein in blood circulation [87] are mainly uptake by the liver (hepatocytes) [88], but also by the spleen, skeletal muscle, bone marrow, kidney, adipose tissue, lung, peripheral blood cells and heart for retinol storage on its esterified form [89,90]. In hepatocytes vitamin A can be stored as retinyl esters or retinyl esters can be hydrolysed. Considering the second alternative, the obtained retinol binds to retinol binding protein (RBP), forming the retinol-RBP complex in the hepatocyte [57]. RBP is a hydrophobic protein capable to protect retinol. This step promotes the transference of retinol-RBP from endoplasmic reticulum to the Golgi complex and its further secretion to the plasma of the blood [91]. Moreover, most of unesterified retinol is displaced to the hepatic stellate cells for its storage as retinyl esters [82,88]. In blood, retinol-RBP binds to transthyretin (TTR) to ensure that retinol is uptaken by target cells/tissue. In fact, RBP of retinol-RBP complex is recognized by the trans-membrane protein called stimulated by retinoic acid 6 (STRA6), which is a RBP receptor present in target cells/tissues [57,92–94]. Retinol is internalized and inside the cells this compound can binds to specific CRBP (I and II) or it is reversibly oxidized to retinal (or all-trans retinaldehyde) by retinol dehydrogenase (RDH) [57,95]. Further irreversible oxidation of retinal by retinaldehyde dehydrogenase (RALDH) results in the formation of RA. This isomer can bind to cellular RA-binding protein (CRABP) and be oxidized to 4-hydroxyretinoic acid and 4-oxoretinoic acid by cytochrome P450 enzyme (*i.e.* CYP26) [39,57,95]. This strategy

enables to regulate the cellular levels of RA. Instead, RA can enter the nucleus of the cells and bind to specific nuclear receptors and regulate the cellular function considering genomic and non-genomic mechanisms (section 2.3.) [39,57]. An overview about the metabolic interconversion between vitamin A (retinol) natural structures is presented in Figure 2.3.

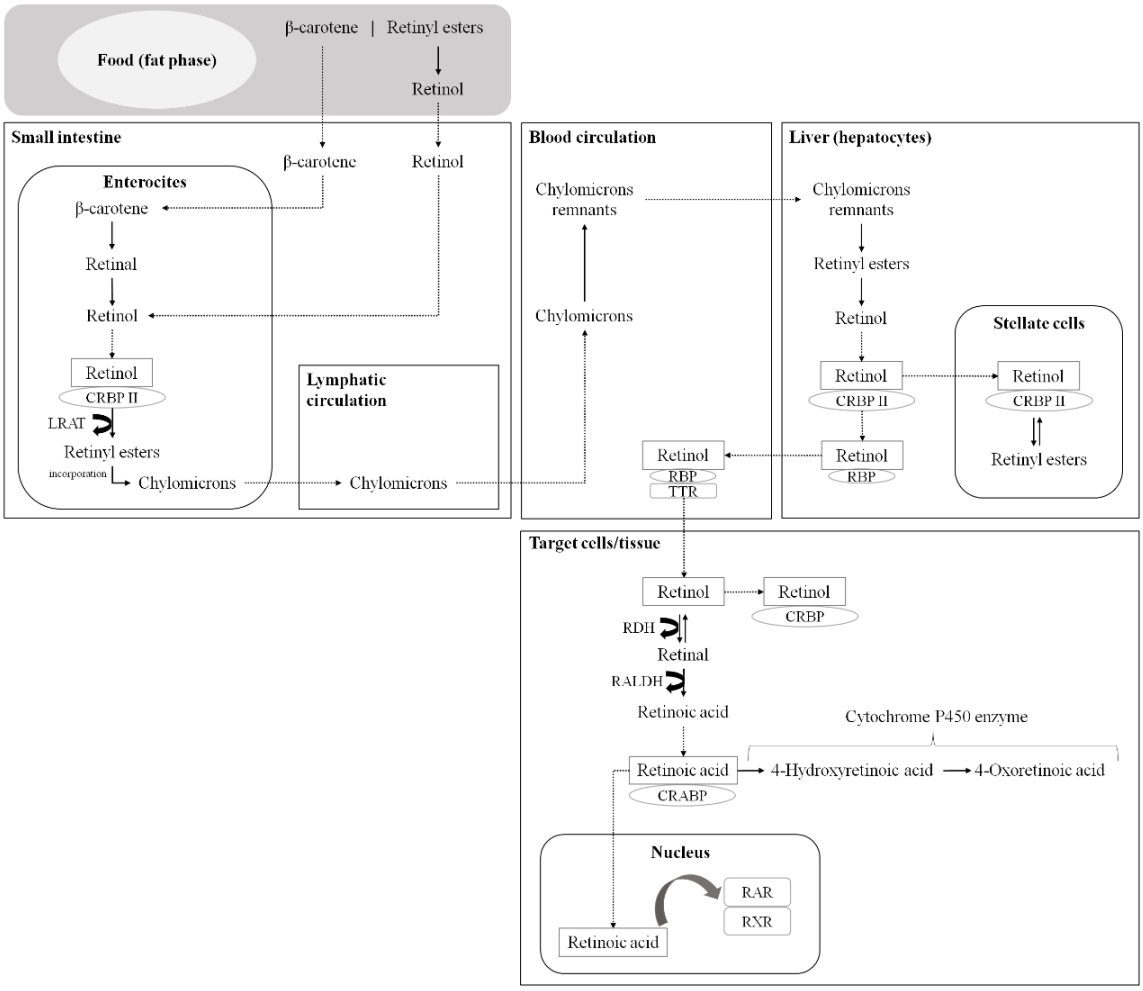


Figure 2.3 – Metabolic interconversion between vitamin A (retinol) natural structures (adapted from [35,37,44,96]). Abbreviations: CRABP: cellular RA-binding protein; CRBP II: cellular retinol-binding protein type II; LRAT: lecithin retinol acyl transferase; RALDH: retinaldehyde dehydrogenase; RBP: retinol binding protein; RDH: retinol dehydrogenase; TTR: transthyretin.

2.3. Mechanisms of action of retinoids

Retinoids act by regulating gene transcription mediated through their bind to RA receptors (RARs) and retinoid X receptors (RXRs) [43]. These specific nuclear receptors comprise the most investigated nuclear hormone receptors [97]. Each family of these receptors is associated to three subtypes (*i.e.* RARα, RARβ and RARγ, and RXRα, RXRβ and RXRγ) and each one of them can present several isoforms [39,98]. Accordingly, RARα and RARγ may be present in the isoforms 1 and 2 (RARα1 and RARα2, RARγ1 and RARγ2), while RARβ may

arise in the isoforms RARβ1, RARβ2, RARβ3, RARβ4, RARβ5 and RARβ1'. In turn, all subtypes of RXR have the isoforms 1 and 2 (RXRα1 and RXRα2, RXRγ1and RXRγ2, RXRβ1 and RXRβ2) [99]. Human RARs activation can be carried out by the ligands all-trans RA, 9-cis RA, isotretinoin, etretinate and acitretin, while the ligands for human RXRs only cover 9-cis RA and bexarotene [43].

Retinoids receptors contain five functional domains [39]. Domain A/B is known by encoding the least conserved N-terminal domain, which has an autonomous transcriptional activation function (AF-1). Domain C is highly conserved and it is composed by two zinc finger modules for the binding of DNA. For this reason, domain C is also referred as the DNA-binding domain. Domain D is a hinge which separates the domains C and E. Moreover, this domain is involved in the interaction with some nuclear receptor coregulators. Domain E contains the ligand-binding domain and the activation function-2 (AF-2) domain. The ligand binding to the ligand-binding domain promotes a conformational change in the receptor complex and modulates their function. AF-2 is also involved in this conformational change due to an amphipathic α-helix. These conformational changes promote the destabilization of corepressors-binding interface and trigger the recruitment and the interaction with specific co-activators [98]. At last, domain F contains a C-terminal domain which might assist in AF-2 activity.

RXRs can form homodimers (two RXRs) or heterodimers (one RXR and one other receptor) with receptors for vitamin D (vitamin D receptor, VDR), bile acids (farnesoid x receptor, FXR), fatty acids (peroxisomal proliferator activated receptors, PPAR) and RA (RARs), among others [57]. Thus, different signalling pathways can be mediated. Considering the numerous subtypes and isoforms of receptors, it is possible to create a large set of different receptor dimers. Dimerization of receptors is carried out through the interaction of the ligand-binding domain (domain E) of each target receptor [39].

The heterodimer RAR/RXR is crucial for biological activity. It is believed that most of the RA effects are mediated by this receptor dimer [95,98]. In the presence of RAR agonists, their binding to the heterodimer RAR/RXR activates a conformation change and the formation of a ligand-receptor complex. This structure is capable to bind to specific DNA sequences at specific RA response elements (RAREs) and modulate the transcription regulators of several genes and the production of specific target peptides [43,98]. Herein, the enzyme histone acetyl transferase is activated, promoting the chromatin decondensation over the promoter region of target gene. Subsequently, the transcription machinery is activated. It is a process which involves other complexes, namely the thyroid hormone receptor-associated protein [98]. Genes regulated by RA have one type of RAREs that is more frequent to be found (*i.e.* the DR-5 type) and another one that is rare (*i.e.* the DR-2 type) [98]. On the other hand, in the presence of antagonist or in absence of ligands for the RAR/RXR heterodimer, the apo-receptor pair binds to RARE and the corepressor which encodes the activity of histone deacetylase is recruited. The deacetylation of histone is stimulated, occurring the condensation of chromatin and the gene silencing [100].

In addition to the genomic mechanisms, retinoids intermediate non-genomic mechanisms, namely retinoylation (RA acylation). It is a post-translational alteration of proteins carried out by eukaryotic cells [39].

2.4. Carrier-based formulations used for controlled delivery of retinoids

Incorporation of retinoids into nano- and/or microparticles has been subject of research in order to improve the performance of these molecules with importance in the pharmaceutical and medical fields. The design of appropriate formulations based on controlled delivery systems has been widely explored to minimize undesirable side-effects due to retinoids administration. Furthermore, this approach might provide an effective protection and stability of retinoids, as well as increase their half-life.

Scientific output reached 81580 and 12114 publications related to “encapsulation” and “microencapsulation”, respectively. Moreover, 192 publications about “encapsulation” and “retinoic acid” are registered on Scopus database (source: www.scopus.pt, 7th May 2019). The most recent studies (from the last five years) propose several lipid-based carriers for RA encapsulation, including micro-, nano- and emulsions, solid lipid nanoparticles (SLN), nanostructured lipid carriers (NLC), liposomes, niosomes, ethosomes, transethosomes. These types of formulations are recognized to provide a sustained delivery system, in addition to be biocompatible and biodegradable carriers [101]. Furthermore, polymeric carriers such as chitosan, collagen-hyaluronate scaffolds, poly(lactic-co-glycolic acid) (PLGA), polyvinyl alcohol (PVA), poly(ε-caprolactone), hollow mesoporous silica and chitooligosaccharide are also described for incorporation of RA. A brief description about these carriers can be reviewed in the following topic (section 2.4.1.). Moreover, examples of these retinoids delivery systems are also discussed, highlighting the impact on the bioavailability, bioaccessibility and stability of RA, as well as the therapeutic effect in *in vitro* and *in vivo* studies (section 2.4.2.).

2.4.1. Most important methods implemented for RA encapsulation

2.4.1.1. Emulsions

Emulsions are thermodynamically unstable formulations. They consist of a mixture of two or more immiscible fluids, wherein the liquid of one phase is dispersed as small droplets within the continuous phase [102]. The formation and stabilization of emulsion droplets is achieved by the usage of an appropriate mixture of surfactants and co-surfactants. More simple or complex emulsions can be prepared considering the relative spatial organization of the water and oil phases. Accordingly, water-in-oil (w/o), oil-in-water (o/w), water-in-oil-in-water (w/o/w), water-in-oil-in-oil (w/o/o), oil-in-water-in-oil (o/w/o), and water-in-oil-in-oil-in-water (w/o/o/w) might be produced [103–106]. The droplet size of emulsions can vary between 10 and 100 nm (nanoemulsions), as well as between 100 nm and 1000 μm (conventional emulsions) [107], considering the formulation composition, the homogenization method and operating conditions of homogenizer [107]. Nanoemulsions are transparent and small droplets with more physical stability to gravitational separation, flocculation and coalescence when compared to conventional emulsions [107–110]. In turn, microemulsions can be distinguished from nanoemulsions, since the first ones are thermodynamically favourable formulations despite of the similarity among structures [101].

2.4.1.2. SLN

SLN are very similar to nanoemulsions, composed of liquid lipids, surfactants and water as previously referred [111]. In case of SLN, the liquid lipids are fully or partly solidified [107,108]. These type of particles are obtained by a controlled crystallization process of the emulsion [112,113], being observed the full crystallization of lipid droplets with the formation of a highly ordered crystalline structure [107].

The main advantages of SNL over nanoemulsions include: (1) the system stability with crystalline lipophilic bioactive compounds (in conventional o/w emulsions the presence of a crystalline lipophilic bioactive compound may cause partial coalescence of the emulsion [114], which might be prevented with the incorporation of the target compound into a lipidic solid matrix), (2) the improvement of lipophilic bioactive compounds stability due to their incorporation into a structured solid matrix and (3) the ability to manage the delivery of the target lipophilic bioactive compound [108]. Moreover, SLN are non-biotoxic carriers, do not require the usage of organic solvents, enable the encapsulation of lipophilic as well as hydrophilic bioactive compounds and their fabrication can be easily scaled-up [115]. The most relevant limitation of using SLN is the high temperatures used during the formation process in order to prevent the crystallization of the lipids [108]. Herein, some heat-sensitive lipophilic compounds may be degraded. Also, the lipids used to form SLN must be highly saturated to ensure the high melting point required to produce the emulsions. This condition implies a damaging effect on human health [108]. Finally, problems related to the low loading capacity, the expulsion of bioactive compounds from particles during storage, the high water content in SLN emulsions and particles aggregation were reported [116–121].

2.4.1.3. NLC

NLC were developed to overcome the limitations related to the SLN (previously described in section (2.4.1.2.). NLC are an unstructured solid lipid matrix composed by a mixture of liquid and solid lipids, as well an aqueous phase which contains surfactants and co-surfactants [119,122,123]. The lipidic phase produces a solid matrix with high imperfections in the crystal lattice. Consequently, a higher space is created in the matrix and a higher amount of bioactive compound can be loaded [119,124–126], reducing leakage during storage [127] and preserving the carrier physical stability [123]. In the final, three different types of NLC can be produced, considering the degree of order found in the matrix: imperfect, amorphous and multiple [119].

NLC are suggested as promising pharmaceutical compounds delivery systems due to the usage of GRAS compounds, safety and the availability of large-scalable production methods [123].

2.4.1.4. Liposomes

Liposome-based systems are the first nano carriers successfully used in clinical applications [128]. Currently, a high number of liposomal formulations has been approved for the cancer treatment. Particularly, the encapsulation of all-trans RA into liposomes is described in clinical trials (phase I/II) - Atragen - to treat advanced renal cell carcinoma by intravenous administration [129]. Furthermore, these products have been also

accepted for viral and fungal infections, pain management and photodynamic therapy [128]. An increasing number of liposomal delivery systems are expected due to undergoing clinical trials [128].

Liposomes consist of spherical vesicles with a bilayer of lipids around an aqueous core, whereby hydrophilic and lipophilic bioactive compounds might be herein encapsulated [101,102,130]. They are mainly composed of phospholipids, whose amphiphilic properties favour thermodynamically the formation of liposomes [128,131]. Moreover, sterols (for example, cholesterol) can be incorporated into liposomes for the bilayer stabilization and enhancement of encapsulation and controlled release features [131–134]. Four types of liposome-based systems were developed, namely conventional liposomes, sterically-stabilized liposomes, ligand-targeted liposomes and, combination systems [130]. They were proposed to deal with relatively short half-life of lipoomes *in vivo*, as well as to improve the retention of the bioactive compounds after *in vivo* administration of liposomes [135].

2.4.1.5. Niosomes

Niosomes are non-ionic surfactant carriers structurally similar to liposomes, considering the presence of a bilayer [136]. The main constituent of niosomes is cholesterol, although other excipients can be integrated. These carrier-based systems are more stable than liposomes considering the materials involved on their production. Other advantages include the osmotic stability and activity of niosomes, their applicability for oral, parenteral and topical administration, their capability to successful delivery of bioactive compounds through the skin using channel-like structures, the ability to improve the stability, oral bioavailability and therapeutic performance of bioactive compound, among others [136,137]. However, it is reported the leaking of bioactive compound from niosomes as well as the hydrolysis of core material which compromises the dispersion shelf life [136].

2.4.1.6. Ethosomes

Ethosomes differs from liposomes by the presence of high content of ethanol in the vesicles (between 20 and 45%) [138]. They are highlighted by their ability to enhance the the skin delivery of several bioactive compounds. In fact, ethosomes enable the bioactive compounds to reach the deep skin layers as well as the systemic circulation [138]. Other advantages regarding this carrier-based system include the low risk profile at a large scale, the high patient compliance due to bioactive compound administration using a gel or a cream and the relative simplicity of ethosomes production [138].

2.4.1.7. Transethosomes

Transethosomes results from the combination of transferosome (with the ability to become deformable and of skin permeation) and ethosomes [139]. Accordingly, bioactive compound-loaded transethosomes can be absorbed by skin and follow for the systemic circulation. This carrier provides high encapsulation efficiency, protection and a slow controlled delivery of bioactive compounds. Moreover, the preparation process does not require the usage of undue pharmaceutical additives [140–142].

2.4.1.8. Polymers

Different biodegradable polymers have been used as encapsulation agents to produce carrier-based systems. Due to their biocompatibility and biodegradability, these polymers are widely considered to be applied in medicine [143].

Natural biodegradable polymers present some limitations related to the defective biomechanical characteristics and the complexity of structure. However, they can be chemically modified and be metabolized by the host [144]. Chitosan is a natural biodegradable polymer capable to adhere to the gastric mucosa, does not trigger allergic or irritant reactions, its permeability increases with decrease of pH and the products resulting from its degradation are not toxic [145]. In turn, the natural polymer collagen-hyaluronate scaffolds might arise as a strategy for tracheal regeneration. In a recent study a tracheobronchial epithelial model was developed using a bilayered collagen-hyaluronate scaffold [146]. Collagen-hyaluronate scaffold provides support for growth and differentiation of respiratory epithelial cells. Consequently, a functional barrier is formed which protects and at the same time avoids the proliferation of bacteria [147].

Synthetic biodegradable polymers arise as an alternative to provide a sustained controlled delivery from over several days to weeks when compared to natural biodegradable polymers. However, they can be involves in toxicity problems and chronic inflammation [148]. PLGA was approved by US FDA and European Medicine Agency to be used in controlled delivery formulations, being one of the most used biodegradable polymers [149]. PVA is reported as safe *in vivo* in addition to present mucoadhesive nature, which is an advantage increasing the residence time of target bioactive compounds within tissues [150]. Poly(ε-caprolactone) is referred as a biodegradable polymer [151]. Hollow mesoporous silica enables the production of nanoparticles with an extensive central hole and an external mesoporous silica shell. The advantages about this type of particles include the large surface area, the ability to control the pore diameter, low density, stability, high loading capacity and the possibility to encapsulate and storage bioactive compounds with volatile properties [152]. Styrene maleic acid is a low-cost copolymer with good durability, non-toxic and no teratogenic effects [153]. Chitooligosaccharide is a depolymerization product of chitosan. It displays antibacterial and antitumor activities, as well as improves immune activity [154].

2.4.2. RA controlled delivery systems for therapeutic applications

Recent studies (from last five years) have reported feasible RA carrier-based formulations to be used to treat acne, photoaging, psoriatic and several types of cancer (Table 2.1). As far as acne therapy is concerned, Lin et al. [155] investigated the usage of two different carrier-based systems – nanoemulsions and NLC – to incorporate a combination of tretinoin and tetracycline to treat this disease. This research reported, for the first time, the impact of encapsulating simultaneously two drugs on the skin permeation and on the antibacterial activity against microorganisms involved in acne (*in vitro* studies). The obtained results evidenced that tretinoin permeation was mostly unchanged after this drug encapsulation, being enhanced the tretinoin delivery via follicular routes when NLC were used. Moreover, the incorporation of tetracycline did not incite a significant

difference in tretinoin skin delivery. However, tetracycline permeation decreased by 2-fold. In terms of the antibacterial activity, it generally was not affected by the usage of a dual-drug system. The usage of nanoemulsions and NLC only improved the antibacterial activity against *Staphylococcus aureus*. Later, Silva et al. [156] combined tretinoin and the antimicrobial lauric acid in SLN as a new strategy for the topical acne treatment. In the study, SNL with and without stearylamine were produced. Retinoid stability was only obtained with SNL composed by stearylamine. Also, SLN loaded with tretinoin and lauric acid showed to be efficient on inhibiting the growth of *Staphylococcus epidermidis*, *Propionibacterium acnes* and *S. aureus* (*in vitro* studies). Gupta et al. [137] suggested another carrier-based system to be used in the treatment of acne. They proposed the encapsulation of tretinoin and benzoyl peroxide (a powerful antibacterial) into niosomes. *In vitro* experiments revealed that a higher amount of tretinoin and benzoyl peroxide is retained in the skin layers when niosomal gel is used instead of a cream and an alcoholic solution. On the other hand, *in vivo* studies showed that niosomal gel is more effective than the antiacne cream, since a 4.16-fold lower dose of benzoyl peroxide in niosomal gel provide the similar therapeutic index of the antiacne cream.

Considering psoriasis disease, Raza et al. [157] developed tretinoin loaded lipid-based carriers – SLN, NLC, liposomes, ethosomes – for improvement of photostability, pharmacodynamic efficacy and skin delivery of this retinoid. *Ex vivo* experiments were performed using bioadhesive hydrogels of the above formulations. Herein, porcine skin (for skin permeation and skin retention analysis) and mouse tail model (for the evaluation of anti-psoriatic activity) were used. The obtained results showed that SLN and NLC provide higher skin transport, photostability and anti-psoriatic activity when compared to liposomes and ethosomes, and even to the marketed product.

Photoaging is referred as the responsible for damage of skin-barrier function. Accordingly, Hung *et al.* [158] examinated the effect of ultraviolet irradiation on the cutaneous penetration of NLC and PLGA polymer nanoparticles loaded with RA (*in vitro studies*). Broadly, UVA exposition increased the RA delivery from NLC and PLGA particles into hair follicles by 4.2- and 4.9-fold, respectively. The *in vivo* skin distribution of particles was also analysed using nude mouse skin.

Other studies were performed, focusing on development and optimization of potential carrier-based formulations for dermal drug delivery. For instance, Mortazavi et al. [159] proposed microemulsions for tretinoin encapsulation considering the acne treatment. The optimized microemulsions were composed of 15% olive oil, 12% propylene glycol (the co-surfactant), 33% Tween® 80 and 40% distilled water. *In vitro* release experiments revealed that tretinoin microemulsion provides an improved release profile when compared to the one obtained by the commercial gels and creams. Moreover, a zero-order kinetics was observed for tretinoin release profile. Bavarsad et al. [160] projected the development and optimization of deformable liposomes for topical delivery of tretinoin. For optimum liposome formulations, the presence of transcutol in the liposomes composition resulted in a higher tretinoin skin penetration when compared to the one obtained for tretinoin cream. Also, this strategy could decrease the side-effects related to conventional tretinoin administration (cream). Castleberry et al. [150] encapsulated all-trans RA by their covalently bonding to PVA using a hydrolytically degradable ester linkage. A complete all-trans RA release was achieved in ten days, considering

in vitro experiments. Moreover, an increase of drug dermal accumulation in explant pig skin was observed. In turn, *in vivo* tests demonstrated a reduction on the side-effects of free all-trans RA (local inflammation), in addition to retain this molecule at the application site at measurable quantities for up to six days.

Design and development of new retinoid-based encapsulation systems to treat cancer have been gathered some new studies. Narvekar et al. [161] evaluated the therapeutic effect of encapsulated all-trans RA against ovarian cancer. A polymer-oil nanostructured carrier with PLGA was used. This formulation was capable to extensively induce apoptosis and provide higher anti-tumorigenic effects for a long-term in the ovarian cancer cell subline SKOV-3_{PR}. Furthermore, Schultze et al. [151] reported, for the first time, the ability of tretinoin-loaded lipid-core nanocapsules (prepared by interfacial deposition of poly(ε-caprolactone)) to solve the huge resistance of human lung adenocarcinoma epithelial cell lines (A549) to the anticancer activity of free tretinoin. Accordingly, apoptosis and cell cycle arrest were induced. Akanda et al. [162] researched the anticancer efficiency of RA loaded SLN over prostate cancer cells. A reduction in viability of these cells was observed when RA concentration was increased in SLN (9.53% at 200 µg/mL). Sun [163] simultaneously encapsulated into a single emulsion all-trans RA and the chemotherapy agent doxorubicin. The final aim was to enable the co-delivery of these compounds and, therefore, provide an efficient strategy for destruction of malignant cells. This approach enhanced the suppression of tumour growth at the same time decreased the incidence of cancer stem cells, considering a synergistic manner. Following the same strategy of Akanda et al., Lei et al. [164] proposed the dual drug encapsulation (in this case, dacarbazine and tretinoin) into transethosomes and liposomes for the treatment of cutaneous melanoma. *In vivo* studies showed that transethosomes contribute for a higher dacarbazine concentration in the plasma. Also, transethosomes showed higher cytotoxic effect when compared to the other formulations. Kong et al. [165] constructed lipid-coated biodegradable hollow mesoporous silica nanoparticles for co-encapsulation of all-trans RA, doxorubicin and interleukin 2. This proposed formulation significantly decreased tumour growth and inhibited metastasis. Li et al. [166] was capable to significantly increase a cytotoxic effect when sorafenib/all-trans RA were both incorporated into SLN. Also, the combination of miRNA coupled with this formulation might be used in gastric cancer treatment. Liu et al. [167] prepared trimethyl chitosan-functionalized RA-loaded SLN to improve the effective treatment of glioblastoma. This carrier-based system increased cell death when compared with the free drug. O'Leary et al. [168] developed all-trans RA-loaded collagen-hyaluronate scaffolds capable to increase functional epithelialisation in primary tracheobronchial cells. Yamamoto et al. [169] prolonged RA in blood circulation when all-trans RA-loaded styrene maleic acid copolymer nanoparticles were injected via intravenous. Silva et al. [170] concluded about the importance of including tributyrin into all-trans RA loaded NLC, in order to increase the encapsulation efficiency. Also, tributyrin- all-trans RA loaded NLC exhibited higher inhibition of cell viability when compared to the free drug. At last, Zhang et al. [171] presented chitooligosaccharide as promising nanoparticles for co-delivery of all-trans-RA and paclitaxel.

Table 2.1 – The most recent RA controlled delivery systems developed for the treatment of several pathologies.

Pathology/Potential application	Administration method	Compound(s)	Carrier-based system/ Encapsulation technique	Main results	Reference
Acne	Topical application	Tretinoin and tetracycline	Nanoemulsions and NLC	It was not observed a significant difference in tretinoin skin delivery with the incorporation of tetracycline (*in vitro* studies). The usage of nanoemulsions and NLC improved the antibacterial activity against *Staphylococcus aureus*.	[155]
	Topical application	Tretinoin and lauric acid	SLN	Tretinoin stability was achieved with SNL composed by stearylamine. SLN loaded with tretinoin and lauric acid revealed growth inhibitory activity against *Staphylococcus epidermidis*, *Propionibacterium acnes* and *S. aureus*.	[156]
	Topical application	Benzoyl peroxide and tretinoin	Niosomes	A higher amount of tretinoin and benzoyl peroxide were retained in the skin layers when niosomal gel is used (*in vitro* experiments). Niosomal gel showed to be more effective than antiacne cream (*in vivo* studies): a 4.16-fold lower dose of benzoyl peroxide in niosomal gels provided a similar therapeutic index when compared to the antiacne cream.	[137]
	Topical application	Tretinoin	Microemulsions	Tretinoin microemulsion provides an improved release profile when compared to the one obtained by commercial gels and creams (*in vitro* experiments). A zero order kinetics was observed for tretinoin release profile.	[159]
Psoriasis	Topical application	Tretinoin	Liposomes, ethosomes, SLN and NLC	SLN and NLC increased the skin transport, photostability, and anti-psoriatic activity when compared to liposomes, ethosomes and marketed product (*ex vivo* studies).	[157]
Photoaging	Topical application	RA	NLC and PLGA nanoparticles	The UVA exposition promoted RA delivery from NLC and PLGA particles into hair follicles by 4.2- and 4.9-fold, respectively (*in vitro* experiments).	[158]
General skin disorders	Topical application	Tretinoin	Optimized deformable liposomes	Optimum liposomes composed by transcutol increase tretinoin skin penetration when compared to the one obtained for tretinoin cream. This formulation could decrease the side-effects related to conventional tretinoin administration (cream).	[160]

(to be continued)

Table 2.1 – The most recent RA controlled delivery systems developed for the treatment of several pathologies (continuation).

Pathology/Potential application	Administration method	Compound(s)	Carrier-based system/ Encapsulation technique	Main results	Reference
General skin disorders	Topical application	All-trans RA	PVA	A complete release of all-trans RA was achieved in ten days, as well as an increase of tretinoin dermal accumulation in explant pig skin (*in vitro* studies). *In vivo* experiments showed a reduction on the side-effects related to free all-trans RA and the retention of this compound at measurable quantities for up to six days.	[150]
Ovarian cancer	-	All-trans RA	Polymer-oil nanostructured carrier (oil and PLGA)	The formulation proposed is capable to induce apoptotic cell death, as well as to provide higher anti-tumorigenic effects for a long-term in the target cells.	[161]
Lung cancer	-	Tretinoin	Poly(ε-caprolactone)	Tretinoin-loaded lipid-core nanocapsules were capable to deal with the high resistance of human lung adenocarcinoma epithelial cell lines and trigger their apoptosis and cell cycle arrest.	[151]
Prostate cancer	-	RA	SLN	A reduction in cell viability of prostate cancer cells was observed when RA concentration was increased in SLN (9.53% at 200 μg/mL).	[162]
Cancer stem cells	-	All-trans-RA and doxorubicin	Emulsions	Co-delivery of all-trans-RA and doxorubicin might enhance the suppression of tumor growth while reduce the incidence of cancer stem cells.	[163]
Cutaneous melanoma	Topical application	Dacarbazine and tretinoin	Transethosomes and liposomes	Transethosomes contribute for a higher dacarbazine concentration in the plasma (*in vivo* studies). Moreover, this formulation showed higher cytotoxic effect when compared to the other one.	[164]
Gastric cancer	-	Sorafenib and all-trans RA	SLN	Sorafenib/all-trans RA-loaded SLN significantly increase a cytotoxic effect when compared to an individual drug.	[166]
Cancer treatment	-	All-trans RA, doxorubicin and interleukin 2	Lipid-coated biodegradable hollow mesoporous silica nanoparticles	All-trans RA/doxorubicin/interleukin-2 co-loaded dHMLB significantly decreased tumour growth and inhibited metastasis.	[165]

(to be continued)

Table 2.1 – The most recent RA controlled delivery systems developed for the treatment of several pathologies (continuation).

Pathology/Potential application	Administration method	Compound(s)	Carrier-based system/ Encapsulation technique	Main results	Reference
Glioblastoma	-	RA	Chitosan and SLN	Trimethyl chitosan-functionalized RA- loaded SLN increased cell death when compared with the free drug.	[167]
Respiratory tissue regeneration	-	All-trans RA	Collagen-hyaluronate scaffolds	All-trans RA-loaded collagen-hyaluronate scaffolds were capable to increase functional epithelialisation in primary tracheobronchial cells.	[168]
-	Intravenous administration	All-trans RA	Styrene maleic acid copolymer	It was observed RA prolonged blood circulation after intravenous injection of all-trans RA-loaded styrene maleic acid copolymer nanoparticles.	[169]
Cancer treatment	Intravenous administration	All-trans RA and tributyrin	NLC	All-trans RA-tributyrin-loaded NLC was more efficient on inhibition of cell viability comparing to the free drug.	[170]
-	-	All-trans RA and paclitaxel	Chitooligosaccharide	Nanoparticles of chitooligosaccharide could be efficiently taken up by HepG2 cells and transported into the nucleus for all-trans RA and paclitaxel delivery.	[171]

2.5. Concluding remarks

The requirement of retinoids in health care forced the creation of strategies to maximize retinoids efficiency. In fact, current administration of retinoids is a challenge not only because the insufficient retinoid concentration which reaches the target cells/tissues (responsible for the brief remission observed in APL patients), but also by the several side-effects reported. Encapsulation technology seems to provide the protection and stability required for retinoids. Moreover, this strategy might beneficiate these compounds in controlled release studies. Accordingly, it is expected to increase the bioavailabity of retinoids in the human body and thus increase retinoids efficiency. The ongoing investigation on encapsulation of retinoids counts with numerous studies which propose properly carrier-based formulations for retinoids application in the pharmaceutical and medical fields. However, the total number of retinoid-controlled delivery systems in clinical trials is still limited, whereby it is important to insist in this investigation topic.

Chapter 3 - Methodologies for simulation of gastrointestinal digestion of different controlled delivery systems and further uptake of encapsulated bioactive compounds

---

The third chapter starts with the presentation of several innovative food products with interest to the consumers. The main carrier-based systems and the encapsulating methods applied to nutraceuticals are further presented. In the last section, an overview about the main simulated gastrointestinal digestion and uptake models are addressed, as well as studies therein performed with delivery systems are discussed.

This chapter is published in:

Gonçalves, A; Estevinho, B N; Rocha, F. Methodologies for simulation of gastrointestinal digestion of different controlled delivery systems and further uptake of encapsulated bioactive compounds. Trends in Food Science & Technology. 2021, 114, 510-520, https://doi.org/10.1016/j.tifs.2021.06.007.

3.1. Introduction

Consumers are increasingly aware of the importance to practice a balanced diet, taking advantage of the intake of different nutrients for health benefit [172]. A diet rich in plant foods (such as fruits and vegetables) stimulates a proper functioning of the human body due to the presence of vitamins, phenolic compounds, phytochemicals (all these compounds with antioxidant properties) and minerals. They are of major importance to prevent/reduce the risk to develop chronic (*i.e.* cancer, cardiovascular diseases and diabetes, among others) and neurodegenerative (*i.e.* Alzheimer) diseases. Furthermore, these compounds act on the immune system boost [113,144,173]. Dietary supplements can be used as a food complement capable to provide specific dietary ingredients (*i.e.* vitamins, minerals, polyunsaturated fatty acids (omega-3), amino acids and herbs or other botanicals [6]) under capsule, pill, tablet or liquid forms.

The increasing demand for novel and high-quality products to assist and improve human health and wellness (beyond basic nutrition) brought some challenges related to their production, sustainability, safety and preservation [174]. Current approaches involve the integration of bioactive compounds (recognized as safe (GRAS) food ingredients, such as carbohydrates, proteins, fats, vitamins and/or probiotics) into food products with the development of functional foods. Some examples of these fortified food products available in the market include yogurts capable to improve digestive health, cereals that benefit cardiac health, margarines/butters that interfere with cholesterol metabolism and energy/protein bars and drinks addressed to reduce hunger [175]. Due to the ability of food-grade bioactive compounds and derived-based food products to act on prevention and/or treatment of several disorders, these nutraceuticals have been explored for improvement of life quality and expectancy. Another class of food products includes the excipient foods, that contain ingredients that are not themselves a bioactive compound but that can improve the efficacy of a food-grade bioactive compounds ingested with these ingredients [176].

The direct incorporation of certain bioactive compounds into food products for oral ingestion is a current challenge due to their highly lipophilic nature and poor chemical stability, as well as the low and/or variable bioavailability [101]. The design and development of effective carrier-based delivery systems might improve the dispersion of bioactive compounds, protect and beneficiate lipophilic molecules in their controlled release and absorption at desired locations within the gastrointestinal tract. The final aim is to increase the bioavailability and improve the efficacy of nutraceuticals in the human body.

During the digestion process, the fraction of bioactive compounds released from food matrix in the gastrointestinal tract and that becomes available for absorption (including intestinal epithelium absorption and presystemic metabolism (intestinal and hepatic)) defines the bioaccessibility. This concept is therefore influenced and determined by the initial concentration of the bioactive compound in the ingested products, the composition of ingested products, the physicochemical characteristics of gastrointestinal fluids and the presence of enzymes [177]. These last conditions may have impact over the most sensitive bioactive compounds, promoting their degradation before they are absorbed. For example, vitamins are known to be chemical unstable and might be easily degraded during digestion due to temperature, moisture, pH and enzymes [174]. Moreover,

they might exhibit low gastrointestinal absorption [17]. Vitamins can also be damaged during processing and storage [35]. Bioaccessibility can be evaluated by simulating gastric and small intestinal digestion (*in vitro* methodologies) and further Caco-2 cells uptake [178].

The exposition of a bioactive compound to the human body triggers a specific effect, which is termed bioactivity. This includes the entrance of bioactive compounds into systemic circulation, tissue uptake and subsequent physiological response. Bioactivity can be determined considering *in vitro*, *ex vivo* and *in vivo* methodologies [179].

Bioavailability is still an unclear term. Broadly, it describes the portion of a bioactive compound from ingested product that is absorbed, reaches the systemic circulation and becomes useful. Hence, bioavailability of a bioactive compound is determined by bioaccessibility and bioactivity [180]. This parameter is usually evaluated thought *in vivo* methods, considering the fraction of bioactive compounds that is digested, absorbed, metabolized and reaches systemic circulation. In fact, the term bioavailability frequently does not include the bioactivity of bioactive compound as a strategy to become the analyses easier [179]. Herein, it is revealed by *in vivo* plasma concentration in animals/ humans after the bioactive compound administration as an isolated compound or as a compound-containing food [177].

This review aims to provide an overall discussion about the carrier-based systems for the controlled delivery of nutraceuticals, as well as the main encapsulation techniques employed in their formation. Furthermore, the most used simulated models for gastrointestinal digestion and uptake are approached. Studies reporting the behaviour of the encapsulated products under the selected simulation models are also presented.

3.2. Delivery systems for encapsulation of nutraceuticals

Nano- and microencapsulation have been increasingly explored for fabrication of controlled delivery systems with application in the food sector [101]. Coating or entrapping of nutraceuticals within a continuous film aims to protect these compounds against the outside surrounding undesirable conditions (*i.e.* light, moisture, heat, pH, oxygen and shear, among others), preventing the loss of the most sensitive molecules during the processing or storage of food products. Moreover, this strategy has been demonstrated to be suitable for the release and controlled delivery of bioactive compounds, improving the stability and optimizing the absorption of nutraceuticals during digestion in the gastrointestinal tract [35,181]. Accordingly, the development of an appropriate delivery system designed for oral ingestion might increase the amount of bioactive compounds capable to reach the target cells/tissues in the desired concentrations to improve their effectivity in the human body.

The most promising and widely used carrier-based systems and encapsulating methods in food sector are presented and discussed in the following topics (Figure 3.1).

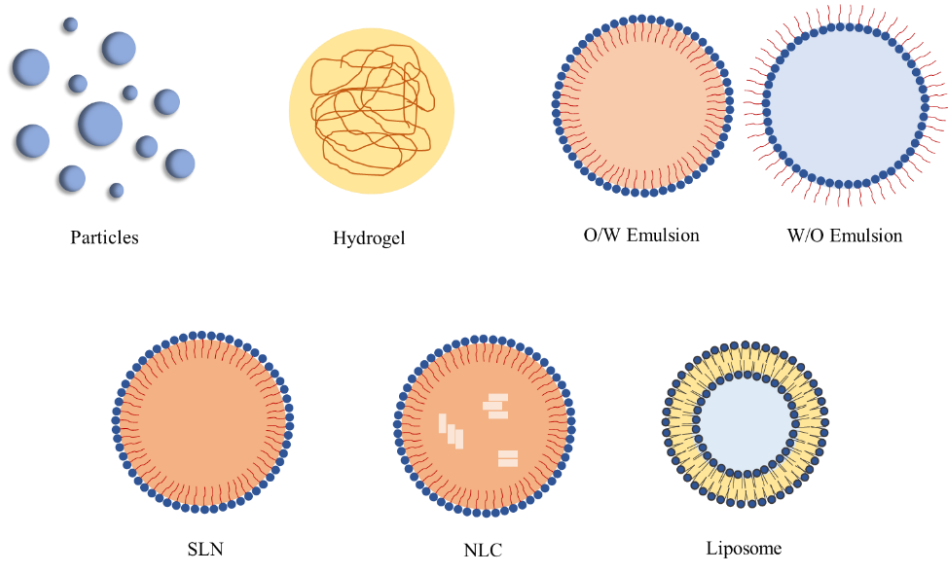


Figure 3.1 – Delivery systems designed for encapsulation of bioactive compounds in food sector (adapted from [101,174]).

3.2.1. Carrier-based systems

3.2.1.1. Particles and capsules

The production of particles and capsules as carrier-based systems for the delivery of bioactive compounds have been widely described in the literature. Several encapsulating methods are used to produce these small vesicular structures, namely spray-drying and coacervation (sections 3.2.2.1. and 3.2.2.3.). Also, various polymers can be considered to create a membrane surrounding the bioactive compound, coating (capsules) or entrapping (particles) the target bioactive compound, providing an effective protection against few desirable conditions in the outside surrounding environment [144]. These structures can be generated at a nano and micro scale. Particularly, spray-drying technology enables to obtain particles with an intern matrix morphology and in a range between 1 µm and 5 mm [182].

3.2.1.2. Hydrogels

Hydrogels consist of a three-dimensional network obtained by gelation methods, wherein hydrophilic polymer chains are crosslinked considering covalent or non-covalent interactions [174,183].

The number, strength, morphology of the structural units and the presence of hydroxyl, carboxyl, ethers, amines and sulphate groups, among others, determine the hydrogel characteristics. Those refer to water-holding capacity, appearance, texture and reaction to specific changes [174]. In fact, hydrogels are considered relevant carrier-based delivery systems due to their ability to react to chemical (*e.g.* ionic strength, pH and solvent composition) and physical (*e.g.* temperature, light and pressure, among others) stimuli, occurring their swelling or shrinking [184,185].

3.2.1.3. Emulsions

Oil-in-water (o/w), water-in-oil (w/o), oil-in-water-in-oil (o/w/o), water-in-oil-in-water (w/o/w), water-in-oil-in-oil (w/o/o) and water-in-oil-in-oil-in-water (w/o/o/w) can be produced, considering the relative spatial organization of water and oil phases. Nanoemulsions (10 - 100 nm, the reason why they appear as transparent) and conventional emulsions (0.1 - 100 μm) can be prepared, influenced by the system composition, operating conditions in the homogenizer and the homogenization method [186,187]. An increasing structure stability is observed from conventional emulsions to nanoemulsions and for microemulsions [101].

3.2.1.4. Solid lipid nanoparticles (SLN)

SLN are composed by liquid lipids, water and surfactants (similarly to the composition of nanoemulsions). However, liquid lipids are partly or fully solidified in the SLN, which is achieved due to an emulsion controlled crystallization process. This lipid-based delivery system does not require the usage of organic solvents and the scale-up is ease. However, it is reported low bioactive compound loading capacity, loss of bioactive compounds during storage and high water content in SLN emulsions [188].

3.2.1.5. Nanostructured lipid carriers (NLC)

NLC are an unstructured solid lipid matrix consisting of liquid and solid lipids and an aqueous phase with surfactants and co-surfactants. A solid matrix with high imperfections is created from the lipidic phase and, therefore, an increased amount of bioactive compounds can be herein encapsulated. Three different types of NLC can be produced, namely imperfect, amorphous and multiple. It was established according to the degree of order of the matrix. NLC arose as an alternative to reduce the limitations reported with SLN (section 3.2.1.4.) [189].

3.2.1.6. Liposomes

Liposomes are spherical vesicles wherein bilayer of lipids are concentric around an aqueous core. The phospholipids present in the composition of these structures promote the thermodynamical formation of liposomes, while sterols (such as cholesterol) may be integrated for the stabilization of the bilayer of liposomes [131]. These carrier-based systems are capable to provide the control release of a bioactive compound at a desirable rate, location and times [190].

3.2.2. Encapsulating methods used in food sector

The most used encapsulating methods for food applications are spray-drying and freeze-drying, coacervation, fluidized bed coating, emulsification, liposome entrapment and inclusion complexation [182,191].

3.2.2.1. Spray-drying

Spray-drying technology is based on the atomization of a liquid (a homogenized system – a solution, suspension or emulsion – containing the bioactive compound(s) to be encapsulated and the encapsulating agent(s)) occurring the formation of a droplet/air contact. The powder formed after water evaporation is separated by a cyclone and recovered [192]. Different parameters influence the process efficiency and characteristics of the final product obtained. Those include the homogenization, stability, viscosity and temperature of fed solutions, as well as the operating conditions implemented during spray-drying process. Particles with variable sizes, density, water content, fluidity and tendency to agglomerate [35]. It is a one-step method capable to incorporate bioactive compounds into good quality particles at low production cost and easy scale-up. Moreover, it is a rapid, continuous and reproducible process [193]. However, it is reported the limiting number of encapsulating agents (they must be soluble in water at an acceptable level) [35] and the usage of relatively high inlet and outlet air temperatures which might be a limitation for the most heat sensitive bioactive compounds [15].

3.2.2.2. Freeze-drying

Freeze-drying or lyophilization is an appropriate method for the encapsulation of the most volatile and heat sensitive compounds [194], which arises as an advantage regarding spray-drying. The mixture composed by the encapsulating agent(s) and the bioactive compound(s) is subjected to freeze and further sublimation. Afterwards, it is carried out the desorption and storage of the dry powder [195]. Freeze-drying enables the samples preservation for a long time. However, the dehydration process is taken for a long period (around 20 h), whereby it is not applied frequently. Moreover, it is reported as an expensive technique [174].

3.2.2.3. Coacervation

Coacervation involves electrostatic interactions capable to promote the separation of the liquid phase from one (simple coacervation) or many (complex coacervation) encapsulating agents, with the formation of a complex composed by two distinct phases. In the phase rich with the encapsulating agent, the liquid drops deposit and harden around the bioactive compound, forming the coacervate. Self-sustaining particles are obtained after this process. Encapsulation by coacervation is a high efficient process, although it is associated with a high cost [196].

3.2.2.4. Fluidized bed coating

In the fluidized bed coating the particles to be encapsulated are suspended by an air stream at a selected temperature, followed by its spraying with an atomized coating material. The main advantages about this method include its good reproducibility, the ability to control of particle size distribution, low energy consumption and low cost. However, fluidized bed coating is not recommended for heat sensitive bioactive compounds due to the direct exposition to hot air during several cycles [197].

3.2.2.5. Emulsification

Emulsification has been carried out to produce emulsions, nanoemulsions and microemulsions (section 3.2.1.3.). In this process, two or more immiscible fluids are mixed, with the dispersion of one liquid (the dispersed phase and wherein the bioactive compound is included) as small droplets within the other liquid (the dispersant phase) [113]. The usage of an appropriate mixture of surfactants and co-surfactants aims to promote the formation and stabilization of emulsion droplets. They act adsorbing to the droplet surfaces with subsequent formation of a thin protective layer around them [173]. According to the emulsion-based delivery systems that are produced, different methods are described. Conventional emulsions are formed by a homogenizer (*e.g.* high shear mixer, high pressure homogenizer, membrane homogenizer, sonicator and colloid mill). In turn, the production of nanoemulsions involve high-energy and low-energy methods. The first one uses mechanical devices to generate intense disruptive forces capable to create tiny oil droplets (*e.g.* high-pressure valve homogenizers, microfluidizers and ultrasonification), while in the second one occurs the spontaneous droplets formation due to the change of the solution or environmental conditions (*e.g.* phase inversion and solvent demixing methods) [112,187].

3.2.2.6. Liposome entrapment

Considering the structure of a liposome (section 3.2.1.6.), the entrapment of bioactive compounds with hydrophilic and lipophilic is enabled. Several methods are described for the liposomes production, including Bangham method, ethanol/ether injection, sonication and reverse phase evaporation [101]. Different characteristics of liposomes are observed according to the production method implemented (*e.g.* size, lamellarity and encapsulation efficiency) [131].

3.2.2.7. Inclusion complexation

Cyclodextrins (α-, β-, and γ-) are widely used for encapsulation by inclusion complexation [198]. Their external part is hydrophilic, while their internal part is hydrophobic and, therefore, appropriate to incorporate slightly polar compounds.

3.3. Behaviour of carrier-based systems under simulated gastrointestinal conditions

Within the human gastrointestinal tract, the ingested food products are submitted to several physicochemical and physiological processes, in a continuous and dynamic approach, until the release of the nutrients and bioactive compounds to be absorbed by the body. The knowledge about the main physical and chemical changes that occur in the different compartments of human body digestive system (*i.e.* mouth, stomach, small intestine and large intestine) is of great importance for the development of effective delivery systems in the control of digestion and, consequently, in the release and absorption of bioactive compounds at target locations of human gastrointestinal tract [199].

The ingested products are exposed in the mouth to mastication and salivation, occurring the reduction of solid, semi-solid food products to small particles with the formation of food bolus [200]. Accordingly, the food products deal with dilution and the human body temperature. Saliva has neutral pH and is composed by water (99.5%), proteins/enzymes (0.3%, including enzymes capable to hydrolyse carbohydrates – *i.e.* amylase) and electrolytes (such as potassium, calcium, magnesium, sodium, phosphate and bicarbonate) [201], which contribute for a low ionic strength. In the stomach, the food products deal with gastric motility as well as acidic pH, high ionic strength, dilution and enzymes (gastric lipase and protease which degrade lipids and proteins, respectively) due to the composition of the gastric fluid. Afterwards in the small intestine, the partially digested food products are subjected to intestinal peristalsis, miceralization with bile salts, neutral pH, high ionic strength and dilution. Moreover, proteins, starch and lipids are hydrolysed by protease, amylase and pancreatic lipase, respectively. In this compartment, the released bioactive compounds are mainly absorbed in the duodenum. The non-absorbed compounds move towards the large intestine, wherein they are exposed to intestinal peristalsis, neutral to slightly acidic pH and high ionic strength. Herein, microbiota acts in a fermentation process of polysaccharides and proteins [174,199].

In the line with the topics above, controlled delivery systems are subject to six key processes during digestion in the human gastrointestinal tract [199]. The pH changes of the aqueous phase promote changes in the electrical charge of surfactants, proteins and polysaccharides that constitute the carrier-based systems. Consequently, their composition, structure and interactions are modified [199]. The variation in the type and concentration of ions, due to the location of human gastrointestinal tract and/or the nature of the products consumed, may influence the electrostatic interactions in the carrier-based systems through electrostatic screening or binding effects [199]. The presence of endogenous (*e.g.* proteins), exogenous (*e.g.* surfactants) and internally generated (*e.g.* lipid digestion products) surface-active components might lead to alterations in the interfacial composition and properties of carrier-based systems [199]. The presence and activity of several enzymes in the human gastrointestinal tract may digest the components of carrier-based systems [199]. Changes in the physical state, molecular conformation or interactions of specific components can be observed in the carrier-based systems due to temperature changes along digestion, which impact their digestibility [199]. At last, the flow/force profile to which the carrier-based systems are exposed may trigger the breaking down of their structure [199].

The behaviour of bioactive compound-loaded delivery systems under gastrointestinal conditions has been assessed considering an *in vitro* approach. Herein, static and dynamic digestion models are used to provide a deeper insight regarding intestinal absorption availability. Further determination of intestinal absorption and presystemic metabolism is performed considering cell culture studies. Eventually, the incorporation of gut microflora to measure intestinal bioaccessibility might be investigated. *In vivo* methodologies are also considered to evaluate the bioaccessibility and bioavailability of bioactive compounds [179]. An overview about these simulated methods is presented in the Table 3.1. These topics are critically reviewed in the following sections. Moreover, some studies in this research field with the digestion of carrier-based delivery systems and the intestinal absorption of released bioactive compounds are also presented.

Table 3.1 – Overview of methodologies used to determine bioaccessibility and bioavailability of bioactive compounds.

Analysis under study	Methodologies
Intestinal absorption availability	*In vitro*: gastrointestinal static digestion models and gastrointestinal dynamic digestion models
Intestinal absorption and presystemic metabolism	*In situ*: intestinal perfusion in animals *Ex vivo*: gastrointestinal organs *In vitro*: cell culture (mainly Caco-2 cells)
Intestinal absorption availability with incorporation gut microflora	*In vitro*: microbial fermentation models
Bioactive compound content in the blood plasma	*In vivo*: rodents, rabbits, pigs and calves

3.3.1. *In vitro* digestion models

Numerous *in vitro* models have been proposed to mimic the physiological processes carried out during gastrointestinal digestion (*i.e.* duration of each digestion step, pH and enzymes, among others), ranging from single static systems to multi-compartmental dynamic systems [177,202]. They are intended to be simple, flexible, inexpensive and reproducible in assessing the bioaccessibility of target bioactive compounds [174,177]. On the other hand, this strategy enables to reduce the ethic, economic and technique constrains related to the *in vivo* studies [199].

The current number of total publications related to "*in vitro* digestion models" reaches 466 and, among these, 279 are related simultaneously to "*in vitro* digestion models" and "foods". Considering this last number, a great contribution was made on this topic in the last five years (from 2017 to 2021) with a total number of 138 publications (source: www.scopus.pt, 8th February 2021).

3.3.1.1. Static models

Most of *in vitro* digestion studies (almost 90%) have been performed using static models [202]. They are single static systems capable to simulate gastric and/or intestinal phases, whereby mono- or multi-compartmental (a succession of stirred vessels is herein used) protocols are considered. A single set of initial biochemical conditions (*i.e.* temperature, pH, concentration of enzymes and bile salts) is stablished to replicate these compartments of gastrointestinal tract and that remain constant during the process [201,203]. Stomach is reproduced by the pepsin hydrolysis of homogenized food at a certain pH (1-2), temperature (37 °C) and period of time (1-3 h). In turn, intestine is simulated by the usage of pancreatic enzymes (with or without bile) at the desired pH (6-7) [177].

Several studies have described the usage of *in vitro* static digestion models to evaluate the behaviour of different delivery systems under the different simulated gastrointestinal conditions. Some of the most recent are compiled in Table 3.2. Guo et al. [204] used a simulated gastrointestinal digestion model composed by gastric and

intestinal phases to investigate the curcumin release from ternary complexes composed by high methoxyl pectin, surfactants (rhamnolipid, tea saponin or ethyl lauroyl arginate hydrochloride) and pea protein isolate. The slowest release of curcumin in the simulated gastrointestinal tract was achieved by the ternary complex which included rhamnolipid. Moreover, this formulation enabled to ensure the functional attribute of curcumin was barely affected in the digestion process. This *in vitro* digestion study was conclusive to propose a more suitable carrier-based delivery system for encapsulation of curcumin with application in commercial food products. In turn, Araiza-Calahorra and Sarkar [205] used a static *in vitro* gastric digestion to validate their proposal on coating Pickering emulsions (prepared using whey protein nanogel particles and emulsions) with a dextran sulphate layer to reduce the destabilization of these emulsions under gastric conditions. The obtained results confirm the production of stable emulsions in gastric medium, which arise as a promising strategy for the delivery in the intestine of encapsulated lipophilic compounds. Furthermore, Peanparkdee et al. [206] used a static simulation model with oral, gastric and intestinal phases to study the stability of capsules produced with two types of gelatin (acid-processed (type A) and alkaline-processed (type B) gelatin) for incorporation of Thai Riceberry bran extract. It was concluded that the stability of this bioactive compound during *in vitro* digestion is influenced by net surface charge and particle size of gelatin. Other studies performed differ from those reported by the implementation of a general standardized *in vitro* digestion protocol proposed by COST INFOGEST network. In fact, despite of the simplicity, lower cost, high-throughput of *in vitro* static models, as well as their ability to analyse multiple samples [174,199], one of the major challenges regarding this methodology are the considerable variations in the digestion parameters that are observed among different models and that prevent the comparison of results across research-groups. Those include the amount of product sample, pH, the amount and type of enzymes, the amount of bile salts, stirring speed and the duration of each stage of digestion, among others [201,207]. Accordingly, the most recent studies usually consider the usage of an uniformized protocol [208]. For example, Beltrán et al. [209] produced high oleic palm oil loaded nanoliposomes by microfluidization and ultrasound and evaluated how the selected production methods could affect the physical stability and intestinal digestibility of these structures. Herein, the standardized protocol published by the COST INFOGEST network was implemented. During oral phase digestion no statistically significant changes in the nanoliposomes stability were observed. However, gastric phase promoted the destabilization of both types of nanoliposomes, while in the intestinal phase the triglycerides that compose the nanoliposomes were degraded due to enzymatic activity. Moreover, Visentini et al. [210] studied the physicochemical and structural modifications of two ovalbumin nanoparticles loaded with conjugated linoleic acid under gastric and intestinal phases, considering the standard *in vitro* static gastrointestinal digestion model developed by the COST INFOGEST network. The obtained results revealed the high retention of conjugated linoleic acid during gastrointestinal simulation. Afonso et al. [211] used the standardized *in vitro* digestion protocol to study the resistance of β-carotene-loaded nanoparticles, individually composed by zein and ethylcellulose, upon gastrointestinal conditions. Both carrier-based delivery systems revealed to be strongly insoluble in the digestion medium, whereby the enzymes and salts therein present could not degrade the

nanoparticles. Consequently, β-carotene release was avoided even in the gastric phase. The highest bioaccessibility of encapsulated β-carotene in the intestinal phase was obtained in zein nanoparticles (37±1%). In turn, Ferrado et al. [212] used the INFOGEST procedure (gastric and intestinal phases) to analyse the potentialities of bovine serum albumin particles loaded with chrysin to be used as supplements to be introduced in functional foods. A high amount of encapsulated chrysin maintains inside the particles during *in vitro* static gastrointestinal digestion, occurring the release of around 14% of this bioactive compound. At last, Zhou et al. [213] used the standardized *in vitro* digestion protocol to evaluate the impact of chitin nanocrystals in the digestion of corn oil-in-water emulsions (stabilized with tween 80) and subsequent bioaccessibility of β-carotene encapsulated into this lipid-based delivery system. The obtained results showed that nanochitin reduces the β-carotene bioaccessibility by reducing lipid digestion. Moreover, the authors compared these results to the one obtained using a regular static *in vitro* digestion model (non-INFOGEST) and some differences were found. Although the same conclusions had been drawn, it was identified, for example, a lower percentage of total free fatty acids released and of carotenoid bioaccessibility (from 68.9 to 99.6 % and from 22.7 to 55.2%, respectively) when the non-INFOGEST method was applied. In fact, one of the main differences between both models are related to the enzymes activity, calcium contractions and bile salt (the first two factors were considered the most relevant for the differences registered). However, the authors reported in their experiments a disadvantage about INFOGEST model, namely the need to carry out a back-titration after the small intestine phase in order to detect all the free fatty acids released.

Although static digestion models have been widely used to investigate the digestion of several food products (they are designed and developed according to their intended purpose), they are oversimplified and do not provide an accurate simulation of the most complex conditions and processes of gastrointestinal tract [174]. In fact, biochemical environment is continually changing in the human body and this behaviour cannot be mimicked using static model, as previously described. Moreover, large volumes of media are used and the implemented continuous stirring does not represent the complexity of peristaltic movements. Also, this methodology does not consider gastric emptying [202]. *In vitro* dynamic digestion models were therefore developed to overcome the limitations related to static models.

3.3.1.2. Dynamic models

In vitro dynamic models emerged in the last decades as an innovative strategy capable to provide an improved and more sophisticated digestion simulation method. They may range from single to multi-compartmental systems and incorporate the dynamic aspects of the digestion process. Those include the shear, mixing, hydration or peristalsis phenomena carried out along the gastrointestinal tract [179]. The aim is the ability of dynamic models to simulate variations in the concentration of enzymes, viscosity, pH, particle size and nutrient partitioning, transport of digested products and continuous secretions of digestive fluids observed in the gastrointestinal tract of human body [179,201]. A better approximation regarding the mechanisms and processes

which occur during digestion and the structural changes of food products can be achieved with this methodology, as well as a more precise evaluation about the bioaccessibility of specific bioactive compounds.

Several *in vitro* dynamic digestion models (with different geometries, physical forces and biochemistry [214]) have been developed and presented in the last years. Dynamic gastric model (DGM), human gastric simulator (HGS), TNO's gastrointestinal model (TIM), gastric digestion simulator (GDS), *in vitro* mechanical gastric system (IMGS), simulator of the human intestinal microbial ecosystem (SHIME), dynamic rat stomach-duodenum system (DRSD) and dynamic human stomach-intestine system (DHIS) are referred as some of the most relevant dynamic models [201]. From those, other digestion simulation models have been developed and proposed [174]. For the best of our knowledge, the studies published so far related to the behaviour of controlled delivery systems of bioactive compounds in dynamic models have been only performed in DGM, HGS, TIM and SHIME. Hence, the main characteristics, advantages and disadvantages and the research studies carried out with these models using carrier-based delivery systems are discussed below.

3.3.1.2.1. DGM

The DGM was developed at the Institute of Food Research (Norwich, UK) and consists of a monocompartmental model designed to simulate the fundus (proximal stomach, the upper part) and antrum (distal stomach, the lower part). Accordingly, two connected compartments/areas were created within a latex vessel. In the one corresponding to the fundus (the main body), the partially digested product is submitted to slight force due to continuous peristaltic contractions from the cyclical pressurization of water jacket (at 37 °C) which involves the main body. Herein are also delivered gastric secretions (gastric acid and enzymes) by computer-controlled pumps, according to the changes registered in the pH and volume of fed product. In turn, in the area correspondent to the antrum, the digested product is subjected to higher shear and grinding forces from the upward and downward movement of the barrel, which promote a high mixing efficiency and ability to reduce the particle size. A valve in the DGM enables to simulate the stomach emptying (the residence time is calculated by a software and is dependent on the variables size, composition and caloric content of the meal), occurring the leaving of the smallest particles, while the bigger ones are refluxed to the top of the vessel to continue the digestion process [201,203,214,215].

DGM has been widely implemented for food investigation since it enables the usage of complex food matrices as the one used in *in vivo* studies. Accordingly, DGM has been applied to study the structural changes during the digestion, with particular interest to understand the impact about the matrix and processing in the hydrolysis rate and extent of nutrients [203]. Other advantage reported regarding DGM includes the possibility to stablish *in vivo* correlation. However, in this dynamic model it is not possible to observe the antral processing since the compartment is not transparent, the simulation of fluid dynamics and distribution of gastric contents might be influenced due to the vertically alignment of main body and antrum, fluctuations in pH can be evidenced and it is not feasible the satiety control [203,215].

Table 3.2 – Studies on the behaviour of different bioactive compound-loaded controlled delivery systems when submitted to various *in vitro* static digestion models (continuation).

Carrier-based system/Encapsulation technique	Bioactive compound	Methodology (Gastrointestinal conditions)			Reference
		Oral phase	Gastric phase	Intestinal phase	
Polysaccharide-surfactant-protein ternary complexes	Curcumin	-	**pH**: 2.0 **Temperature:** 37 °C **Secretion**: Simulated gastric fluid (3.2 mg·mL^{-1} pepsin) **Agitation:** - **Duration:** 1 h	**pH**: 7.4 **Temperature:** 37 °C **Secretion**: Simulated intestinal fluid (consisting of 2 mg·mL^{-1} pancreatin, 13.6 mg·mL^{-1} monopotassium phosphate and 12 mg·mL^{-1} bile salts) **Agitation:** - **Duration:** 2 h	[204]
Corn oil-in-water emulsions stabilized by tween 80	β-carotene	**pH**: - **Temperature:** 37 °C **Secretion**: Simulated salivary fluid (inorganic salts, calcium and 3 mg·mL^{-1} mucin) **Agitation:** - **Duration:** 2 min	**pH**: 3.0 (HCl) **Temperature:** 37 °C **Secretion**: 2000 U·mL^{-1} pepsin **Agitation:** Yes **Duration:** 2 h	**pH**: 7.0 (NaOH) **Temperature:** 37 °C **Secretion**: Simulated intestinal fluid (consisting of bile salt (10mM in final mixture), $CaCl_2$, trypsin and lipase (to ensure 100 U·mL^{-1} trypsin and 2000 U·mL^{-1} lipase) **Agitation:** - **Duration:** 2 h	[213]
Zein nanoparticles and ethylcellulose nanoparticles	β-carotene	**pH**: - **Temperature:** 37 °C **Secretion**: Simulated salivary fluid, 0.3 M $CaCl_2(H_2O)_2$ and water **Agitation:** Yes **Duration:** 2 min	**pH**: 3.0 (HCl) **Temperature:** 37 °C **Secretion**: Simulated gastric fluid, 2000 U·mL^{-1} pepsin, 0.3 M $CaCl_2(H_2O)_2$, 1 M HCL and water **Agitation:** Yes **Duration:** 2 h	**pH**: 7.0 **Temperature:** 37 °C **Secretion**: Simulated intestinal fluid (consisting of 60 mg·mL^{-1} bile salt and 100 U·mL^{-1} pancreatin), 0.3 M $CaCl_2(H_2O)_2$, 1 M HCL and water **Agitation:** Yes **Duration:** 2 h	[211]

(to be continued)

Table 3.2 – Studies on the behaviour of different bioactive compound-loaded controlled delivery systems when submitted to various *in vitro* static digestion models (continuation).

Carrier-based system/Encapsulation technique	Bioactive compound	Methodology (Gastrointestinal conditions)			Reference
		Oral phase	Gastric phase	Intestinal phase	
Bovine serum albumin particles	Chrysin	-	**pH:** 3.0 **Temperature:** 37 °C **Secretion**: Simulated gastric fluid (which includes 0.15 mM $CaCl_2$, 2000 $U \cdot mL^{-1}$ pepsin and 60 $U \cdot mL^{-1}$ gastric lipase) **Agitation:** Yes **Duration:** 2 h	**pH: 7**.0 **Temperature:** 37 °C **Secretion**: Simulated intestinal fluid (which includes 10 mM bile salts and 0.6 mM $CaCl_2$) and pancreatin (to ensure 100 $U \cdot mL^{-1}$ trypsin) **Agitation:** Yes **Duration:** 2 h	[212]
Biopolymer-coated Pickering emulsions	-	-	**pH**: 3.0 **Temperature:** 37 °C **Secretion**: Simulated gastric fluid (consisting of 0.257 $g \cdot L^{-1}$ KCl, 0.061 $g \cdot L^{-1}$ KH_2PO_4, 1.05 $g \cdot L^{-1}$ $NaHCO_3$, 1.38 $g \cdot L^{-1}$ NaCl, 0.0122 $g \cdot L^{-1}$ $MgCl_2(H_2O)_6$, 0.024 $g \cdot L^{-1}$ $(NH_4)_2CO_3$) and 2000 $U \cdot mL^{-1}$ pepsin **Agitation:** Yes **Duration:** 2 h	-	[205]

(to be continued)

Table 3.2 – Studies on the behaviour of different bioactive compound-loaded controlled delivery systems when submitted to various *in vitro* static digestion models (continuation).

Carrier-based system/Encapsulation technique	Bioactive compound	Methodology (Gastrointestinal conditions)			Reference
		Oral phase	Gastric phase	Intestinal phase	
Nanoliposomes	Oleic palm oil	**pH:** - **Temperature:** 37 °C **Secretion**: Simulated salivary fluid (without adding α-amylase) **Agitation:** Yes **Duration:** 2 min	**pH:** 3.0 (1 M HCl) **Temperature:** 37 °C **Secretion**: Simulated gastric fluid **Agitation :** Yes (100 rpm) **Duration :** 2 h	**pH:** 7.0 **Temperature:** 37 °C **Secretion**: Simulated intestinal fluid (consisting of electrolyte stock, bile extract (10mM in final mixture), pancreatin and pancreatic lipase (to ensure 100 $U \cdot mL^{-1}$ trypsin and 2000 $U \cdot mL^{-1}$ lipase) **Agitation:** Yes **Duration:** 2 h	[209]
Ovalbumin nanoparticles	Conjugated linoleic acid	-	**pH:** 3.0 (1 M HCl) **Temperature:** 37 °C **Secretion**: Simulated gastric fluid (consisting of 6.9 mM KCl, 0.9 mM KH_2PO_4, 25 mM, $NaHCO_3$, 47.2 mM NaCl, 0.1 mM $MgCl_2$ and 0.5 mM $(NH4)_2CO_3$), 0.15 mM $CaCl_2$ (to a final concentration of 0.075 mM CaCl2) and 2000 $U \cdot mL^{-1}$ pepsin **Agitation :** Yes (60 rpm) **Duration :** 2 h	**pH :** 7.0 **Temperature :** 37 °C **Secretion** : Simulated intestinal fluid (consisting of 6.8 mM KCl, 0.8 mM KH_2PO_4, 85 mM $NaHCO_3$, 38.4 mM NaCl, 0.33 mM $MgCl_2$), 0.3 mM CaCl2 (final concentration), 10 mM bile salts (final concentration) and pancreatin to ensure 100 $U \cdot mL^{-1}$ trypsin) **Agitation :** Yes (60 rpm) **Duration :** 2 h	[210]

(to be continued)

Table 3.2 – Studies on the behaviour of different bioactive compound-loaded controlled delivery systems when submitted to various *in vitro* static digestion models (continuation).

Carrier-based system/Encapsulation technique	Bioactive compound	Methodology (Gastrointestinal conditions)			Reference
		Oral phase	Gastric phase	Intestinal phase	
Gelatin capsules	Thai Riceberry bran extract	**pH:** 6.75 **Temperature: -** **Secretion**: Simulated salivary fluid (consisting of 2.38 $g \cdot L^{-1}$ Na_2HPO_4, 0.19 $g \cdot L^{-1}$ KH_2PO_4 and 8 $g \cdot L^{-1}$ NaCl) and α-amylase (200 U) **Agitation: -** **Duration: -**	**pH:** 1.2 (1 M HCl) **Temperature: -** **Secretion**: 0.31% pepsin (from porcine gastric mucosa: pepsin A, EC 3.4.23.1) and 0.03M NaCl **Agitation: -** **Duration: -**	**pH:** 6.0 (0.1 M $NaHCO_3$) **Temperature:** 37 °C **Secretion**: A mixture composed by 0.05 g of pancreatin and 0.3 g of bile extract porcine dissolved in 35 mL of NaHCO3 (0.1M). **Agitation: -** **Duration: -**	[206]

A few studies report the usage of DGM (and of the other dynamic models described in the following) to simulate *in vitro* digestion of controlled delivery systems. For example, Manson et al. [216] used DGM to investigate the impact of the polymer content of hydrophilic matrices (between 10 and 30% of hydroxypropyl methylcellulose) in the release of caffeine considering fasted and fed dissolution environments. The obtained results showed that in the fed state the caffeine release was highly influenced by the presence of a high fat meal. Herein, a delay before initial drug release. Moreover, for the highest hydroxypropyl methylcellulose content used (30% (w/w)) similar release rates were observed under fasted and fed conditions, while for the lowest content of this polymer (10% (w/w)) a faster release was achieved in the fasted state. In this study the erosion mechanisms appeared to dominate drug release in the DGM due to the cylindrical forces exerted during simulated antral cycling. The results obtained using DGM were compared to the performed using compendial USP I and USP II dissolution tests. The last ones enabled to clearly distinguish between the formulations composed by polymer content. In turn, DGM test under fasted conditions enabled to group release profiles into three groups, in addition to not be able to distinguish between some different formulations.

3.3.1.2.2. HGS

HGS was designed and developed with the aim to replicate the peristaltic activity of antrum contraction waves and, therefore, to provide an improved simulation regarding the mechanical shear and grinding forces capable to generate the disintegration of ingested products and promote the mixing of gastric components [217]. In fact, HGS can simulate the peristaltic movements with a comparable amplitude and frequency to the one registered in *in vivo* gastric phase.

Similarly to DGM, HGS is also a monocompartmental model. It consists of (i) a cylindrical latex chamber in an inverted conical shape with a volume of 5.7 L corresponding to the gastric compartment, (ii) a mechanical driving system responsible by the reproduction of antral contraction wave action; herein, a set of rollers secured on belts pushes the chamber walls driven by motor, (iii) peristaltic pumps to control the delivery rate of the simulated gastric juice into the gastric chamber (2.5 $mg \cdot mL^{-1}$) as well as the simulating stomach emptying (3 $mg \cdot mL^{-1}$; the bottom of the gastric compartment contain a thin polyester mesh bag with pore size of around 1.5 mm to simulate the sieving) and (iv) temperature control systems (at 37 °C) based on two light bulbs and a mini-fan [201,203,217].

Some limitations regarding the HGS model are related to secretion and emptying rates of gastric fluid and the time of residence do not consider the properties of food products. Moreover, the digestion cannot be observed (such as in the DGM) [203].

3.3.1.2.3. TIM

TIM was developed at TNO Nutrition and Food Research (Zeist, The Netherlands). TIM-1 encompasses four compartments simulating the stomach, duodenum, jejunum and ileum [203]. Temperature control of each compartment is operated by the pumping water (at 37 °C) into the space between the inner and outer walls of

glass jackets, which compose these compartments. Flexibility of inner wall enables to replicate peristaltic movements due to its consecutive compression and expansion. The connection between the compartments of TIM is carried out by peristaltic valve pumps, which enable the chyme to move among them. pH of each compartment is computer-monitored and controlled by the usage of pH electrodes. In turn, gastric and duodenal secretions are controlled by specific pumps. Membranes with a molecular weight cut off of around 10 kDa are connected to jejunum and ileum compartments for removal of water-soluble compounds and further bioaccessibility determination [201,203].

In the line with this overall description, due to ability of TIM to include key parameters of human digestion, this *in vitro* dynamic model is reported to provide a full recreation of gastrointestinal tract. Hence, TIM has been used to study the digestion of food products [201].

Lu et al. [218] compared the bioaccessibility of curcumin with and without a controlled delivery system – Pickering emulsions stabilized by milled starch particles - under *in vitro* digestion using TIM-1 model and *in vitro* pH-stat lipolysis model (the latter has not been described or discussed in this review). Broadly, integration of curcumin into milled starch particles resulted in a higher bioaccessibility of this bioactive compound. The TIM-1 model was described to enable a good analysis about the digestion of milled starch particles stabilized Pickering emulsions in the upper gastrointestinal tract.

3.3.1.2.4. SHIME

SHIME is reported as the first *in vitro* multi-compartmental system with almost whole integrated gastrotestinal tract (only mouth phase is not included), comprising six double-jacketed vessels which simulate the stomach, duodenum/jejunum, ileum, caecum/ascending colon, transverse colon and descending colon [174]. The last five vessels are continuously stirred with the usage of a magnetic stirrer. SHIME enables to obtain more reproducible results when compared to *in vivo* methodologies, being specifically developed to investigate the interactions of ingested components with human resident microbiota. However, the magnetic stirring provided by this model is distinct from the peristaltic movements *in vivo*, which compromises mechanistic agitation and digestion behaviours. Moreover, the human fecal bacteria used is not representative of the *in vivo* microbial community. Also, SHIME does not include absorption methods, the effects of microbiota colonization, the adhesion of microorganisms to the vessels and tubing [219].

3.3.2. Intestinal absorption and presystemic metabolism evaluation

Before intestinal absorption of bioactive compounds, the hydrolysis products obtained from the digestion of carbohydrates, lipids and proteins are still degraded by brush border membrane enzymes at the small intestinal epithelium of human body [203]. The activity of these enzymes increases from the proximal duodenum to the distal ileum, with the chyme decreases. Different procedures have been used for the simulation of this last step of intestinal digestion. One of the most simplified approach is based on isolated brush border membrane vesicles [220]. Herein, brush border membrane enzymes are mostly isolated from the jejunum of rat, pig and cow [221].

In fact, a standard protocol is still not currently available for application in this type of studies [220]. It can be explained by the lack of consensus about the incubation conditions to be stablished, namely the media composition, the ration between enzyme and substrate and pH, among others. On the other hand, it must be pointed out the limited availability brush border membrane enzymes, the incomplete data about their activity and adequate validation of the used of these enzymes [203]. Accordingly, this step is not included in most of *in vitro* digestion models. Particularly, intestinal digestion seems not to be reported when simulated gastrointestinal digestion studies of carrier-based delivery systems loaded with bioactive compounds were performed.

Methodologies involved in the determination of the amount of target bioactive compounds that are absorbed by intestinal wall cells include the usage of *in vitro* systems that vary from simple membranes to cell cultures, the combination of *ex vivo* (gastrointestinal organs operated under controlled conditions) with *in vitro* models and *in vivo* models (animals are submitted to intestinal perfusion – *in situ* method) [177]. Intestinal digestion using brush border membrane enzymes can be connected with intestinal absorption [203].

Among *in vitro* systems, the most used cell culture is Caco-2 human colorectal cancer epithelial cell lines [222], which is the more realistic model of the human intestinal epithelium. However, other cell cultures might be selected for simulation studies regarding intestinal absorption [179]. The selection of cell culture is of major importance since each one exhibits specific characteristics regarding its preservation and suitability for the expression of transporters. Considering this last topic, changes in the expression of transporters and enzymes might trigger an under- or overestimation of intestinal permeability [177]. Cell culture experiments consider a simplification of procedure, being assumed that a simple filtration or centrifugation of *in vitro* digested product is enough to quantify the amount of bioactive compounds transported through the intestinal epithelium cells. However, it must be tested and validated. Moreover, the amount of bioactive compound present in the decantation/centrifugation supernatant and in the residue must be confirmed to correspond to the amount of bioactive compound accessible in the small and large intestine, respectively [177]. In fact, decantation/centrifugation may not be capable to replicate the separation of the fraction in the intestinal lumen, as well as the passage of bioactive compounds into the intestinal epithelium. Herein, a relatively cheap and straightforward strategy based on the usage of dialysis membranes can be applied, despite of the impossibility to simulate the biochemical phenomena occurring at intestinal cells. Another reported limitation is related to the investigation of the bioaccessibility of lipophilic bioactive compounds [177]. They solubilize in the digestion after the release from digested products, whereby micellarization of bioactive compounds is a limiting factor. To overcome these problems, the bioaccessibility of several bioactive compounds has been studied using a two-stage *in vitro* digestion model, which may include ultracentrifugation method. Herein it is assumed that *in vitro* processes become a fraction of the digest containing the absorbable micelles. Accordingly, the amount of bioactive compound in the ultracentrifugation supernatant can be used to determine the amount of bioactive compounds transferred from the digest to the micelle fraction (micellarization efficiency) [177].

Various studies are currently published about intestinal absorption of bioactive compounds incorporated into carrier-based delivery systems. Liu et al. [223] used Caco-2 cells and monolayers to evaluate the cellular uptake and simulated intestinal wall transportation, respectively, of encapsulated (into zein/pectin nanoparticles) and

free resveratrol. *In vivo* methods for the bioavailability analyses were also considered with oral administration to rats. The cellular uptake and transmembrane transport were significantly higher in the case of encapsulated resveratrol. Furthermore, the usage of a controlled-based delivery system enables to increase the bioavailability of resveratrol in rats, as well as to prolong its existence in the plasma. Studies that combine *in vitro* digestion models and cellular uptake of bioactive compounds provide a better understanding about the potentialities of a carrier-based system for oral applications. Costa et al. [224] produced alginate and chitosan nanoparticles for encapsulation of grape pomace extract. Both delivery systems were subjected to *in vitro* gastrointestinal digestion and the results evidenced the protection of the extract in these conditions, occurring an increase in the bioaccessibility of different polyphenols. A reduction in the permeability of bioactive compounds through a Caco-2/HT29-MTX co-culture was observed, probably due to an increase in the residence time in the intestine. *Ex vivo* models enable a better representation of the morphological and physiological characteristics of intestine, by the inclusion of the most important cell types and architecture and of mucus layer wherein intestinal digestion by brush border membrane enzymes can be investigated [225]. *Ex vivo* models are usually obtained from rats, rabbits and pigs (the limited availability from human intestinal tissue must be considered) and they are valuable for studies related to the transport (across the epithelium), permeability, absorption and interaction with the mucus layer. However, the tissue is viable for a short time (1 to 3 hours) [203].

3.3.3. Incorporation of gut microflora

A strategy based on *in vitro* simulation of microbial fermentation has been used to evaluate the impact of gut microflora in the intestinal bioaccessibility of bioactive compounds. Herein, an inoculum of colonic microbiota is used to determine the colonic metabolism in the non-digestible fraction [177].

Recently, Santos et al. [177] reviewed some of the methodologies involving *in vitro* digestion of several food products containing phenolic compounds and antioxidants and subsequent gut microflora processing. Broadly, some challenges are described regarding the usage of *in vitro* fermentation models, including the difficulty to ensure the functional stability and reproducibility of human gut microbiota in order to conclude that the effects on microbial composition and metabolic activity are just explained by the experiment. Furthermore, it is considered the absence of a true biological replication in *in vitro* gut fermentation modelling due to the temporal modification of microbiota during consecutive sampling, among others [177].

This methodology might be eventually incorporated into simulation studies for gastrointestinal digestion of encapsulated bioactive compounds.

3.3.4. *In vivo* methodologies

In vivo experiments might be performed to evaluate bioavailability of specific bioactive compounds after the digestion process under a real gastrointestinal tract. However, several ethical issues might be presented and discussed in these circumstances. Rodents, rabbits, pigs and calves are the animals frequently used for *in vivo* studies [174]. For example, Zheng et al. [226] studied the bioaccessibility and bioavailability of lecithin-based

nanoemulsion loaded with carnosic acid considering a complementary *in vitro* and *in vivo* approach. *In vivo* pharmacokinetic evaluation was performed on rat model (Male Sprague Dawley) and showed that bioavailability of encapsulated carnosic acid was 2.2-fold higher when compared to carnosic acid in a suspension. Bioavailability can be measured by changes in the blood plasma concentration as a function of time (postprandial or after meal), as well as by quantifying the plasma concentration of a target bioactive compound over a prolonged period of time of constant feed intake [177].

3.4. Conclusion

Several food products that provide a set of bioactive compounds and other relevant molecules capable to promote the well-being are currently available in the market. The integration of nutraceuticals into these formulations requires to the industries to deal with their exposition to eventual undesirable temperature and moisture conditions during processing and storage. Moreover, during digestion processes, the bioactive compounds present in the ingested product must be protected from the pH changes and enzymatic activity. Accordingly, encapsulation technology has been reported as a suitable strategy to increase the stability of the most sensitive bioactive compounds. Additionally, controlled delivery systems are intended to promote the release of the bioactive compounds in the target place and at a desirable release rate. With the increase of the shelf-life of the obtained final products and of bioactive compounds bioavailability, the activity of bioactive compound in the human body is beneficiated. *In vitro* static models (considering standardized and non-standardized protocols) have been the most described to evaluate the behaviour of carrier-based delivery systems designed for the encapsulation of nutraceuticals under gastrointestinal conditions. The obtained results showed to be conclusive about the most resistant formulations according to bioaccessibility data. Regarding the *in vitro* dynamic models, the number of publications in this field is still scarce. Some of the main generated conclusions are related to the impact of using simulation of peristaltic phenomena on the release of bioactive compounds from the delivery systems. The usage of intestinal absorption models (cell cultures) associated to *in vitro* digestion models is of major importance to more accurately identify the most promising carrier-based systems for oral administration capable to enhance the bioavailability of nutraceuticals in the human body.

Chapter 4 – Characterization of biopolymer-based systems obtained by spray-drying for retinoic acid controlled delivery

---

The fourth chapter proposes the inclusion of RA into arabic gum, modified chitosan and alginic acid sodium microcapsules using spray-drying technology.

This chapter is published in:

Gonçalves, A; Estevinho, B N; Rocha, F. Characterization of biopolymer-based systems obtained by spray-drying for retinoic acid controlled delivery, Powder Technology. 2019 345, 758-765, https://doi.org/10.1016/j.powtec.2019.01.062.

4.1. Introduction

Retinoic acid (RA) is a carboxylic acid and corresponds to the oxidized form of vitamin A (retinol). RA is recognized as a successful chemopreventive and therapeutic agent in the treatment of several types of cancer [18,50,73,227–229]. Furthermore, it is also used for treatment of some dermatological disorders, such as acne vulgaris, psoriasis and photo damaged skin, among others [67,68]. However, the efficacy of RA as a medical agent is often compromised, whereby RA administration and delivery is currently a challenge. It has been reported for cancer patients that continuous oral administration or intravenous injection significantly reduces RA half-life in the blood [25,26], decreasing RA concentration in patients plasma [58]. As a consequence, many patients became resistant to RA despite continued treatment. The reduction of RA half-life in continuous administration might be explained by three hypothesis, according to Muindi et al. [58] (1) biliary excretion is involved for at least in 60% of RA elimination, whereby an unreal malabsorption or a nonspecific binding to the intestinal proteins compromised RA oral bioavailability, (2) RAR-α mutations might arise due to the continued treatment with RA and (3) the enzymes involved in RA catabolism might be induced as a consequence of continuous treatment with this drug. The daily dose of Vesanoid® (trade name of all-trans RA) is 45 mg/m^2 body surface (prescribing information). Other limitations about RA include its short gastrointestinal absorption and its rapid metabolism [27]. Moreover, several side effects related to RA administration, including hypertriglyceridemia, mucocutaneous dryness and headache, have been described [58–60]. Topical application of retinoids (skin treatment) leads to skin irritation (*e.g.* erythema, peeling and burning at the application site) and increased susceptibility to the sunlight which limits RA therapy acceptance by patients [42,73]. At last, RA is poorly soluble in aqueous systems due to its low polarity, which favours its inactivity or rapid degradation.

In the last years, several efforts have been made for development of carrier-based formulations for RA administration. The aim is to optimize the absorption and increase RA in the human body considering a sustained drug delivery and, consequently, improve the treatment efficiency against several malignancies [32,170,230,231]. This procedure might also reduce the side effects described for RA [74,158,160] as well as increase the protection and stability of RA [161]. In fact, these formulations expect to be appropriate controlled release systems to ensure the delivery of the core material at the target site and at the desirable rate and time.

The present work proposes the usage of spray-drying technology for the production of RA loaded biopolymer-based microcapsules. To date, it has been reported encapsulation of RA into liposomes, nanoemulsions, solid lipid nanoparticles (SLN), polyethylene glycol-coated poly-lactic-co-glycolic acid copolymer (PLGA) and PLGA combined with poly(vinyl alcohol), among others [229,232,233]. However, some of these processes use toxic organic solvents (*i.e.* dichloromethane, chloroform and ethyl acetate), which triggers undesirable reactions in the human body due to irritancy and toxicity [229].Accordingly, the main advantage about spray-drying technology include the non-usage of organic solvents. Encapsulation by spray-drying is also a rapid, continuous and reproducible process. Other advantages of this method include the good quality of microcapsules produced, the low production costs and the easy scale up [145,234]. Biopolymers are considered very attractive and even ideal materials to be used as encapsulation agents for incorporation of drugs and nutraceuticals [113]. Biopolymer-based delivery systems are biodegradable, biocompatible with cells and tissues, non-toxic, stable

in blood and non-thrombogenic, whereby different sources of biopolymers are valuable for pharmaceutical, medical and food industries [235,236]. Additionally, biopolymers have great mechanical and barrier properties [237]. Among the variety of biopolymers described in the literature, gums and carbohydrates constitute excellent candidates for RA encapsulation. Vitamin A is absorbed in the small intestinal lumen [83], whereby the biopolymers to be used for RA encapsulation must be selected considering their capability to protect RA against harsh gastric conditions and to enable RA release in the small intestine. Arabic gum is considered one of the most popular encapsulating agent due to its low viscosity, solubility and ability to produce stable emulsions, despite of the arabic gum high cost and its low availability [145,234,238,239]. Currently, some studies report the usage of arabic gum in formulations for encapsulation of probiotic cells for delivery in the intestine [240,241].

Alginates enable the production of microcapsules for controlled delivery of active compounds in the ileum or colon, considering the chemical nature of microcapsules [113]. In fact, alginates enable the protection of bioactive compounds from the acidic stomach environment while provide further release in the basic conditions of intestine [242]. However, the disadvantages regarding the usage of this gum include their very porous and permeable membranes, the high cost at industrial scale and the difficult scale-up [145]. Modified chitosan emerges also as a good strategy for the delivery of drugs into the intestine, as this encapsulating agent can bypass the acidic environment of the stomach [243].

Arabic gum, modified chitosan and alginic acid sodium were individually used to encapsulate RA in order to evaluate RA controlled release and its kinetics. Moreover, microcapsules formulations, load and unload with RA, were analysed regarding its average size and morphology. The final aim of RA encapsulation is to protect and to beneficiate RA in controlled release experiments for further medical application.

4.2. Material and Methods

4.2.1. Materials

All-trans retinoic acid (≥ 98%, R2625-1G, CAS 302-79-4) and alginic acid sodium (180947-500G, Lot#MKBS5877V, CAS 9005-38-3) were purchased from Sigma-Aldrich (Saint Louis, USA). Arabic gum from acacia tree (30888-1KG, Lot#BCBK8649V) was obtained from Fluka (Germany). Modified chitosan (pharmaceutical grade water-soluble chitosan) was supplied by China Eastar Group (Dong Chen, China) (Batch no. SH20091010). Ethanol (99%) was obtained from Valente e Ribeiro, Lda® (Alcanena, Portugal). 1-Octanol for synthesis (820931, CAS 111-87-5) was purchased from Merck (Darmstadt, Alemanha).

4.2.2. Preparation of solutions to be fed to the spray-dryer

Two sets of solutions were prepared and fed to the spray-dryer in order to produce two different types of microcapsules: empty microcapsules (only composed by the encapsulating agent and without core material) (Mc1) and RA-loaded microcapsules (Mc2). The first set of solutions concerns three aqueous solutions, each

one composed by one of the three biopolymers selected as encapsulating agent for RA encapsulation: arabic gum, modified chitosan and alginic acid sodium. These solutions were prepared at 1% (w/V) in 100 mL of ultra-pure water. Moreover, they were prepared in the day before to be spray-dried (biopolymer hydration overnight) and stored until use at 4 °C. In turn, the second set of solutions differs from the first set of solutions by the incorporation of RA in the biopolymer solutions previously described. Herein, 7 mL of a RA solution prepared in ethanol (99%) and with a concentration of 0.2% (w/V) were dispersed in each encapsulating agent solution. The concentration of the encapsulating agents to be used was selected considering the characteristics of the encapsulating agents, as well as the restriction of the laboratorial spray-dryer. Alginate is characterized by its viscosity, whereby concentrations between 0.5 and 4% of alginate are described for encapsulation [244]. Accordingly, 1% was the concentration selected to prepare the alginate microcapsules. Subsequently, this concentration was also used to prepare the arabic gum and modified chitosan microcapsules in order to keep the same concentration. The RA concentration was selected considering the ratios mass of core material/total mass of microcapsules used in a previous work performed by the authors for incorporation of vitamin A into arabic gum [245]. RA solution was prepared immediately before the final solutions to be fed to the spray-dryer. All the solutions were prepared under stirred conditions. Encapsulating agent solutions and RA solution were prepared at 35 °C and at room temperature, respectively.

4.2.3. Spray-drying conditions

Spray-drying technique was performed using a mini spray-dryer B-290 from BÜCHI (Flawil, Switzerland) with a standard 0.5 mm nozzle. The air and solution flow rates, air pressure and inlet temperature were set at 35 $m^3 \cdot h^{-1}$ (90%), 3.5 $mL \cdot min^{-1}$, 5-6 bar and 150 ºC, respectively. The outlet temperature, a parameter influenced by the other experimental conditions and the properties of each solution, varied between 81 and 88 ºC. These operating conditions were selected considering previous studies about vitamin A encapsulation performed by several researchers, including the authors of this research work [245–248].

The product yield (%) of the obtained microcapsules was determined by the ratio between the mass of dry powder recovered in the cyclone and in the collection vessel of spray-dryer and the total mass of materials used to prepare the solution fed to the spray-dryer (Eq. 4.1).

$$Product\ yield\ (\%) = \frac{Mass\ of\ dry\ powder\ recovered\ in\ the\ cyclone\ and\ in\ the\ collection\ vessel\ of spray-dryer}{Total\ mass\ of\ materials\ used\ to\ prepare\ the\ solution\ fed\ to\ the\ spray-dryer} \times 100 \quad \textbf{(4.1)}$$

4.2.4. Particle size distribution

Particle size distribution of the obtained spray-dried powders was assessed by laser granulometry using a Coulter LS 230 Particle Size Analyser (Miami, FL, USA). The microcapsules were first dispersed in ethanol and exposed to ultrasound radiation (3 to 4 min) in order to prevent their agglomeration. The sizes distribution and the average sizes of microcapsules, considering volume and number distributions, were determined for three 30 s runs (three analyses were performed for each sample and each analysis had the duration of 30 seconds). A

number distribution approach considers that each particle has equal weighting once the final distribution is calculated. In turn, a volume distribution approach considers the volume of each particle, whereby particles with higher volume have a higher contribution.

4.2.5. Scanning electron microscopy (SEM)

Surface morphology of microcapsules was evaluated by SEM using a Fei Quanta 400 FEG ESEM/EDAX Pegasus X4M (Eindhoven, The Netherlands). Herein, a brass stub using double-sided adhesive tape was used to fix the microcapsules, which were further coated in vacuum by a thin layer of gold (electrically conductive).

4.2.6. Analytical method validation

RA concentration was measured through an UV/VIS spectrometer (SPEC RES+, Sarspec, Porto, Portugal) at 348 ± 5 nm. The validation of analytical method was performed over linearity range, detection limit (LOD), quantification limit (LOQ), specificity (regarding the biopolymers used to produce the microcapsules), precision (intra-day) and accuracy. Additionally, the global uncertainty associated to the results was determined.

4.2.7. Controlled release experiments

An appropriate amount of spray-dried powders was used for RA controlled release experiments. This amount of microcapsules was estimated by mass balance considering the total amount of RA present in the microcapsules, as previously described by Estevinho et al. [249]. Herein, no losses of RA were assumed, as well as the proportion of core material/encapsulating agent was considered constant during the spray-drying process. RA-loaded microcapsules were placed on top of a cuvette with octanol inside. In turn, the cuvette was placed in an external device connected to the UV/VIS spectrometer, which enabled RA controlled release under magnetic stirring conditions. Another external device was used to control the heating during RA controlled release (at 37 ± 2 ºC). This spectrophotometric method enabled to determinate the amount of RA released from the capsules over the time by absorbance (at 348 ± 5 nm) in a continuous mode (intervals of 60 s) and to trace the RA controlled release profiles.

4.3. Results and discussion

Biopolymer-based microcapsules were produced for RA encapsulation using spray-drying technology. Arabic gum, modified chitosan and alginic acid sodium were individually used as encapsulating agents in the production of empty microcapsules (only composed by the biopolymer and without RA – microcapsules Mc1) and RA-loaded microcapsules (microcapsules Mc2). The impact of the usage of these different materials was evaluated in terms of microcapsules characterization and RA controlled release.

The product yield (amount of powder recovered in the spray-dryer regarding to the total mass of materials fed to the spray-dryer) varied between 26 and 38% for all the microcapsules produced, the highest value being registered for the microcapsules Mc2 composed by alginic acid sodium (Table 4.1). The product yield is a

parameter influenced not only by the operating conditions used in the spray-dryer (*e.g.* inlet temperature) and the volume of the solution fed to the spray-dryer, but also by the microcapsules formulation. Briefly, the usage of higher inlet temperatures leads to a reduction of the final moisture content in the microcapsules due to the increase of microcapsules drying rate [234]. Accordingly, the amount of microcapsules obtained increases, which results in a higher product yield. Herein, thermogravimetry studies were not considered on that time considering the information existent in the literature for these encapsulating agents and for the spray-drying process. In fact, the effect of the temperature is minimized by the short period of time (miliseconds) that the microcapsules and the encapsulating agents are exposed to high temperatures during the spray drying process. Hence, the spray-drying process is safe for sensitive compounds and as well as for the encapsulating agents. Concerning the volume of the solution fed to the spray-dryer, when a small volume is used the obtained product yield is compromised. About the effect of the constituents of microcapsules, the main factor associated to the product yield differences are associated to the encapsulating agents used and the type of solution fed to the spray-dryer. For instance, Gonçalves et al. [245] observed a marked decrease on the product yield of arabic gum carrier-based microcapsules (from 2.1 to 5.2. times) when the microcapsules contained coconut oil (loaded or unloaded with vitamin A (retinol)) instead of being composed only by the encapsulating agent. In the present study, the product yield obtained among all the microcapsules can be discussed and compared based on the different biopolymers used as encapsulating agents. Several works report a higher product yield when modified chitosan or alginic acid sodium carrier-based microcapsules (between around 30 and 75% and around 42 and 54%, respectively) are produced by spray-drying process [249–252]. However, for arabic gum carrier-based microcapsules the product yield value reported is very similar to the one herein obtained (around 31%) [250]. Comparing the product yield between microcapsules Mc1 and Mc2, the addition of an RA solution (dissolved in ethanol) to the formulations used to produce the microcapsules Mc2 seems to not interfere with the product yield. As observed, a similar product yield is obtained when comparing microcapsules Mc2 and microcapsules Mc1, whose formulation is only based on the encapsulating agent solutions.

Table 4.1 – Product yield of empty and RA-loaded microcapsules obtained by spray-drying technology using different biopolymers as encapsulating agents.

Microcapsules content	Encapsulating agent	Product yield (%)
Mc1	Arabic gum	30
	Modified chitosan	27
	Alginic acid sodium	31
Mc2	Arabic gum	31
	Modified chitosan	26
	Alginic acid sodium	38

Mc1 – microcapsules composed only by the encapsulating agent and without RA (empty microcapsules).

Mc2 – RA-loaded microcapsules.

4.3.1. Microcapsules analysis

The average size of microcapsules was assessed considering a differential volume distribution and a differential number distribution (Table 4.2). Microcapsules Mc1 exhibited a similar average size for all the encapsulating agents used, being registered a differential volume distribution between 2.44 and 2.54 μm. In turn, the average size of microcapsules Mc2 did not follow this tendency. The usage of the biopolymers alginic acid sodium, arabic gum and modified chitosan resulted in an increase in the average size of microcapsules Mc2 from 3.28 to 5.35 and 10.88 μm, respectively. Herein, the higher values registered (particularly related to modified chitosan carrier-based microcapsules) might be associated to the microcapsules aggregation despite of the exposition of microcapsules to the ultrasound radiation (section 4.2.4.) [253]. The presence of RA in the microcapsules might be associated to the observed aggregation tendency, considering the bindings formed between the encapsulating agents and RA. Regarding differential number distribution, the average size of microcapsules Mc1 and Mc2 varied from 0.12 to 0.99 μm. The surface of microcapsules evidenced different morphologies according to the biopolymers used as encapsulating agents (Figure 4.1). The presence/absence of RA in the microcapsules did not influence their morphology. Arabic gum microcapsules (Figure 4.1 A and D) presented a spherical form and rough surface. A similar morphology was observed by Gonçalves et al. [245] when vitamin A was encapsulated into arabic gum microcapsules using different concentrations of this biopolymer. Also, Estevinho et al. [250] observed the same characteristics in arabic gum microcapsules produced for *Gulosibacter molinativorax* ON4^{T} cells encapsulation. In turn, modified chitosan microcapsules (Figure 4.1 B and E) showed a spherical form and smooth surface. This morphology was shown by Estevinho et al. [254] and Estevinho et al. [249] when modified chitosan was used for β-galactosidase encapsulation and when vitamin B12 and vitamin C were individually incorporated into modified chitosan microcapsules, respectively. At last, alginic acid sodium microcapsules (Figure 4.1 C and F) showed a spherical form and slightly rough surface when compared to the obtained arabic gum microcapsules. These results are quite different from those reported in the literature when the same encapsulating agent was used. For example, in the study performed by Gonçalves et al. [255] a regular shape and smooth surface was observed for chlorogenic

Table 4.2 – Average size of all microcapsules formulations produced considering a differential volume distribution and a differential number distribution.

Microcapsules content	Encapsulating agent	Average size of microcapsules	
		Differential volume distribution (μm)	Differential number distribution (μm)
Mc1	Arabic gum	2.49 ± 1.35	0.12 ± 0.17
	Modified chitosan	2.44 ± 1.26	0.99 ± 0.57
	Alginic acid sodium	2.54 ± 1.41	0.70 ± 0.53
Mc2	Arabic gum	5.35 ± 5.06	0.17 ± 0.26
	Modified chitosan	10.88 ± 6.72	0.25 ± 0.28
	Alginic acid sodium	3.28 ± 2.31	0.31 ± 0.34

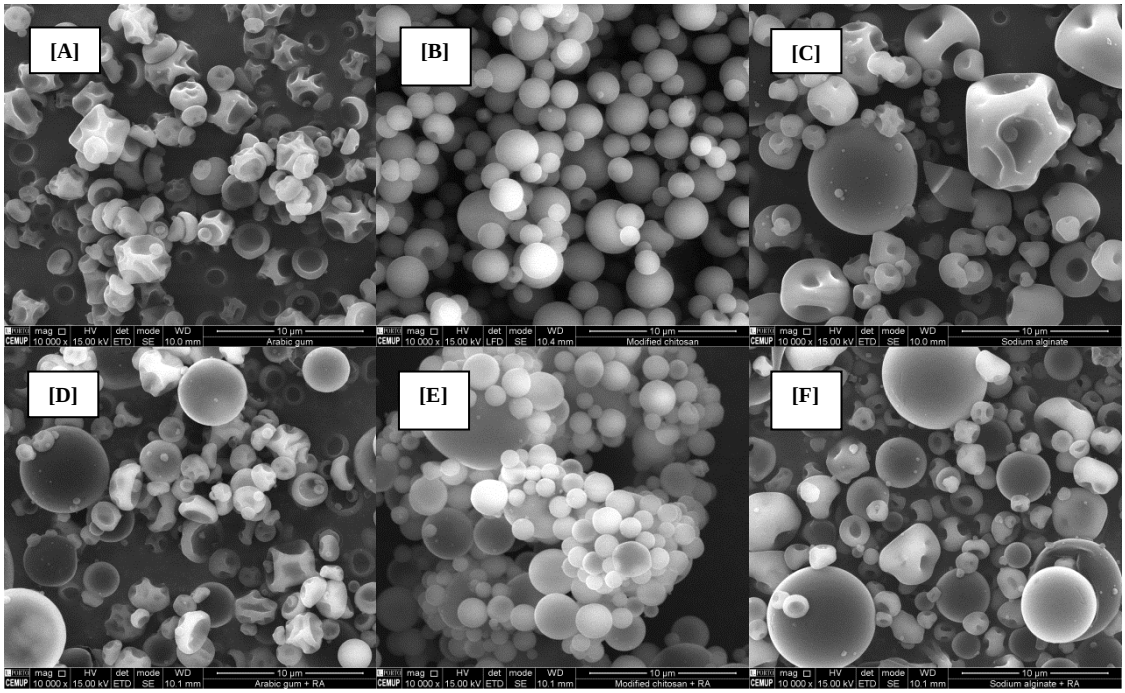


Figure 4.1 – SEM images of empty (A, B and C) and RA-loaded polymeric-based microcapsules (D, E and F) using arabic gum (A and D), modified chitosan (B and E) and alginic acid sodium (C and F) as encapsulating agents. Magnification =10,000 times, beam intensity (HV) 15.00 kV, distance between the sample and the lens (WD) around 10 mm.

acid-loaded microparticles prepared with sodium alginate. Moreover, Estevinho et al. [256] reported the incorporation of β-galactosidase into sodium alginate microcapsules characterized by a very smooth surface.

4.3.2. RA controlled release

4.3.2.1. Analytical method validation

The analysis and measurement of RA was accomplished through a spectroscopic method using a linear calibration curve validated in the range between 0.0003 $mg \cdot mL^{-1}$ and 0.006 $mg \cdot mL^{-1}$ (eight standard solutions were prepared in octanol) with a correlation coefficient of 0.9952. LOD and LOQ were 0.0003 $mg \cdot mL^{-1}$ and 0.0009 $mg \cdot mL^{-1}$, respectively. Precision was determined in terms of repeatability (intra-day) at three concentration levels: 0.0003, 0.002 and 0.006 $mg \cdot mL^{-1}$. The relative standard deviation obtained for all of these solutions (triplicate assays) was lower than 7.5%. Accuracy was calculated by the ratio between the concentration obtained for the RA standard solutions and the predictable concentration (recovery factor). The percentage of recovery is registered in the Table 4.3 and varied between 88.2 and 111.7%. Specificity was evaluated by the interference of the biopolymer solutions (prepared in octanol) with the baseline signal. No peak was observed for all the encapsulating agents tested, particularly at the wavelength where RA is detected (348

± 5 nm). However, an increase of the baseline signal was observed which influences the final absorbance values analysed.

Table 4.3 – Accuracy of RA at different concentration level.

RA (mg·mL^{-1})	Recovery (%)
3.33x10^{-4}	88.2
5.00x10^{-4}	99.1
6.67x10^{-4}	96.6
1x10^{-3}	99.2
2x10^{-3}	93.8
3x10^{-3}	111.7
5x10^{-3}	97.2
6x10^{-3}	99.9

Global uncertainty was determined considering the uncertainties associated to the standard preparation (U1), calibration curve (U2), precision (U3) and accuracy (U4) [257] (Figure 4.2).

The global uncertainty was lower than 5% for all the standard solutions concentrations (Figure 4.2 A). Regarding the relative weight of each individual source of uncertainty, the uncertainty associated to the calibration curve (U2) has the strongest weight in the registered variation. The influence of standard preparation (U1) increases with the standard solutions concentration, while the influence of precision (U3) decreases with the standard solutions concentration. The impact of accuracy (U4) is very small for all the standard solutions concentration (Figure 4.2 B).

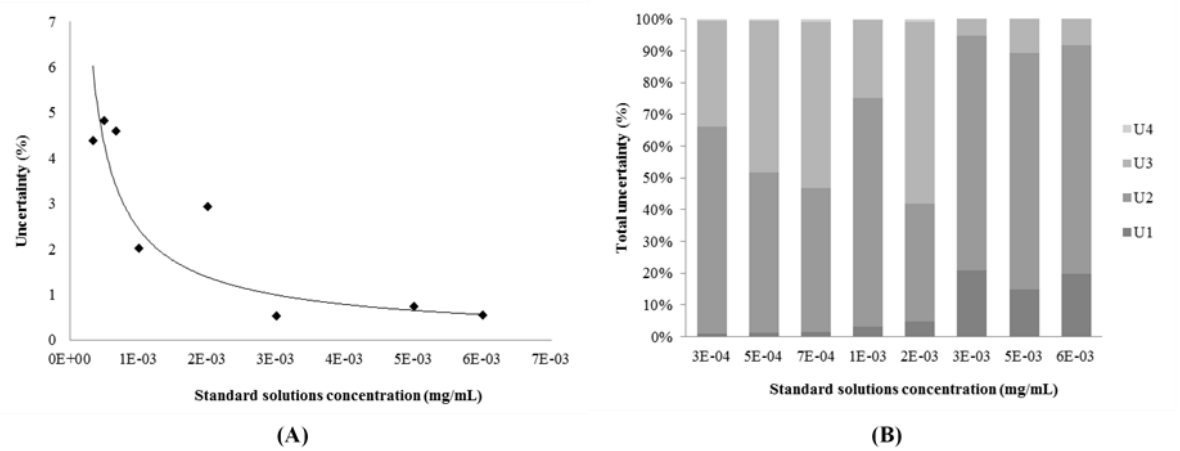


Figure 4.2 – Global uncertainty considering the uncertainties associated to the standard preparation (U1), calibration curve (U2), precision (U3) and accuracy (U4). (A) Variation of global uncertainty for all the standard solutions concentrations. (B) Relative weight of each individual source of uncertainty for all the standard solutions concentration.

4.3.2.2. Controlled release profiles

RA controlled release studies were carried out in octanol, an organic solved widely used to simulate the possibility of this lipophilic molecule to cross the lipid membranes of living system [258,259]. The amount of RA released from all biopolymer-based microcapsules enabled to draw the RA release profiles, expressed as the percentage of cumulative RA over time (Figure 4.3).

Modified chitosan microcapsules enabled the fastest RA release when compared to the other microcapsules formulations used. In fact, a very fast release of RA to octanol was observed in the first 7 min of the experiment, its stabilization occurring 92 min after. For arabic gum and alginic acid sodium microcapsules very similar RA release profiles were obtained in the first 36 min. Afterwards, a slower RA release was registered with alginic acid sodium formulation, which prolonged for more than 7 h. In turn, arabic gum microcapsules provided a RA controlled release for 102 min. Considering the final aim of achieving a RA release in the last part of digestion (in the small intestine), a slow release in the ideal medium is desired. The final aim is to maximize RA absorption and improve RA action as a medical agent as well as decrease RA side-effects.

The obtained results demonstrate the effect of the encapsulating agent in the controlled release of target active compounds. The same evidences were reported by Estevinho et al. [249], which compared the release profiles of vitamin B12 and vitamin C, each one individually encapsulated in different biopolymer-based formulations. The authors observed a complete release of both vitamins in around 10, 15 and 120 min when modified chitosan, sodium alginate and chitosan were used as encapsulating agents, respectively. Furthermore, comparing these stabilization times with the one obtained in the present work, different results are obtained particularly regarding to modified chitosan. This suggests the effect of the release media in the outside surrounding environment of microcapsules. A recent number of studies have been carried out to analyse the RA controlled release profiles from different carrier-based systems in order to validate their application. Castleberry et al. [150] propose polyvinyl alcohol bound to all-trans RA for controlled transdermal delivery. They demonstrated the active all-trans RA for out to ten days (*in vitro* experiments). Moreover, *in vivo* experiments showed that pro-drug formulation reduces the inflammation in the application site, in addition to retain the drug at the application site for measurement for up to six days. Akanda et al. [162] optimized RA-loaded solid lipid nanoparticles for prostate anticancer treatment. After almost 40% of RA was released in the first 10 h, a sustained release was followed for five days.

Preliminary studies related to RA stability for at least three months storage were also performed in the present work. The samples were conserved in the fridge at 4 ºC and protected from light with aluminium foil. A spectrophotometric method was used to compare the amount of RA present in the new and the old microcapsules. The obtained results suggested the total loss of RA in the arabic gum-based microcapsules after this period of time. Moreover, for the modified chitosan and alginic acid sodium formulations a significant loss of RA was observed (data not shown). The percentage of loss of RA was around 48 and 83% from modified chitosan and alginic acid sodium, respectively. These results inform about the microcapsules resistance over time. Accordingly, an improvement on microcapsules formulation might be required considering its eventual further commercialization.

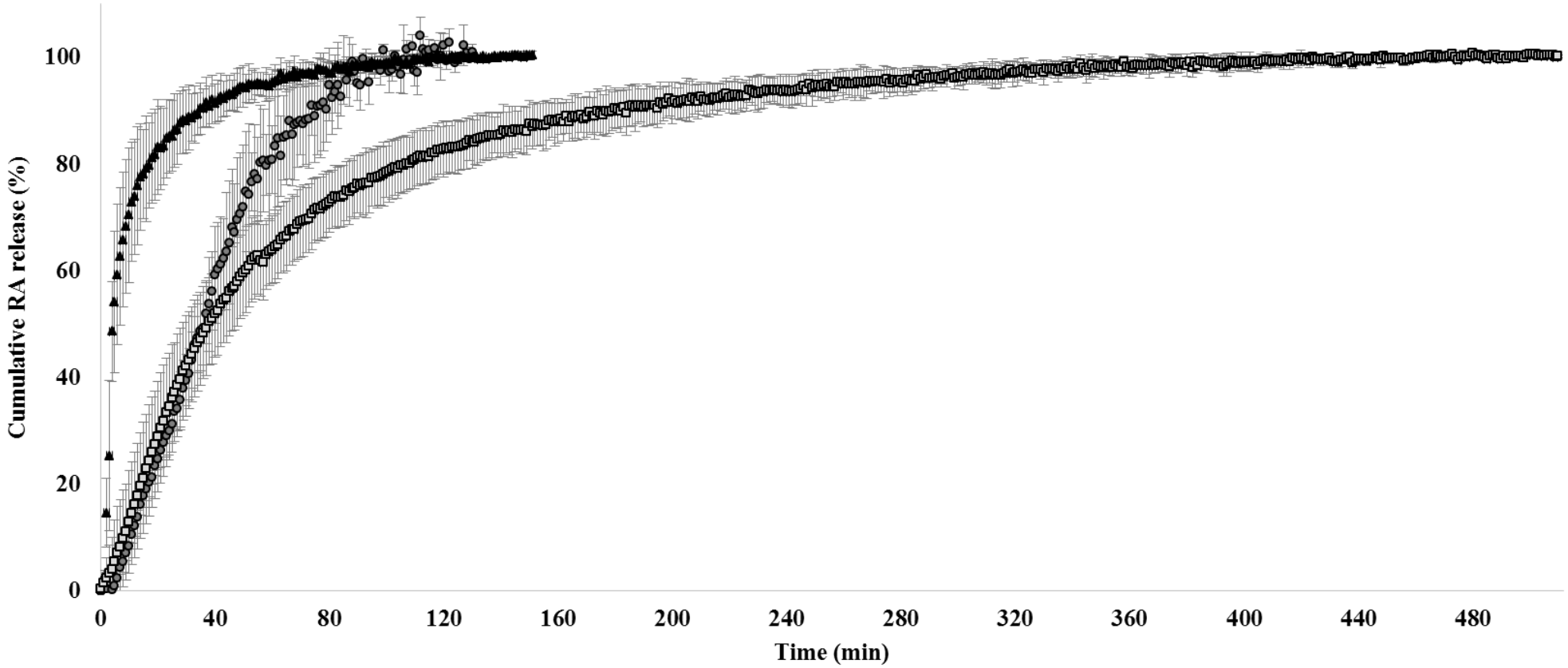


Figure 4.3 – RA release profiles obtained from different biopolymers-based systems using arabic gum (●), modified chitosan (▲) and alginic acid sodium (■) as encapsulating agents. Results are presented as the average and standard deviation of three independent assays.

4.3.2.3. Kinetic models

Several release mechanisms are described in the literature, namely statistical methods, model dependent methods and model independent methods [260]. They are influenced by the encapsulation methods applied, the kind and amount of encapsulating agent(s) used and the conditions selected for the release experiments [145]. Furthermore, the physicochemical phenomena involved in the drug /bioactive compound release from the carrier-based system include the individual or combined action of diffusion-controlled, barrier-controlled, pressure-activated, solvent-activated, osmotically-controlled, pH-controlled, temperature-sensitive and melting-activated processes [145].

The main mathematical models related to the model dependent methods were used to describe the controlled release profiles obtained from the RA biopolymer-based release systems developed in this work. Those include zero-order, first-order, Higuchi, Korsmeyer-Peppas and Weibull models [260–262].

The kinetics of zero-order (Eq. 4.2) describes a slow and constant release rate. Moreover, it is observed when the core material is a pure compound and its release from the carrier-based system is also carried out as a pure compound [145,263,264]. Although kinetics of zero-order designates ideal release behaviour in theory, in practice it is very difficult to achieve due to the short adjustment factors equated by the model [262].

$$Q_t = Q_0 + K_0 t \quad \textbf{(4.2)}$$

where Q_t is the cumulative amount of the drug/active compound released at the time t, Q_0 is the initial amount of the drug/active compound in solution (usually $Q_0 = 0$) and K_0 is the zero-order release constant.

In the present work, the adjustment of the kinetics of zero order to the RA controlled release profiles presented a correlation coefficient which varied between 0.948 for the modified chitosan-based microcapsules, 0.996 for the alginic acid sodium-based microcapsules and 0.997 for the arabic-based microcapsules (Table 4.4). The zero-order release constant, K_0, registered the lowest value with the usage of arabic gum as encapsulating agent (8.0×10^{-5} mg·min^{-1}) (Table 4.4). For the microcapsules composed by alginic acid sodium and by modified chitosan, this parameter increased to 2.0×10^{-4} and 5.0×10^{-4} mg·min^{-1} (Table 4.4), respectively. This tendency of results is in the agreement with an increase of RA release rate in the same conditions.

The kinetic of first-order (Eq. 4.3) is observed when the core material is in a solution [145,263,264]. Accordingly, this model was not applied to the experimental results obtained in this work, since the encapsulating method used leads to the production of solid RA-loaded biopolymer-based microcapsules (a powder).

$$Q_t = Q_0 e^{-K_1 t} \quad \textbf{(4.3)}$$

where K_1 is the first-order release constant.

Higuchi, Korsmeyer-Peppas and Weibull are more complex models when compared to the above presented. They include several factors that might be involved in the release of active compounds [262].

Considering Higuchi model (Eq. 4.4) the correlation coefficient obtained from the adjustment of the model to the registered experimental results varied between 0.820 and 0.858 (Table 4.4). The Higuchi constant, K_H, followed the same tendency when compared to the zero-order release constant, K_0, influenced by the RA release rate. K_H changed between 5.0×10^{-4} and 1.2×10^{-3} mg·min^{-1} (Table 4.4).

$$Q_t = K_H \sqrt{t} \quad \textbf{(4.4)}$$

where K_H is the Higuchi constant.

The Korsmeyer-Peppas model (Eq. 4.5) provides information related to the structural and geometric characteristics of the dosage form (Korsmeyer constant, K_K). Furthermore, it enables to identify the major mechanism responsible for the active compound controlled release (release exponent – diffusional, n) [145,264,265].

The Korsmeyer-Peppas model was adjusted to the linear RA controlled release profiles considering the Q_t/Q_∞ is lower than 0.6 [262] and the correlation coefficients obtained changed between 0.702 and 0.997 (Table 3.4.). The parameter n was higher than 0.85 for the arabic gum microcapsules (n = 1.1) (Table 4.4), suggesting a drug transport mechanism based on a super case-II transport and a t^{n-1} rate as a function of time [145]. In turn, for modified chitosan and alginic acid sodium formulations the parameter n changed between 0.43 and 0.85 (n = 0.4 and n = 0.7, respectively) (Table 4.4), whereby an anomalous transport and a t^{n-1} rate as a function of time was evidenced for these microcapsules [145]. The Korsmeyer constant, K_K, increased from the arabic gum-based microcapsules (9.3×10^{-3} min^{-n}) to alginate acid sodium-based microcapsules (0.1 min^{-n}) and to modified chitosan-based microcapsules (0.2 min^{-n}) (Table 4.4). Again, this parameter increased with the increase of RA release rate.

$$Q_t/_{Q\infty} = K_K \, t^n \quad \textbf{(4.5)}$$

where Q_t/Q_∞ is the fraction of active compound released until time t and K_K is the Korsmeyer constant.

Weibull model (Eq. 4.6) is reported as the most appropriate model to describe the active compound release profiles from a matrix-based delivery system [260]. Since the powders obtained by spray-drying technology are microcapsules with a matrix morphology [266], it is expected that the Weibull model will fully fit to the RA release profiles obtained in the present work.

$$M_t = M_\infty \left[1 - e^{-\left(\frac{t - t_0}{\tau d}\right)^\beta}\right] \quad \textbf{(4.6)}$$

where M_t is the dissolution/release (%) of the active compound at time t, M_∞ is the dissolution/release (%) of the active compound at infinite time, t_0 is the lag-time of the dissolution (usually t_0=0), β indicates the shape parameter of the curve and τ_d is the time when 63.2% of M has been dissolved/released [260,262,267].

The correlation coefficients obtained from the adjustment of the Weibull model to the registered experimental results was 0.993, 0.995 and 0.983 for the RA-loaded microcapsules composed by arabic gum, modified chitosan and alginic acid sodium, respectively (Table 4.4). The β parameter, which provides information regarding the shape of the release curve, registered a value higher than 1 for the RA release profiles obtained from arabic gum-based microcapsules (β = 1.4) (Table 4.4). In this case, the shape of the curve gets sigmoidal with a turning point [262]. In turn, for the other biopolymer-based microcapsules the β was lower than 1 (β = 0.5 for modified chitosan and β = 0.9 for alginic acid sodium) (Table 4.4), whereby the shape of the curve would show a steeper increase regarding the shape of the release curve that corresponds exactly to the shape of an exponential profile [262]. The τ_d parameter, calculated from the RA release profiles when 63.2% of the active compound was released, showed different values for all the encapsulating agents used. The lowest value was registered for RA-loaded modified chitosan microcapsules (6.9 min) while the highest one was obtained for RA-loaded alginic acid sodium microcapsules (67.4 min) (Table 4.4).

Table 4.4 – Parameters and correlation coefficients of the kinetics of zero-order, Higuchi, Korsmeyer-Peppas and Weibull applied to the experimental RA release profiles.

	Parameters		Biopolymers (encapsulating agents)		
			Arabic gum	Modified chitosan	Alginic acid sodium
Kinetic models	Zero-order	K_0 (mg·min^{-1})	8.0x10^{-5}	5.0 x10^{-4}	2.0x10^{-4}
		Q_0 (mg)	-7.0x10$^{-5*)}$	2.0x10^{-5}	1.0x10^{-4}
		R^2	0.997	0.948	0.996
	Higuchi	K_H (mg·min$^{-0.5}$)	5.0x10^{-4}	1.2x10^{-3}	1.1x10^{-3}
		R^2	0.820	0.823	0.858
	Korsmeyer-Peppas	K_k (min^{-n})	9.3x10^{-3}	0.2	0.1
		n	1.1	0.4	0.7
		R^2	0.997	0.702	0.887
	Weibull	τ_d (min)	43.4	6.9	67.4
		β	1.4	0.5	0.9
		R^2	0.993	0.995	0.983

*) Consider $Q_0 \geq 0$.

Among the models used in the present work, the Weibull model is the best capable to describe the RA controlled release profiles obtained from the different microcapsules formulations used. However, several studies related to this topic suggest other suitable mathematical models for the same active compound. Jeong et al. [268]

observed that all-trans RA released from core-shell type nanoparticles of poly(ε-caprolactone)/poly(ethylene glycol) diblock copolymer considering a almost pseudo-zero-order kinetic. Also, Dinarvand et al. [269] observed a Higuchi kinetics and a zero order release profile for the all-trans RA release from gelatin microspheres and from a cream formulation (*in vitro* studies), respectively.

4.4. Conclusion

In this study, biopolymer-based delivery systems were produced for RA encapsulation using the spray-drying technology. Controlled release studies evidence the impact of the encapsulating agent on the RA release profiles. The fastest release was observed in 99 min and it was registered for the modified chitosan-based formulation. In turn, alginic acid sodium microcapsules enabled the longer RA release period, which took place for more than 7 h. The most appropriate kinetic model capable to describe the RA release profiles considering the carrier-based systems proposed is the Weibull model.

Chapter 5 – Spray-drying of oil-in-water emulsions for encapsulation of retinoic acid: polysaccharide- and protein-based microparticles characterization and controlled release studies

---

The fifth chapter proposes oil-in-water emulsions to produce RA-loaded biopolymer-based delivery systems applying spray-drying technology. Alginic acid sodium, modified chitosan, arabic gum, xanthan gum and gelatin were individually used as encapsulating agents.

This chapter is published in:

Gonçalves, A; Estevinho, B N; Rocha, F. Spray-drying of oil-in-water emulsions for encapsulation of retinoic acid: Polysaccharide- and protein-based microparticles characterization and controlled release studies. Food Hydrocolloids. 2022, 124, Part A, 107193, https://doi.org/10.1016/j.foodhyd.2021.107193.

5.1. Introduction

The treatment of several types of cancer has been carried out by retinoic acid (RA), a metabolite of vitamin A (retinol). RA acts against malignant cells by the regulation of gene transcription mediated through their bind mostly to RA receptors (RARs), members of the nuclear receptor superfamily [97]. Consequently, cellular proliferation, migration and invasion are inhibited, while cell differentiation and apoptosis are promoted [232,270–273]. Particularly, for the treatment of acute promyelocytic leukaemia (APL) the only effective approach is based on chemopreventive and/or chemotherapeutic action of all-trans RA [274].

Clinical use of RA handles with several challenges, such as the poor solubility in water and physicochemical instability of this retinoid [275]. Furthermore, the major drawback about RA oral administration is the significant decrease of RA half-life in blood due to its continuous repetitive administration. Consequently, a marked decrease of RA concentration is detected in the plasma [25,26,58,276] and the patients become resistant to RA (relapses have occurred in many patients with APL) despite of the continued treatment. This behaviour is related, among other factors, to the cytochrome P450 activity. These enzymes regulate the cellular levels of RA, being induced even at a low amount of this bioactive compound. Accordingly, repeated RA administration promotes the degradation of this retinoid and its levels are not possible to be maintained in the plasma [277]. The design and development of an appropriate carrier-based system for a slow and continuous RA controlled delivery may beneficiate its anticancer activity, preventing repetitive administration of this retinoid and subsequently reducing the activity of cytochrome P450. This strategy aims to increase the RA bioavailability in the human body. Moreover, the severe side-effects related to high levels of RA administration (*i.e.* nausea, headache, abdominal pain and retinoid acute resistance, among others [28,58–60]) might be minimized.

Encapsulation by spray-drying is hypothesized as a promising strategy for incorporation of RA into biopolymer-based microparticles to treat patients with APL and other types of cancer. The advantages about this technology compared to others already investigated for RA encapsulation (*i.e.* solid lipid nanoparticles (SLN), liposomes, nanoemulsions and poly-lactic-co-glycolic acid copolymer (PLGA), among others [229,232]) include the non-usage of toxic organic solvents, as well as the rapid, continuous and reproducible production of microparticles with good quality, at low cost and easy scale up [145,234].

In our previous work, biopolymer-based microparticles were prepared for RA encapsulation (RA solution was prepared in ethanol) considering the individual usage of alginic acid sodium, modified chitosan and arabic gum as encapsulating agents (prepared in ultra-pure water) [278]. RA controlled release in octanol prolonged for more than 7 h from alginic acid sodium-based microparticles. In the present work, oil-in-water emulsions containing RA in the oily phase, a surfactant (tween 80) and a biopolymer (polysaccharides or a protein for the entrapment of the core material) in the aqueous phase were proposed to be fed to the spray-dryer to produce loaded microparticles. The same encapsulating agents used in the previous work were individually used herein, in addition to gelatin and xanthan gum. The biopolymers to be used in the formulation of microparticles for RA oral administration must ensure the protection of this retinoid during passage through the stomach and enable its release and absorption in the intestine. Accordingly, most of the biopolymers were selected as encapsulating agents considering the information described in the literature for the release of the active compounds in the

intestine. Moreover, biopolymers with high emulsifying and film forming properties are of major importance. However, a better understanding of the real effect of body fluids (namely, saliva) on the stability of RA loaded biopolymer-based microparticles produced might be analysed in gastrointestinal simulation studies. The production of microparticles coated with chitosan might be considered to improve the final product characteristics [252]. Alginate [242] and modified chitosan [243] are resistant to the acidic stomach environment, arising as a good solution for the bioactive compound release in the intestine. Arabic gum has a great ability to produce stable emulsions with several oils and over a wide range of pH, in addition to present low viscosity [234,239]. Gelatin is recognized by the high emulsifying and stabilizing activity, having the tendency to form a fine dense structure upon drying [279]. At last, xanthan gum is very stabilizing, thickening and emulsifying agent [280]. Moreover, it is resistant to enzymatic degradation and pH variations, being stable at low pHs [281]. Screening of the the most appropriate formulations for medical use was carried out based on characterization of RA-loaded microparticles (*i.e.* encapsulation efficiency, morphology, particle size and controlled release studies) (preliminary studies).

5.2. Material and Methods

5.2.1. Materials

All-trans RA (≥ 98%, R2625-1G, CAS 302-79-4), alginic acid sodium salt (180947-500G, Lot#MKBS5877V, CAS 9005-38-3, MW: between 120,000 and 190,000 g·moL^{-1}, ratio of mannuronic acid to guluronic acid (M/G ratio): 1.56, country of manufacture: United Kingdom), arabic gum from acacia tree (30888-1KG, Lot#BCBK8649V, country of manufacture: Germany), gelatin tested according to Ph. Eur. (48723-500G-F, Lot#BCBM9678V, CAS 9000-70-8, biological origin: animal (species of animal: bovine (Ruminant-Cow, Ox, Buffalo) and porcine (swine, pig), tissue type: hide/bones), country of manufacture: Germany), xanthan gum from *Xanthomonas campestris* (G1253-100G, Lot#SLCC2817, CAS 11138-66-2, country of manufacture: USA), coconut oil from *Cocos nucifera* (C1758-500G, Lot#MKCK3631, CAS 8001-31-8) and tween 80 (P1754-1L, Lot#BCBT8094, CAS 9005-65-6) were purchased from Sigma-Aldrich. Modified chitosan (pharmaceutical grade water-soluble chitosan) was supplied by China Eastar Group (Dong Chen, China) (Batch no. SH20091010). It was obtained by carboxylation and had a deacetylation degree of 96.5% and a viscosity of 5 mPa·s (1%; 25 °C). 1-Octanol for synthesis (820931, CAS 111-87-5) was obtained from Merck (Darmstadt, Alemanha). Ethanol (99%) was purchased from Valente e Ribeiro, Lda® (Alcanena, Portugal).

5.2.2. Emulsions preparation

Aqueous phase of emulsions was composed by encapsulating agents' solutions. Biopolymers (modified chitosan, alginic acid sodium, arabic gum, gelatin and xanthan gum) were individually dissolved in ultra-pure water (1% (w/v)) 24 h before being emulsified and spray-dried to ensure the fully hydration of compounds. In turn, the oily phase was composed by a RA solution prepared in coconut oil (0.1% (w/v)). All the solutions were

prepared under stirred conditions and at 35 ± 2 ºC. Tween 80 surfactant was added to the RA solution (0.5% (w/v) regarding to this oily solution) and the obtained final mixture was dispersed with each encapsulating agent solution at 12000 rpm for 5 min (the emulsion prepared with xanthan gum was produced at 20000 rpm for 10 min due to the properties of this biopolymer), using a mechanical homogenizer (CAT, Germany). The proportion of encapsulating agent and coconut oil was 2.77 $g \cdot g^{-1}$. This parameter was optimized considering previous studies performed by the authors [245,278]. The emulsions produced were immediately fed to the spray-dryer for the microparticles production. The pH value of emulsions was 7.41, 7.42, 5.31, 5.73 and 5.13, when modified chitosan, alginic acid sodium, arabic gum, gelatin and xanthan gum were used, respectively.

5.2.3. Spray-drying technology

A mini spray-dryer B-290 from BÜCHI (Flawil, Switzerland) with a standard 0.5 mm nozzle and a standard cyclone was used for drying the emulsions and the production of RA loaded-biopolymer-based microparticles. Three inlet air temperatures were tested for drying modified chitosan-based emulsions – 115, 130 and 150 ºC – and the best condition identified was selected to dry the other emulsions, individually composed by alginic acid sodium, arabic gum, gelatin and xanthan gum. Atomization air flow rate and air pressure were set at 35 $m^3 \cdot h^{-1}$ (90%) and 5-6 bar, respectively. Emulsion feed flow rate varied between 2 and 6 $mL \cdot min^{-1}$ to enable outlet air temperatures kept in the range between 60 and 70 ºC. Outlet temperature is influenced by the properties of the fed system, as well as the other operating conditions implemented in the spray-dryer. The starting point for the operating conditions herein used relies on vitamin A encapsulation studies previously reported [245–248,278]. The obtained microparticles (dry powder) were recovered in the cyclone and in the collection vessel of spray-dryer and stored under refrigeration and protected from the light with aluminium foil until further analysis. The product yield (%) was determined according to the Eq. 5.1.

$$Product\ yield\ (\%) = \frac{Dry\ powder\ weight\ recovered\ in\ the\ cyclone\ and\ in\ the\ collection\ vessel\ of spray-dryer}{Total\ mass\ of\ compounds\ used\ to\ prepare\ the\ systems\ fed\ to\ the\ spray-dryer} \times 100 \qquad \textbf{(5.1)}$$

5.2.4. Emulsions viscosity

Emulsions viscosity was evaluated from steady-shear flow curves using an Anton Paar MCR 92 rheometer (Austria). Analyses were performed in triplicate at 25 ºC, with an increasing shear rate from 1 to 100 s^{-1}, using a measuring plate PP50 (Part No.: 79045, Serial No.: 55422, Cat No.: 79045, Del No.: 80352243, Anton Paar) with 50 mm of diameter and a gap of 0.5 mm. Flow curves with a total number of 50 points were obtained for each sample.

5.2.5. Emulsions zeta potential

Zeta potential (a good indication of droplet surface electrical charge) of emulsions was measured by dynamic light scattering using a Zetasizer Nano-ZS90 (Malvern Instruments, Worcestershire, UK). Measurements were performed in triplicate.

5.2.6. Droplet and particle size distribution

Emulsions droplet size and particle size of microparticles obtained by spray-dryer were assessed by laser granulometry using a Coulter LS 230 Particle Size Analyser (Miami, FL, USA). A suspension of microparticles dispersed in ethanol was used for the analyses, considering particle size measurements. These parameters were reported as the average of droplet mean diameter, considering volume and number distributions. A volume distribution considers the volume of each particle (particles with a higher volume have higher contribution), while in a number distribution each particle has equal weight. Measurements were performed in triplicate and each analysis had the duration of 30 seconds.

5.2.7. Microparticle morphology

Scanning electron microscopy was performed with a Fei Quanta 400 FEG ESEM/EDAX Pegasus X4M (Eindhoven, The Netherlands) to evaluate the surface morphology of microparticles. Microparticles were fixed into a brass stub with double-sided adhesive tape and further coated in vacuum by a thin layer of gold-palladium using a SPI module sputter coater.

5.2.8. Encapsulation efficiency and loading capacity

Encapsulation efficiency (%) was determined by the ratio between the mass of RA present in the microparticles and the mass of RA used to prepare the oily phase of emulsions fed to the spray-dryer, adapting the method described by Côrrea-Filho et al. [282]. A suspension of microparticles prepared in octanol (the fluid considered for controlled release studies (section 5.2.9.)) was stirred at 2000 rpm during 2 min and kept at room temperature overnight. Afterwards, the suspension was again stirred at 2000 rpm during 5 min to ensure the microparticles break, put on a bath at 37 ± 2 ºC for 3 h and then centrifuged (Centromix mod. S-549, Porto, Portugal) at 50000 rpm during 20 min. Supernatant was recovered and RA concentration was determined using an UV/VIS spectrometer (SPEC RES+, Sarspec, Porto, Portugal) at 352 ± 8 nm. A calibration curve with a correlation coefficient of 0.9973 was validated in a concentration range between 0.00005 and 0.01200 $mg \cdot mL^{-1}$. LOD and LOQ were 0.0002 $mg \cdot mL^{-1}$ and 0.0007 $mg \cdot mL^{-1}$, respectively.

Loading capacity of microparticles was calculated by the ratio between the mass of RA and microparticles weight.

5.2.9. Controlled release experiments

RA controlled release studies were performed according to the method described by Gonçalves et al. [278]. Briefly, RA loaded-biopolymer-based microparticles were placed on top of a cuvette with octanol, an organic solvent referred as a good mimic of phospholipids membrane characteristics due to its amphiphilic nature [258,259,283,284]. RA controlled release was performed at 37 ± 2 ºC and under magnetic stirring conditions. Monitorization of RA release profiles was carried out using an UV/VIS spectrometer (section 5.2.8.) by absorbance (at 352 ± 8 nm) in a continuous mode (intervals of 2 min). The main mathematical models related

to the model dependent methods (zero-order (Eq. 5.2), Higuchi (Eq. 5.3), Korsmeyer-Peppas (Eq. 5.4) and Weibull (Eq. 5.5) [260–262,267]) were fitted to the obtained controlled release profiles.

$$Q_t = Q_0 + K_0 t \quad \textbf{(5.2)}$$

where Q_t is the cumulative amount of the drug/active compound released at the time t, Q_0 is the initial amount of the drug/active compound in solution (usually $Q_0 = 0$) and K_0 is the zero-order release constant.

$$Q_t = K_H \sqrt{t} \quad \textbf{(5.3)}$$

where K_H is the Higuchi constant.

$$Q_t/Q_\infty = K_K t^n \quad \textbf{(5.4)}$$

where Q_t/Q_∞ is the fraction of active compound released until time t and K_K is the Korsmeyer constant. The parameter n is the release exponent (diffusional), a parameter that defines the release mechanism.

$$M_t = M_\infty \left[1 - e^{-\left(\frac{t-t_0}{\tau d}\right)^\beta}\right] \quad \textbf{(5.5)}$$

where M_t is the dissolution/release (%) of the active compound at time t, M_∞ is the dissolution/release (%) of the active compound at infinite time, t_0 is the lag-time of the dissolution (usually t_0=0), β indicates the shape parameter of the curve and τ_d is the time when 63.2% of M has been dissolved/released.

5.2.10. Statistical analysis

Apparent viscosity and droplet size of the emulsions produced was evaluated regarding the biopolymer individually used. Moreover, encapsulation efficiency and particle size distribution were compared for each inlet air temperature operated in the spray-dryer. Also, particle size distribution was analysed among all microparticle formulations prepared at the inlet air temperature of 130 °C. At last, encapsulation efficiency and loading capacity were evaluated for the RA-loaded microparticles composed by different biopolymers as encapsulating agents. One-way analysis of variance (ANOVA) at $p < 0.05$ and subsequent Tukey test were conducted by Minitab® 19 software.

5.3. Results and discussion

5.3.1. Emulsions characterization

5.3.1.1. Viscosity

Rheological properties of an emulsion play an important role in determining encapsulation efficiency and oil retention. Increasing emulsions viscosity up to an optimal value deals with a decrease of oscillation and internal droplets circulation, contributing to improve both parameters. In turn, emulsions with high viscosity may compromise the encapsulation efficiency and oil retention due to the slower droplet formation and longer exposition during atomization [285]. Also, rheological properties enable to predict the droplet and particle sizes. Emulsions with lower viscosities exhibit smaller droplets and enable the production of particles with smaller size [286].

The emulsions prepared with the biopolymers alginic acid sodium, arabic gum, modified chitosan and gelatin evidenced characteristics relatively close of a Newtonian fluid. Shear stress linearly increased with shear rate (in the case of the arabic gum-based emulsion, this behaviour was registered for a shear rate higher than 9.08 s^{-1}) (Figure 5.1). Apparent viscosity of these emulsions varied between 17.6 ± 0.2, 1.5 ± 0.3, 3.53 ± 0.06 and 2.77 ± 0.06 mPa·s, respectively, considering a shear rate of 100 s^{-1} (Table 5.1). Consistency index (*k*) and flow behaviour index (*n*) (parameters from the Ostwald–de Waele power law (Eq. 5.6), which are used to describe the behaviour of non-Newtonian fluids [287]), were also determined. Consistency index informs about the flow properties of the system (mixture) [288]. For the described emulsions, this parameter increased from 0.0020 ± 0.0003 (arabic gum-base emulsion) to 0.018 ± 0.001 (alginic acid sodium-based emulsion) mPa·s^n (Table 5.1), providing an indication about the increasing of emulsion viscosity (from 1.5 ± 0.3 to 17.6 ± 0.2, respectively (Table 5.1)). The viscosity of emulsions is related to the chemical structure and molecular weight of biopolymers used as encapsulating agents, whereby molecules with long chains and high molecular weights increase the viscosity of emulsions due to the increase of resistance of the aqueous phase to flow [285,286]. In turn, flow behaviour index increased from 0.91 ± 0.01 to 0.99 ± 0.01 with the usage of gelatin, arabic gum, modified chitosan and alginic acid sodium, by this order. Parameter *n* provides an indication about how close the system is to a Newtonian fluid, whereby $n < 1$ indicates a system with pseudoplastic behaviour, $n = 1$ evidence a system with Newtonian behaviour and $n > 1$ show a system with dilatant behaviour [288,289]. The emulsions produced with the mentioned biopolymers revealed, therefore, to be systems close to a Newtonian fluid, as already previously referred.

$$\tau = K\left(\frac{d\mu}{dy}\right)^n \quad \textbf{(5.6)}$$

Where τ is the shear stress, *K* is the consistency index, $\frac{d\mu}{dy}$ is the shear rate and *n* is the flow behaviour index.

An increase of shear rate resulted in the apparent viscosity decrease for the emulsion composed by xanthan gum (from 6228 ± 63 to 99.3 ± 0.2 mPa·s), whereby it showed to be non-Newtonian fluid (Figure 5.2). Goëlo et al. [290] also characterized xanthan-based solutions (without the bioactive compound, with curcumin and with turmeric powder) as non-Newtonian fluids. The flow behaviour index and consistency index were 0.109 ± 0.001

and 6.06 ± 0.02 (mPa·s^n), respectively, for the xanthan emulsion produced in this work. Accordingly, this system was indicated as pseudoplatic fluid. In fact, pseudoplastic fluids usually refer to polymer solutions with high molecular weight compounds. Xanthan gum is a high molecular weight polysaccharide with a molecular weight probably of the order of 2 million but could also be as high as 13-50 million. At low shear rates, it occurs for these systems the formation of shear stress with reordering of the molecules to reduce the overall stress. A higher degree of order in the system enables to reduce the shear stress, with observation of the nonproportionality between the shear rate and the shear force (data not shown) [291].

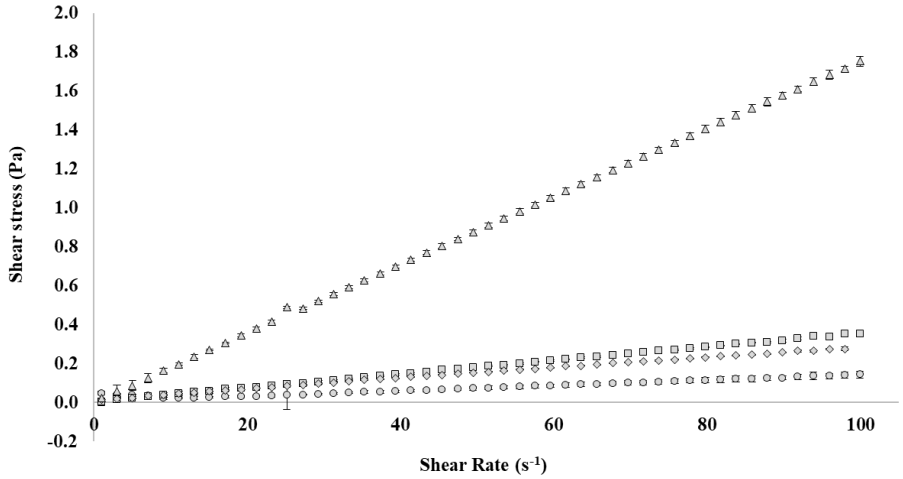


Figure 5.1 – Relation between shear stress and shear rate for the emulsions prepared with modified chitosan (■), arabic gum (▲), alginic acid sodium (●), gelatin (♦). Results are presented as the average and standard deviation of three independent assays

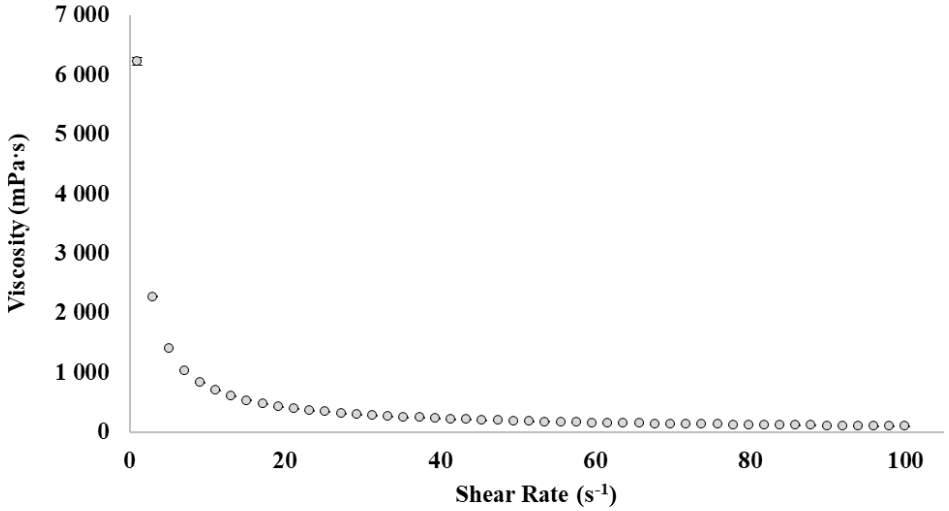


Figure 5.2 – Viscosity curve of the emulsion prepared with xanthan gum. Results are presented as the average and standard deviation of three independent assays.

Table 5.1 – Rheological parameters, apparent viscosity, zeta potential and droplet size of emulsions prepared with different biopolymers.

Emulsions (biopolymeric composition)	**Rheological parameters**		**Apparent viscosity at 100 s^{-1} (mPa·s)**	**Zeta potential (mV)**	**Droplet mean diameter**	
	Consistency index, k ($mPa \cdot s^n$)	**Flow behaviour index, n**			**Differential volume distribution (µm)**	**Differential number distribution (µm)**
Modified Chitosan	0.0041 ± 0.0007	0.97 ± 0.04	3.53 ± 0.06^{b}	-38 ± 6	3.80 ± 0.02^{a}	0.75 ± 0.03^{a}
Arabic gum	0.0020 ± 0.0003	0.92 ± 0.02	1.5 ± 0.3^{d}	-25.8 ± 0.2	1.93 ± 0.09^{b}	0.5 ± 0.3^{ab}
Alginic acid sodium	0.018 ± 0.001	0.99 ± 0.01	17.6 ± 0.2^{a}	-59 ± 9	2.3 ± 0.7^{b}	0.706 ± 0.004^{a}
Gelatin	0.0043 ± 0.0002	0.91 ± 0.01	2.77 ± 0.06^{c}	3.1 ± 0.2	4.8 ± 0.9^{a}	0.13 ± 0.01^{b}
Xanthan gum	6.06 ± 0.02	0.109 ± 0.001	-	0.3 ± 0.6	1.65 ± 0.09^{b}	0.65 ± 0.01^{a}

Different letters in the same column indicate significant differences ($p<0.05$)

5.3.1.2. Stability of colloidal systems

Stability of colloidal systems fed to the spray-dryer is commonly evaluated by the analyses of the percentage of emulsion separation (creaming index) generally 24 h after its preparation [292,293]. This parameter is influenced by the addition of surfactants, as well as the emulsifying properties and viscosity of biopolymers present in the emulsion formulations [293]. In this study, the high proportion of aqueous phase when compared to the oily phase of emulsions prevented the accurate measurement regarding the percentage of emulsion separation. Accordingly, only the zeta potential of emulsions was measured. Zeta potential is referred as a magnitude index of the interaction among colloidal particles, being used to investigate the stability of colloids by measuring the electrokinetic potential of droplets [294].Broadly, particles with a zeta potential value above of $\left|30\right|$ mV are normally considered stable [294]. Among the evaluated emulsion, only the one composed by alginic acid sodium (-59 ± 9 mV) and modified chitosan (-38 ± 6 mV) fulfil this requirement (Table 5.1). The second higher zeta potential value was revealed for arabic gum-based emulsions (-25.8 ± 0.2 mV) (Table 5.1).

The most unstable emulsions were shown to be related to the presence of biopolymers gelatin (3.1 ± 0.2 mV) and xanthan gum (0.3 ± 0.6 mV) (Table 5.1). Stability of emulsions is referred to be related to the encapsulation efficiency of microparticles produced, although in this study this may not be the factor that most influences the encapsulation efficiency. Accordingly, emulsions with a lower stability result in a lower bioactive retention during spray-drying [295]. In this work, modified chitosan- and alginic acid sodium-based microparticles evidenced the higher RA encapsulation efficiency (65 ± 6 and 62 ± 5%, respectively). A lower encapsulation efficiency was registered for arabic gum-, xanthan gum- and gelatin-based microparticles (49 ± 4, 48 ± 2 and 27 ± 1%, respectively)) (section 5.3.6., Table 5.4).

5.3.1.3. Droplet size distribution

Emulsions droplet size is another indication about stability of colloids, influencing the retention of bioactive compounds in the carrier-based delivery systems [285,295]. Generally, larger emulsion droplets are related to a decrease in the encapsulation efficiency [295]. The emulsions produced in this work with the biopolymers alginic acid sodium, arabic gum, modified chitosan, gelatin and xanthan gum exhibited an average droplet diameter that ranged from 1.65 ± 0.09 to 4.8 ± 0.9 μm (differential volume distribution) and from 0.13 ± 0.01 to 0.75 ± 0.03 μm (differential number distribution) (Table 5.1). Arabic gum and gelatin have good emulsifier properties, as previously described (section 5.1.), resulting in the production of emulsions with the smaller droplets (differential number distribution) (Table 5.1). In turn, modified chitosan, alginic acid sodium and xanthan gum contributed for the larger droplets obtained. These results did not enable to deduce about the encapsulation efficiency of microparticles produced. In fact, the higher encapsulating efficiency was achieved for the microparticles composed by modified chitosan and the microparticles composed by alginic acid sodium (65 ± 6 and 62 ± 5%, respectively) and the lower encapsulating efficiency was observed for the microparticles composed by gelatin (27 ± 1%) (section 5.3.6., Table 5.4).

5.3.2. Optimization of the spray-drying inlet air temperature

Poor solubility of retinoids in aqueous systems and their high instability under heat, light and oxidant conditions are some of the major concerns regarding these compounds, as previously mentioned [17,76]. Particularly, RA is extremely sensitive to air, oxidizing agents and UV light (product information from Sigma Aldrich). The operational conditions to be used in the spray-dryer for RA encapsulation must be selected considering these properties of the core material.

Previous studies about vitamin A microencapsulation using spray-drying process report the usage of inlet air temperatures in a range between 120 and 200 ˚C [246–248,296]. Although one of the advantages of this method is the relatively short drying contact time (a few seconds) [15,266], the relatively high temperatures used for the sample drying (usually, inlet and outlet air temperatures are 150-200 ºC and 50-80 ˚C, respectively [297]) might compromise the properties of most heat sensitive compounds [15]. For example, Quek et al. [298] encapsulated watermelon juice into maltodextrin at four different inlet air temperatures (145, 155, 165 and 175 ˚C). The content of β-carotene and lycopene in the spray-dried watermelon particles decreased with the inlet air temperatures increase.

Inlet air temperature is considered the most relevant parameter influencing the properties of microparticles obtained by spray-drying. Its optimization is therefore of great importance to produce microparticles with the an appropriate moisture content, water activity, fluidity and density, considering their final purpose [234]. Higher inlet air temperature increases the drying rate and reduces the moisture content of final microparticles [234]. Consequently, the product yield, encapsulation efficiency, morphology and particle size of microparticles are also affected.

5.3.2.1. Product yield

The product yield of modified chitosan microparticles loaded with RA ranged between 15 and 20% with the inlet air temperature increase (Table 5.2). As the moisture content of microparticles decreases, the amount of microparticles remaining in the cylinder or/and on the cyclone wall is lower, moving towards the recovery vessel of spray-dryer [254]. The relationship existing between these two variables was reported by other authors, such as Santhalakshmy et al. [299] when they spray-dried jamun juice using maltodextrin (with 20 DE). Herein, the highest product yield (8.25%) was registered at 150 ºC.

Table 5.2 – Product yield and physical properties of RA loaded-modified chitosan-based microparticles produced at different inlet air temperatures.

Inlet air temperature (˚C)	Product yield (%)	Encapsulation efficiency (%)	Particle mean diameter	
			Differential volume distribution (μm)	Differential number distribution (μm)
115	15	48 ± 4^{b}	1.712 ± 0.004^{c}	0.641 ± 0.006^{a}
130	18	65 ± 6^{a}	12.9 ± 0.3^{a}	0.59 ± 0.04^{a}
150	20	56 ± 5^{b}	11.7 ± 0.6^{b}	0.38 ± 0.01^{b}

Different letters in the same column indicate significant differences ($p<0.05$)

Also, Jog and Burgess [300] recorded an increased product yield of spray-dried nanocrystalline zileuton (≥ 75%) with the increase of the inlet air temperature (> 115 ºC).

5.3.2.2. RA retained in the microparticles

RA content effectively retained in the microparticles produced (encapsulation efficiency) was significantly influenced by the inlet air temperature ($p<0.05$). The increasing inlet air temperature from 115 to 130 ºC benefited modified chitosan-based microparticles with the significant increase of the encapsulation efficiency ($p<0.05$) from 48 ± 4 to 65 ± 6% (Table 5.2). In fact, the highest encapsulation efficiency was recorded for the microparticles produced at the inlet air temperature of 130 ℃. This condition increased the droplets drying rate, occurring the rapid formation of a particle crust with a firm membrane due to the higher water evaporation rate [234,301]. Accordingly, the core material composed by oily phase with RA is prevented to leak from the microparticles formed. Aghbashlo et al. [301] registered a similar behaviour when encapsulated fish oil into several formulations using different drying air temperatures (140, 160 and 180 ºC). On the other hand, the lower moisture content of microparticles obtained reduces the RA exposition against feasible damaging conditions. The increase of inlet air temperature up to 150 ºC significantly decreased the encapsulation efficiency from 65 ± 6 to 56 ± 5% (Table 5.2). An over water evaporation might have been occurred with the formation of microparticles with a fragile membrane [234,302]. Consequently, the RA release might have been induced. Furthermore, considering that RA is a heat sensitive compound, its exposition to higher temperatures may have favoured the thermal and/or oxidative degradation of this retinoid.

5.3.2.3. Morphology

Modified chitosan-based microparticles loaded with RA produced at different inlet air temperatures exhibited a surface structure overall similar (Figure 5.3). They are characterized as small spheres with small concavities overall distributed, which gives the microparticles the rough appearance. Other studies report a different morphology for microparticles also composed by modified chitosan as encapsulating agent [249,303]. In these cases, modified chitosan microparticles present a very smooth surface. The formulation composition used in the present work (section 5.2.2.) may have affected the final aspect of surface of the microparticles obtained. The increase of inlet air temperatures in microparticles production had some impact on their morphology. The microparticles produced at 115 ℃ of inlet air temperature exhibited a slightly unstructured appearance when compared to the ones obtained at 130 ºC (Figure 5.3 A, B, D and E). In turn, microparticles formed at 150 ºC showed to be the most unstructured, in addition to show some cracks on the surface (Figure 5.3 C and F). These characteristics can be related to the drying process involved in the microparticles formation at different inlet air temperatures, as previously referred [234]. Santiago-Adame et al. [304] used maltodextrin for the production of cinnamon Infusions loaded microparticles by spray-drying at 140, 160 and 180 ºC of

inlet air temperature. Microparticles with more defined and smoother surfaces were obtained with the inlet air temperature increase.

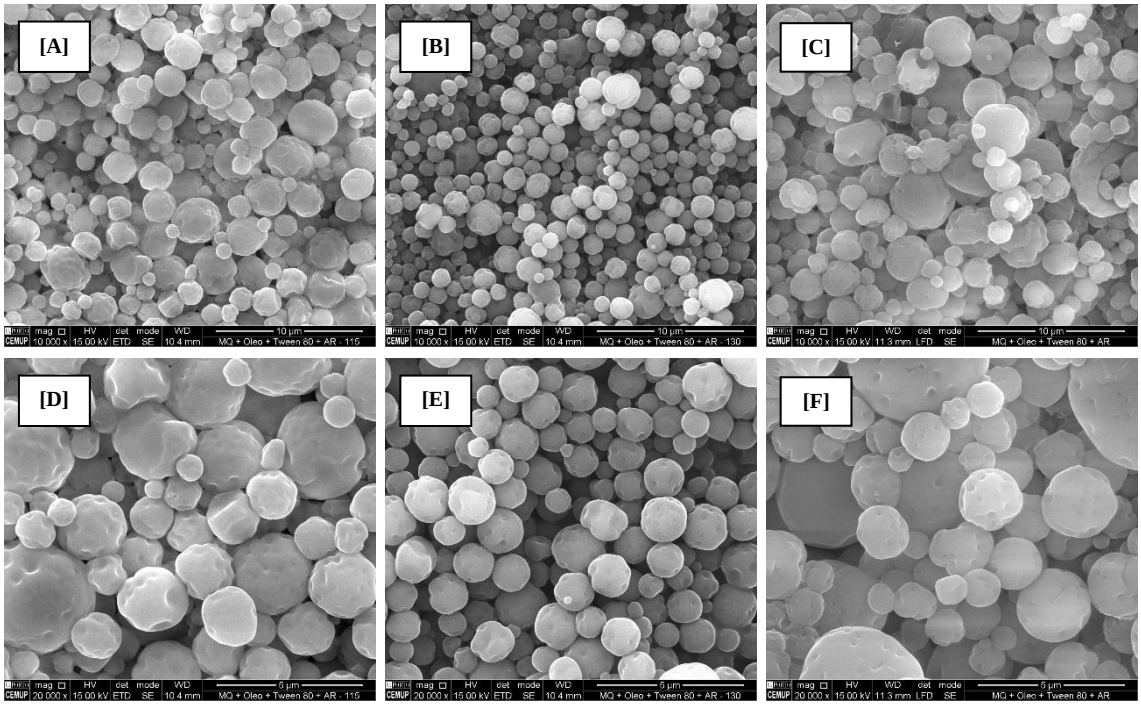


Figure 5.3 – Surface morphology of RA-loaded-modified chitosan-based microparticles produced at 115 ̊C (A and D), 130 ̊C (B and E) and 150 ̊C (C and F) of inlet air temperature. Magnification =10,000 (A, B and C) and 20,000 (D, E and F) times, beam intensity (HV) 15.00 kV, distance between the sample and the lens (WD) around 10 mm.

5.3.2.4. Particle size

Particle mean diameter of modified chitosan-based microparticles significantly varied with the inlet air temperatures tested ($p<0.05$) (differential volume distribution) (Table 5.2). Particularly, with the increase of inlet air temperature from 115 to 130°C and from 115 to 150 °C, the particle size increased from 1.712 ± 0.004 to 12.9 ± 0.3 µm and from 1.712 ± 0.004 to 11.7 ± 0.6 µm, respectively (Table 5.2). Zare et al. [305] observed the same tendency when produced sour orange powder at constant air flow rate and increased the inlet air temperature conditions. Regarding the differential number distribution, the lowest particle mean diameter of microparticles was registered at 150 °C of inlet air temperature. Accordingly, the increase of inlet air temperature seems to promote the production of microparticles with higher volume (it can be explained by the aggregation of microparticles) under the evaluated inlet air temperature conditions, which explains the discrepancy of particle mean diameter showed in terms of volume and number distribution.

5.3.2.5. Controlled release profiles

The fastest RA controlled release was observed from modified chitosan-based microparticles produced at 130 ˚C of inlet air temperature. The release profile stabilized (*i.e.* the cumulative amount of RA present in the surrounding environment (octanol) reached a constant value due to its complete release) 138 min after the beginning of the assay (Figure 5.4). For microparticles composed with the same encapsulating agent but produced at 115 ºC and 150 ºC, similar RA release profiles were registered and they prolonged for 178 and 232 min, respectively (Figure 5.4). The higher amount of RA retained in the microparticles produced at 130 ˚C (Table 2) may have impacted the increased release rate of RA to the surrounding environment.

In the line with these topics discussed, 130 ºC is the most appropriate inlet air temperature for drying the emulsions and the production of RA loaded biopolymer-based microparticles. This condition was selected for further experiments, wherein arabic gum, alginic acid sodium, gelatin and xanthan gum were investigated for RA encapsulation.

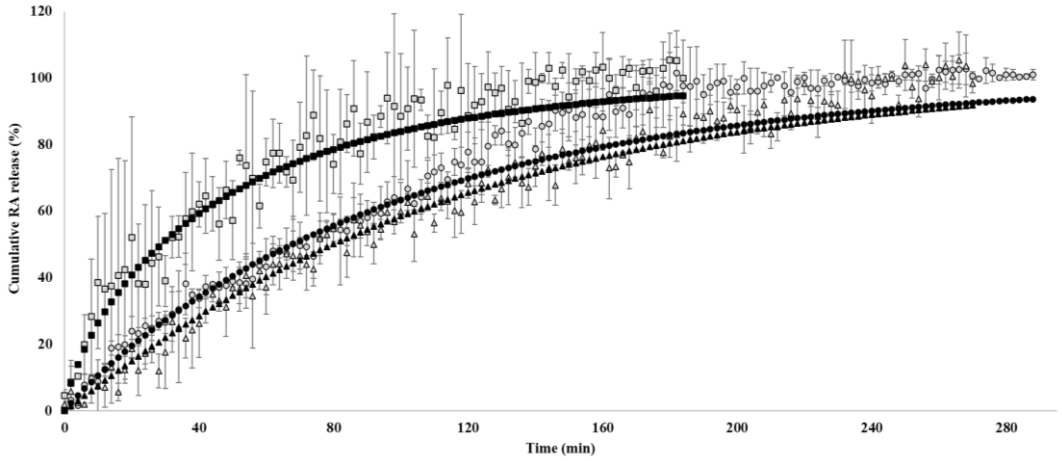


Figure 5.4 – Cumulative RA release from modified chitosan-based microparticles produced at 115 ˚C (●), 130 ˚C (■) and 150 ˚C (▲) of inlet air temperature. Results are presented as the average and standard deviation of three independent assays. Weibull model was fitted to the obtained controlled release profiles: 115 ˚C (●), 130 ˚C (■) and 150 ˚C (▲).

5.3.3. Biopolymer-based microparticles characterization

Microparticles only composed by the encapsulating agent (unloaded microparticles – microparticles MpE), loaded with coconut oil and tween 80 (microparticles MpOT) and loaded with RA dissolved in coconut oil and mixed with tween 80 (microparticles MpRA) were produced using different biopolymers as encapsulating agents. Product yield varied from 28 to 41% among microparticles MpE, 12 to 26% among microparticles MpOT and 18 to 30% among microparticles MpRA (Table 5.3). Product yield is influenced by the volume and the composition of the system fed to the spray-dryer, in addition to the operational conditions implemented in the spray-dryer as previously discussed (section 5.3.2.1.).

Table 5.3 – Product yield, emulsion volume and particle diameter of microparticles produced using different formulations.

Microparticles content		Particle mean diameter		Product yield (%)	Emulsion volume used in the spray-dryer (mL)
Formulation	**Encapsulating agent**	**Differential volume distribution (µm)**	**Differential number distribution (µm)**		
MpE	Modified Chitosan	4.95 ± 0.02^{d}	0.168 ± 0.006^{h}	41	100
	Arabic gum	4.3 ± 0.4^{ef}	0.628 ± 0.006^{d}	29	100
	Alginic acid sodium	2.87 ± 0.04^{gh}	0.15 ± 0.01^{h}	39	100
	Gelatin	3.89 ± 0.02^{f}	0.29 ± 0.04^{g}	32	200
	Xanthan gum	3.30 ± 0.03^{g}	0.529 ± 0.005^{f}	28	200
MpOT	Modified Chitosan	2.97 ± 0.02^{gh}	0.92 ± 0.02^{bc}	18	100
	Arabic gum	3.31 ± 0.02^{g}	0.61 ± 0.01^{de}	26	100
	Alginic acid sodium	2.79 ± 0.01^{h}	1.03 ± 0.02^{a}	17	100
	Gelatin	4.4 ± 0.1^{e}	0.121 ± 0.003^{h}	12	200
	Xanthan gum	2.90 ± 0.02^{gh}	0.99 ± 0.04^{ab}	16	200
MpRA	Modified Chitosan	12.9 ± 0.3^{a}	0.59 ± 0.04^{def}	18	200
	Arabic gum	7.9 ± 0.2^{b}	0.54 ± 0.02^{ef}	27	200
	Alginic acid sodium	5.9 ± 0.2^{c}	1.045 ± 0.005^{a}	30	200
	Gelatin	7.8 ± 0.1^{b}	0.60 ± 0.04^{de}	30	300
	Xanthan gum	5.5 ± 0.2^{c}	0.62 ± 0.41^{c}	24	500

Different letters in the same column indicate significant differences ($p<0.05$)

A larger volume used increases the product yield. In turn, the encapsulating agent' properties and the type of formulation fed to the spray-dryer are the main factors affecting the product yield. In this work, for all the microparticles produced (MpE, MpOT and MpRA) a larger volume of xanthan gum- (200, 200 and 500 mL, respectively) and gelatin-based emulsions (200, 200 and 300 mL, respectively) was required to increase and obtain a product yield closer to the one recorded when alginic acid sodium-, modified chitosan- and arabic gum-based emulsions, prepared with a lower volume (100, 100 and 200 mL to produce microparticles MpE, MpOT and MpRA, respectively), were fed to the spray-dryer (Table 5.3). The properties of biopolymers used as encapsulating agents may have influenced the amount of powder that was possible to be collected in the spray-dryer. High viscosity of xanthan gum-based solutions and also xanthan gum-based emulsions clearly led to the preparation of the largest emulsion volume to produce microparticles MpRA (Table 5.3). Regarding microparticle formulations, the addiction of coconut oil to the system fed to the spray-dryer (to produce an emulsion together with the encapsulating agent solutions, with and without the core material) decreased the product yield. This behaviour is less evident for the microparticles MpRA due to the preparation of a larger volume of emulsions (in most of the cases, double or more than double of the volume) when compared to the volume of emulsions and solutions considered to produce the microparticles MpOT and MpE,

respectively (Table 5.3). Other studies reported show a more pronounced reduction of this parameter due to the usage of an oily-based formulation to encapsulate liposoluble bioactive compounds [245].

5.3.4. Surface morphology of microparticles

Microparticles MpE showed to be spherical structures with different morphologies due to the biopolymers used in their formulation (Figure 5.5 – A, B, C, D and E). Modified chitosan-based microparticles exhibited a very smooth surface (Figure 5 – A), while alginic acid sodium showed a smooth surface with scarce concavities (Figure 5.5– C). As previously described, some studies report the production of microparticles with a similar morphology when modified chitosan was used as encapsulating agent [249,303]. Moreover, Chaumun et al. [306] produced different types of microparticles using alginate for incorporation of *Laurus nobilis* L. extract, but therein the microparticles evidenced several concavities, which provided a slightly rough surface. In turn, microparticles composed by arabic gum and microparticles composed by gelatin evidenced a rough surface (Figure 5.5 – B and D, respectively). Di Battista et al. [307] produced arabic gum-based microparticles for encapsulation of phytosterols, which evidenced a similar rough surface. Also, Estevinho et al. [308] observed this morphology when they produced folic acid-loaded microparticles using arabic gum. However, Li et al. [309] produced a novel gelatin microcapsule to benefit ibuprofen, which showed a smooth surface. At last, xanthan-based microparticles evidenced a high rough and irregular surface (Figure 5.5 – E).

The inclusion of an oily phase (coconut oil, with or without RA) and surfactant to the encapsulating agent solution resulted in several changes regarding the morphology of several microparticles. Microparticles MpOT and MpRA composed by modified chitosan (Figure 5.5 – F and K, respectively) and alginic acid sodium (Figure 5.5 – H and M, respectively) gained relief by the presence of several concavities on their surface. In turn, arabic gum-based microparticles (Figure 5.5– G and L) evidenced a smoother surface.However, microparticles with gelatin (Figure 5.5– I and N) as well as with xanthan gum (Figure 5.5– J and O) do not evidence modifications on their morphology. These results point out the effect of microparticles composition in their surface structure.

5.3.5. Microparticle particle size measurement

Microparticles MpE and MpOT showed a particle mean diameter between 2.79 ± 0.01 and 4.95 ± 0.02 μm (Table 5.3), considering a differential volume distribution. Incorporation of RA into the biopolymer-based formulations resulted in microparticles with a higher size, which ranged between 5.5 ± 0.2 (with xanthan gum) and 12.9 ± 0.3 μm (with modified chitosan) (Table 5.3). Differential number distribution evidenced an overall particle mean diameter between 0.121 ± 0.003 and 1.045 ± 0.005 μm (Table 5.3). Herein, the smaller and higher size refer to microparticles MpOT composed by gelatin and microparticles MpRA composed by alginic acid sodium, respectively.

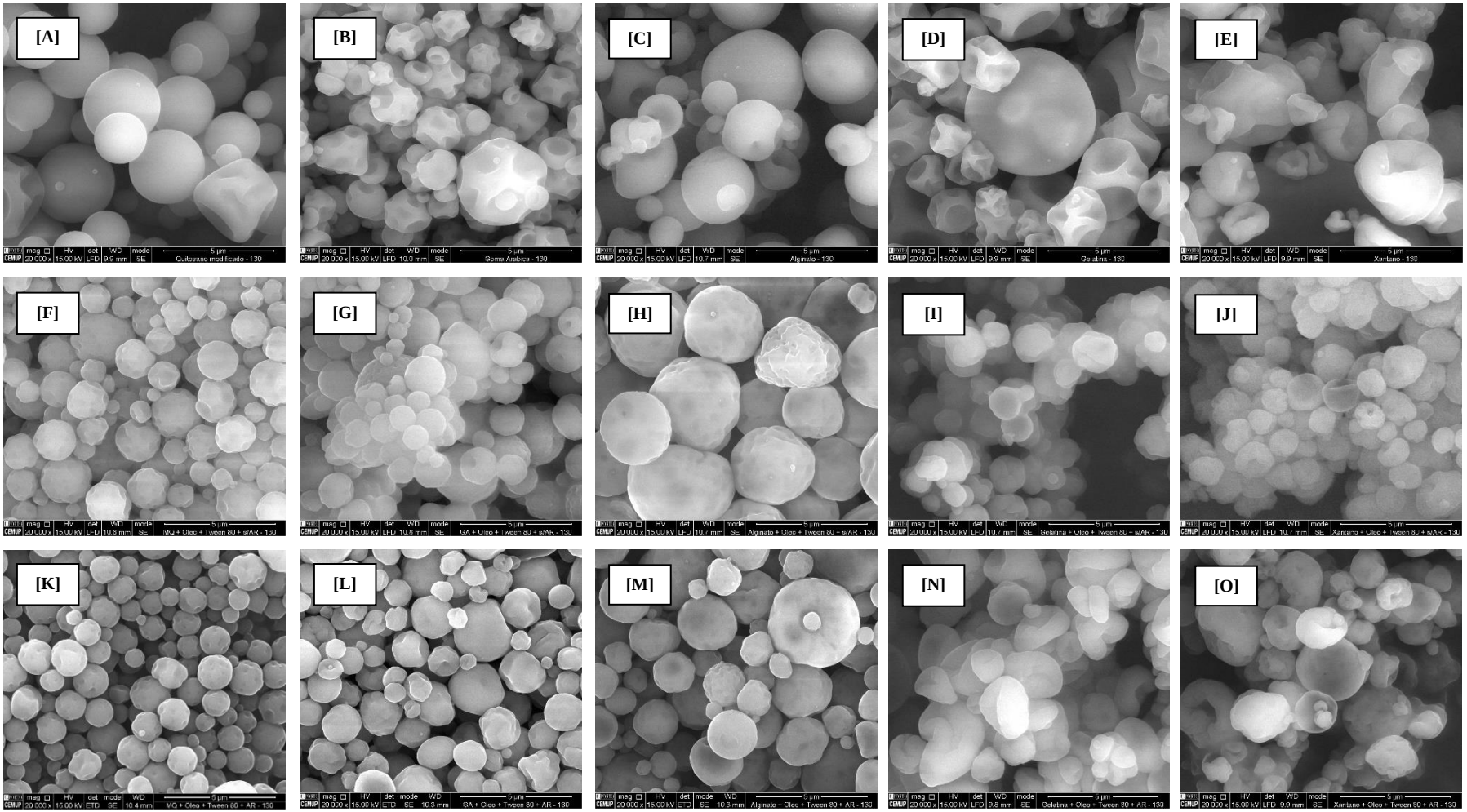


Figure 5.5 – Surface morphology of MpE (A, B, C, D and E), MpOT (F, G, H, I and J) and MpRA (K, L, M, N and O) microparticles composed by modified chitosan (A, F and K), arabic gum (B, G and L), alginic acid sodium (C, H and M), gelatin (D, I and N) and xanthan gum (E, J and O). Magnification = 20,000 times, beam intensity (HV) 15.00 kV, distance between the sample and the lens (WD) around 10 mm.

5.3.6. Encapsulation efficiency and loading capacity

Encapsulation efficiency and loading capacity varied from 27 to 65% and from 0.0078 to 0.019%, respectively (Table 5.4). An increase in both parameters was registered in the order of gelatin, xanthan gum, arabic gum, alginic acid and modified chitosan. Encapsulation efficiency was significantly higher for modified chitosan- and alginic acid sodium-based microparticles (65 ± 6% and 62 ± 5%, respectively) ($p<0.05$) (Table 5.4). The ability of microparticles to retain the core material is largely dependent on the encapsulating agent composition [234]. Polysaccharides provide an effective encapsulation efficiency due to their large molecular structure. The presence of different reactive groups in their structure promotes the interaction with several molecules. Moreover, it must be pointed out the high stability of polysaccharides, while proteins can be denatured during processing at high temperatures. However, both polysaccharides and proteins have been reported as good carrier-based delivery systems [310]. Other studies using spray-drying technology report general higher values of encapsulation efficiency when the same biopolymers were used as encapsulating agents. Chaumun et al. [306] encapsulated gallic acid and *Laurus nobilis* L. extract into modified chitosan- and alginate-based microparticles with an efficiency between 95.4 ± 3.5 – 97.6 ± 3.3 and 90.2 ± 1.5– 99.3 ± 0.6%, respectively. In turn, arabic gum enabled an encapsulation efficiency of 72.9 ± 6.7% for gallic acid and 96.1 ± 3.7% for *L. nobilis* L. extract. On the other hand, Carlan et al. [311] reached a full encapsulation when incorporated vitamin B1 into xanthan-based microparticles. At last, Aguiar et al. [312] obtained an encapsulation efficiency of orange essential oil into gelatin between 9.37 and 97%.

Table 5.4 – Encapsulation efficiency and loading capacity of RA-loaded microparticles obtained using different encapsulating agents.

Encapsulating agent	Encapsulation efficiency (%)	Loading capacity (%)
Modified Chitosan	65 ± 6^{a}	0.019 ± 0.002^{a}
Arabic gum	49 ± 4^{bc}	0.014 ± 0.001^{bc}
Alginic acid sodium	62 ± 5^{ab}	0.018 ± 0.001^{ab}
Gelatin	27 ± 1^{d}	0.0078 ± 0.0004^{d}
Xanthan gum	48 ± 2^{c}	0.0141 ± 0.0007^{c}

Different letters in the same column indicate significant differences ($p<0.05$)

5.3.7. Drug controlled release assay

The release behavior of RA from microparticles composed by different biopolymers was performed in octanol at 37 ℃. The aim is to understand the ability of RA to cross the lipid membranes of the living system [258,259,283]. For this study it was considered that RA-loaded microparticles remain relatively intact until reaching the intestine. However, the effective behaviour of microparticles along gastrointestinal tract only can be achieved in gastrointestinal simulation studies. These studies are of major importance for the microparticles that show a greater prospective for the treatment of acute promyelocytic leukaemia. An improvement in the microparticles formulation might be eventually required.

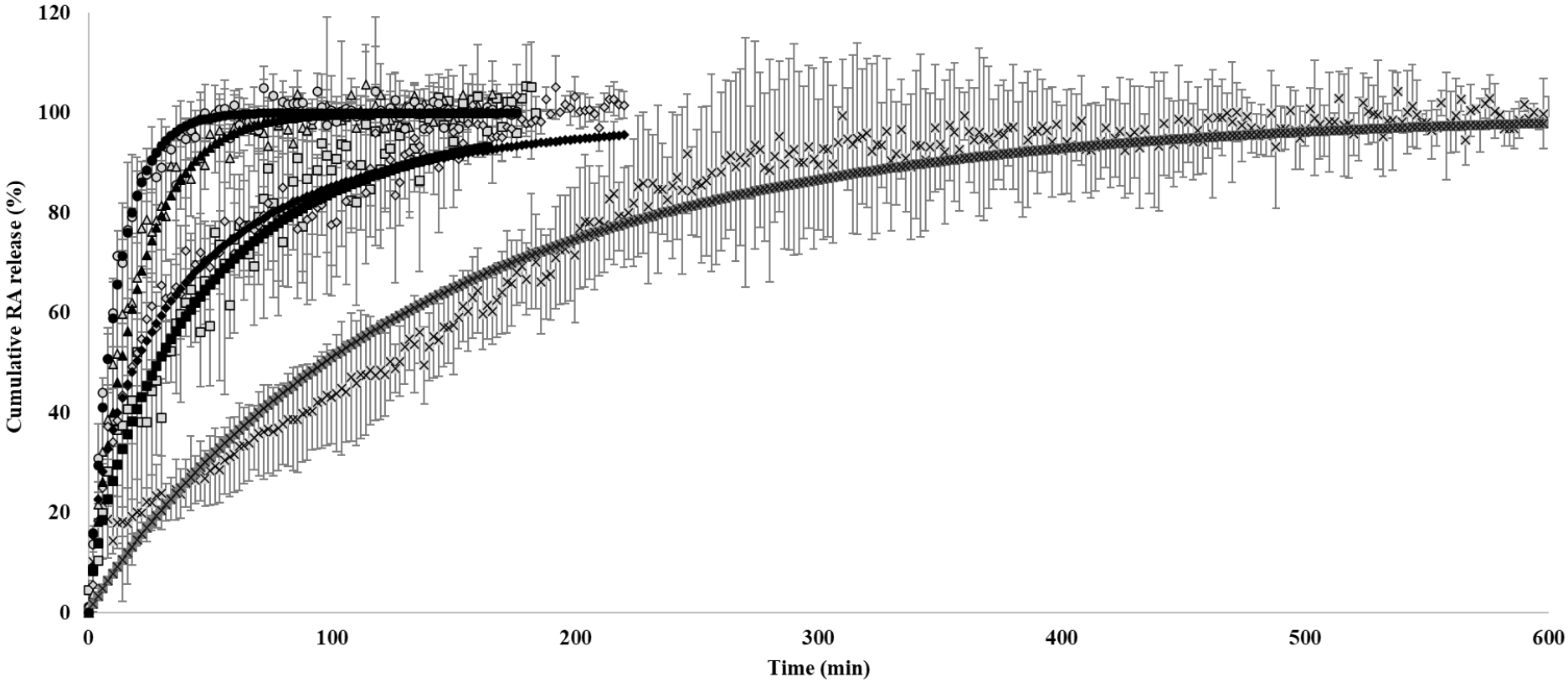


Figure 5.6 – Cumulative RA release from biopolymer-microparticles individually composed by modified chitosan (■), arabic gum (▲), alginic acid sodium (×), gelatin (♦) and xanthan gum (●). Results are presented as the average and standard deviation of three independent assays. Weibull model was fitted to the obtained controlled release profiles: modified chitosan (■), arabic gum (▲), alginic acid sodium (×), gelatin (♦) and xanthan gum (●).

Controlled release profiles obtained by cumulative percentage of RA over time are presented in Figure 5.6. Xanthan gum- and arabic gum-based microparticles enabled the fastest release of RA to the surround environment, which occurred in 48 and 94 min, respectively. A slightly slower release was obtained from microparticles composed by modified chitosan and gelatin. Herein, RA controlled release profile stabilization was observed 138 and 156 min (more than 2 h) after the beginning of the experiment. The slowest release of core material was recorded when the microparticles formulation included alginic acid sodium, prolonging for almost 8 h. Within the scope of APL treatment, the proposal of a slower drug controlled delivery system is the most appropriate to reduce the activation of cytochrome P450.

Other studies report the impact about the formulation composition in the drug controlled release behaviour, but also of the release media used. For instance, Ribeiro et al. [313] produced elderberry extract-loaded microparticles using modified chitosan, sodium alginate and arabic gum as encapsulating agents, considering a spray-drying method. The faster release in deionised water was achieved with modified chitosan (600 s), followed by arabic gum (1000 s) and sodium alginate (1140 s). Moreover, and considering a recent study about RA encapsulation, Gonçalves et al. [278] investigated the incorporation of RA (dissolved in ethanol) into arabic gum, alginic acid sodium and modified chitosan microparticles also using the spray-drying technology. An increase of RA controlled release rate was observed with the usage of alginic acid sodium (more than 7 h), arabic gum (36 min) and modified chitosan (7 min) as encapsulating agents.

5.3.8. Kinetic models

A correlation coefficient in a range from 0.911 and 0.990 was obtained when the kinetics of zero order (describes a slow and constant release rate) was fitted to the RA controlled release profiles (Table 5.5). The zero-order release constant, K_0, increased from 5.0×10^{-6} to 8.0×10^{-5} mg·min^{-1}, considering the usage of alginic acid sodium, gelatin, modified chitosan, arabic gum and xanthan gum as encapsulating agents (Table 5.5). This behaviour is in agreement with an increase of RA release rate in the same conditions. For Higuchi model the Higuchi constant, K_H, followed the same tendency of K_0, varying from 9.0×10^{-5} and 3.0×10^{-4} mg·min$^{-0.5}$ (Table 5.5). Herein, the correlation coefficient varied from 0.982 to 0.992.

Korsmeyer-Peppas model was fitted to the linear RA controlled release profiles considering the Q_t/Q_∞ is lower than 0.6 [262]. For all the biopolymer-based microparticles the parameter n varied between 0.43 and 0.85 (n = 0.5 for alginic acid sodium and gelatin formulations, n = 0.6 for modified chitosan formulations and n = 0.7 for arabic gum and xanthan gum formulations (Table 5.5), suggesting an anomalous transport which results from the combination of diffusion mechanisms and swelling release (case II transport) and a t^{n-1} rate as a function of time was evidenced for these microparticles [145,262]. The Korsmeyer constant, K_K, increased from 0.04 (considering alginic acid sodium-based microparticles) to 0.1 min^{-n} (for all the other biopolymer-based microparticles) in the same line with the increase of RA release rate (Table 5.5). The correlation coefficients with Korsmeyer-Peppas model varied from 0.831 to 0.938 (Table 5.5).

Table 5.5 – Parameters and correlation coefficients of the models of zero-order, Higuchi, Korsmeyer-Peppas and Weibull applied to the experimental RA release profiles.

	Parameters		Encapsulating agents				
			Modified chitosan	**Arabic gum**	**Alginic acid sodium**	**Gelatin**	**Xanthan gum**
Kinetic models	**Zero-order**	K_0 **(mg·min^{-1})**	2.0×10^{-5}	5.0×10^{-5}	5.0×10^{-6}	2.0×10^{-5}	8.0×10^{-5}
		Q_0 **(mg)**	4.0×10^{-4}	1.0×10^{-4}	2.0×10^{-4}	7.0×10^{-5}	6.0×10^{-5}
		R^2	0.911	0.940	0.990	0.931	0.984
	Higuchi	K_H **(mg·min$^{-0.5}$)**	2.0×10^{-4}	2.0×10^{-4}	9.0×10^{-5}	9.0×10^{-5}	3.0×10^{-4}
		R^2	0.992	0.986	0.989	0.992	0.982
	Korsmeyer-Peppas	K_k **(min^{-n})**	0.1	0.1	0.04	0.1	0.1
		n	0.6	0.7	0.5	0.5	0.7
		R^2	0.937	0.831	0.920	0.860	0.938
	Weibull	τ_d **(min)**	46	19	143	35	11
		β	0.8	1.03	0.9	0.6	1.02
		R^2	0.937	0.884	0.916	0.966	0.986

Weibull model was fitted to the RA controlled release profiles with correlation coefficients varying from 0.884 to 0.986 (Table 5.5). The β parameter was lower than 1 for modified chitosan- (β = 0.8), alginic acid sodium- (β = 0.9) and gelatin-based microparticles (β = 0.6) (Table 5.5). Accordingly, the shape of the curve would show a steeper increase regarding the shape of the release curve that corresponds exactly to the shape of an exponential profile [262]. In turn, for arabic gum- and xanthan gum-based microparticles the β parameter was higher than 1 (β = 1.03 and β = 1.02, respectively) (Table 5.5), suggesting the shape of the curve gets sigmoidal with a turning point [262]. T_d parameter was determined from RA release profiles when 63.2% of the active compound was released. It varied from 11 min to 143 min, when xanthan gum and alginic acid sodium were used as encapsulating agents, respectively (Table 5.5).

Weibull model enabled a full fitting of the RA controlled release profiles obtained from all the microparticles produced in this work. In fact, it is described as the most appropriate model to describe the release of an active compound from a matrix-based delivery system [260], the typical morphology of powders produced by spray-drying technology [266]. Gonçalves et al. [278] also reported the Weibull model as the most capable to characterize the RA release profiles from biopolymer-based microparticles obtained by spray-drying.

5.4. Conclusion

Microparticles composed by alginic acid sodium, modified chitosan, arabic gum, gelatin and xanthan gum were successfully produced from oil-in-water emulsions by spray-drying technology for controlled delivery of RA. Inlet air temperature of spray-dryer significantly interferes with the encapsulation efficiency, being achieved the highest RA retention for the modified chitosan-based microparticles produced at 130 °C (65 ± 6%). The usage of different biopolymers in the formulations influences the characteristics of the emulsions (*i.e.* viscosity, stability and droplet size) as well as the product yield and the main characteristics of carrier-based systems produced, including their morphology and RA controlled release profiles. Xanthan gum and arabic gum-based microparticles enable the faster release of RA, while the slower RA release was obtained from alginic acid sodium-based microparticles (almost 8 h).

Chapter 6 – Microencapsulation of retinoic acid by atomization into biopolymeric matrices: binary and ternary blends of alginic acid sodium, xanthan gum and modified chitosan

---

The sixth chapter presents binary and ternary blends of biopolymers – xanthan gum + alginic acid sodium, modified chitosan + alginic acid sodium, modified chitosan + xanthan gum and modified chitosan + xanthan gum + alginic acid sodium – to prepare oil-in-water emulsions for the preparation of RA-loaded biopolymer-based delivery systems using spray-drying technology.

This chapter is published in:

Gonçalves, A; Estevinho, B N; Rocha, F. Microencapsulation of retinoic acid by atomization into biopolymeric matrices: Binary and ternary blends of alginic acid sodium, xanthan gum and modified chitosan. Food Hydrocolloids. 2022, 124, Part B, 107310, https://doi.org/10.1016/j.foodhyd.2021.107310.

6.1. Introduction

Encapsulation technology has been requested for the development of carrier-based systems capable to improve the chemopreventive and chemotherapeutic action of retinoic acid (RA) in the treatment of several pathologies [17]. Low aqueous solubility, high instability under unfavourable conditions (*i.e.* moisture, pH, oxygen, heat and light, among others) and gastrointestinal malabsorption of RA contribute to decrease the bioavailability of this retinoid in the human body. Moreover, in the treatment of acute promyelocytic leukaemia (APL), continuous repetitive oral administration of RA is associated to a significant decrease of RA half-life in blood, occurring a notable decrease of RA concentration in the plasma [25,26,58]. Some hypothesis were proposed to explain this behaviour [58], one of which is related to the activation of cytochrome P450 enzymes. They are involved in the regulation of cellular levels of RA, triggering the catabolism of this bioactive compound even when it is present in a small amount [277]. Although RA is the only effective strategy to treat APL [274], patients ultimately become resistant to this retinoid despite of the continued treatment.

The usage of a formulation for oral RA administration oriented towards a drug controlled delivery system might promote the stabilization of RA until its release at the target site (in the intestine) and at an appropriate rate reducing the activity of cytochrome P450 enzymes. RA absorption can be therefore optimized with a consequent improvement of RA bioavailability in APL patients, contributing for a more efficient treatment. Furthermore, this strategy might also beneficiate the patients decreasing the side-effects related to the administration of this antitumor agent (*i.e.* headache, nausea, abdominal pain and retinoid acute resistance, among others [28,58–60]).

Spray-drying technique has been explored by the authors for the encapsulation of RA into biopolymer-based microparticles for therapeutic applications, particularly related to the treatment of APL. It is a one-step method recognized as a rapid, continuous (continuous batch), reproducible, low cost and of easy scale up process [193]. Microparticles with good quality are produced by spray-drying without resorting to organic solvents. Gonçalves et al. [278] incorporated RA (dissolved in ethanol) into microparticles individually composed by alginic acid sodium, modified chitosan and arabic gum as encapsulating agents (prepared in ultra-pure water). The RA release rate slightly decreased from modified chitosan- to arabic gum-based microparticles (from 99 to 102 min). The slowest RA release was verified from alginic acid sodium-based microparticles and lasted for more than 7 hours. Afterwards, Gonçalves et al. [314] spray-dried oil-in-water emulsions composed by RA dissolved in coconut oil (oily phase), a surfactant (tween 80) and a biopolymer aqueous solution (alginic acid sodium, modified chitosan, arabic gum, gelatin and xanthan gum were individually used as encapsulating agents). For the modified chitosan- and alginic acid sodium-based microparticles the encapsulation efficiency was significant higher (65 and 62%, respectively) when compared to the one obtained for the other microparticles formulations loaded with RA. Regarding RA controlled release studies, the fastest release was achieved from xanthan- and arabic gum-based microparticles (48 and 94 min, respectively), while the alginic acid sodium-based microparticles enabled the slowest release for almost 8 hours.

In the present work, biopolymers blends-based delivery systems for RA encapsulation were proposed, attending to the biopolymers that individually enabled the production of RA-loaded microparticles with the most advantageous characteristics (of which, encapsulation efficiency and RA release rate were evaluated so far) for

further RA oral administration in the treatment of APL – alginic acid sodium, xanthan gum and modified chitosan – [314]. Binary and ternary blends (xanthan gum + alginic acid sodium, modified chitosan + alginic acid sodium, modified chitosan + xanthan gum and modified chitosan + xanthan gum + alginic acid sodium) were considered to prepare oil-in-water emulsions for the RA-loaded microparticles formation using spray-drying technology. The obtained formulations were compared to each other, as well as compared regarding to the formulations wherein these encapsulating agents were individually used. An updated screening of the most satisfactory microsystems for the delivery of RA into APL patients was accomplished. Data on encapsulation efficiency, morphology, particle size and RA controlled release were herein considered.

6.2. Material and Methods

6.2.1. Materials

All-trans RA (≥ 98%, R2625-1G, CAS 302-79-4), coconut oil from *Cocos nucifera* (C1758-500G, Lot#MKCK3631, CAS 8001-31-8), tween 80 (P1754-1L, Lot#BCBT8094, CAS 9005-65-6), alginic acid sodium salt (180947-500G, Lot#MKBS5877V, CAS 9005-38-3, MW: between 120,000 and 190,000 $g \cdot moL^{-1}$, ratio of mannuronic acid to guluronic acid (M/G ratio): 1.56, country of manufacture: United Kingdom) and xanthan gum from *Xanthomonas campestris* (G1253-100G, Lot#SLCC2817, CAS 11138-66-2, country of manufacture: USA) were purchased from Sigma-Aldrich (Saint Louis, USA). Modified chitosan (pharmaceutical grade water-soluble chitosan, obtained by carboxylation, deacetylation degree of 96.5%, viscosity of 5 mPa·s (1%; 25 °C)) was obtained by China Eastar Group (Dong Chen, China) (Batch no. SH20091010). 1-Octanol for synthesis (820931, CAS 111-87-5) was supplied from Merck (Darmstadt, Alemanha). Ethanol (99%) was obtained from Valente e Ribeiro, Lda® (Alcanena, Portugal).

6.2.2. Preparation of emulsions

Emulsions were prepared using a proportion of encapsulating agents and coconut oil of 2.77 $g \cdot g^{-1}$ (optimized in a previous study regarding the maximum amount of coconut oil that was possible to incorporate in the microparticles without their quality being compromised) and following the method described by Gonçalves et al. [314]. Binary and ternary biopolymers blends (xanthan gum + alginic acid sodium (50%-50%), modified chitosan + alginic acid sodium (50%-50%), modified chitosan + xanthan gum (50%-50%) and modified chitosan + xanthan gum + alginic acid sodium (33.3%-33.3%-33.3%)) were used to prepare solutions of encapsulating agents in ultra-pure water (final concentration of 1% (w/v)). Coconut oil was used to dissolve RA (0.1% (w/v)) and to the obtained solution the surfactant tween 80 was added (0.5% (w/v)). Oil-in-water emulsions were produced by dispersing this final mixture with each encapsulating agents blending solution at 20000 rpm for 10 min (the emulsion prepared with modified chitosan + alginic acid sodium was prepared at 12000 rpm for 5 min) using a mechanical homogenizer (CAT, Germany).

6.2.3. Spray-drying technique

Emulsions were dried using a mini spray-dryer B-290 from BÜCHI (Flawil, Switzerland) with a standard cyclone and a standard 0.5 mm nozzle. For the microparticles production, inlet air temperature, air pressure and atomization air flow rate were set at 130 ºC, 5-6 bar and 35 $m^3 \cdot h^{-1}$ (90%), respectively. These conditions were previously optimized, particularly regarding the inlet air temperature [314]. Feed flow rate varied between 3 and 5 $mL \cdot min^{-1}$ to maintain the outlet air temperatures close to 70 ºC. The obtained dry powder with encapsulated RA was recovered from the cyclone and the collection vessel of spray-dryer, covered with aluminium foil (protection against light exposition) and stored under refrigeration until further analysis. The product yield (%) was determined according to Eq. 6.1.

$$Product\ yield\ (\%) = \frac{Microparticles\ weight\ recovered\ in\ the\ cyclone\ and\ the\ collection\ vessel\ of spray-dryer}{Total\ mass\ of\ raw\ materials\ used\ to\ prepare\ the\ systems\ fed\ to\ the\ spray-dryer} \times 100 \quad \textbf{(6.1)}$$

6.2.4. Emulsions viscosity

Steady-shear flow curves were used to assess the emulsions viscosity. Flow curves with a total number of 50 points were obtained using an Anton Paar MCR 92 rheometer (Austria). The shear rate was increased from 1 to 100 s^{-1} using a measuring plate PP50 (Part No.: 79045, Serial No.: 55422, Cat No.: 79045, Del No.: 80352243, Anton Paar) with 50 mm of diameter and a gap of 0.5 mm. The experiment was performed in triplicate at 25 ºC.

6.2.5. Emulsions zeta potential

Emulsions zeta potential was measured by dynamic light scattering using a Zetasizer Nano-ZS90 (Malvern Instruments, Worcestershire, UK). Analyses were performed in triplicate.

6.2.6. Emulsions droplet size and microparticle size

The size distribution of emulsion droplets and dry powder obtained by spray-drying was evaluated by laser granulometry using a Coulter LS 230 Particle Size Analyser (Miami, FL, USA). For the microparticle size measurements, the dry powder was first dispersed in ethanol. Measurements were performed in triplicate and each analysis had a run of 30 seconds. The obtained results express the average of droplet mean size and the average of particle mean size (volume and number distributions). Volume distribution considers the volume of each particle, whereby particles with a higher volume have higher contribution. In a number distribution each particle has equal weight.

6.2.7. Morphology of microparticles

Microparticles surface morphology was performed by scanning electron microscopy using a Fei Quanta 400 FEG ESEM/EDAX Pegasus X4M (Eindhoven, The Netherlands). The dry powder was fixed into a brass stub with double-sided adhesive tape and then coated in vacuum by a thin layer of gold-palladium using a SPI module sputter coater.

6.2.8. Encapsulation efficiency and loading capacity

Encapsulation efficiency (%) was calculated by the ratio between the mass of RA detected in the microparticles formed and the mass of RA used to prepare the oily phase of emulsions fed to the spray-dryer, considering the method carried out by the authors in a previous work. Briefly, an appropriate amount of RA-loaded microparticles was dispersed in octanol and maintained at room temperature overnight. The suspension was further vigorously stirred, put on a bath at 37 ± 2 ºC and centrifuged. The amount of RA present in the supernatant was measured using an UV/VIS spectrometer (SPEC RES+, Sarspec, Porto, Portugal) at 352 ± 7 nm. Calibration curve was validated in a concentration range between 0.000250 and 0.005000 mg·mL^{-1} with a correlation coefficient of 0.9928. LOD and LOQ were 0.0002 mg·mL^{-1} and 0.0008 mg·mL^{-1}, respectively. Loading capacity was determined by the ratio between the mass of RA and mass of microparticles.

6.2.9. Controlled release assays

The experiments performed for RA controlled release from biopolymers blend-based microparticles were carried out considering the methodology described in previous works of the authors Gonçalves et al. [278,314]. RA-loaded microparticles were placed on top of a cuvette with octanol (this organic solvent attempts to mimic the phospholipids membrane characteristics, considering the amphiphilic nature of octanol) [258,259,283,284]) under magnetic stirring conditions and at 37 ± 2 ºC. An UV/VIS spectrometer (section 6.2.8.) was used to assess the RA release profiles in a continuous mode (intervals of 2 min) by absorbance (at 352 ± 7 nm). The models of zero-order (Eq. 6.2), Higuchi (Eq. 6.3), Korsmeyer-Peppas (Eq. 6.4) and Weibull (Eq. 6.5) [260,262] were further applied to these experimental release profiles.

$$Q_t = Q_0 + K_0 t \quad \textbf{(6.2)}$$

where Q_t is the cumulative amount of the drug/active compound released at the time t, Q_0 is the initial amount of the drug/active compound in solution (usually $Q_0 = 0$) and K_0 is the zero-order release constant.

$$Q_t = K_H \sqrt{t} \quad \textbf{(6.3)}$$

where K_H is the Higuchi constant.

$$Q_t / Q_\infty = K_K t^n \quad \textbf{(6.4)}$$

where Q_t/Q_∞ is the fraction of active compound released until time t, and K_K is the Korsmeyer constant and the parameter n is the release exponent (diffusional) that defines the release mechanism.

$$M_t = M_\infty \left[1 - e^{-\left(\frac{t-t_0}{\tau d}\right)^\beta}\right] \quad \textbf{(6.5)}$$

where M_t is the dissolution/release (%) of the active compound at time t, M_∞ is the dissolution/release (%) of the active compound at infinite time, t_0 is the lag-time of the dissolution (usually t_0=0), β indicates the shape parameter of the curve and τ_d is the time when 63.2% of M has been dissolved/released.

6.2.10. Statistical analysis

The effect of using different biopolymers blends in the preparation of emulsion was evaluated in terms of the droplet size of these colloidal systems. Moreover, particle size distribution was compared among all the microparticle formulations produced. RA-loaded microparticles were further assessed regarding encapsulation efficiency and loading capacity. One-way analysis of variance (ANOVA) at $p < 0.05$ and subsequent Tukey test were conducted by Minitab® 19 software.

A statistical simplex centroid experimental design with three components was used to evaluate encapsulation efficiency, loading capacity and release times (response variables) of RA-loaded microparticles produced regarding the blends of biopolymers used as encapsulating agents. Herein, a triangular diagram is built wherein the three points at the vertices correspond to each one of biopolymers, *i.e.* modified chitosan, xanthan gum and alginic acid sodium. Each midpoint of the sides of the triangle corresponds to 1:1 binary blend of the biopolymers. At last, the center point of the triangle represents a three-biopolymer blend of equal portions.

6.3. Results and discussion

6.3.1. Emulsions characterization

6.3.1.1. Viscosity

The emulsion with an aqueous phase composed by the modified chitosan + alginic acid sodium blend exhibited characteristics relatively close of a Newtonian fluid (Table 6.1). Apparent viscosity of this emulsion was 7.9 ± 0.4 mPa·s for a shear rate of 100 s^{-1} (Table 6.1), which is close to an intermediate value between the apparent viscosities verified for emulsions prepared with the same oily phase and surfactant, but wherein modified chitosan and alginic acid sodium were individually used in the formulations. Herein, apparent viscosities of modified chitosan- and alginic acid sodium-based emulsions were 3.53 ± 0.06 and 17.6 ± 0.2 mPa·s, respectively [314]. Consistency index (provides information about the flow properties of the system, informing about the emulsion viscosity [288]) and flow behaviour index (indicates how close the system is to a Newtonian fluid [288]) were also determined (Table 6.1). Gonçalves et al. [314] verified that emulsions individually composed by modified chitosan and alginic acid sodium also showed being relatively close of Newtonian fluids

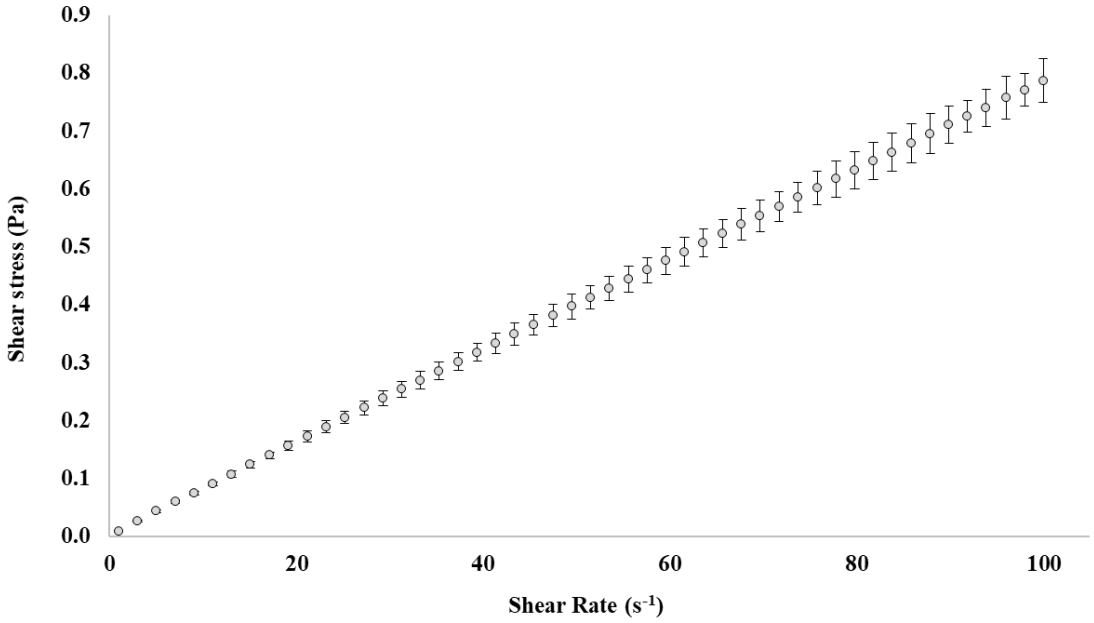


Figure 6.1 – Increase between shear stress and shear rate for the emulsion composed by the modified chitosan + alginic acid sodium blend. Results are presented as the average and standard deviation of three independent assays.

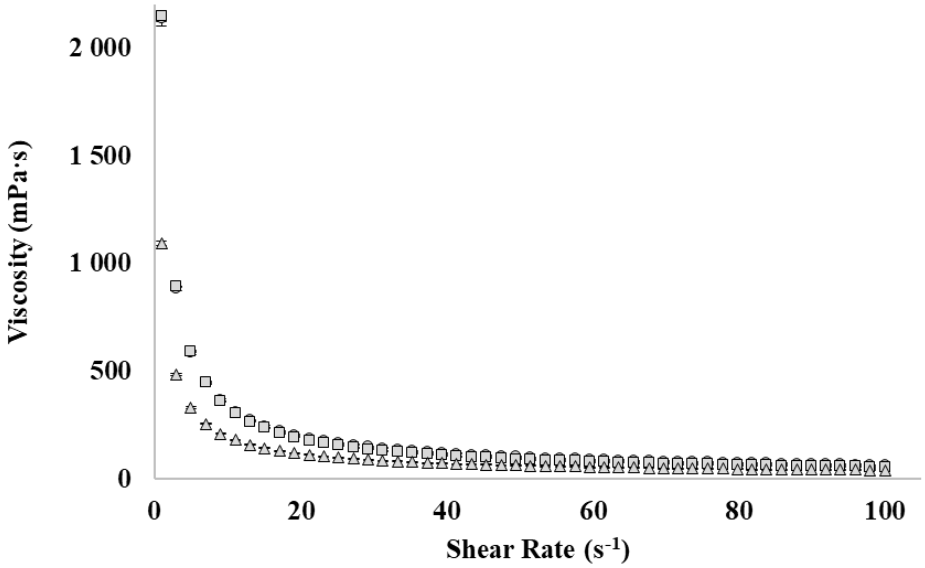


Figure 6.2 – Viscosity curves of the emulsions prepared with different biopolymers blends (xanthan gum + alginic acid sodium (●), modified chitosan + xanthan gum (■) and modified chitosan + xanthan gum + alginic acid sodium (▲)). Results are presented as the average and standard deviation of three independent assays

(n = 1). For the emulsions containing xanthan gum in the blend of biopolymers (*i.e.* xanthan gum + alginic acid sodium, modified chitosan + xanthan gum and modified chitosan + xanthan gum + alginic acid sodium) the increase of shear rate decreased the apparent viscosity (Figure 6.2). Accordingly, these systems are non-

Newtonian fluids. Other studies revealed xanthan gum-based systems as non-Newtonian fluids [290]. Consistency index ranged from 0.98 ± 0.01 to 2.042 ± 0.005 mPa·s^n (Table 6.1) among these emulsions, while flow behaviour index varied from 0.215 ± 0.001 to 0.306 ± 0.002 indicating the emulsions containing xanthan in the encapsulating agents blend as pseudoplatic fluids (n < 1) [288]. In fact, pseudoplastic fluids commonly refer to polymer solutions with high molecular weight compounds, the case of the polysaccharide xanthan gum.

6.3.1.2. Stability of colloids

Stability of colloidal systems is usually analysed through the percentage of emulsion separation (creaming index) 24 h after its preparation [292,293]. However, due to the high proportion of aqueous phase regarding the oily phase of emulsions prepared in this work, this methodology showed not being the most appropriate. Alternatively, the stability of emulsions can be determined by zeta potential, measuring the electrokinetic potential of droplets [294].

The only stable emulsion (zeta potential value above of │30│ mV [294]) was composed by the modified chitosan + alginic acid sodium blend (-51 ± 5 mV) (Table 6.1). The individual usage of these biopolymers also generates stable emulsions [314]. Among the other emulsions produced in the present work, zeta potential decreased with the usage of the modified chitosan + xanthan gum, xanthan gum + alginic acid sodium and modified chitosan + xanthan gum + alginic acid sodium blends, by this order (Table 6.1). Previous studies reported that xanthan gum-based emulsions are highly unstable (around 0.3 mV) [314], whereby the addition of this biopolymer to an original stable emulsion may have contributed to produce an unstable final emulsion.

6.3.1.3. Droplet size distribution

In addition to zeta potential, emulsions droplet size also indicate the stability of colloids [285]. In fact, larger emulsion droplets are related to a lower encapsulation efficiency [295]. In this work, the droplet mean diameter of the emulsions produced varied between 1.290 ± 0.007 and 2.69 ± 0.01µm (differential volume distribution) and 0.0651 ± 0.0002 and 0.146 ± 0.007 µm (differential number distribution) (Table 6.1). The biopolymers blend composed by xanthan gum + alginic acid sodium resulted in an emulsion with the smaller droplets (0.068 ± 0.005% considering differential number distribution) (Table 6.1), which is in agreement with the higher encapsulation efficiency obtained for the microparticles composed by these encapsulating agents (section 6.3.5.) (76 ± 4%) (Table 6.2). Moreover, the higher droplet size was registered for the emulsion composed by modified chitosan + alginic acid sodium (2.69 ± 0.01% considering differential volume distribution) (Table 6.1), dealing with the obtainment of the lower encapsulation efficiency among all the microparticles produced (section 6.3.5.) (27.1 ± 0.9%) (Table 6.2). Emulsions individually composed by modified chitosan, alginic acid sodium and xanthan gum evidenced larger droplets diameter (3.80 ± 0.02 and 0.75 ± 0.03, 2.3 ± 0.7 and 0.706 ± 0.004, and 1.65 ± 0.09 and 0.65 ± 0.01, respectively, considering differential volume and number distributions) [314] when compared to the droplets of the emulsions herein produced from several blends of these biopolymers.

Table 6.1 – Rheological parameters, apparent viscosity, zeta potential and droplet size of emulsions prepared with different blends of alginic acid sodium, xanthan gum and modified chitosan.

Emulsions (biopolymeric composition)	**Rheological parameters**		**Apparent viscosity at 100 s^{-1} (mPa·s)**	**Zeta potential (mV)**	**Droplet mean diameter**	
	Consistency index, k ($mPa \cdot s^n$)	**Flow behaviour index, n**			**Differential volume distribution (µm)**	**Differential number distribution (µm)**
Xanthan gum + Alginic acid sodium	1.89 ± 0.02	0.262 ± 0.001	-	14.8 ± 0.4	1.41 ± 0.02[c]	0.068 ± 0.005[c]
Modified chitosan + Alginic acid sodium	0.0087 ± 0.0004	0.980 ± 0.04	7.9 ± 0.4	-51 ± 5	2.69 ± 0.01[a]	0.121 ± 0.002[b]
Modified chitosan + Xanthan gum	2.042 ± 0.005	0.215 ± 0.001	-	17.2 ± 0.9	1.290 ± 0.007[d]	0.0651 ± 0.0002[c]
Modified chitosan + Xanthan gum + Alginic acid sodium	0.98 ± 0.01	0.306 ± 0.002	-	2.73 ± 0.04	1.95 ± 0.02[b]	0.146 ± 0.007[a]

Different letters in the same column indicate significant differences ($p<0.05$)

6.3.2. Biopolymers blends-based microparticles production

Formulations based on biopolymers blends (modified chitosan, alginic acid sodium and xanthan gum) were considered to produce unloaded microparticles (empty microparticles only composed by the encapsulating agents - microparticles BBMpE), microparticles loaded with coconut oil and tween 80 (microparticles BBMpOT) and microparticles loaded with RA dissolved in coconut oil and mixed with tween 80 (microparticles BBMpRA). The selection of the biopolymers to be blended was based on the study carried out by Gonçalves et al. [314]. Herein, the amount of RA retained in the microparticles was significantly higher for modified chitosan- and alginic acid sodium-based microparticles (65 and 62%, respectively, as previously referred). Moreover, the slower release rate (for several hours) was obtained when alginic acid sodium was used as encapsulating agent. The most relevant benefits about xanthan gum might be further evaluated in the simulation gastrointestinal digestion studies, wherein the presence of this biopolymer shall provide high resistance to enzymatic degradation and pH variations to microparticles produced. In fact, xanthan gum is recognized by its stability at low pHs.

Product yield ranged between 28 and 41% for microparticles BBMpE, while for microparticles BBMpOT and BBMpRA it ranged between 16-21% and 21-36%, respectively (Table 6.2). The volume and the properties of the system content to be spray-dried highly influence the product yield. Moreover, the operational conditions to be used in the spray-dryer (*e.g.* inlet air temperature) also interfere with the product yield. In the present work, the production of microparticles containing an oily phase due to the incorporation of coconut oil (with or without RA dissolved) resulted in an overall slight decrease of the product yield, except for the microparticles BBMpRA composed by the modified chitosan + alginic acid sodium blend, wherein a higher product yield was registered (36%). The product yield was slightly higher for microparticles BBMpRA composed by xanthan gum when compared to microparticles BBMpOT also composed by this polysaccharide, probably due to the larger volume of emulsion prepared and fed to the spray-dryer (500 and 200 mL, respectively).

Several works related to the encapsulation of lipophilic bioactive compounds by spray-drying technology describe a higher or lower decrease in the product yield of loaded microparticles due to their increased adhesion to the walls of spray-dryer [245,290,315]. Particularly, Gonçalves et al. [314] registered similar values of product yield to the one obtained in this work when modified chitosan-, alginic acid sodium- and xanthan gum-based microparticles were produced at 130℃ of inlet air temperature, considering unloaded microparticles (41, 39 and 28%, respectively), microparticles loaded with coconut oil and tween 80 (18, 17 and 16%, respectively) and microparticles loaded with RA dissolved in coconut oil and mixed with tween 80 (18, 30 and 24%, respectively).

6.3.3. Particle size distribution

Diameter (considering differential volume distribution) of biopolymer blends-based microparticles decreased with the incorporation of coconut oil and surfactant (comparison between microparticles BBMpE and BBMpOT) and decreased even more with the incorporation of RA dissolved in coconut oil and surfactant

Table 6.2 – Product yield, RA encapsulation efficiency, RA loading capacity and particle diameter of microparticles produced using different formulations.

Microparticles content		Product yield (%)	RA encapsulation efficiency (%)	RA Loading capacity (%)	Particle mean diameter	
Formulation	**Encapsulating agents blend**				**Differential volume distribution (µm)**	**Differential number distribution (µm)**
BBMpE	Xanthan gum + Alginic acid sodium	30	-	-	4.70 ± 0.05^{de}	0.934 ± 0.008^{c}
	Modified chitosan + Alginic acid sodium	41	-	-	4.04 ± 0.04^{fgh}	0.465 ± 0.003^{d}
	Modified chitosan + Xanthan gum	28	-	-	6.2 ± 0.3^{b}	0.110 ± 0.003^{g}
	Modified chitosan + Xanthan gum + Alginic acid sodium	32	-	-	6.9 ± 0.4^{a}	0.156 ± 0.004^{fg}
BBMpOT	Xanthan gum + Alginic acid sodium	19	-	-	3.60 ± 0.02^{h}	1.1323 ± 0.0006^{a}
	Modified chitosan + Alginic acid sodium	21	-	-	5.0 ± 0.4^{d}	0.41 ± 0.01^{d}
	Modified chitosan + Xanthan gum	16	-	-	4.22 ± 0.04^{fg}	1.082 ± 0.005^{ab}
	Modified chitosan + Xanthan gum + Alginic acid sodium	18	-	-	4.49 ± 0.04^{ef}	1.064 ± 0.003^{b}
BBMpRA	Xanthan gum + Alginic acid sodium	24	76 ± 4^{a}	0.022 ± 0.001^{a}	2.923 ± 0.002^{i}	0.938 ± 0.007^{c}
	Modified chitosan + Alginic acid sodium	36	27.1 ± 0.9^{c}	0.0080 ± 0.0003^{c}	5.76 ± 0.03^{c}	0.29 ± 0.04^{e}
	Modified chitosan + Xanthan gum	21	49 ± 2^{b}	0.0144 ± 0.0007^{b}	3.75 ± 0.09^{gh}	0.19 ± 0.07^{f}
	Modified chitosan + Xanthan gum + Alginic acid sodium	21	54 ± 5^{b}	0.016 ± 0.001^{b}	2.88 ± 0.01^{i}	0.925 ± 0.009^{c}

Different letters in the same column indicate significant differences ($p<0.05$)

(comparison between microparticles BBMpOT and BBMpRA) in the formulations (Table 6.2). Accordingly, particle mean diameter varied between 2.923 ± 0.002 and 4.70 ± 0.05 μm among microparticles composed by the xanthan gum + alginic acid sodium blend, 3.75 ± 0.09 and 6.2 ± 0.3μm among microparticles composed by the modified chitosan + xanthan gum blend and 2.88 ± 0.01 and 6.9 ± 0.4 μm among microparticles composed by the modified chitosan + xanthan gum + alginic acid sodium blend. For the microparticles composed by the modified chitosan + alginic acid sodium blend the particle diameter increased from 4.04 ± 0.04 to 5.0 ± 0.4 and to 5.76 ± 0.03 μm when microparticles BBMpE, BBMpOT and BBMpRA were produced, respectively. Considering a differential number distribution, an overall particle mean diameter between 0.110 ± 0.003 (microparticles BBMpE composed by the modified chitosan + xanthan gum blend) and 1.1323 ± 0.0006 μm (microparticles BBMpOT composed by the xanthan gum + alginic acid sodium blend) was registered (Table 6.2).

6.3.4. Microparticles morphology

All the microparticles produced (BBMpE, BBMpOT and BBMpRA) evidenced a spherical form (Figure 6.3). Microparticles BBMpE composed by the xanthan gum + alginic acid sodium, modified chitosan + xanthan gum and modified chitosan + xanthan gum + alginic acid sodium blends were characterized by a rough surface with several concavities (Figure 6.3 – A, C and D). In turn, microparticles BBMpE composed by the modified chitosan + alginitic acid sodium blend showed a smooth surface with only one apparent concavity (Figure 6.3 – B). The surface morphology exhibited by these biopolymers blends-based microparticles is in agreement with a combination of the structures typically observed in microparticles individually composed by modified chitosan, xanthan gum and alginic acid sodium. In fact, Gonçalves et al. [314] produced modified chitosan- and alginic acid-based microparticles with a very smooth and a smooth surface with few concavities, respectively. Moreover, xanthan-based microparticles were produced evidencing a high rough and irregular surface. In the present work, the microparticles containing xanthan gum in their formulations presented an evident less rough surface certainly influenced by the presence of modified chitosan and/or alginic acid sodium biopolymers. Similar conclusions regarding the impact of using biopolymers blends in the morphology of microparticles produced was reported by Ribeiro et al. [316] when binary and ternary blends were prepared with the biopolymers gum arabic, starch and maltodextrin for encapsulation of vitamin A (retinol). Microparticles BBMpOT and BBMpRA revealed alterations regarding the morphologies exhibited by microparticles BBMpE, whereby the microparticles loaded with coconut oil (with or without RA) and surfactant impacted their surface structures. Microparticles BBMpOT composed by the xanthan gum + alginic acid sodium blend appeared with small protuberances on their surface (Figure 6.3 – E). For all the other microparticles BBMpOT and BBMpRA produced (Figure 6.3 – F, G, H, I, J, K and L), it was observed the presence of several concavities (in a higher or lower number) with an appreciable smaller size when compared to the dimension of the concavities observed among microparticles BBMpE. This morphological change observed in the microparticles composed by the

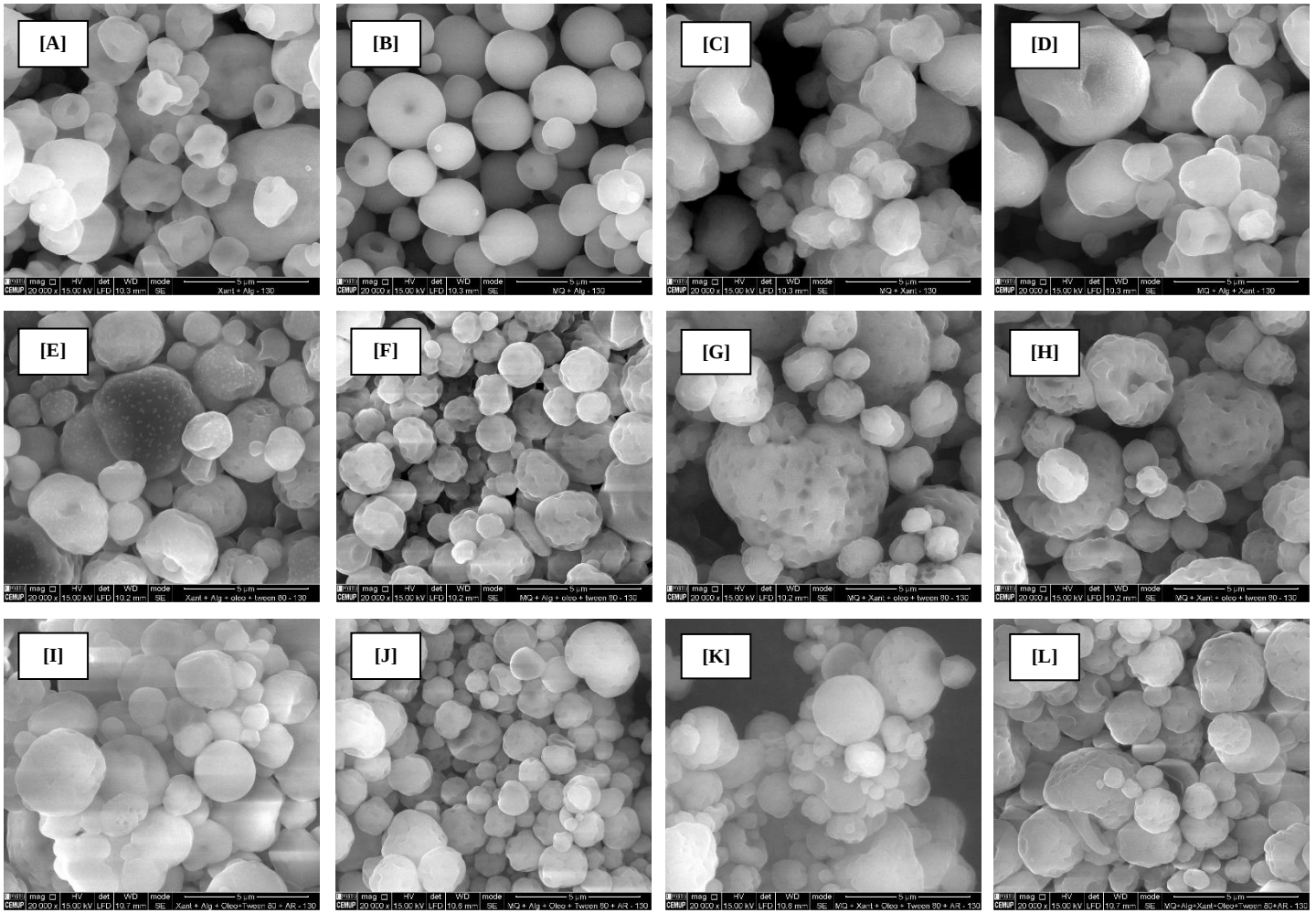
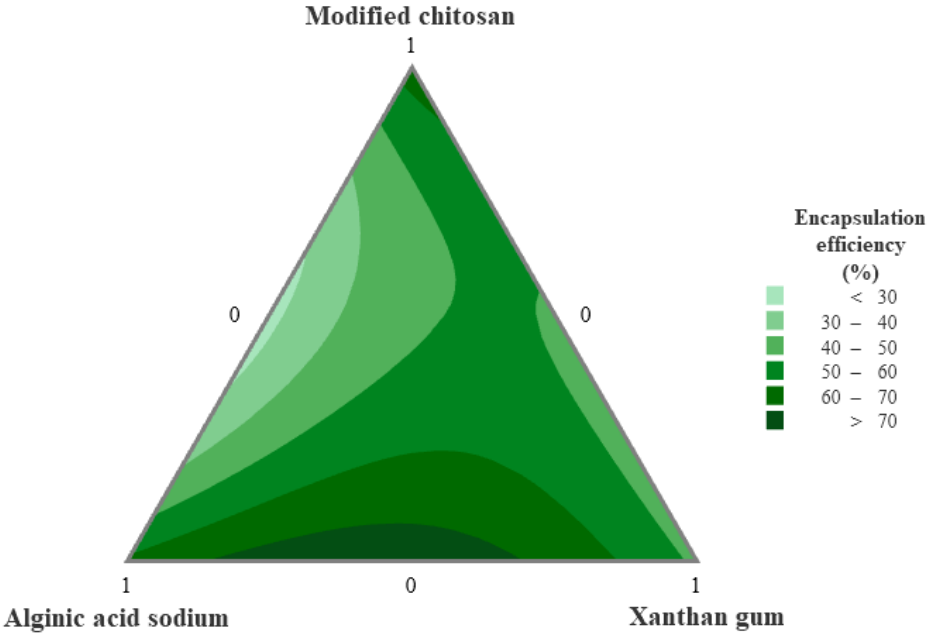
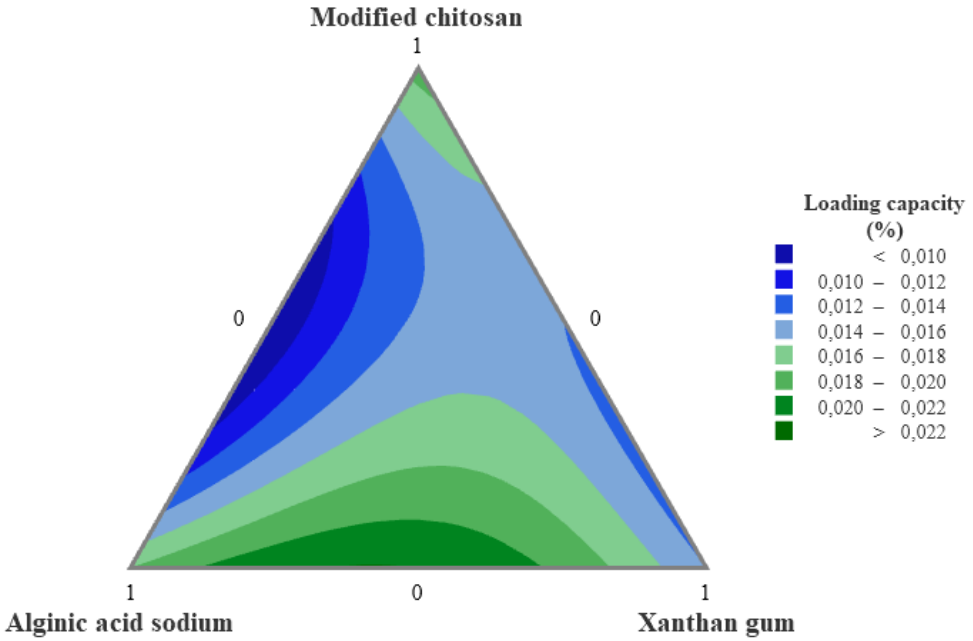


Figure 6.3 – Surface morphology of BBMpE (A, B, C and D), BBMpOT (E, F, G and H) and BBMpRA (I, J, K and L) microparticles composed by xanthan gum + alginic acid sodium blend (A, E and I), modified chitosan + alginic acid sodium blend (B, F and J), modified chitosan + xanthan gum blend (C, G and K) and modified chitosan + xanthan gum + alginic acid sodium blend (D, H and L). Magnification = 20,000 times, beam intensity (HV) 15.00 kV, distance between the sample and the lens (WD) around 10 mm.



(A)



(B)

Figure 6.4 – Response surfaces of encapsulating efficiency (A) and loading capacity (B) based on a simplex centroid design.

modified chitosan + alginic acid sodium blend resulted in the production of microparticles with a rough surface (Figure 6.3 – F and J).

6.3.5. Encapsulation efficiency and loading capacity

Encapsulation efficiency and loading capacity were highly influenced by the biopolymers blends used in the microparticles formulation. A significant higher amount of RA was effectively incorporated in the microparticles composed by the xanthan gum + alginic acid sodium blend (76 ± 4%) ($p<0.05$) (Table 6.2 and Figure 6.4 - A). This value was even higher when compared to the encapsulation efficiency obtained for xanthan gum- and alginic acid sodium-based microparticles [314] (Figure 6.4 – A). However, incorporation of modified chitosan in biopolymers blends seems to not benefit the microparticles regarding this parameter (Figure 6.4 – A). Herein, encapsulation efficiency decreased from 54 ± 5 to 49 ± 2 and to 27.1 ± 0.9% when microparticles composed by the modified chitosan + xanthan gum + alginic acid sodium, modified chitosan + xanthan gum and modified chitosan + alginic acid sodium blends were produced, respectively (Table 6.2). Particularly, the amount of RA retained in the microparticles composed by modified chitosan + alginic acid sodium blend was highly lower when compared to the one registered for the microparticles individually composed by modified chitosan and alginic acid sodium biopolymers [314]. In turn, for the other microparticles formulations containing modified chitosan in the biopolymers blend, the encapsulation efficiency showed to be relatively close to an intermediate value regarding the encapsulation efficiency values obtained for alginic acid sodium-, modified chitosan- and xanthan gum-based microparticles [314]. In fact, modified chitosan only provided a high encapsulation efficiency when this biopolymer is individually used as encapsulating agent [314] (Figure 6.4 – A).

Loading capacity varied from 0.0080 ± 0.003 to 0.022 ± 0.001% (Table 6.2). This parameter was influenced by the biopolymers used (individually or as a blend) in the production of microparticles in a behaviour similar to the observed for the encapsulation efficiency (Figure 6.4 – B).

In other works, RA encapsulation using different encapsulation methods registered higher values of encapsulation efficiency when compared to this work. Schultze et al. [151] obtained lipid-core nanocapsules by interfacial deposition of polymer with an encapsulation efficiency higher than 80%. Also, Akanda et al. [162] registered an encapsulation efficiency of 90.5 ± 1.2% when RA-loaded solid lipid nanoparticles (SLN) were produced.

6.3.6. Controlled release

Cumulative percentage of RA released over time from different biopolymers blends-based microparticles is presented in Figure 6.5. Microparticles composed by the xanthan gum + alginic acid sodium and modified chitosan + xanthan gum + alginic acid sodium blends enabled the highest release times, promoting RA release in 416 and 414 min, respectively (almost 7 h). Herein, a slightly faster RA release was observed in the first hours when the modified chitosan + xanthan gum + alginic acid sodium blend was used. However, an overall

slower release was observed for this formulation when compared to the microparticles composed by the xanthan gum + alginic blend. Globally, microparticles with lower diameter (0.19 ± 0.07 and 0.29 ± 0.04 μm in the case of microparticles composed by modified chitosan + xanthan gum and composed by modified chitosan + alginic acid sodium, respectively (Table 6.2) enable the faster release of bioactive compound. The individual usage of alginic acid sodium has been associated to the longest release times in controlled release studies of RA [278,314]. Particularly, microparticles composed by the same core material and alginic acid sodium as encapsulating agent enabled a RA release time of almost 8 h [314]. Accordingly, RA release times from the biopolymers blends-based microparticles previously described slightly decreased possibly by the interference of the lower release times associated to the biopolymers modified chitosan and xanthan gum (138 and 48 min, respectively) [314] (Figure 6.6). The modified chitosan + alginic acid sodium blend evidenced the fastest RA release from microparticles, contrary to the expected RA slow release due to the presence of alginic aid sodium. It might be due to the eventual creation of a porous network that promoted the RA release from microparticles. At last, RA release prolonged for 218 min (more than 3 h) from microparticles composed by modified chitosan + xanthan gum. Individual usage of this biopolymers resulted in a lower release time from microparticles as described above [314] (Figure 6.6).

Ribeiro et al. [316] also evaluated the impact of using biopolymers blends on retinol release times. The ternary blend of biopolymers (composed by gum arabic, starch and maltodextrin) enabled an intermediate release time due to the contribution of the three encapsulating agents.

The most suitable biopolymers blends-based microparticles to regulate RA catabolism in APL patients are the microparticles composed by the xanthan gum + alginic acid sodium and modified chitosan + xanthan gum + alginic acid sodium blends. They evidenced a slow RA release profile and higher encapsulation efficiency.

Studies involving other methods for RA encapsulation report longer release profiles when compared to the one obtained in this work. Narvekar et al [161] produced a polymer-oil nanostructured carrier composed by oil and poly(lactic-co- glycolic) acid (PLGA) for incorporation of all-trans RA, using an emulsification-solvent evaporation technique. This nanoparticle formulation, aiming to act against ovarian cancer, evidenced a 5-day controlled release profile in PBS at pH 7.4. Moreover, Akanda et al [162] optimized RA-loaded SLN nanoparticles with potential to be used in the treatment of prostate cancer. Herein, 40% of the bioactive compound was released in the first 10 h and release was also registered for 5 days. It was performed in a mixture of double-distilled water and ethanol (50:50, v/v).

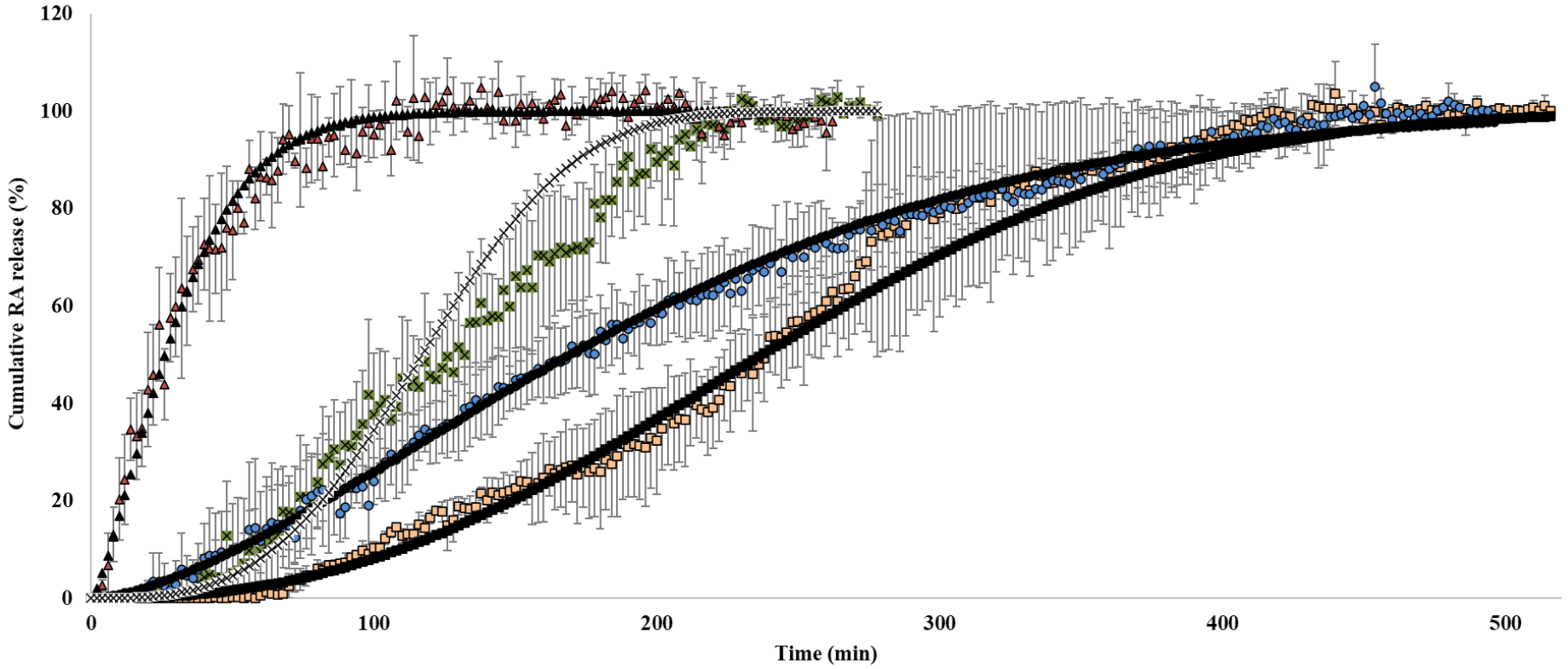


Figure 6.5 – Cumulative RA release from microparticles composed by modified chitosan + alginic acid sodium blend (pink triangles), modified chitosan + xanthan gum blend (green filled crosses), modified chitosan + xanthan gum + alginic acid sodium blend (blue circles) and xanthan gum + alginic acid sodium blend (orange squares). Results are presented as the average and standard deviation of three independent assays. Weibull model was fitted to the obtained controlled release profiles: modified chitosan + alginic acid sodium blend (black triangles), modified chitosan + xanthan gum blend (black filled crosses), modified chitosan + xanthan gum + alginic acid sodium blend (black circles) and xanthan gum + alginic acid sodium blend (black squares).

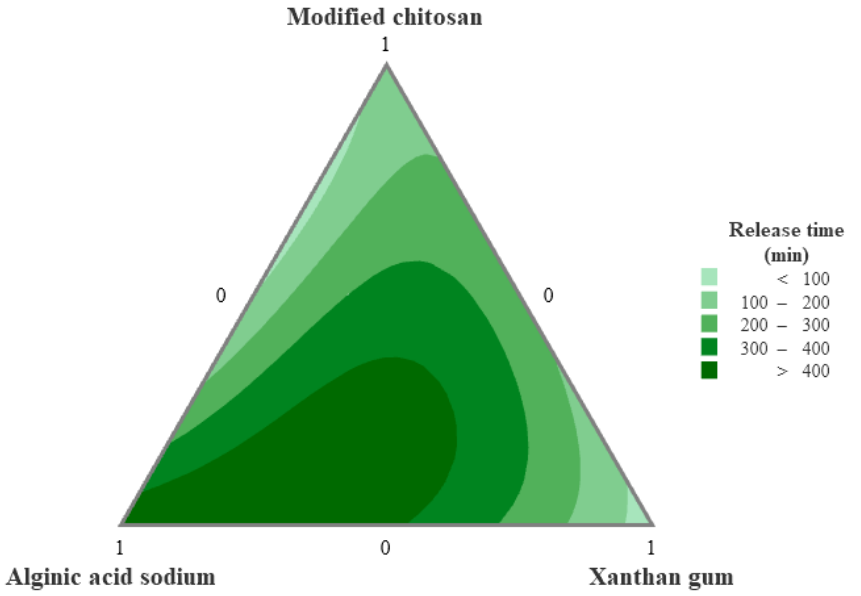


Figure 6.6 – Response surface of RA release times based on a simplex centroid design.

6.3.7. Kinetic models

Zero-order release constant, K_0, increased from 5.0×10^{-6} to 2.0×10^{-5} mg·min^{-1} with the increase of RA release rate observed for biopolymer blends-based microparticles composed by modified chitosan + xanthan gum + alginic acid sodium, xanthan gum + alginic acid sodium, modified chitosan + xanthan gum and modified chitosan + alginic acid sodium blends, by this order. Kinetics of zero order was fitted to RA release profiles with a correlation coefficient between 0.968 and 0.991 (Table 6.3).

Higuchi constant, K_H, varied from 6.0×10^{-5} to 8.0×10^{-5} mg·min$^{-1/2}$, corresponding to the slower (from microparticles composed by the modified chitosan + xanthan gum + alginic acid sodium blend) and fastest (from microparticles composed by the modified chitosan + alginic acid sodium blend) RA release rate. A correlation coefficient for Higuchi model between 0.899 and 0.962 was achieved (Table 6.3).

Korsmeyer-Peppas model was fitted to the RA release profiles considering the Q_t/Q_∞ is lower than 0.6 [262]. Korsmeyer constant, K_K, increased from 3.6×10^{-6} (for the microparticles composed by the xanthan gum + alginic acid sodium blend) to 1.4×10^{-2} (for the microparticles composed by the modified chitosan + alginic acid sodium blend) min^{-n}. For Korsmeyer-Peppas model the correlation coefficients varied from 0.767 to 0.935 (Table 6.3). Parameter n was higher than 0.85 among all the microparticles formulations (n = 1.1 for the modified chitosan + alginic acid sodium blend, n = 1.4 for the modified chitosan + xanthan gum + alginic acid sodium blend, n = 2.2 for the xanthan gum + alginic acid sodium blend and n = 3.0 for the modified chitosan + xanthan gum blend (Table 6.3), whereby a super case-II transport and a t^{n-1} rate as a function of time was suggested [145].

Correlation coefficients between 0.825 and 0.988 enabled to fit the Weibull model to RA release profiles (Table 6.3). β parameter was higher than 1 for the microparticles produced (1.4, 1.6, 2.4 and 3.1 for the modified chitosan + alginic acid sodium, modified chitosan + xanthan gum + alginic acid sodium, xanthan gum + alginic acid sodium and modified chitosan + xanthan gum blends, respectively (Table 6.3). Accordingly, it was

Table 6.3 – Application of the models of zero-order, Higuchi, Korsmeyer-Peppas and Weibull to the experimental RA release profiles.

	Parameters		Encapsulating agents blends			
			Xanthan gum + Alginic acid sodium	Modified chitosan + Alginic acid sodium	Modified chitosan + Xanthan gum	Modified chitosan + Xanthan gum + Alginic acid sodium
Kinetic models	**Zero-order**	K_0 **(mg·min^{-1})**	7.0×10^{-6}	2.0×10^{-5}	8.0×10^{-6}	5.0×10^{-6}
		Q_0 **(mg)**	-5.0×10^{-4} *)	8.0×10^{-7}	-3.0×10^{-4} *)	-9.0×10^{-5} *)
		R^2	0.978	0.968	0.991	0.989
	Higuchi	K_H **(mg·min$^{-1/2}$)**	8.0×10^{-5}	8.0×10^{-5}	7.0×10^{-5}	6.0×10^{-5}
		R^2	0.899	0.959	0.917	0.945
	Korsmeyer-Peppas	K_k **(min^{-n})**	3.6×10^{-6}	1.4×10^{-2}	4.3×10^{-7}	3.0×10^{-4}
		n	2.2	1.1	3.0	1.4
		R^2	0.767	0.909	0.864	0.935
	Weibull	τ_d **(min)**	276	34	132	213
		β	2.4	1.4	3.1	1.6
		R^2	0.825	0.963	0.892	0.988

*) Consider $Q_0 \geq 0$.

suggested the shape of the curve gets sigmoidal with a turning point [262]. τ_d parameter was determined from RA release profiles when 63.2% of this retinoid was released and varied between 34 (for the xanthan gum + alginic acid sodium blend) and 236 (for the xanthan gum + alginic acid sodium blend) min (Table 6.3).

Weibull model enabled the better fitting to the RA release profiles obtained in this work. Similar results were previously obtained by the authors considering the production of different biopolymer-based microparticles also addressed for RA encapsulation [278,314]. Weibull model is reported as the most appropriate model to describe a bioactive compound release from a matrix-based delivery system [260].

6.4. Conclusions

Binary and ternary blends of biopolymers (modified chitosan, xanthan gum and alginic acid sodium) were considered for development of RA-loaded delivery systems from oil-in-water emulsions using spray-drying. The biopolymers used in the biopolymers blends affect the viscosity, stability and droplet size of emulsions, as well as the overall characteristics of microparticles. The highest encapsulation efficiency was registered when the xanthan gum + alginic acid sodium blend was used (76 ± 4%). Biopolymers blends-based microparticles containing alginic acid sodium enable slower RA release, which extends for almost 7 h. As exception, microparticles composed by the modified chitosan + alginic acid sodium blend enable a fast release of RA (100 min).

Chapter 7 - Application of ethyl cellulose and ethyl cellulose + polyethylene glycol for the development of polymer-based formulations by spray-drying technology for retinoic acid encapsulation

---

The seventh chapter proposes EC-based microparticles, with and without the incorporation of PEG as a second encapsulating agent, prepared by spray-drying process for the encapsulation of RA.

This chapter is in the form of submitted paper:

Gonçalves, A; Rocha, F; Estevinho, B N. Application of ethyl cellulose and ethyl cellulose + polyethylene glycol for the development of polymer-based formulations by spray-drying technology for retinoic acid encapsulation.

7.1. Introduction

Retinoic acid (RA) is a natural derivative of vitamin A considered as a chemopreventive and/or chemotherapeutic agent [17]. To treat several malignances, this signalling molecule is involved in inhibition of cellular proliferation, migration and invasion and the triggering of differentiation, apoptosis and cellular cycle arrest in pre malignant and malignant cells. These processes are carried out by gene transcription regulation due to RA binding predominantly to RARs (RA receptors) [97,232,270–273].

Despite high efficacy of all-trans RA to treat acute promyelocytic leukemia (APL) (induction agent), the concentration of this retinoid that reach and is therefore maintained in the target cells and tissues may not be in the required amount to activate target genes [317]. Consequently, therapeutic efficiency is compromised with patients becoming resistant to RA. Moreover, as a result of continuous repetitive RA oral administration, a high decline in the RA half-life in blood and further reduction in the concentration of this retinoid in the plasma of patients is reported [25,26,58,276]. Muindi et al. [58] presented some hypotheses for this reduction of RA half-life, including (1) a marked elimination of RA by biliary excretion (at least 60%); herein, a nonspecific binding to the intestinal proteins or an unreal malabsorption decreased oral bioavailability of RA, (2) RAR-α mutations and (3) the induction of RA catabolism due to the continued treatment with RA. Considering this last possibility, the regulation of cellular levels of RA is related to cytochrome P450 enzymes. They are activated for low amounts of this retinoid, whereby repeated RA administration may stimulate RA degradation with the formation of 4-oxo-all-trans RA [17,277].

In the line with these topics, incorporation of RA into proper carrier-based delivery systems for its slow and continuous release is of major importance to boost the treatment of APL. Repetitive RA administration is herein avoided which enables to decrease the activity of cytochrome P450 enzymes and thus improve the bioavailability of RA. This approach also may help to deal with inactivity or rapid degradation of RA due to its poor aqueous solubility and high physicochemical instability (e.g. under oxidant and heat conditions). Also, minimization of RA side-effects due to high amount of RA administrated might be achieved [318].

Development of polymeric microparticles using spray-drying for RA encapsulation has been proposed by the authors as a strategy to treat patients with APL. Gonçalves et al. [278] evaluated the incorporation of RA (ethanolic solution) into alginic acid sodium-, modified chitosan- and arabic gum-based microparticles. Alginic acid sodium-based microparticles evidenced a RA release for more than 7 h. Afterwards, oil-in-water emulsions containing RA (solutions prepared in coconut oil), tween 80 and biopolymers (individually used [314] and combined in advantageous binary and ternary blends [319]) resulted in RA-loaded microparticles with variable characteristics. The higher encapsulation efficiency was registered for alginic acid sodium-, modified chitosan- and xanthan gum + alginic acid sodium- based microparticles (62, 65 and 76%, respectively). Also, RA controlled release prolonged for almost 8 h for alginic acid sodium-based microparticles and for almost 7 h for the majority of microparticles with alginic acid sodium in the biopolymers blends (the exception refers to microparticles composed by the modified chitosan + alginic acid sodium blend, wherein RA release was carried out in 100 min).

Spray-drying is a one-step procedure that enables the continuous (continuous batch), rapid and reproducible production of microparticles as carrier-based delivery systems at low cost. It is also an easy scale up process and enables the production of microparticles with good quality [13]. In the present work, two synthetic polymers – ethyl cellulose (EC) and polyethylene glycol (PEG) – were considered to design microparticle formulations for RA oral administration and provide its controlled delivery in the intestine. These materials are hypothesized as an approach to prepare carrier-based systems to be fed to the spray-dryer with a significantly higher mass of RA when compared to the maximum mass of RA that was possible to add to the biopolymer-based systems previously designed by the authors [278,314,319]. Moreover, the possibility to increase the encapsulation efficiency using synthetic polymer-based microparticles is also considered. This step is of major importance to ensure that the microparticles produced have a suitable amount of RA for the treatment of APL. The usual daily dose of Vesanoid® is 80 mg for one adult (patient information leaflet). EC-based microparticles and microparticles composed by the EC + PEG blend were produced. EC is a cellulose-derived polymer with biocompatible, non-allergic, non-irritant, tasteless and non-biodegradable properties. It is not water soluble, but soluble in several organic solvents (*e.g.* alcohols). EC is generally recognized as safe (GRAS) and has been widely explored in the pharmaceutical industry for the development of a drug carrier for preparation of microparticles capable to provide a sustained-release. In fact, EC has been described as a retardant of drug release despite of the acidity of the medium, being therefore used in the composition of oral delivery systems [320,321]. In turn, PEG is biocompatible and presents water solubility. Accordingly, the PEG inclusion in an EC formulation is carried out to increase drug release rate due to solubilization of PEG during gastrointestinal tract. The concentration of EC and PEG can be used to manage and reach a desired release rate [322].

7.2. Material and Methods

7.2.1. Materials

All-trans RA (≥ 98%, R2625-1G, CAS 302-79-4) and EC tested according to Ph. Eur. (28244-250G, Lot#BCBQ4872V, CAS 9004-57-3, viscosity: 10 mPa.s, ethoxy groups (dried substances): 48.0-49.5%, country of manufacture: USA) were obtained from Sigma-Aldrich. PEG 4000 for synthesis (807490-1KG, LOT#5191687, average molecular mass: 3500 - 4500) and 1-octanol for synthesis (820931, CAS 111-87-5) were supplied by Merck (German). Absolute ethanol (83813.360, Lot 21B104029, CAS 64-17-5) was acquired from VWR BDH Chemicals.

7.2.2. Formulation of RA loaded-polymer-based microparticles by spray-drying technology

EC was used individually (EC, 100%) and as a blend of materials (EC+PEG, 50%-50%) to prepare solutions in absolute ethanol (1% (w/v)). RA was added to the polymer-based solutions 24 h after their preparation (after fully hydration of polymers) in a final concentration of 0.1% (w/v). Each solution was prepared at 35 ± 2 ºC and under stirring conditions and immediately fed to the spray-dryer. A mini spray-dryer B-290 from BÜCHI

(Flawil, Switzerland) with a standard cyclone and a standard 0.5 mm nozzle, coupled to an Inert Loop B-295 also from BÜCHI (Flawil, Switzerland), was used to produce microparticles for RA encapsulation. Nitrogen pressure, aspiration rate and solution feed flow were set at 2 bar, 36 $m^3 \cdot h^{-1}$ (100%) and 4 $mL \cdot min^{-1}$, respectively. Inlet air temperature was set at 95 °C and outlet temperature varied between 41 and 51 °C. The temperature of Inert Loop B-295 was set to −5 °C. The microparticles produced were collected from the cyclone and the collection vessel of spray-dryer. Then the dry powder was stored under refrigeration and covered with aluminium foil until further analysis. The product yield (%) was determined based on Eq 7.1.

$$Product\ yield\ (\%) = \frac{Dry\ powder\ weight\ recovered\ in\ the\ cyclone\ and\ in\ the\ collection\ vessel\ of spray-dryer}{Total\ mass\ of\ materials\ used\ to\ prepare\ the\ systems\ fed\ to\ the\ spray-dryer} \times 100 \quad \textbf{(7.1)}$$

7.2.3. Microparticle morphology

A Fei Quanta 400 FEG ESEM/EDAX Pegasus X4M (Eindhoven, The Netherlands) was used to assess microparticles morphology by scanning electron microscopy. Herein, microparticles were placed into a brass stub with double sided adhesive tape and subsequently coated in vacuum by a thin layer of gold-palladium using a SPI module sputter coater.

7.2.4. Particle size distribution

Mean diameter of microparticles was assessed using a Coulter LS 230 Particle Size Analyser (Miami, FL, USA) by laser granulometry. A suspension of microparticles was prepared in water and analysed regarding volume and number distributions. The volume of each particle is considered in volume distribution, whereby a higher contribution is attributed to particles with a higher volume. In turn, in number distribution each particle has equal weight. Measurements were performed in triplicate and each analysis had the duration of 30 s.

7.2.5. Encapsulation efficiency and loading capacity

Encapsulation efficiency (%) was evaluated by the ratio between the mass of RA evidenced in the microparticles and the mass of RA added to the polymer-based solutions prior their feeding to the spray-dryer, considering the approach implemented by Gonçalves et al. [314,319] and adapted from Côrrea-Filho et al. [282]. RA loaded microparticles were suspended in octanol, stirred (2000 rpm, 2 min) and maintained on the laboratory bench overnight. Then the suspension was stirred again (2000 rpm, 5 min), put on a bath at 37 ± 2 ºC for 3 h and centrifuged. The quantification of RA in the supernatant was assessed by an UV/VIS spectrometer (SPEC RES+, Sarspec, Porto, Portugal) at 352 ± 7 nm. Calibration curve was validated in a concentration range between 0.00008 and 0.006 $mg \cdot mL^{-1}$ with a correlation coefficient of 0.9927. LOD and LOQ were 0.0002 $mg \cdot mL^{-1}$ and 0.0007 $mg \cdot mL^{-1}$, respectively.

Loading capacity was determined by the ratio between the mass of RA and mass of microparticles used.

7.2.6. Controlled release experiments

Loaded microparticles were put on a beaker with octanol (an organic solvent capable to imitate the characteristics of phospholipids membrane, considering its amphiphilic nature) [258,259,283,284]) at 37 ± 2 ºC and under magnetic stirring conditions. At appropriate time intervals samples were recovered, analysed in an UV/VIS spectrometer (section 2.5.) by absorbance (at 350 nm) and returned to the beaker. With the data obtained, RA release profiles from each type of microparticles were drawn. The models of zero-order (Eq. 7.2), Higuchi (Eq. 7.3), Korsmeyer-Peppas (Eq. 7.4) and Weibull (Eq. 7.5) [260–262,267]) were fitted to the obtained controlled release profiles.

$$Q_t = Q_0 + K_0 t \quad \textbf{(7.2)}$$

where Q_t is the cumulative amount of the drug/active compound released at the time t, Q_0 is the initial amount of the drug/active compound in solution (usually $Q_0 = 0$) and K_0 is the zero-order release constant.

$$Q_t = K_H \sqrt{t} \quad \textbf{(7.3)}$$

where K_H is the Higuchi constant.

$$Q_t/_{Q\infty} = K_K t^n \quad \textbf{(7.4)}$$

where Q_t/Q_∞ is the fraction of active compound released until time t and K_K is the Korsmeyer constant. The parameter n is a parameter that defines the release mechanism and is the release exponent (diffusional).

$$M_t = M_\infty \left[1 - e^{-\left(\frac{t-t_0}{\tau d}\right)^\beta}\right] \quad \textbf{(7.5)}$$

where M_t is the dissolution/release (%) of the active compound at time t, M_∞ is the dissolution/release (%) of the active compound at infinite time, t_0 is the lag-time of the dissolution (usually t_0=0), β indicates the shape parameter of the curve and τ_d is the time when 63.2% of M has been dissolved/released.

7.2.7. Statistical analysis

Particle size of microparticles was evaluated for all the microparticle formulations. Moreover, encapsulation efficiency and loading capacity was analysed for RA-loaded microparticles with different polymers on their composition. One-way analysis of variance (ANOVA) at $p < 0.05$ and consequent Tukey test were performed in Minitab® 19 software.

7.3. Results and discussion

EC-based microparticles and microparticles composed by the EC+PEG blend were designed as RA controlled delivery systems considering spray-drying technology. PEG-based microparticles were also produced. However, the solution composed by RA and PEG dissolved in absolute ethanol fed to the spray-dryer resulted in microparticles with a crystalline appearance that remained adhered to the cyclone of spray-dryer.

Accordingly, RA-loaded PEG microparticles were not possible to be recovered. Product yield of unloaded microparticles (microparticles MpPE – only composed by the polymer(s) as encapsulating agent(s)) and RA-loaded microparticles (microparticles MpPRA) changed between 12 and 28% (Table 7.1). This parameter is mostly affected by the formulation (*i.e.* solution, suspension or emulsion) fed to the spray-dryer and the properties of the materials used as encapsulating agents. Moreover, the volume of formulation prepared and the conditions used in the spray-drying technique also influence the product yield. In this work, spray-dryer was operated based on conditions previously used by some of the authors [323]. All the solutions were prepared with 100 mL, varying their composition in terms of the polymers used and the presence/absence of bioactive compound. The usage of EC as an individual encapsulating agent or in a blend with PEG resulted in a similar product yield among microparticles MpPE (Table 7.1). In turn, incorporation of RA in the microparticles decreased the product yield of EC-based microparticles, while increased the product yield of EC + PEG-based microparticles (Table 7.1). The type of polymers used seems to not interfere with product yield. However, the impact of the encapsulating agents' properties in the product yield is clear in several studies. For example, the high viscosity of xanthan gum requires the preparation of a higher volume of solutions/emulsions based on this polysaccharide when compared to the one used to prepare solutions/emulsions composed of low viscosity biopolymers, in order to obtain a similar product yield [314]. Furthermore, the product yield of polymer-based microparticles obtained in this work was lower when compared to the biopolymer-based microparticles produced in other works using the same encapsulating method [290,324,325]. Herein, a great amount of EC- and EC + PEG-based microparticles remained deposited on the cyclone of spray-dryer, which compromised the recovery of the dried powder. Several authors report the production of EC-based microparticles with a product yield mostly higher than 40%. Waghulde and Naik [326] produced EC microparticles by spray-drying technique for vildagliptin (an antihyperglycemic drug) encapsulation with a product yield between 40.85 and 75.73%. This experiment was carried out considering a two-factor three-level factorial design wherein the surfactant concentration (span-80, between 0.3 and 0.8 % w/v) and mass of EC (between 0.5 and 1.5 g) were selected as independent variables. EC solutions were prepared in methanol. The obtained particles exhibited a mean size of 1.026 µm. Also, Stocker et al. [327] and Tsolaki et al. [328] spray-dried active pharmaceutical ingredients-ionic liquids into EC with a product yield that ranged between 67.9 and 87.8% (only in two cases the product yield was 24.8% and 29.9%), using a mini spray-dryer combined with the B-295 inert loop and two-fluid nozzle (1.5 mm cap and 0.7 mm tip). The EC concentration used was 2.5% (w/v).

7.3.1. Surface morphology of microparticles

Microparticles MpPE and MpPRA, both composed by EC and by the EC + PEG blend, exhibited an irregular form that varied between a spherical and elliptic structure (Figure 7.1). Moreover, they evidenced several concavities that determined a rough surface. In this case, the production of microparticles with different formulations did not result in different microparticle morphologies. Waghulde and Naik [326] also evaluated

Table 7.1 – Characterization of polymer-based microparticles for RA encapsulation: product yield, particle diameter, encapsulation efficiency and loading capacity.

Microparticles content		Product yield (%)	Particle mean diameter		Encapsulation efficiency (%)	Loading capacity (%)
Formulation	**Encapsulating agent**		**Differential volume distribution (µm)**	**Differential number distribution (µm)**		
MpPE	EC	19	22 ± 2^{bc}	0.090 ± 0.002^{c}	-	-
	EC + PEG	21	6.0 ± 0.1^{c}	0.54 ± 0.02^{a}	-	-
MpPRA	EC	12	44 ± 8^{a}	0.13 ± 0.01^{b}	107 ± 23^{a}	10 ± 2^{a}
	EC + PEG	28	31 ± 13^{ab}	0.0987 ± 0.0004^{c}	109 ± 19^{a}	10 ± 2^{a}

Different letters in the same column indicate significant differences ($p<0.05$)

the morphology of microparticles produced, being very similar to the one registered for the microparticles obtained in this work. On the other hand, Wagh et al. [329] obtained by spray-drying EC micro-/nanospheres loaded with ketorolac tromethamine that showed a spherical form and a very slight rough surface. In the preparation of micro-/nanospheres the drug and polymer were dissolved in a mixture of dichloromethane and acetone along with magnesium stearate.

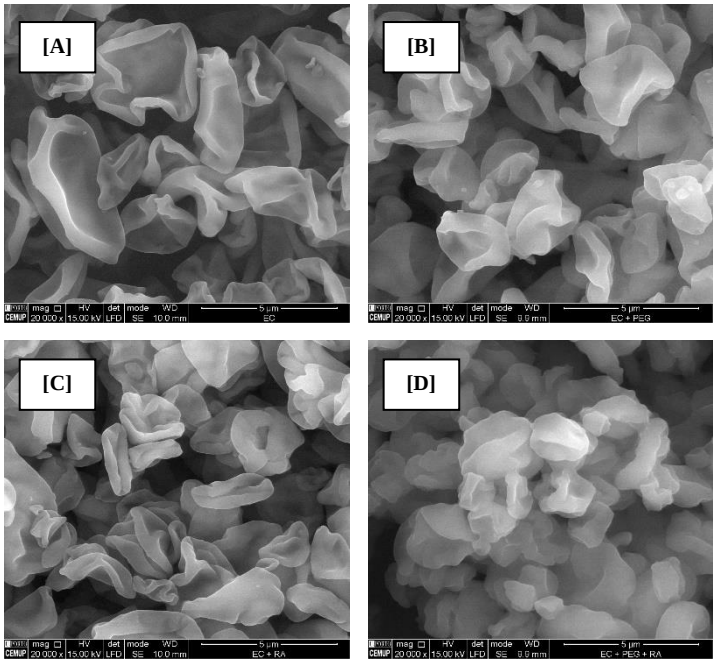


Figure 7.1 – Surface morphology of MpPE (A and B) and MpPRA (C and D) microparticles composed by EC (A and C) and EC + PEG blend (B and D). Magnification = 20,000 times, beam intensity (HV) 15.00 kV, distance between the sample and the lens (WD) around 10 mm.

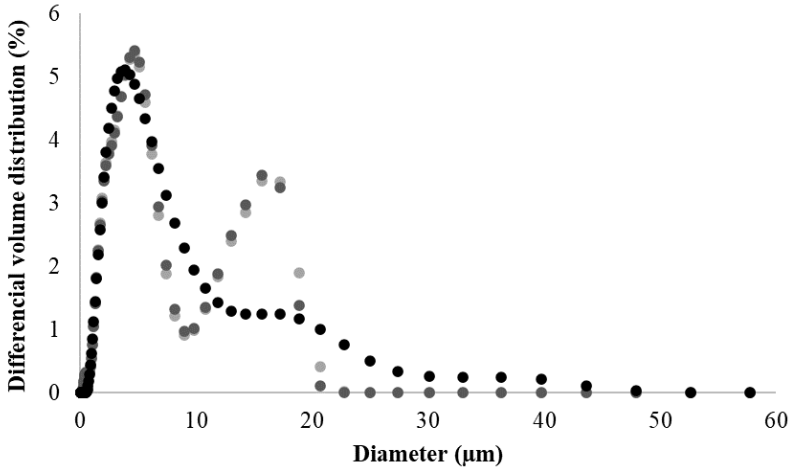


Figure 7.2 – Particle size distribution of microparticles MpPE composed by EC + PEG blend, considering differential volume distribution: replicate 1 - grey circles, replicate 2 - dark grey circles, replicate 3 – black circles.

7.3.2. Microparticle particle size

Mean diameter of all microparticle formulations ranged between 0.090 ± 0.002 and 0.54 ± 0.02 μm (Table 7.1) (differential number distribution). In other studies, the usage of spray-drying technology to produce microparticles composed by different biopolymers (individual or as a blend) for the controlled delivery of several bioactive compounds resulted in a powder with a mean size higher than 0.100 μm [278,303,316]. In turn, differential volume distribution showed an overall particle mean diameter between 6.0 ± 0.1 and 44 ± 8 μm, being the smaller size related to microparticles MpPE composed by EC + PEG blend (Table 7.1). These results suggest the aggregation of microparticles, which was identified on volume weighted size distribution (Figure 7.2). This explains the marked divergence of particle mean diameter exhibited comparing volume and number distribution. Waghulde and Naik [326] obtained EC microparticles by spray-drying with a mean size of 1.026 μm, as previously described (section 7.3.).

7.3.3. Encapsulation efficiency and loading capacity

Encapsulation efficiency was experimentally calculated as 107 ± 23 and 109 ± 19% for EC- and EC + PEG-based microparticles, while loading capacity was 10 ± 2% for both types of microparticles (Table 7.1). In this work, the production of polymer-based delivery microparticles capable to incorporate the total mass of RA used to formulate the systems fed to the spray-dryer is a major achievement. It must be pointed out the usage of an increased amount of RA up to a suitable amount for the treatment of APL. With an encapsulation efficiency of 100%, the amount of EC- and EC+PEG- based microparticles capable to incorporate the current daily amount of RA administrated for APL is less than 1 g.

In previous studies, biopolymer-based microparticles produced by spray-drying technology for RA encapsulation were designed by mixing a RA solution (prepared in coconut oil at 0.1% (w/v)), tween 80 (0.5% (w/v) regarding to RA solution) and each encapsulating agent solution. Herein, the higher encapsulation efficiency was 65 ± 6% using modified chitosan-based microparticles [314] and 76 ± 4% for microparticles composed by the xanthan gum + alginic acid sodium blend [319].

The encapsulating agents used in the microparticle production highly influence the bioactive compound content effectively retained in the carrier-based systems [234]. Waghulde and Naik [326] registered an encapsulation efficiency between 71.42 and 89.87% for the vildagliptin loaded microparticles composed by EC. In turn, Wagh et al. [329] observed an encapsulation efficiency between 70.74 and 79.68% for the ketorolac tromethamine-loaded micro-/nanospheres also composed by EC.

7.3.4. Drug controlled release

RA release from EC-based microparticles and microparticles composed by the EC + PEG blend was performed at 37 ˚C in octanol. This solvent will enable to assume about RA ability to cross the lipid membranes [258,259,283]. Carrier-based delivery systems composed by EC are resistant to acidic environments and enable to prolong the drug release for a long time, as previously referred (section 7.1.) [320,321]. In turn, the EC +

PEG blend arises as a strategy to increase the drug release due to PEG solubilization [322]. Accordingly, in this study it was assumed that the microparticles produced are not significantly damaged until they reach the intestine, wherein the release and absorption of RA is carried out in contact with lumen membrane.
The obtained cumulative RA release profiles are presented in Figure 7.3.

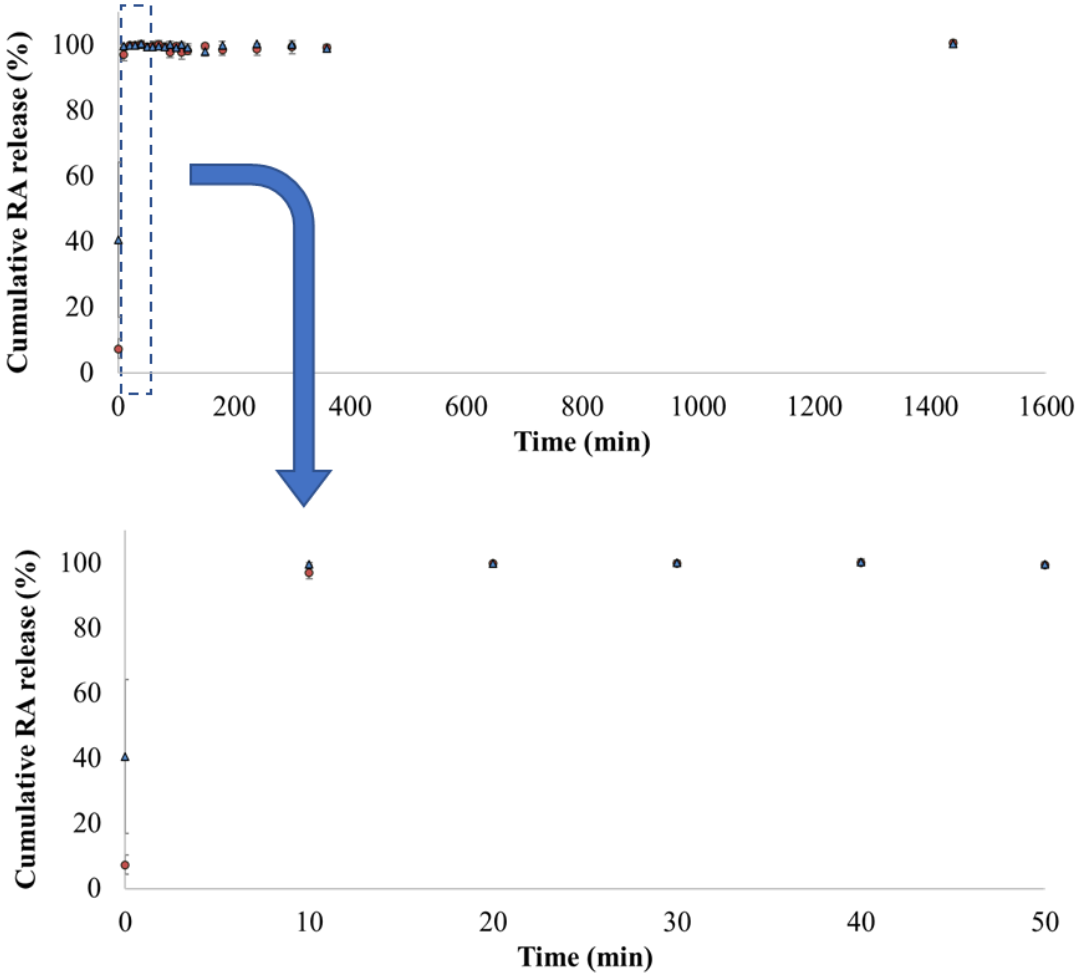


Figure 7.3 – Cumulative RA release from polymer-microparticles composed by EC (pink circles) and by the EC + PEG blend (blue triangles). Results are presented as the average and standard deviation of three independent assays.

The release RA behaviour from both types of microparticles was very similar and is characterized by a fast release of this drug to the surrounding environment. Complete RA release was achieved in 40 min when the polymer EC and the EC + PEG blend were considered as encapsulating agents. Several studies report the influence of different controlled release conditions in the drugs release rate from EC-based microparticles. For example, Waghulde and Naik [326] registered a continuous and constant release rate of vildagliptin from spray-dried EC microparticles in a phosphate buffer (pH 7.4) up to 12 h. At the end of 12 h between 89.45 and 97.4% of the drug was released. Wagh et al. [329] also used a phosphate buffer (pH 6.8) to investigate the release of

ketorolac tromethamine from EC microparticles obtained by spray-drying. Herein, drug release varied from 32.68 to 45.48% considering 12 h of experiment. de Francisco et al. [330] evaluated the fluoride release from EC microparticles and a fast release of sodium fluoride, sodium monofluorophosphate and aminofluoride in purified water was evidenced in the first 30 min.

7.3.5. Kinetic models

Kinetics of zero order (considers a slow and constant release rate) was adjusted to the RA controlled release profiles obtained from EC- and from EC + PEG-based microparticles with a determination coefficient of 0.774 and 0.751, respectively (Table 7.2). The zero-order release constant, K_0, was 7.1×10^{-3} and 7.2×10^{-3} mg·min^{-1}, suggesting a similar release rate of RA from both types of microparticles.

Regarding the Higuchi model, the Higuchi constant, K_H, registered the values 3.6×10^{-2} and 3.7×10^{-2} when the polymer EC and the EC + PEG blend were used in the microparticle formulations, respectively. Furthermore, the determination coefficient was 0.977 and 0.972.

The Korsmeyer-Peppas model was fitted to the RA controlled release profiles for Q_t/Q_∞ lower than 0.6 [262]. Again, for all the microparticles produced the parameter n was lower than 0.43 (n = 0.02 for EC-based microparticles and n = 0.004 for the microparticles composed by the EC + PEG blend (Table 7.2), whereby a Fickian diffusion (case I transport) and a rate as a function of time of $t^{-0.57}$ is suggested [145,262]. The Korsmeyer constant, K_K, and the determination coefficients were 9.1×10^{-1} and 9.8×10^{-1}, and 0.809 and 0.875, for the EC and the EC + PEG microparticles, respectively (Table 7.2).

Table 7.2 – Parameters and correlation coefficients of zero-order, Higuchi, Korsmeyer-Peppas and Weibull models fitted to the experimental RA release profiles.

	Parameters		Encapsulating agents	
			EC	**EC + PEG**
Kinetic models	**Zero-order**	K_0 (mg·min^{-1})	7.1×10^{-3}	7.2×10^{-3}
		Q_0 (mg)	2.2×10^{-2}	2.4×10^{-2}
		R^2	0.774	0.751
	Higuchi	K_H (mg·min$^{-0.5}$)	3.6×10^{-2}	3.7×10^{-2}
		R^2	0.977	0.972
	Korsmeyer-Peppas	K_k (min^{-n})	9.1×10^{-1}	9.8×10^{-1}
		n	0.02	0.004
		R^2	0.809	0.875
	Weibull	τ_d (min)	0.2	0.0004
		β	0.3	0.2
		R^2	0.841	0.768

Weibull model was adjusted to the controlled release profiles with determination coefficients of 0.841 and 0.768 for EC-based microparticles and microparticles composed by the EC + PEG blend, respectively (Table 7.2). The β parameter was lower than 1 for both types of microparticles (β = 0.3 for EC-based microparticles and β = 0.2 for EC + PEG-based microparticles (Table 7.2), indicating that the shape of the curve would show a steeper increase regarding the shape of the release curve that corresponds exactly to the shape of an exponential profile [262]. At last, τ_d parameter was 0.2 and 0.0004 min when the polymer EC and the EC + PEG blend were used as encapsulating agents, respectively (Table 7.2).

Weibull was the most appropriate model to describe the release of RA from all polymer-based microparticles proposed in this work. It is explained by the internal morphological structure of spray-dried microparticles [260]. Gonçalves et al. [278,314,319] observed that this model also enabled the best fit to the obtained RA controlled release profiles from different formulations of biopolymer-based microparticles produced by spray-drying.

7.4. Conclusion

The synthetic polymers EC and PEG were successfully used to produce RA-loaded microparticles by spray-drying. Herein, controlled delivery systems individually composed by EC and composed by the EC + PEG blend were developed. All the formulations enabled to obtain microparticles with a global small size (differential number distribution) and similar surface morphology. Loaded microparticles incorporated the total amount of RA fed to the spray-dryer, obtaining an encapsulation efficiency of around 100%. At last, both EC- and EC+PEG-based microparticles enabled a very fast complete release of RA (in 40 min). The incorporation of PEG in the EC-based microparticles did not change the RA release profiles.

Chapter 8 - *In vitro* bioaccessibility and intestinal transport of retinoic acid in ethyl cellulose-based microparticles and impact of meal co-ingestion

---

The eighth chapter proposes the evaluation of RA bioaccessibility after in vitro static digestion of RA loaded synthetic polymer-based microparticles (composed by EC and the EC + PEG blend), with and without co-ingestion of a reference diet. Moreover, the study of RA intestinal transport was presented considering an intestinal absorption model (Caco-2 cells).

This chapter is in the form of submitted paper:

Gonçalves, A; Viegas, O; Faria, M; Ferreira, I M.P.L.V.O.; Rocha, F; Estevinho, B N. *In vitro* bioaccessibility and intestinal transport of retinoic acid in ethyl cellulose-based microparticles and impact of meal co-ingestion

8.1. Introduction

Retinoic acid (RA) is a naturally occurring endogenous retinoid recognized for its anticancer activity [17]. This chemopreventive and chemotherapeutic agent acts in the regulation of gene transcription (involvement of a family of nuclear receptors comprising RA receptors (RARs)) [331], inhibiting the proliferation, migration and invasion of cells and promoting the differentiation, apoptosis and cellular cycle arrest [49,332–335].

The only effective strategy in the treatment of acute promyelocytic leukaemia (APL) is based on the usage of all-trans RA [274]. However, routine oral administration of this retinoid to the patients has been a challenge. Continuous repetitive RA administration leads to a marked reduction of RA half-life, occurring a high decrease of RA concentration in the plasma [25,26,58,276]. The concentration of RA reaching the target cells/tissues may therefore be insufficient to activate target genes. Moreover, the patients become resistant to this retinoid. For these reasons, the efficiency of RA as a pharmacological agent may be compromised.

The reasons for the RA half-life decrease are pointed out by Muindi et al. [58] and include the elimination of RA by biliary excretion (at least 60%), RAR-α mutations and the triggering of RA catabolism as a result of the continued treatment with this retinoid. Cytochrome P450 is involved in the RA cellular levels regulation, promoting the degradation of this retinoid with the production of 4-oxo all-trans RA. These enzymes are activated even in the presence of a low amount of RA, whereby the repeated RA administration during APL treatment promotes RA conversion and does not enable to maintain the RA levels in the plasma [17,277]. In the line with these topics, the development of a carrier-based system for oral administration capable to provide a slow and sustained release of RA in the small intestine might beneficiate the activity of this retinoid. This approach aims to avoid RA repetitive administration with impact on the reduction of the activity of cytochrome P450. Encapsulation of RA can also minimize the severe side-effects due to the high amount of RA administration as well as protect RA from the undesirable conditions in the gastrointestinal tract [318].

Spray-drying technology has been explored for RA encapsulation into several biopolymer-based microparticles formulations addressed for the treatment of APL [278,314,319,336]. It is a one-step, rapid, continuous (continuous batch), reproducible, low cost and of easy scale up method [193]. In our most recent work, microparticles composed by ethyl cellulose (EC) and the EC + polyethylene glycol (PEG) blend were proposed for RA oral administration and the controlled release and absorption in the intestine [336]. EC is described as a synthetic polymer used in oral delivery systems to protect the drugs from the acidity of the medium and retard the release [320,321]. The incorporation of PEG into EC formulations can be used to increase the drug release rate due to the solubilization of PEG in gastrointestinal tract [322]. The obtained carrier-based delivery systems were characterized in terms of encapsulation efficiency, morphology, particle size and controlled release studies. The best achievement was the production of RA-loaded microparticles with an encapsulation efficiency of 100%. These particles can incorporate an amount of RA, comparable to the recommended dose of Vesanoid® currently used in the treatment of APL, in a reasonable volume. The present work configures the next logical step in the study of the developed particles which involves its evaluation and validation to be used for RA oral administration. Carrier-based systems addressed for RA oral administration must be resistant to the stomach harsh environment and enable the RA delivery in the small intestinal lumen wherein vitamin A is absorbed [83].

This strategy also protects RA against the gastrointestinal aqueous environment and oxidant conditions [17,76]. Within the scope of APL treatment, the selection of the polymers to be used in the microparticles formulation is therefore of major importance. The aim of this work was thus to evaluate EC- and EC+PEG (ECP)-based microparticles loaded with RA towards its applicability by *in vitro* simulation of gastrointestinal digestion coupled to an intestinal absorption model (Caco-2 cells). The influence of digesting these microparticles with and without meal (following a western diet) was evaluated regarding RA bioaccessibility (gastric and intestinal phases) and RA intestinal transport. Several *in vitro* models are currently described to mimic the physiological processes performed in the gastrointestinal digestion [337]. *In vitro* static models are simple, low cost and reproducible in the evaluation of bioaccessibility [174,177]. Moreover, they are not usually used to evaluate the bioaccessibility of drugs. In this study, a general standardized *in vitro* digestion protocol proposed by the INFOGEST network was implemented [208]. The Caco-2 human colorectal cancer epithelial cell line is the most used among *in vitro* intestinal transport systems [222] covering a wide range of compounds [338,339]. Moreover, a few studies report the usage of this type of cells to evaluate the intestinal absorption of bioactive compounds incorporated into carrier-based delivery systems [223,224].

8.2. Material and Methods

8.2.1. Materials

All-trans RA (≥ 98%, R2625), EC tested according to Ph. Eur. (28244), bovine bile (B3883), porcine pepsin (P7012), porcine pancreatin (P7545), CaCl2(H2O)2 (C1016), MTT (3-(4,5-dimethylthiazol-2-yl)-2,5-diphenyltetrazolium bromide) (M2128) were supplied by Sigma-Aldrich. PEG 4000 for synthesis (807490), 1-octanol for synthesis (820931), NaOH (9141) and acetonitrile (HPLC grade, 100030) were obtained from Merck. Acetic acid (LC-MS grade) was obtained from Biosolve Chimie (Dieuze, France). Absolute ethanol (83813.360) was obtained from VWR BDH Chemicals. HCl (6081) was purchased from J. T. Baker. DMSO (D1370) was obtained at Duchefa Biochemie B.V (Haarlem, The Netherlands). High glucose Dulbecco's modified Eagle's medium (DMEM) (11965092), fetal bovine serum, MEM nonessential amino acids 100 X (11140050), GlutaMAX™ 100 X (11140050), penicillin/streptomycin 100 X solution (10,000 Units·ml^{-1}/10,000 mg·ml^{-1}) (15140122) and Hanks balanced salt solution (HBSS) were all purchased from Gibco/Life Technologies corporation (Paisley, United Kingdom). Transwell permeable polycarbonate 0.4 µm pore size 12-well supports and inserts (83.3931.040) were supplied from Sarstedt (Nümbrecht, Germany). Ultrapure water was obtained from distilled water by a Milli-Q gradient system (18.2 mΩcm^{-1}) from Millipore (Milford, MA, USA).

8.2.2. RA encapsulation into microparticles composed by EC and the EC+PEG blend by spray-drying

Two solutions composed by EC (100%) and the EC+PEG blend (50%-50%) were prepared in absolute ethanol at 1% (w/v) under stirred conditions and at 35 ± 2 ºC. After fully polymers hydration (24 h) RA was added to these solutions (0.1% (w/v)) and the final mixture was immediately fed to the spray-dryer. A mini spray-dryer B-290 (with a standard 0.5 mm nozzle and a standard cyclone) coupled to an Inert Loop B-295, all from BÜCHI (Flawil, Switzerland), was used to obtain the RA-loaded microparticles. Nitrogen pressure, aspiration rate, solution feed flow, inlet air temperature and the temperature of Inert Loop B-295 were set at 2 bar, 32 $m^3 \cdot h^{-1}$ (80%), 4 $mL \cdot min^{-1}$, 100 °C and −5 °C, respectively. The outlet air temperature varied between 44 and 59 °C. The microparticles produced were protected from the light with aluminium foil and stored at 4 °C. RA-loaded microparticles composed by EC and the EC + PEG blend were denominated microparticles EC and microparticles ECP, respectively. The product yield was determined by the ratio between the amount of dry powder recovered in the cyclone and in the collection vessel of spray-dryer and the total mass of compounds used to prepare the systems fed to the spray-dryer (Eq. 8.1).

$$Product\ yield\ (\%) = \frac{Dry\ powder\ weight\ recovered\ in\ the\ cyclone\ and\ in\ the\ collection\ vessel\ of spray-dryer}{Total\ mass\ of\ compounds\ used\ to\ prepare\ the\ systems\ fed\ to\ the\ spray-dryer} \times 100 \qquad \textbf{(8.1)}$$

8.2.3. Encapsulation efficiency and loading capacity

Encapsulation efficiency (%) was determined by the ratio between the amount of RA present in the microparticles and the amount of RA added to the synthetic polymers-based solutions fed to the spray-dryer, adapting the method described by Côrrea-Filho et al. [282]. Microparticles were suspended in octanol and stirred at 2000 rpm during 2 min and kept at room temperature overnight. Then, the suspension was stirred at 2000 rpm during 5 min, put on a bath at 37 ± 2 ºC for 2 h and centrifuged (Centromix mod. S-549, Porto, Portugal) at 50 000 rpm during 20 min. The supernatant was recovered and diluted in methanol for further determination of RA concentration by high-performance liquid chromatography (HPLC) at 355 nm (section 8.2.8.).

Loading capacity of microparticles was determined by the ratio between the amount of RA and microparticles weight.

8.2.4. Characterization of RA-loaded microparticles

Surface morphology and particle size were analysed by scanning electron microscopy using a Fei Quanta 400 FEG ESEM/EDAX Pegasus X4M (Eindhoven, The Netherlands). Microparticles were fixed into a brass stub with double-sided adhesive tape and then coated in vacuum by a thin layer of gold-palladium using a SPI module sputter coater.

8.2.5. Preparation of meal

The meal was prepared considering a common western dietary pattern, according to Silva et al. [340]. The food

ingredients used were beef (semi-fat) (200 g/800 g of meal), homemade french fries (fried in sunflower oil) (200 g/800 g of meal) and coke-type soft drink (400 g/800 g of meal), without salt addition (Table 8.1). At the end the meal was mixed using a Thermomix® (Vorwerk, Germany) to produce a homogeneous sample. Macro and micronutrientes composition of this Western Diet (88 compounds) can be assessed in a cured database [341].

Table 8.1 – Proximal composition of the meal used in *in vitro* digestion experiments following a western diet.

		Western diet		
		Beef (semi-fat)	Homemade french fries (cooked in vegetable oil)	Coke-type soft drink (mL)
Total amount (g)	800	200	200	400
Energy	982	384	454	144
Humidity	593.6	121.8	108.6	363.2
Protein	61.2	53.8	7.4	0
Fat	40.4	18.8	21.6	0
Saturated fatty acids	10.8	8	2.8	0
Monounsaturated fatty acids	13.2	8.4	4.8	0
Total polyunsaturated fatty acids	11.4	1.2	10.2	0
Trans fatty acids	1	0.8	0.2	0
Carbohydrates	91.2	0	55.2	36
Total sugars	39.4	0	3.4	36
Sucrose	21.4	0	1.8	19.6
Glucose	0	0	0	0
Frutose	0	0	0	0
Total fibers	4.8	0	4.8	0
Cholesterol	178	178	0	0
Ashes	6.4	3.6	2.4	0.4
Ca	88	36	28	24
Mg	104	60	40	4
K	2084	700	1380	4
Na	588	540	28	20
P	708	540	128	40
Fe	5.6	5	0.6	0
Zn	10.8	10.2	0.6	0
Mn	0	0	0	0
Cu	0	0	0	0
Se	0	0	0	0
Vitamin A	0	0	0	0
β-carotene	0	0	0	0
Vitamin D	0.6	0.6	0	0
Vitamin E	7.66	0.06	7.6	0
Thiamine	0.54	0.1	0.44	0
Riboflavin	0.44	0.38	0.06	0
Niacin	11.8	8.2	3.6	0
Trp/60	12.8	11.4	1.4	0
Niacin equivelants	22.2	19.6	2.6	0
Vitamin B6	1.56	0.56	1	0
Vitimanin B12	4	4	0	0
Vititamin C	26	0	26	0
Folates	113	39	74	0

8.2.6. INFOGEST *in vitro* digestion

The *in vitro* digestion was performed according to the internationally standardised methods described by Brodkorb et al. [208], simulating oral, gastric and small intestinal digestion. Briefly, 25 mg of EC-based microparticles or 22 mg of ECP-based microparticles (each type of microparticles contained a total of 2 mg of RA), with and without 5 g of meal, were mixed with 4 mL of simulated salivary fluid (SSF), 25 µL of 0.3 M $CaCl_2$ solution and 975 of µL of ultrapure water. The oral mixture was incubated at 37 °C under gentle stirring for 2 min. The obtained oral bolus was then mixed with 8 mL of simulated gastric fluid (SGF), 5 µL of 0.3 M $CaCl_2$, 0.5 mL of pepsin (2000 U·mL^{-1}), 1 N HCl to adjust pH to 3.0 and water (to reach a total volume of 20 mL) to form the gastric phase. The gastric mixture was incubated at 37 °C for 2 h under gentle stirring. Half of gastric chime was collected for further analysis while the other half was used to proceed with the intestinal digestion. Accordingly, 4.25 mL of simulated intestinal fluid (SIF), 20 µL 0.3 M $CaCl_2$, 2.5 mL of pancreatin solution (100 U·mL^{-1} based on trypsin activity), 1.25 mL of bile solution (10 mM), 1 N NaOH to adjust pH to 7.0 and water (to reach a total volume of 20 mL) were added to gastric chime to form the intestinal phase. The intestinal mixture was also at 37 °C for 2 h under gentle stirring. The samples obtained after gastric and intestinal digestion were immediately put on an ice bath for 10 min and then centrifuged at 5000 g and 4 °C during 10 min (Centrifuge Model 5810R, Eppendorf). The supernatant, correspondent to the bioaccessible fraction, was frozen at −20 °C. All the digestions were performed in triplicates plus one blank for pH adjustment. The two blanks of digestion, with and without meal, were performed with only one replicate. An overview about the *in vitro* digestion procedure as well as the RA intestinal transport assay (section 8.2.7.) is presented in Figure 8.1.

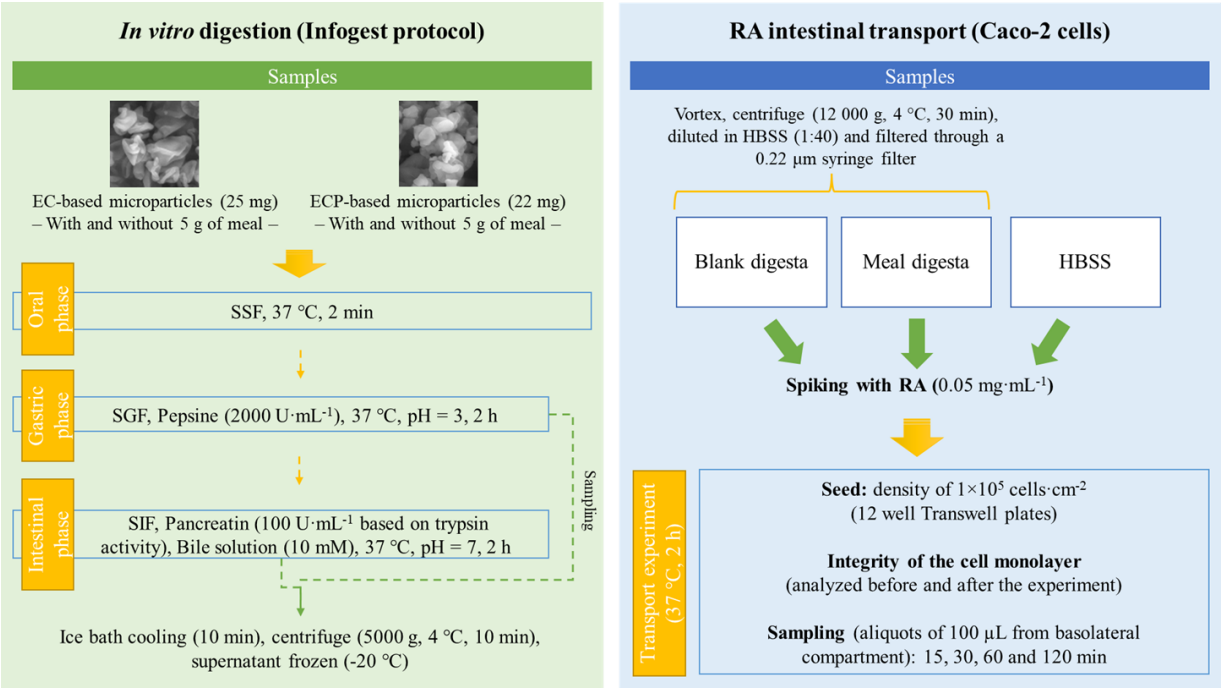


Figure 8.1 – *In vitro* digestion of RA-loaded EC- and ECP-based microparticles, with and without diet, and intestinal transport of RA.

8.2.7. Cell culture and intestinal transport

The human cell line Caco-2 cells were kindly provided by the "Molecular Physical-Chemistry" group of the University of Coimbra. Cells were cultured in a supplemented culture medium composed by DMEM, 10% of fetal bovine serum, 1% of non-essential amino acids solution, 1% GlutaMAX™ solution, 100 units·ml^{-1} penicillin and 100 mg·ml^{-1} streptomycin, at 37 °C and 5% CO_2. Culture medium was changed every two days until 60% confluence when cells were passaged. Experiments were carried out between passages 61 and 67.

For the evaluation of RA intestinal transport cells were seeded in a density of 1×10^5 cells·cm^{-2} in 12 well Transwell plates. The volumes of culture medium in the apical and basolateral compartments were 0.8 and 1.5 mL, respectively, changed with fresh medium every two days. The transport experiment was carried out between 21 and 28 days after the cells seeding in the inserts. Herein, the cell monolayers were washed twice with HBSS and then incubated at 37 °C for 30 min for cells stabilization. The integrity of the cell monolayer was analysed by measuring the transepithelial electric resistance (TEER) using the Millicell ERS-2 Voltohmmeter (Merck Millipore, Darmstadt, Germany). Only monolayers with a TEER value > 1000 Ω·cm^2 were considered for the experiment. A BSA in HBSS solution 1% (w/v) was added to the basolateral compartment to prevent plastic binding of compounds [342]. In turn, in the apical compartment cells were exposed to the bioaccessible fractions of the blank of digestion (blank digesta); the meal digestion (meal digesta) that were 1:40 diluted in HBSS and then spiked with RA (0.05 mg·mL^{-1}) to simulate a fasted state intestinal lumen. Moreover, the cells were also exposed to RA dissolved in HBSS (0.05 mg·mL^{-1}) as a control condition. Bioaccessible fractions were previously treated according to Garrett et al. [343]. Broadly, the blanks of final intestinal digestion were vortexed, centrifuged at 12 000 g at 4 °C for 30 min, diluted in HBSS and filtered through a 0.22 μm syringe filter.

The minimal digests dilution to be used in the transport assays was determined by a preliminary cellular viability (MTT test performed in a 96 well plate considering a cell density of $5x10^4$ cell·mL^{-1} (10000 cell/200 μL)) and monolayer integrity after 3 h of cells expositions to different dilutions of digests (1:3; 1:5 and 1:10).

Transport experiment was performed in triplicate for 120 min. Aliquots of 100 μL were taken from basolateral compartment after 15, 30 and 60 min and these volumes replenished with the same volume of basolateral medium. At the end of the experiment the whole volume from the apical and basolateral compartments were collected. All aliquots were kept at −20 °C until further analysis. At last, both compartments were washed twice with HBSS and then the monolayer integrity was evaluated after 30 min stabilization in HBSS at 37 ºC.

8.2.8. RA extraction and HPLC analyses

Bioaccessible fractions from gastric and intestinal phases, as well as the aliquots obtained from intestinal transport experiment were subjected to an extraction using acetonitrile. This solvent was added to each sample in an appropriate dilution and after 30 min (protein precipitation) the mixture was centrifuged at 17,000 x g (Heraeus Fresco 17 Centrifuge, Thermo Scientific™) for 5 min. The supernatant with RA was recovered for further quantification of this retinoid. In the case of aliquots corresponding to 15, 30 and 60 min of intestinal

transport, they were first lyophilized (Freeze Dryer Cryodos, Telstar, Terrassa, Spain) and then dissolved in acetonitrile. The supernatant obtained after centrifugation was evaporated to dryness by nitrogen stream and the analytes were redissolved in an appropriate volume of acetonitrile for further RA quantification.

Separation and quantification of RA was performed by high performance liquid chromatography (HPLC) using an analytical HPLC unit (Jasco, Japan) equipped with PU-1580 HPLC pump, a MD-2010 PLUS multiwavelength detector, an automatic injector AS-2057 Plus with a 20 µL injector and a column C18 reversed phase YMC-Triart C18 (25 cm length; 4.6 mm internal diameter; 5 µm particle size) was used. Samples were eluted at 0.9 $mL \cdot min^{-1}$ by an isocratic mobile phase composed by acetonitrile and acetic acid 1% (v/v) (90/10, v/v) was used (adapted from [344]. The wavelength was set at 355 nm [344] and the retention time was 11.3 min. The system was controlled by Borwin PDA Controller Software (JMBS Developments, Le Fontanil, France).

RA calibration curve with correlation coefficients of 0.9997 was validated in a concentration range between 0.005 and 10 $mg \cdot L^{-1}$. LOD and LOQ were 0.054 and 0.183 $mg \cdot L^{-1}$, respectively.

8.2.9. Statistical analysis

RA bioaccessibility was compared among digests of EC- and ECP-based microparticles, with and without diet, at gastric and intestinal level. Moreover, apical retention and intestinal transport was evaluated regarding the blank digesta and meal digesta spiked with RA and RA dissolved in HBSS. One-way analysis of variance (ANOVA) and ANOVA multiple comparison tests at $p<0.05$ with Tukey test were conducted by GraphPad Prism version 6.0 for Windows.

8.3. Results and discussion

8.3.1. Production and characterization of EC- and ECP-based microparticles loaded with RA

Microparticles EC and microparticles ECP, both loaded with RA, were obtained by spray-drying method with a product yield of 4 and 37%, respectively (Table 8.2). The composition of the system fed to the spray-dryer highly affects the product yield due to the influence of the properties of the polymers used as encapsulating agents and the type of formulations used (*i.e.* solution, suspension or emulsion). Moreover, the volume of formulation prepared and the operational conditions applied during the spray-drying (*i.e.* inlet air temperature) also influence the product yield. In this work, both solutions were prepared with 100 mL and the operating conditions used in the spray-dryer were similar to the one previously used by the authors to produce the same type of microparticles [336]. Accordingly, the differences pointed out in the product yield can be explained by the microparticles formulation used. The low product yield related to EC-based microparticles can be explained by the high amount of microparticles that moved towards the filter and the amount of microparticles that remained adhered to the walls of cyclone and the collection vessel of spray-dryer (visually observed). Gonçalves

et al. [336] produced EC- and EC + PEG- based microparticles for RA encapsulation and the product yield was also higher for the second set of microparticles (12 and 28 %, respectively).

Encapsulation efficiency and loading capacity were 91 ± 12 and 8 ± 4% for EC-based microparticles, respectively (Table 8.2). In turn, for ECP-based microparticles these parameters were 100 ± 7 and 9.1 ± 0.6%, respectively (Table 8.2). Broadly, encapsulation efficiency is influenced by the characteristics of the encapsulating agent(s) and the bioactive compound(s), the properties of the system fed to the spray-dryer and the parameters of the spray-drying process (*i.e.* inlet and outlet air temperature and aspiration rate, among others) [345]. In this work, the polymers used as encapsulating agents and their final concentration enabled them to obtain an encapsulation efficiency higher than 90%. Particularly, the EC + PEG blend enabled the total retention of RA inside the microparticles. Furthermore, these synthetic polymer-based microparticles enabled the incorporation of a significantly higher mass of RA when compared to the mass of RA that was possible to incorporate in microparticles composed by several biopolymers (*e.g.* modified chitosan, alginic acid sodium, arabic gum, xanthan gum and gelatin [314,319]), individually used or as a blend. This achievement may become the formulations herein proposed with higher interest for the treatment of APL. The daily dose of Vesanoid® is around 80 mg of RA for an adult (patient information leaflet).

Table 8.2 – Product yield, encapsulation efficiency and loading capacity of RA-loaded microparticles composed by different synthetic polymer formulations.

Microparticles formulations	Product yield (%)	Encapsulation efficiency (%)	Loading capacity (%)
EC	4	91 ± 12	8 ± 4
ECP	37	100 ± 7	9.1 ± 0.6

Microparticles EC and microparticles ECP evidenced a very irregular form and several concavities. Moreover, they exhibited an estimated size of 2 µm (Figure 8.2). A similar morphology was observed by the authors when they produced RA-microparticles using the same formulations [336].

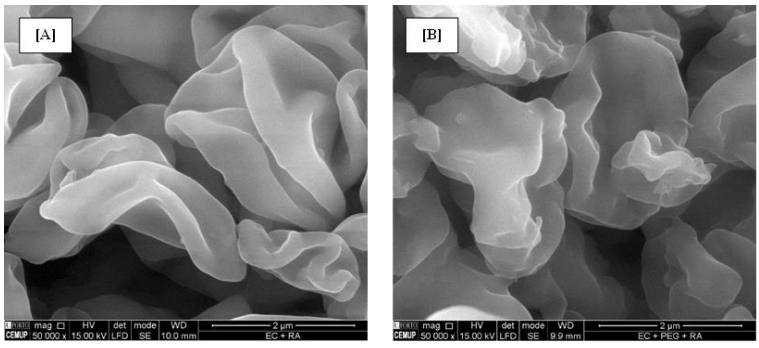


Figure 8.2 – Surface morphology of microparticles EC (A) and microparticles ECP (B). Magnification = 50,000 times, beam intensity (HV) 15.00 kV, distance between the sample and the lens (WD) around 10 mm.

8.3.2. RA bioaccessibility at gastric and intestinal levels

The bioaccessibility of RA at gastric and intestinal levels was evaluated when RA-loaded microparticles composed by EC and the EC+PEG blend were subjected to the INFOGEST *in vitro* digestion method. The effect of digesting the microparticles together with a meal (following a western diet) on RA bioaccessibility was also assessed. No significant changes were observed on RA bioaccessibility at gastric level (Figure 8.3). Herein, the highest percentage was 3 ± 2%, when microparticles EC without diet were digested. These results evidenced

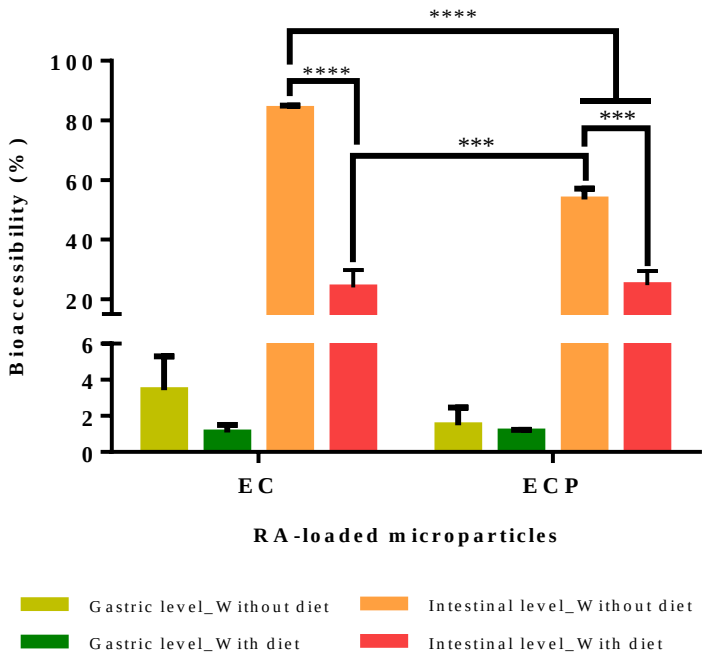


Figure 8.3 – Gastric and intestinal bioaccessibility (%) of RA after the *in vitro* digestion of RA-loaded microparticles with and without diet. **** $p < 0.0001$, *** $p < 0.001$.

the ability of the synthetic polymers used as encapsulating agents to maintain the RA-loaded microparticles relatively intact and, consequently, to preserve RA inside the microparticles during gastric digestion. In fact, EC is widely used in the pharmaceutical industry for the development of oral delivery-based systems due to its ability to prevent drugs exposure to the stomach conditions, at the same time enabling a sustained drug release in the intestinal tract for further absorption [320,321], as previously described (section 8.1.). Moreover, the inclusion of PEG in the EC-based formulation does not seem to have promoted the RA release from microparticles ECP in the stomach due to the expected PEG solubilization in water and subsequent creation of spaces in the matrix. Accordingly, this current formulation proposed, due to the concentration and/or the proportion of polymers used, may not benefit the final microparticles in controlled release studies for the delivery of RA in the intestine.

At intestinal level, RA bioaccessibility was significantly influenced by the type of microparticles and the presence of diet (Figure 8.3). Microparticles EC without diet enabled a significant higher bioaccessibility of this retinoid (84 ± 1%) when compared to microparticles EC with diet (24 ± 6%), as well as microparticles ECP

with and without diet (54 ± 4 and 25 ± 5%, respectively) ($p < 0.0001$). Also, the diet significantly decreased RA bioaccessibility when microparticles ECP were considered ($p < 0.001$). At last, microparticles EC with diet showed a lower bioaccessibility of RA when compared to microparticles ECP without diet. The presence of PEG in the microparticles ECP did not beneficiate RA bioaccessibility after a total of 4 h of digestion (gastric + intestinal), whereby the highest bioaccessibility was achieved from microparticles EC. In turn, the integration of a diet in the digestion of RA-loaded microparticles globally led to a lower bioaccessibility of RA. This might be caused by the amount of RA released from microparticles EC and ECP that are adsorbed to the digesta solids and fibers. Food matrix may impact the bioaccessibility of bioactive compounds and drugs, as described by several authors. For example, Sobral et al. [346] observed that the addiction of herbs and/or beer did not significantly change the bioaccessibility of several antibacterial and coccidiostat drugs – chlortetracycline, doxycycline and tylosin – on chicken meat burgers oven cooked and microwaved. However, the bioaccessibility of most sulfonamides tested was increased when they were cooked with herbs. In turn, Faria et al. [347] registered a decrease on the bioaccessibility of some food contaminants when they were spiked in western, mediterranean and vegetarian diet matrices. With exception, benzo[*b*]fluoranthene, benzo[α]pyrene and ochratoxin A (pure compounds) showed a similar bioaccessibility when compared the bioaccessibility of these compounds spiked in western diet. Moreover, the dietary pattern itself showed to significantly affect the bioaccessibility of some contaminants.

For the best of our knowledge, there is no published studies exploring the bioaccessibility of RA upon RA oral administration, considering free RA or RA encapsulated into a carrier-based delivery systems.

8.3.3. Intestinal transport of RA

The simulation of the intestinal transport in a Caco-2 monolayers, using digesta obtained from *in vitro* simulation, requires previous testing to assure the digesta does not compromise the cell barrier integrity, in the conditions used. The bile acids and enzymes present in the bioaccessible fraction obtained in the end of digestion may compromise cellular viability hindering the accurate assessment of RA intestinal transport [347]. Preliminary experiments showed a marked loss in Caco-2 monolayer integrity after 3 h of cells exposition to micelar fractions of the digests of microparticles EC and ECP, with and without diet, diluted 1:3; 1:5 and 1:10 with HBSS (data not shown). The obtained results evidenced a notable loss of cellular viability for all dilutions of the digests, wherein the global highest cellular viability was 14%. As exception, for the digest without microparticles and without diet with the 1:10 dilution it was registered a cellular viability of 89%. Another experiment was thus performed using higher dilutions: 1:3, 1:10, 1:20 and 1:40. The 1:40 dilution was the only one that enabled to maintain the integrity of cells after 3 h of cells exposition to the digests, whereby it was considered the most appropriate for further intestinal transports assays.

This dilution is higher than the needed in other previous studies, where in some cases a 1:3 dilution is enough in this type of experiments to maintain the cellular viability, according previously tests performed in the lab [347]. However, in our previous studies using the 1:3 dilution, a flash heating step of 5 min at 98 ºC for enzymes

inactivation was performed, which could not be applied in the present study since RA is a thermolabile substance thus a higher dilution had to be used.

Intestinal transport of RA from apical to basolateral compartment was then evaluated along 2 h. The amount of RA in the basolateral compartment that crossed the Caco-2 monolayer at 15, 30 and 60 min after the beginning of experiment was below the LOQ for all the samples and even below the LOD for most of them. Notwithstanding, after 120 min of transport, the percentage of RA reaching the basolateral compartment was detectable for all the samples and it was significantly higher for the blank digesta with RA (7.8 ± 0.6%) when compared to RA dissolved in HBSS (5.2 ± 0.4%) ($p < 0.01$) (Figure 8.4). Although transported in low percentages during the 2 h experiment RA was capable of crossing the intestinal barrier with a tendency to higher efficiency when a digesta matrix was present.

After 2 h of transport, the percentage of RA retained in the apical compartment was significantly influenced by the matrix (blank digesta or HBSS) in which RA was dissolved (Figure 8.4). A significant higher percentage of RA was retained in the apical compartment when blank digesta ($p < 0.01$) and meal digesta ($p < 0.05$) spiked with RA were used. Moreover, the presence of diet in the digests decreased RA retention from 44 ± 6 to 38 ± 1% (statistically non-significant) (Figure 8.4). This can be related to the ability of the fat component of diet to promote the aggregation of RA and further transport it to the cells which would be a beneficial situation although no significant increase in the RA fraction transported was denoted for these samples.

The obtained results suggest that an important fraction of RA was up taken by the cells or was adsorbed in the plastic surfaces and did not reach the basolateral compartment. For blank digesta and meal digesta spiked with RA and RA dissolved in HBSS, this fraction corresponds to 48 ± 6, 56 ± 1 and 69 ± 1%, respectively. Notwithstanding, to establish a better correlation with the *in vivo* situation, dynamic data on the transport at 15, 30, 60 and 120 minutes would be useful to calculate the apparent permeability of the substance and infer the percentage in which the RA is absorbed in the tested conditions.

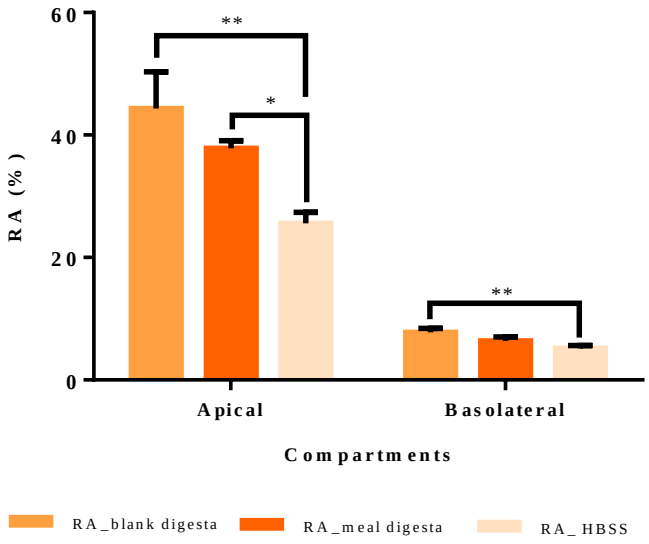


Figure 8.4 – Apical retention and intestinal transport of RA after 2 h of transport. ** $p < 0.01$, * $p < 0.05$.

8.4. Conclusion

Synthetic polymer-based microparticles composed by EC and the EC + PEG blend were successfully produced for RA encapsulation by spray-drying. However, the product yield was around 9-fold lower for the EC-based microparticles. Both carrier-based delivery systems enabled the incorporation of an amount of RA that make them comparable to the current dosage administrated to APL patients. The polymers used as encapsulating agents enabled the necessary protection of RA in the gastric phase of digestion. The simultaneous administration of the particles with a meal and the microparticle formulation significantly influenced the bioaccessibility of RA at intestinal level *in vitro*. The digestion of RA-loaded microparticles composed by EC without diet ensured the highest RA bioaccessibility. The digestion of both microparticles with diet significantly decrease RA bioaccessibility probably due to the adsorption of this retinoid to the meal matrix. Regarding intestinal transport, the maximum percentage of RA that reached the basolateral compartment was 7.8 ± 0.6% from the blank digesta spiked with RA after 2 hr of simulated transport. Also, the percentage of RA retained in the apical compartment was significantly influenced by the matrix. These are important findings ensuring that the inclusion of RA in the proposed particles can protect the substance from gastric degradation and does not significantly hinder its intestinal release and transport to the systemic circulation.

Chapter 9 - (Bio)polymer-based microparticles obtained by spray drying as co-encapsulation systems for co delivery of retinoic acid, curcumin and/or resveratrol

---

The nineth chapter proposes co-encapsulation of RA, curcumin and/or resveratrol into microparticles composed by alginic acid sodium (spray-drying of an oil-in-water emulsion) and the EC + PEG blend (spray-drying of an ethanolic solution) for protection and co-delivery of these bioactive compounds.

This chapter is in the form of submitted paper:

Gonçalves, A; Rocha, F; Estevinho, B N. (Bio)polymer-based microparticles obtained by spray drying as co-encapsulation systems for co delivery of retinoic acid, curcumin and/or resveratrol.

9.1. Introduction

The treatment of acute promyelocytic leukemia (APL) was revolutionized with the introduction of all-trans retinoic acid (all-trans RA) in 1988 [18] and arsenic trioxide in 1996 [348]. In the last three decades the studies showed the efficacy of all-trans RA combined with chemotherapy and then the efficacy of all-trans RA combined with arsenic trioxide, with or without chemotherapy [274,349]. Accordingly, clinical trials have promoted the development of several regimens for the treatment of APL [349]. In fact, all-trans RA is referred as the only effective in the treatment of APL. This retinoid acts in the activation of blocked genes transcription and in the degradation of PML/RARα, the oncogenic fusion protein obtained due to the reciprocal and translocation involving the retinoic acid receptor (RARα) located on chromosome 17 and PML gene located on chromosome 15 [350–352]. In turn, arsenic trioxide promotes the apoptosis further degradation of PML/RARα. Moreover, arsenic trioxide has pro-oxidant effect [24].

Several studies have been performed to explore and suggest new retinoids and the combination of different molecules with all-trans RA or arsenic trioxide to trigger alternative mechanisms of action and therefore lead to a synergistic effect on growth control and apoptosis of cancerous cells in APL [24]. In the line with this topic, curcumin and resveratrol has been indicated as potential bioactive compounds to be used as therapeutic agents in the treatment of APL.

Curcumin is a phenolic compound with yellow-orange colour and the active ingredient from *Curcuma longa* (Turmeric). This hydrophobic compound has received great attention due to its pharmacological functions, including antitumor agent [353]. The anticancer activity of curcumin is considered to be related to its antioxidant and pro-oxidant actions. In fact, as an antioxidant, curcumin acts against two critical initiators of cancer, inhibiting free radicals from mediating peroxidation of membrane lipids or oxidative DNA damage [354]. In the treatment of APL, curcumin inhibits and arrests the proliferation of leukemic cells derived from APL by stabilizing the misfolded nuclear receptor co-repressor (N-CoR) protein. N-CoR proteins are involved in the transcription of genes that regulate the proliferation, differentiation and apoptosis of cells, participating in the development of blood and immune cells (erythrocytes and thymocytes, respectively) [355,356]. These proteins are recruited by the oncogenic fusion protein PML/RARα and the N-CoR/PML/RARα complex formed represses the RA target genes and reduces the differentiation of APL cells [357,358]. Moreover, PML/RARα promotes the N-CoR misfolding and its accumulation in the cytosol, which induces the endoplasmic reticulum stress and the activation of the unfolded protein response with cytoprotective or cytotoxic action [359,360]. Curcumin inhibits specific proteases and the proteasome that degrade misfolded N-CoR, contributing to increase the endoplasmic reticulum stress and then to sensitize APL cells to apoptosis induced by unfolded protein response [21,361,362]. A study performed by Kini et al. [363] enabled to understand how curcumin can influence the differentiation of NB4 APL cells. These cells can differentiate in response to all-trans RA, while NB4-R1 cells are resistant to this retinoid. The obtained results evidenced that the usage of curcumin alone does not promote the differentiation of NB4 cells and higher concentrations of this bioactive compound can trigger the apoptosis. Moreover, the treatment of NB4 cells with curcumin enabled to increase the differentiation of

cells promoted by all-trans RA. In addition, the combination of all-trans RA and curcumin was capable to induce the differentiation of the NB4-R1 cells. This result was not achieved using individually each bioactive compound.

Resveratrol is recognized as the best-known compound of the stilbene group. It is also a polyphenol and can be naturally found in the mulberry tree, berries, grape skins, peanuts and red wine, among others. The health benefits of this bioactive compound are widely described and include the ability of resveratrol to prevent cancer [315,364]. Briefly, resveratrol induces the apoptosis and arrests the cell cycle, reducing the risk of mutation [365–367]. Several authors report the ability of resveratrol to act against leukemic cells preventing proliferation and inducing apoptosis of cells [364,368]. Meng et al. [368] indicated that these processes can be related to the ability of resveratrol to up-regulate PTEN expression as well as to inhibit the activity of PI3K/AKT pathway. The combination of all-trans RA and resveratrol may benefit the treatment of APL, according to the studies performed by Cao et al. [369]. They reached the induction of 100% of NB4 cells into NBT-positive. The individual usage of these bioactive compounds only enabled a small conversion of the cells. The combination of resveratrol with arsenic trioxide also evidenced to be an advantage in the treatment of APL. Fan et al. [370] observed that resveratrol displays a synergetic effect with arsenic trioxide, whereby their co-administration significantly increased the anticancer action of arsenic trioxide in NB4 cells. Moreover, it was noted that resveratrol decreased the cardiotoxicity induced by arsenic trioxide. This bioactive compound can also reduce the hepatotoxicity related to arsenic trioxide administration [371].

This work proposes the co-encapsulation of RA with curcumin and/or resveratrol into (bio)polymer-based microparticles obtained by spray-drying to beneficiate the APL treatment due to the co-delivery of these bioactive compounds in the intestine.

Encapsulation of RA by spray-drying technology has been studied by the authors as a strategy to overcome the clinical limitations observed in the treatment of APL and related to the oral administration of this retinoid [245,314,319,336]. Continuous repetitive RA administration handles with a significant decline of RA half-life in blood and consequently a noticeable decrease of RA concentration is observed in the plasma [25,26,58,276]. The activity of cytochrome P450 can be involved in this behaviour, whereby these enzymes regulate the cellular levels of RA and they are activated even at a low amount of RA [277]. Moreover, RA presents high physicochemical instability and poor solubility in water [17]. The usage of a carrier-based system capable to provide a slow and continuous controlled release of RA in the intestine may reduce the activity of cytochrome P450 and therefore increase the RA bioavailability in the human body. The severe side-effects related to RA administration and described in the treatment of APL can also be minimized using this encapsulation-based approach. Encapsulation of curcumin and resveratrol can also beneficiate these bioactive compounds in order to deal with their poor solubility in water and chemical instability, among others [290,315].

Spray-drying technology enables the production of loaded microparticles in a rapid, continuous (continuous batch) and reproducible mode. Moreover, it is a one-step, low cost and easy scale up method [193]. Previous studies evidenced that alginic acid sodium-based microparticles evidenced an encapsulation efficiency of 62% and enabled a slower RA release that prolonged for more than 7 h [314]. Also, ethyl cellulose (EC) +

polyethylene glycol (PEG)-based microparticles showed an encapsulation efficiency of 100% and enabled the incorporation of an amount of RA comparable to the amount of RA orally administrated [336]. Moreover, *in vitro* digestion studies (INFOGEST protocol) evidenced the ability of these synthetic polymer-based microparticles to protect RA from the gastric phase conditions and enable its release in the intestinal phase [372]. Accordingly, both carrier-based delivery systems were selected in this study for co-encapsulation of RA with curcumin and/or resveratrol. RA-loaded microparticles were characterized in terms of encapsulation efficiency, particle size, surface morphology and *in vitro* controlled release profiles.

9.2. Material and Methods

9.2.1. Materials

All-trans RA (≥ 98%, R2625-1G, CAS 302-79-4), Resveratrol (≥ 99%, R5010-100MG, CAS 501-36-0), Curcumin from *Curcuma longa* (Turmeric) powder (≥ 65%, C1386-10G, 458-37-7), alginic acid sodium salt (180947-500G, Lot#MKBS5877V, CAS 9005-38-3, MW: between 120,000 and 190,000 $g \cdot moL^{-1}$, ratio of mannuronic acid to guluronic acid (M/G ratio): 1.56, country of manufacture: United Kingdom), EC tested according to Ph. Eur. (28244-250G, Lot#BCBQ4872V, CAS 9004-57-3, country of manufacture: USA), coconut oil from *Cocos nucifera* (C1758-500G, Lot#MKCK3631, CAS 8001-31-8) and tween 80 (P1754-1L, Lot#BCBT8094, CAS 9005-65-6) were purchased from Sigma-Aldrich. PEG 4000 for synthesis (807490-1KG, LOT#51916871) and 1-octanol for synthesis (820931, CAS 111-87-5) were obtained from Merck (German). Absolute ethanol (83813.360, Lot 21B104029, CAS 64-17-5) was supplied by VWR BDH Chemicals.

9.2.2. Preparation of systems to be fed to the spray-dryer

Two different approaches were tested, using emulsions and solutions. Four emulsions and four solutions were prepared to be fed to the spray-dryer for co-encapsulation of RA with curcumin and/or resveratrol into carrier-based microparticles.

The emulsion-based systems were prepared considering encapsulating agent/coconut oil ratio of 2.77 $g \cdot g^{-1}$. This proportion was based in previous studies performed by the authors, which evaluated the largest amount of coconut oil that was possible to incorporate in the microparticles and ensure the high quality of final microparticles [245,278]. Aqueous phase of emulsions was composed by alginic acid sodium dissolved in ultra-pure water (1% (w/v)). In turn, the oily phase was composed by a RA, RA + curcumin, RA + resveratrol or RA + curcumin + resveratrol solution prepared in coconut oil (0.1% (w/v) of each bioactive compound). The surfactant tween 80 was added to the core material solutions (0.5% (w/v) regarding to this oily solution) and the final mixture was dispersed with the encapsulating agent solution at 12000 rpm for 5 min using a mechanical homogenizer (CAT, Germany).

The solution-based systems were composed by the EC + PEG blend (50%-50%) prepared in absolute ethanol (1% (w/v)) and RA, RA + curcumin, RA + resveratrol or RA + curcumin + resveratrol further dissolved in this synthetic polymer solution (final concentration of 0.1% (w/v) of each bioactive compound).

All the solutions were prepared under stirred conditions and at 35 ± 2 ºC. Moreover, the encapsulating agent solutions were prepared 24 h before their usage to ensure fully hydration of biopolymer and synthetic polymers. At last, the emulsions produced were immediately fed to the spray-dryer for the microparticles production.

9.2.3. Spray-drying technology

A mini spray-dryer B-290 from BÜCHI (Flawil, Switzerland) with a standard 0.5 mm nozzle and a standard cyclone was used to dry the emulsions and the solutions with RA, RA + curcumin, RA + resveratrol or RA + curcumin + resveratrol and produce loaded microparticles. An Inert Loop B-295 from BÜCHI (Flawil, Switzerland) was coupled to the spray-dryer when the solutions were fed to this equipment. For the emulsions, air pressure, aspiration rate, solution feed flow and inlet air temperature were set at 5-6 bar, 35 $m^3 \cdot h^{-1}$ (90%), 4 $mL \cdot min^{-1}$ and 130 °C, respectively. The outlet air temperature varied between 63 and 71 °C. In turn, for the solutions, nitrogen pressure, aspiration rate, solution feed flow, inlet air temperature and the temperature of Inert Loop B-295 were set at 2 bar, 32 $m^3 \cdot h^{-1}$ (80%), 4 $mL \cdot min^{-1}$, 100 °C and −5 °C, respectively. The outlet air temperature varied between 52 and 56 °C. The obtained dry powder (microparticles) was recovered in the cyclone and in the collection vessel of spray-dryer and protected from the light with aluminium foil and stored at 4 °C until further analysis. The product yield was determined according to the Eq. 9.1.

$$Product\ yield\ (\%) = \frac{Dry\ powder\ weight\ recovered\ in\ the\ cyclone\ and\ in\ the\ collection\ vessel\ of spray-dryer}{Total\ mass\ of\ materials\ used\ to\ prepare\ the\ systems\ fed\ to\ the\ spray-dryer} \times 100 \quad \textbf{(9.1)}$$

9.2.4. Emulsions viscosity

Emulsions viscosity was assessed from steady-shear flow curves (a total number of 50 points for each sample) using an Anton Paar MCR 92 rheometer (Austria). An increasing shear rate from 1 to 100 s^{-1} was applied using a measuring plate PP50 (Part No.: 79045, Serial No.: 55422, Cat No.: 79045, Del No.: 80352243, Anton Paar) with 50 mm of diameter and a gap of 0.5 mm. Analyses were performed in duplicate at 25 ºC.

9.2.5. Emulsions zeta potential

Zeta potential (as an indication of droplet surface electrical charge) of emulsions was measured by dynamic light scattering using a Zetasizer Nano-ZS90 (Malvern Instruments, Worcestershire, UK). Measurements were performed in duplicate.

9.2.6. Droplet and particle size distribution

Emulsions droplet size and the size of microparticles obtained by spray-dryer were evaluated by laser granulometry using a Coulter LS 230 Particle Size Analyser (Miami, FL, USA). In the case of alginic acid

sodium-based microparticles, they were first dispersed in ethanol and the obtained suspension was considered for the size assessment. Droplet and particle size measurements were performed in duplicate and each analysis had the duration of 30 seconds. The obtained results were expressed as the average of droplet and particle mean diameter, considering volume and number distributions. In the volume distribution, the volume of each particle is considered (particles with a higher volume have higher contribution). In turn, in the number distribution, each particle has equal weight.

9.2.7. Microparticle morphology

Scanning electron microscopy was performed with a Fei Quanta 400 FEG ESEM/EDAX Pegasus X4M (Eindhoven, The Netherlands) for the analysis of the surface morphology of microparticles. Herein, microparticles were fixed into a brass stub with double-sided adhesive tape and then coated in vacuum by a thin layer of gold-palladium using a SPI module sputter coater.

9.2.8. Encapsulation efficiency and loading capacity

Encapsulation efficiency (%) was determined by the ratio between the mass of each bioactive compound present in the microparticles (RA, curcumin and/or resveratrol) and the mass of each bioactive compound used to prepare the oily phase of emulsions and the solutions fed to the spray-dryer, adapting the method described by Côrrea-Filho et al. [282] and considering the procedure carried out by the authors in previous works. Briefly, loaded microparticles were dispersed in octanol, stirred at 2000 rpm during 2 min and maintained at room temperature overnight. The suspension was then stirred at 2000 rpm during 5 min, put on a bath at 37 ± 2 ºC for 3 h and centrifuged (Centromix mod. S-549, Porto, Portugal) at 50000 rpm for 20 min. The concentration of RA, curcumin and resveratrol present in the supernatant was determined using an UV/VIS spectrometer (SPEC RES+, Sarspec, Porto, Portugal) at 356.098 ± 19.7, 438.614 ± 21.388 and 315.0415 ± 17.091 nm, respectively. Calibration curves of RA, curcumin and resveratrol were validated over a range of concentrations registered in Table 9.1. The correlation coefficients, LODs and LOQs are also indicated.

Loading capacity of microparticles was determined by the ratio between the mass of each bioactive compound and the mass of microparticles.

Table 9.1 – Concentration range, LOD and LOQ and correlation coefficients related to the calibration curves of RA, curcumin and resveratrol.

Calibration curve	Concentration range ($mg \cdot mL^{-1}$)	LOD ($mg \cdot mL^{-1}$)	LOQ ($mg \cdot mL^{-1}$)	R^2
RA	0.0001 - 0.008	0.000224	0.000746	0.9953
Curcumin	0.00005 - 0.005	0.000225	0.000750	0.9951
Resveratrol	0.000200 - 0.007000	0.000338	0.001128	0.9943

9.2.9. Controlled release experiments

Controlled release experiments were performed in octanol, an organic solvent capable of good mimic of phospholipids membrane characteristics due to its amphiphilic nature [258,259,283,284], at 37 ± 2 ºC and under magnetic stirring conditions. Alginic acid sodium-based microparticles were placed on top of a cuvette with octanol and the bioactive compound(s) release was performed in a continuous mode (intervals of 2 min). In turn, EC + PEG-based microparticles were placed on top of a beaker with octanol and samples were taken for each 10 min and then returned to the beaker. In both cases, monitorization of the bioactive compound(s) release was performed in an UV/VIS spectrometer (section 9.2.8.) by absorbance. The main mathematical models related to the model dependent methods (zero-order (Eq. 9.2), Higuchi (Eq. 9.3), Korsmeyer-Peppas (Eq. 9.4) and Weibull (Eq. 9.5) [260–262,267]) were fitted to the obtained controlled release profiles.

$$Q_t = Q_0 + K_0 t \quad \textbf{(9.2)}$$

where Q_t is the cumulative amount of the drug/active compound released at the time t, Q_0 is the initial amount of the drug/active compound in solution (usually $Q_0 = 0$) and K_0 is the zero-order release constant.

$$Q_t = K_H \sqrt{t} \quad \textbf{(9.3)}$$

where K_H is the Higuchi constant.

$$Q_t/Q_\infty = K_K t^n \quad \textbf{(9.4)}$$

where Q_t/Q_∞ is the fraction of active compound released until time t and K_K is the Korsmeyer constant. The parameter n is the release exponent (diffusional), a parameter that defines the release mechanism.

$$M_t = M_\infty \left[1 - e^{-\left(\frac{t-t_0}{\tau d}\right)^\beta}\right] \quad \textbf{(9.5)}$$

where M_t is the dissolution/release (%) of the active compound at time t, M_∞ is the dissolution/release (%) of the active compound at infinite time, t_0 is the lag-time of the dissolution (usually t_0=0), β indicates the shape parameter of the curve and τ_d is the time when 63.2% of M has been dissolved/released.

9.2.10. Statistical analysis

Apparent viscosity and droplet size of the emulsions were evaluated among all the formulations prepared. Particle size distribution, encapsulation efficiency and loading capacity were compared for all the loaded microparticles composed by different encapsulating agents. One-way analysis of variance (ANOVA) at $p < 0.05$ and subsequent Tukey test were conducted by Minitab® 19 software.

9.3. Results and discussion

9.3.1. Emulsions characterization

9.3.1.1. Viscosity

For all the emulsions prepared the shear stress linearly increased with the shear rate (Figure 9.1). Accordingly, alginic acid sodium-based emulsions composed by RA, RA + curcumin, RA + resveratrol and RA + curcumin + resveratrol demonstrated characteristics relatively close of a Newtonian fluid. Apparent viscosity of these emulsions varied between 13.8 ± 0.2 and 14.1 ± 0.0 mPa·s considering a shear rate of 100 s^{-1} (Table 9.2). Gonçalves et al. [314] observed that oil-in-water emulsions composed by alginic acid sodium, tween 80 and RA dissolved in coconut oil exhibited a slightly higher apparent viscosity (17.6 ± 0.2 mPa·s) when compared to the one registered in this study. Consistency index ranged from 0.01374 ± 0.00009 (emulsion composed by RA + curcumin) to 0.01407 ± 0.00006 (emulsion composed by RA) mPa·s^n (Table 9.2). Broadly, this parameter indicates the flow properties of the system and consequently informs about the emulsion viscosity [288]. It turn, flow behaviour index points to how close the system is to a Newtonian fluid [288]. In this study, flow behaviour index maintained around 1 for all the emulsions prepared (Table 9.2), whereby the systems evidenced a Newtonian behaviour, as previously referred [288,289].

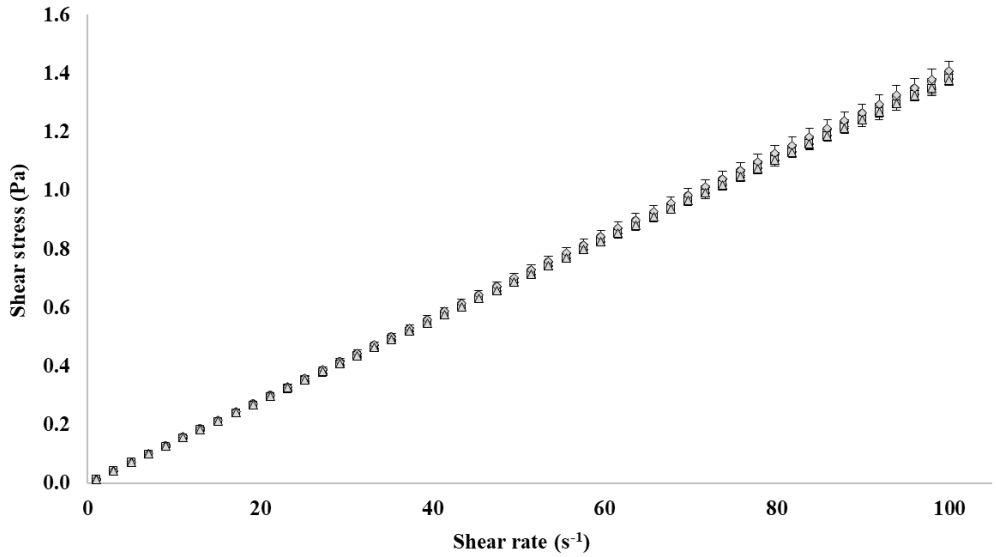


Figure 9.1 – Relation between shear stress and shear rate for the alginic acid sodium-based emulsions composed by RA (circles), RA + curcumin (diamonds), RA + resveratrol (squares) and RA + curcumin + resveratrol (triangles). Results are presented as the average and standard deviation of two independent assays.

Table 9.2 – Rheological parameters, apparent viscosity, zeta potential and droplet size of alginic acid sodium based-emulsions composed by RA, RA + curcumin, RA + resveratrol and RA + curcumin + resveratrol.

Emulsions (composition in bioactive compounds)	**Rheological parameters**		**Apparent viscosity at 100 s^{-1} (mPa·s)**	**Zeta potential (mV)**	**Droplet mean diameter**	
	Consistency index, k ($mPa·s^n$)	**Flow behaviour index, n**			**Differential volume distribution (µm)**	**Differential number distribution (µm)**
RA	0.01407 ± 0.00006	1.000 ± 0.009	14.0 ± 0.4[a]	-50 ± 3	3.25 ± 0.02[b]	0.883 ± 0.000[b]
RA + curcumin	0.01374 ± 0.00009	1.007 ± 0.001	14.1 ± 0.0[a]	-45.8 ± 0.5	3.61 ± 0.02[a]	0.934 ± 0.001[a]
RA + resveratrol	0.0138 ± 0.0004	1.001 ± 0.006	13.8 ± 0.0[a]	-47 ± 3	3.62 ± 0.02[a]	0.843 ± 0.003[c]
RA + curcumin + resveratrol	0.0139 ± 0.0006	0.999 ± 0.006	13.8 ± 0.2[a]	-47.1 ± 0.6	3.579 ± 0.002[a]	0.9345 ± 0.0007[a]

Different letters in the same column indicate significant differences ($p<0.05$)

9.3.1.2. Stability of colloidal systems

The methodology usually used to evaluate the stability of colloidal systems is based on the percentage of emulsion that separates (creaming index) 24 h after its preparation [292,293]. This approach must not be used in this work due to the high ratio aqueous phase volume/oily phase volume of emulsions prepared. Another strategy that can be used is related to the analysis of zeta potential of emulsions with the measurement of the electrokinetic potential of droplets [294]. All alginic acid sodium-based emulsions showed to be stable (zeta potential value above of $\left|30\right|$ mV [294]). The lower and higher value of zeta potential were registered for the emulsions composed by RA + curcumin (-45.8 ± 0.5) and RA (-50 ± 3), respectively (Table 9.2). The stability of emulsions influences the encapsulation efficiency of obtained carrier-based delivery systems. A higher amount of bioactive compound(s) is retained during spray-drying when emulsions exhibit higher stability [295]. In this work, encapsulation efficiency of RA, curcumin and resveratrol into alginic acid sodium-based microparticles globally varied between 26 ± 3 and 34 ± 1% (section 9.3.6., Table 9.3). In the previous study performed by the authors, spray-drying of the oil-in-water emulsion composed by alginic acid sodium ensured a higher RA encapsulation efficiency (62 ± 5%) [314].

9.3.1.3. Droplet size distribution

Stability of colloids can also be analysed by the emulsions droplet size [285]. Emulsions with larger droplets are generally related to a lower encapsulation efficiency of carrier-based delivery systems [295]. The alginic acid sodium-based emulsion composed by RA evidenced a significant lower average droplet diameter (3.25 ± 0.02 μm) when compared to the other emulsions composed by the same biopolymer and two or more bioactive compounds, considering differential volume distribution ($p<0.05$) (Table 9.2). Herein, emulsions composed by RA + curcumin, RA + resveratrol and RA + curcumin + resveratrol showed an average droplet diameter around 3.61 ± 0.02, 3.62 ± 0.02 and 3.579 ± 0.002 μm, respectively (Table 9.2). In turn, the emulsions composed by RA + curcumin, with or without resveratrol, enabled a significant higher average droplet diameter, considering differential number distribution (0.9345 ± 0.0007 and 0.934 ± 0.001 μm, respectively). A significant lower average droplet diameter was achieved for emulsions composed by RA + resveratrol (0.843 ± 0.003) (Table 9.2). Microparticles obtained from the spray-drying of these emulsions did not evidence significant differences regarding the encapsulation efficiency of each bioactive compound (section 9.3.6., Table 9.3).

9.3.2. Characterization of carrier-based loaded microparticles

Formulations composed by different polymers – biopolymers and synthetic polymers – were proposed for the co-encapsulation of retinoic acid, curcumin and/or resveratrol. Alginic acid sodium-based microparticles loaded with coconut oil and tween 80 (microparticles MpB) and microparticles composed by the EC + PEG blend (microparticles MpP) were produced for the incorporation of the selected combination of bioactive compounds. Product yield ranged from 29 to 35% among microparticles MpB and 10 to 27% among microparticles MpP (Table 9.3). Product yield is affected by the volume, the composition and the type of the system fed to the spray-

Table 9.3 – Characterization of MpB and MpP microparticles: product yield, particle diameter, encapsulation efficiency and loading capacity.

Microparticles content		Product yield	Particle mean diameter		Encapsulation efficiency (%)			Loading capacity (%)		
Formulation	Bioactive compounds	(%)	Differential volume distribution (μm)	Differential number distribution (μm)	RA	Curcumin	Resveratrol	RA	Curcumin	Resveratrol
MpB	RA	35	6.3 ± 0.2^{c}	0.437 ± 0.006^{c}	32.9 ± 0.3^{b}	-	-	0.00964 ± 0.00009^{d}	-	-
	RA + curcumin	31	2.97 ± 0.04^{c}	1.11 ± 0.01^{b}	31 ± 1^{b}	26 ± 3^{b}	-	0.0090 ± 0.003^{d}	0.0077 ± 0.0008^{c}	-
	RA + resveratrol	30	3.45 ± 0.05^{c}	1.174 ± 0.005^{a}	30 ± 1^{b}	-	28 ± 2^{b}	0.0088 ± 0.0004^{d}	-	0.0081 ± 0.0006^{c}
	RA + curcumin + resveratrol	29	3.61 ± 0.05^{c}	1.1615 ± 0.0007^{a}	34 ± 1^{b}	32 ± 3^{b}	33 ± 3^{b}	0.0098 ± 0.0004^{d}	0.0095 ± 0.0008^{c}	0.010 ± 0.001^{c}
MpP	RA	10	4.5 ± 0.4^{c}	0.0942 ± 0.0003^{e}	97 ± 8^{a}	-	-	10 ± 1^{a}	-	-
	RA + curcumin	22	88 ± 3^{a}	0.25 ± 0.02^{d}	92 ± 10^{a}	92 ± 9^{a}	-	7.6 ± 0.4^{bc}	7.5 ± 0.5^{a}	-
	RA + resveratrol	21	49 ± 4^{b}	0.0987 ± 0.0008^{e}	93 ± 6^{a}	-	91 ± 6^{a}	8.6 ± 0.5^{ab}	-	8.4 ± 0.6^{a}
	RA + curcumin + resveratrol	27	79 ± 7^{a}	0.108 ± 0.003^{e}	96 ± 5^{a}	92 ± 4^{a}	93 ± 4^{a}	7.0 ± 0.3^{c}	6.7 ± 0.2^{b}	6.8 ± 0.3^{b}

Different letters in the same column indicate significant differences ($p<0.05$)

dryer. The operating conditions used in the spray-dryer also influence this parameter. In this work, the volume of emulsions prepared was larger when compared to the volume of solutions prepared in ethanol (200 mL and 50 mL, respectively), which contributed to the global higher product yield of alginic acid sodium-based microparticles. However, the oily phase of emulsions adversely impacted the product yield due to the amount of microparticles that kept adhered to the walls of spray-dryer (visually observed). Other studies report the impact of producing microparticles by spray-drying from oily-based formulations [245,314,319].

9.3.3. Surface morphology of microparticles

Microparticles MpB evidenced a spherical configuration and a slightly rough surface due to the presence of concavities overall distributed (Figure 9.2 – A, B, C and D). In turn, microparticles MpP showed a very irregular shape combined with several concavities on the surface, which gives the microparticles a high rough presentation (Figure 9.2 – E, F, G and H). Both formulations were previously described for RA encapsulation also by spray-drying technology [314,336]. The obtained RA-loaded microparticles exhibited a similar morphology to the one herein observed. In other study, Bajac et al. [373] encapsulated juniper berry essential oil into sodium alginate microparticles by spray-drying and the obtained microparticles showed a semi-spherical form with deep concavities on the surface. Also, Wasilewska and Winnicka [320] compiled several images related to the surface morphology of powders obtained by the spray-drying of EC in different forms. The powders obtained from drying of EC ethanolic solutions evidenced a structure similar to the one registered in

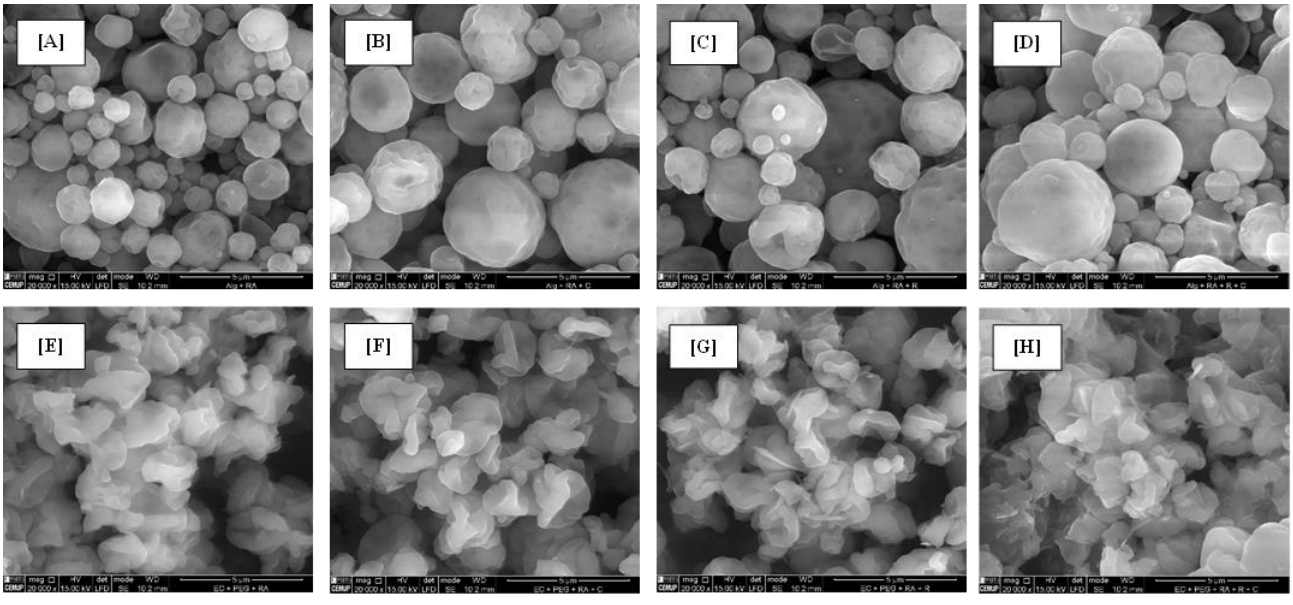


Figure 9.2 – Surface morphology of MpB (A, B, C and D) and MpP (E, F, G and H) microparticles loaded with RA (A and E), RA + curcumin (B and F), RA + resveratrol (C and G) and RA + curcumin + resveratrol (D and H). Magnification = 20,000 times, beam intensity (HV) 15.00 kV, distance between the sample and the lens (WD) around 10 mm.

this work by microparticles MpP. Changes in the surface morphology between microparticles MpB and microparticles MpP are explained by the different composition of microparticles. However, for each type of microparticles, the appearance of microparticles was not modified by the incorporation of curcumin and/or resveratrol (Figure 9.2 – B, C, D, F, G, H). Moreover, none of the microparticles has surface cracks.

9.3.4. Particle size

Particle mean diameter varied between 2.97 ± 0.04 and 6.3 ± 0.2 μm among microparticles MpB (differential volume distribution) (Table 9.3). In turn, microparticles MpP exhibited a significant global higher size ($p<0.05$) that ranged from 49 ± 4 (RA + resveratrol-loaded microparticles) and 88 ± 3 μm (RA + curcumin-loaded microparticles) (Table 9.3). This discrepancy can be due to the high aggregation of microparticles. With exception, microparticles MpP loaded with RA evidenced a particle size of 4.5 ± 0.4 μm (Table 9.3). Accordingly, the incorporation of curcumin and/or resveratrol into the synthetic polymer-based formulations seems to promote the aggregation phenomena. Differential number distribution showed a particle mean diameter between 0.437 ± 0.006 and 1.174 ± 0.005 μm among microparticles MpB and between 0.0942 ± 0.0003 (microparticles MpP loaded with RA) and 0.25 ± 0.02 μm (microparticles MpP loaded with RA + curcumin) (Table 9.3). Oil-in-water-based formulations seem to promote the production of microparticles with higher size.

9.3.5. Encapsulation efficiency and loading capacity

Encapsulation efficiency of RA, curcumin and resveratrol was significantly higher for all microparticles MpP (ranged between 91 ± 6 and 97 ± 8%) ($p<0.05$) (Table 9.3). Microparticles MpB enabled a lower encapsulation efficiency that varied between 26 ± 3 and 34 ± 1% (Table 9.3). In turn, loading capacity varied between 0.0077 ± 0.0008 and 0.010 ± 0.001% among microparticles MpB and 10 ± 1 and 6.7 ± 0.2% among microparticles MpP (Table 9.3). The obtained results clearly indicate that the capacity of microparticles to retain the core material is largely influenced by the selected encapsulating agent(s) [234]. Moreover, they indicate that the co-encapsulation of bioactive compounds do not compromise the encapsulation efficiency of each bioactive compound considered in the blend. In a previous study performed by the authors wherein alginic acid sodium-based microparticles were obtained from oil-in-water emulsions for RA encapsulation, the encapsulation efficiency registered was higher when compared to the one registered in this work (62 ± 5%) [314]. Another study performed by the authors related to the preparation of EC + PEG dissolved in absolute ethanol also for RA encapsulation evidenced an encapsulation efficiency of around 100% [336]. Both formulations can be compared to the one prepared in this work regarding the amount of RA incorporated in the system fed to the spray-dryer.

9.3.6. Drug controlled release assay

Controlled release profiles obtained by cumulative percentage of RA, curcumin and resveratrol over time from different microparticles formulations (microparticles MpB and microparticles MpP) were performed at 37 ̊C in

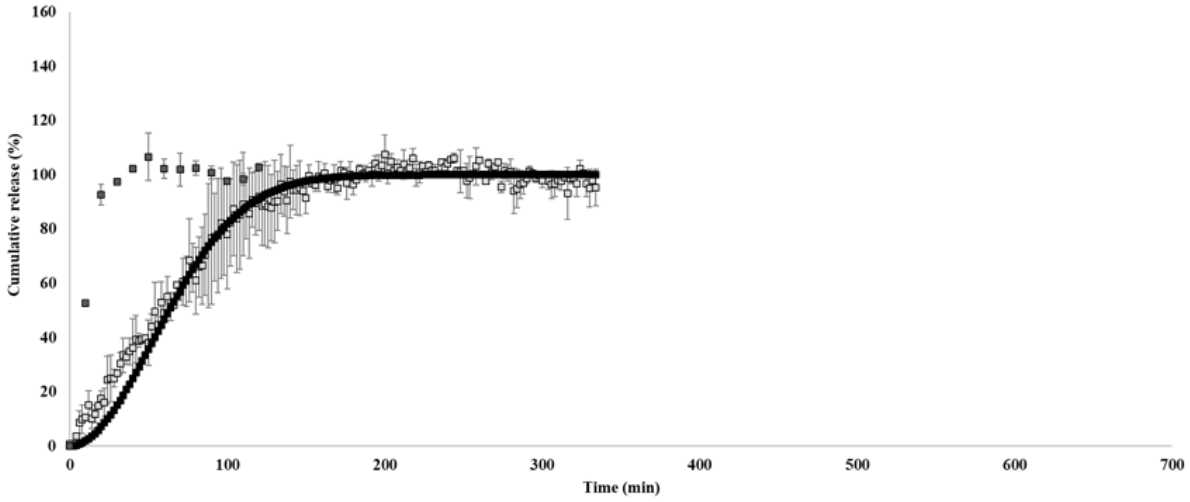
octanol (Figure 9.3). The usage of this organic solvent is related to comprehension about the ability of these bioactive compounds to cross the lipid membranes of the living system [258,259,283].

RA controlled release profiles seem to vary according to the microparticles formulation, considering microparticles MpB. A slower initial release of RA was observed from RA-loaded microparticles. Herein, the release prolonged for 154 min (Figure 9.3 - A). The other RA release profiles obtained from microparticles MpB stabilized 48, 100 and 362 min after the beginning of the experiment, when RA was co-encapsulated with resveratrol, curcumin + resveratrol and curcumin, respectively (Figure 9.3). Regarding curcumin and resveratrol, both exhibited a release profile that was very similar to the one recorded for the RA co-encapsulated with these bioactive compounds in the same formulations. Accordingly, the controlled release of curcumin from microparticles MpB loaded with RA + curcumin and RA + curcumin + resveratrol lasted for 380 and 124 min, respectively. In turn, the resveratrol controlled release extended for 48 and 100 min from microparticles MpB loaded with RA + resveratrol and RA + curcumin + resveratrol, respectively (Figure 9.3). A previous study reported a RA controlled release that lasted beyond the 2.5 h herein registered and prolonged for almost 8 h from alginic acid sodium-based microparticles [314]. Those microparticles evidenced a higher encapsulation efficiency when compared to the value obtained in this study, as previously referred (section 9.3.5.). The higher amount of RA effectively retained in the microparticles may have contributed to increase the time for stabilization of release profile of this bioactive compound.

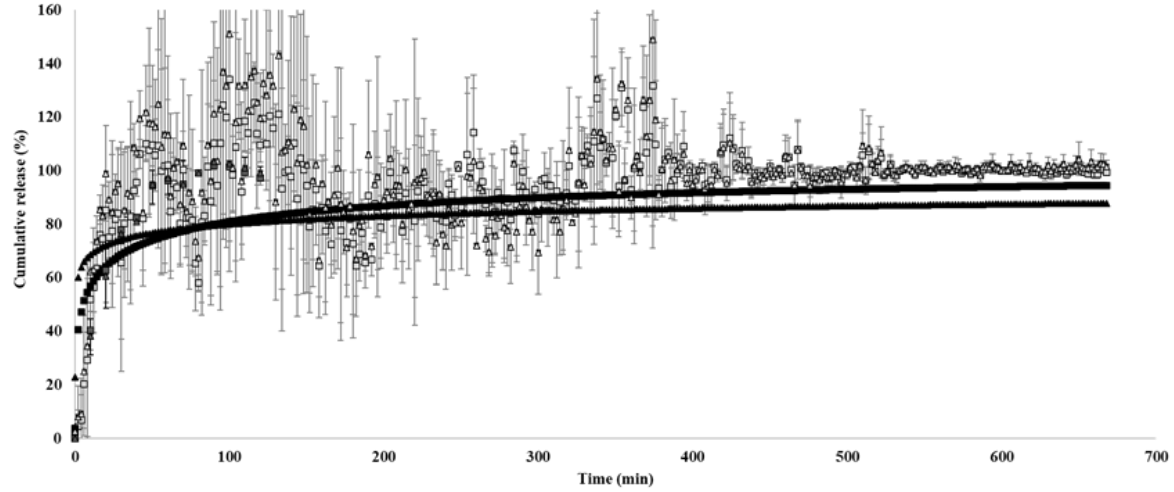
The controlled release profiles of RA, curcumin and resveratrol obtained from all microparticles MpP are very similar. They are characterized by a fast release of bioactive compounds and the release profiles were stabilized between 60 and 80 min after the beginning of the assay (Figure 9.3).

The obtained results evidence the importance of the formulation used in the controlled release behaviour of the bioactive compounds. With the aim of using the obtained microparticles in the treatment of APL to reduce the activation of cytochrome P450 and, at the same time, benefit the combination of RA and curcumin and/or resveratrol, alginic acid sodium-based microparticles might be most advantageous on its current formulation. Microparticles composed by the EC + PEG blend must be optimized to increase the controlled release time. A previous study evidences the ability of this last formulation to protect RA against the stomach harch conditions and release this bioactive compound in the intestine [372].

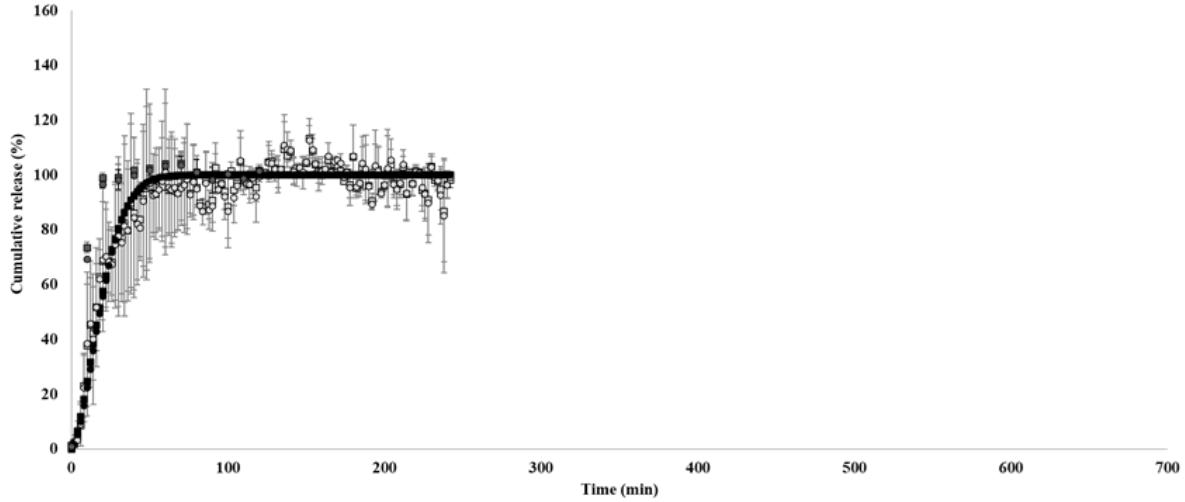
Other studies show the release profiles of co-encapsulated bioactive compounds. Han et al. [374] encapsulated ginkgolide A, ginkgolide B, ginkgolide C and bilobalide from Ginkgo terpenes extracted from *Ginkgo biloba* leaves into injectable PELGE (mPEG–PLGA–mPEG) nanoparticles and the obtained released profiles performed in 0.9% NaCl at 37 ºC were very similar and prolonged for 36 h.


Cumulative release (%)
Time (min)
0
20
40
60
80
100
120
140
160
0
100
200
300
400
500
600
700

[A]


Cumulative release (%)
Time (min)
0
20
40
60
80
100
120
140
160
0
100
200
300
400
500
600
700

[B]


Cumulative release (%)
Time (min)
0
20
40
60
80
100
120
140
160
0
100
200
300
400
500
600
700

[C]

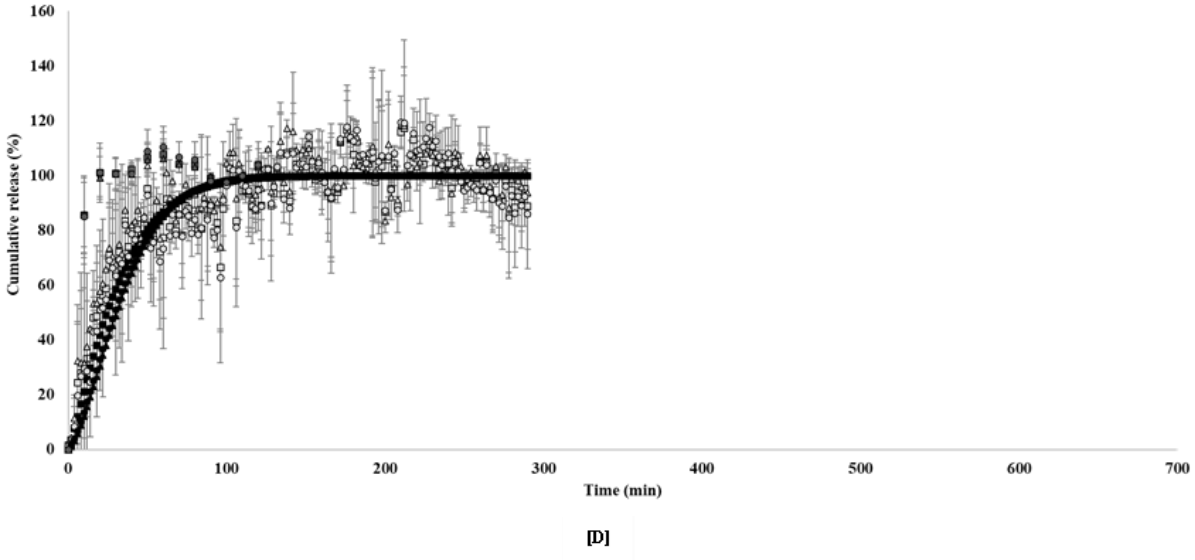


Figure 9.3 – Cumulative release of RA (squares), curcumin (triangles) and resveratrol (circles) from MpB (light grey) and MpP (dark grey) microparticles loaded with RA (A), RA + curcumin (B), RA + resveratrol (C) and RA + curcumin + resveratrol (D). Results are presented as the average and standard deviation of two independent assays. Weibull model was fitted to the obtained controlled release profiles from MpB microparticles: RA (black squares), curcumin (black triangles) and resveratrol (black circles).

9.3.7. Kinetic models

Kinetics of zero order (describes a slow and constant release rate) was fitted to the RA, curcumin and resveratrol controlled release profiles with a correlation coefficient that varied from 0.739 and 0.988 (Table 9.4 and Table 9.5). The zero-order release constant, K_0, increased from 8.0×10^{-6} to 4.4×10^{-3} mg·min^{-1} among all the bioactive compounds released from microparticles MpB and microparticles MpP (Table 9.4 and Table 9.5), which is in agreement with an increase of the release rate. Regarding the Higuchi model, the Higuchi constant, K_H, ranged from 6.0×10^{-5} to 3.2×10^{-2} mg·min$^{-0.5}$ and the correlation coefficient from 0.939 to 0.998 (Table 9.4 and Table 9.5).

Korsmeyer-Peppas model was fitted to the linear controlled release profiles considering the Q_t/Q_∞ is lower than 0.6 [262]. For the microparticles MpB loaded with RA + curcumin and the microparticles MpP loaded with RA + resveratrol and RA + curcumin + resveratrol the parameter *n* was lower than 0.43 (Table 9.4 and Table 9.5), suggesting a Fickian diffusion and a $t^{-0.57}$ rate as a function of time. It turn, for the microparticles MpP loaded with RA and RA + curcumin the parameter *n* varied between 0.43 and 0.85 suggesting an anomalous transport which results from the combination of diffusion mechanisms and swelling release (case II transport) and a t^{n-1} rate as a function of time. At last, for the microparticles MpB loaded with RA, RA + resveratrol and RA + curcumin + resveratrol the parameter *n* was higher than 0.85, suggesting a super case-II transport and a t^{n-1} rate as a function of time (Table 9.4 and Table 9.5) [145,262]. The Korsmeyer constant, K_K, ranges from 0.0004 to

Table 9.4 – Parameters and correlation coefficients of the models of zero-order, Higuchi, Korsmeyer-Peppas and Weibull applied to the experimental RA, curcumin and resveratrol release profiles from MpB microparticles.

	Parameters		MpB microparticles							
			Loaded with RA	Loaded with RA + Curcumin		Loaded with RA + Resveratrol		Loaded with RA + Curcumin + Resveratrol		
			RA	RA	Curcumin	RA	Resveratrol	RA	Curcumin	Resveratrol
Kinetic models	Zero-order	K_0 (mg·min^{-1})	8.0×10^{-6}	1.0×10^{-5}	1.0×10^{-5}	1.0×10^{-5}	1.0×10^{-5}	2.0×10^{-5}	2.0×10^{-5}	1.0×10^{-5}
		Q_0 (mg)	-6.0×10^{-5} *)	3.0×10^{-4}	3.0×10^{-4}	2.0×10^{-4}	1.0×10^{-4}	7.0×10^{-5}	-9.0×10^{-6} *)	1.0×10^{-4}
		R^2	0.988	0.792	0.739	0.883	0.872	0.920	0.895	0.769
	Higuchi	K_H (mg·min$^{-0.5}$)	6.0×10^{-5}	1.0×10^{-4}	1.0×10^{-4}	1.0×10^{-4}	1.0×10^{-4}	1.0×10^{-4}	1.0×10^{-4}	9.0×10^{-5}
		R^2	0.939	0.982	0.979	0.989	0.985	0.972	0.948	0.964
	Korsmeyer-Peppas	K_k (min^{-n})	0.0004	0.3	0.6	0.01	0.009	0.03	0.009	0.009
		n	1.7	0.2	0.09	1.3	1.4	0.9	1.2	1.2
		R^2	0.898	0.193	0.048	0.871	0.847	0.906	0.811	0.864
	Weibull	τ_d (min)	76	18	3	22	23	33	39	38
		β	2.0	0.3	0.1	1.6	1.7	1.2	1.5	1.4
		R^2	0.934	0.187	0.060	0.910	0.886	0.902	0.859	0.880

*) Consider $Q_0 \geq 0$.

Table 9.5 – Parameters and correlation coefficients of the models of zero-order, Higuchi, Korsmeyer-Peppas and Weibull applied to the experimental RA, curcumin and resveratrol release profiles from MpP microparticles.

	Parameters		MpP microparticles							
			Loaded with RA	Loaded with RA + Curcumin		Loaded with RA + Resveratrol		Loaded with RA + Curcumin + Resveratrol		
			RA	RA	Curcumin	RA	Resveratrol	RA	Curcumin	Resveratrol
Kinetic models	Zero-order	K_0 (mg·min^{-1})	4.4×10^{-3}	2.0×10^{-3}	1.0×10^{-5}	2.2×10^{-3}	2.4×10^{-3}	1.2×10^{-3}	1.2×10^{-3}	1.2×10^{-3}
		Q_0 (mg)	4.9×10^{-2}	4.2×10^{-2}	2.0×10^{-4}	9.5×10^{-2}	8.4×10^{-2}	1.1×10^{-1}	1.0×10^{-1}	1.0×10^{-1}
		R^2	0.826	0.944	0.952	0.759	0.795	0.761	0.827	0.765
	Higuchi	K_H (mg·min$^{-0.5}$)	3.2×10^{-2}	1.9×10^{-2}	1.0×10^{-4}	3.1×10^{-2}	3.0×10^{-2}	2.9×10^{-2}	2.8×10^{-2}	2.9×10^{-2}
		R^2	0.988	0.998	0.995	0.990	0.992	0.980	0.981	0.981
	Korsmeyer-Peppas	K_k (min^{-n})	0.1	0.09	0.06	0.4	3	0.5	0.6	0.6
		n	0.7	0.6	0.7	0.3	0.3	0.2	0.1	0.1
		R^2	0.909	0.973	0.971	0.829	0.835	0.875	0.841	0.789
	Weibull	τ_d (min)	13	22	25	8	9	5	6	5
		β	1.6	1.0	1.1	1.3	1.2	0.9	1.2	1.1
		R^2	0.960	0.991	0.988	0.896	0.969	0.894	0.972	0.888

3 min^{-n} also indicating a general increase of release rate (Table 9.4 and Table 9.5). The correlation coefficients with Korsmeyer-Peppas model ranged from 0.048 to 0.971 (Table 9.4 and Table 9.5).A correlation coefficient from 0.187 to 0.991 was obtained when the Weibull model was fitted to the controlled release profiles (Tables 4 and 5). The β parameter is lower than 1 for microparticles MpB loaded with RA + curcumin and RA + curcumin + resveratrol (in this last case for the RA release profile) (Table 9.4 and Table 9.5). The shape of the curve would show therefore a steeper increase regarding the shape of the release curve that corresponds exactly to the shape of an exponential profile [262]. For all the other microparticles and respective controlled release profiles the β parameter was higher than 1 (Table 9.4 and Table 9.5). Accordingly, the shape of the curve gets sigmoidal with a turning point [262]. τ_d parameter varied from 3 (microparticles MpB loaded with RA + curcumin, considering the curcumin release profile) to 76 min (microparticles MpB loaded with RA) (Table 9.4 and Table 9.5).

Among all the microparticle formulations, the Weibull model was the most suitable to ensure the full fitting of all bioactive compounds controlled release profiles obtained from alginic acid sodium-based microparticles and EC + PEG-based microparticles. Weibull model is reported as the most appropriate to describe the release of bioactive compounds from a matrix-based microparticles [260], which is related to the typical morphology obtained by spray-drying technology [266]. Gonçalves et al. [278,314,336] identified Weibull model as the most capable to describe RA release profiles obtained from biopolymer- and synthetic polymer-based microparticles obtained by spray-drying.

9.4. Conclusion

Alginic acid sodium-based microparticles and microparticles composed by EC + PEG were successfully produced by spray-drying technology for co-encapsulation and co-delivery of RA, curcumin and/or resveratrol encapsulation. The usage of biopolymers or synthetic polymers as encapsulating agents influences the product yield, the amount of bioactive compound that is possible to incorporate in the system fed to the spray-dryer, the encapsulation efficiency, particle size, morphology and controlled release profiles from loaded microparticles. Particularly, both types of microparticles enabled a similar encapsulation efficiency among the co-encapsulated bioactive compounds (from 26 ± 3 to 34 ± 1% for microparticles MpB and 91 ± 6 to 97 ± 8% for microparticles MpP). The bioactive compounds that were co-encapsulated in the same formulation evidenced a similar release profile, with their release occurring between 48 min and more than 6 h from alginic acid-based microparticles, and the achievement of release stabilization between 60 and 80 min after the begging of assay from EC + PEG-based microparticles.

Chapter 10 - Conclusions and future perspectives

The tenth chapter aims to present a critical overview of the main findings achieved in this research. Moreover, some recommendations for future work are presented.

10.1. Conclusions

This thesis focused on the design and development of microparticle formulations for RA encapsulation using spray-drying technology. An approach based on the incorporation of RA into appropriate carrier-based delivery systems has been subject of research in pharmaceutical and medical fields (Chapter 2). This strategy aims to provide an effective protection and stability to RA. In general, retinoids are poor aqueous soluble and can be damaged due to heat, presence of oxidants and light. Particularly, RA is highly sensitive to oxidizing compounds, air and UV light. Moreover, a sustained RA delivery can also be achieved and at the desired place. At last, undesirable side-effects related to RA administration might be mitigated. In this research, the encapsulation of RA aimed to increase the efficiency of this retinoid in the treatment of APL. Herein, continuous repetitive RA oral administration (Vesanoid®) leads to a marked decline of RA half-life in blood and consequent decrease of RA concentration in the plasma. Despite of the continued treatment the patients become resistant to RA. Providing a slow and continuous RA controlled delivery may reduce the activity of cytochrome P450 enzymes involved in catabolism of this retinoid and ultimately beneficiate the anticancer activity of RA.

Chapter 4 proposed the first microparticles for RA encapsulation, individually composed by alginic acid sodium, modified chitosan and arabic gum. The slower release was achieved from alginic acid sodium-based microparticles (> 7 h) in octanol, whereby this encapsulating agent showed to be the most promising for RA controlled release. In turn, the faster release was observed from modified chitosan-based microparticles (99 min). However, for these both formulations a high loss of RA was evidenced over time. This situation required the presentation of an improved system for RA delivery. Accordingly, oil-in-water emulsions individually composed by alginic acid sodium, modified chitosan, arabic gum, xanthan gum and gelatin (Chapter 5) and oil-in-water emulsions composed by binary and ternary blends of these biopolymers (Chapter 6) were further proposed to be dried to produce RA loaded-biopolymer-based microparticles. Considering Chapter 5, RA encapsulation efficiency of modified chitosan-based microparticles showed to be significantly affected by inlet air temperature. The highest RA retention was observed at 130 °C (65 ± 6%). In agreement with this result, further spray-drying operations were performed using this inlet air temperature. Among the microparticles herein produced the highest encapsulation efficiency was obtained for modified chitosan- and, in second place, for alginic acid sodium-based microparticles (62 ± 5%). Regarding controlled release studies, xanthan gum and arabic gum-based microparticles resulted in a faster release of RA, while the alginic acid sodium-based microparticles enabled again to register the slower release of this retinoid (almost 8 h). In Chapter 6, the biopolymers that individually enabled in Chapter 5 the production of RA-loaded microparticles with the most promising characteristics (alginic acid sodium, modified chitosan and xanthan gum) were proposed to produce the xanthan gum + alginic acid sodium, modified chitosan + alginic acid sodium, modified chitosan + xanthan gum and modified chitosan + xanthan gum + alginic acid sodium blends for RA encapsulation. The xanthan gum + alginic acid sodium blend enabled the production of RA-loaded microparticles with the highest encapsulation efficiency (76 ± 4%). Most of microparticles composed by alginic acid sodium also enabled to prolong the RA release for a longer time (almost 7 h). Exceptionally, microparticles composed by the modified chitosan + alginic acid sodium blend resulted in a complete release of RA after 100 min. In order to significantly

increase the amount of RA that is possible to incorporate in the system fed to the spray-dryer and then increase the amount of RA encapsulated in the microparticles, Chapter 7 proposes EC- and EC + PEG-based microparticles for encapsulation of this retinoid. These both formulations increased at least 250-fold the mass of RA added to the system to be fed to the spray-dryer, when compared to the biopolymer-based systems proposed. The encapsulation efficiency herein obtained was around 100%, which become these carrier-based delivery systems more suitable for the treatment of APL when compared to the biopolymer-based microparticles previously presented (Chapters 4, 5 and 6). However, the RA release from these synthetic polymer-based microparticles was very fast (40 min). Subsequently, *in vitro* bioaccessibility and intestinal transport of RA encapsulated into EC- and EC + PEG- based microparticles were assessed in Chapter 8. This study is of major importance to evaluate these microparticles regarding their behaviour during gastrointestinal tract and then validate the EC- and EC + PEG- based microparticles for RA release and delivery in the intestine. Currently, the number of recent studies in this field and applied to carrier-based delivery systems is limited (Chapter 3). RA bioaccessibility after *in vitro* static digestion of RA-loaded synthetic polymer-based microparticles, with and without co-ingestion of a reference diet, was significantly affected at intestinal level by the type of microparticles and the presence of meal. The digestion of EC- and EC+PEG-based microparticles without diet significantly increased the RA bioaccessibility from 24 ± 6 to 84 ± 1% and 25 ± 5 to 54 ± 4%, respectively. Moreover, comparing these both type of microparticles, the bioaccessibility of this retinoid was significantly higher for EC-based microparticles digested without diet. At last, co-ingestion of EC- and ECP-based microparticles with diet enabled a similar RA bioaccessibility among both formulations. Regarding intestinal transport, it was observed that the amount of RA that reached the basolateral compartment was significantly influenced by the samples used in the experiments. The best results were obtained from blank digesta spiked with RA. All the studies presented so far in this thesis enable to point out the most promising microparticle formulation for RA encapsulation and those include: (i) alginic acid sodium-based microparticles (obtained from oil-in-water emulsion), due the relatively high encapsulation efficiency and slow controlled release profiles of RA; and (ii) EC + PEG-based microparticles, due to the *in vitro* digestion results and the ability to encapsulate RA in an amount closer to the current daily dosage administrated. Accordingly, these both formulations were proposed as co-encapsulation systems for the co-delivery of RA, curcumin and/or resveratrol. Encapsulation efficiency was significantly influenced by the encapsulating agent(s) used in the microparticles formulations, whereby the biopolymer-based microparticles and synthetic polymers-based microparticles enabled an encapsulation efficiency for all the bioactive compounds that varied between 26 ± 3-34 ± 1% and 91 ± 6-97 ± 8%, respectively. The bioactive compounds that were co-encapsulated showed a similar release profile and it was more prolonged from alginic acid-based microparticles (between 48 min and more than 6 h). This work showed that different polymers can be used to produce microsystems by spray-drying for RA encapsulation and controlled release. Synthetic polymers evidenced to be the most promising to be used in formulations for application in the treatment of APL. Moreover, this work provided knowledge regarding the behaviour of microparticles composed by EC and the EC + PEG blend during *in vitro* digestion). At last, a preliminary

approach regarding the effect of RA, curcumin and/or resveratrol co-encapsulation in the co-release of these bioactive compounds was understood.

10.2. Future perspectives

In this thesis, several carrier-based delivery systems were proposed for RA encapsulation to be used for the treatment of APL. However, we are still far from the final pharmaceutical product. New experiments must be performed, including:

- Optimization of the concentration and ratio of synthetic polymers used in the EC + PEG blend of encapsulating agents. The final aim is the development of microparticles capable to provide a sustained release of RA for hours and, therefore, reduce the activation of cytochrome P450 and increase RA efficiency. In this work, EC + PEG-based microparticles exhibited relevant features to be used in the treatment of APL, including the ability to incorporate an increased amount of RA that is comparable to the daily dose of Vesanoid® and to protect RA during gastrointestinal tract and enable the release in the intestine.
- Evaluation of RA bioaccessibility and intestinal transport after *in vitro* digestion of EC + PEG-based microparticles co-ingested with a suitable diet for patients with APL.
- Integration of EC + PEG-based microparticles into a food-based matrix for oral administration of RA-loaded microparticles. Gastrointestinal behaviour of the obtained food/microparticle combined formulation might be assessed by *in vitro* digestion.

References

[1] M. Hadidi, S. Pouramin, F. Adinepour, S. Haghani, S.M. Jafari, Chitosan nanoparticles loaded with clove essential oil: Characterization, antioxidant and antibacterial activities, Carbohydr. Polym. 236 (2020) 116075. https://doi.org/10.1016/j.carbpol.2020.116075.

[2] Z. Ban, J. Zhang, L. Li, Z. Luo, Y. Wang, Q. Yuan, B. Zhou, H. Liu, Ginger essential oil-based microencapsulation as an efficient delivery system for the improvement of Jujube (Ziziphus jujuba Mill.) fruit quality, Food Chem. 306 (2020) 125628. https://doi.org/10.1016/j.foodchem.2019.125628.

[3] G. Vinner, Z. Rezaie-Yazdi, M. Leppanen, A. Stapley, M. Leaper, D. Malik, Microencapsulation of Salmonella-Specific Bacteriophage Felix O1 Using Spray-Drying in a pH-Responsive Formulation and Direct Compression Tableting of Powders into a Solid Oral Dosage Form, Pharmaceuticals. 12 (2019) 43. https://doi.org/10.3390/ph12010043.

[4] E. Juère, J. Florek, M. Bouchoucha, S. Jambhrunkar, K.Y. Wong, A. Popat, F. Kleitz, In Vitro Dissolution, Cellular Membrane Permeability, and Anti-Inflammatory Response of Resveratrol-Encapsulated Mesoporous Silica Nanoparticles, Mol. Pharm. 14 (2017) 4431–4441. https://doi.org/10.1021/acs.molpharmaceut.7b00529.

[5] J. de A. Figueiredo, C.R. de P. Silva, M.F. Souza Oliveira, L.B. Norcino, P.H. Campelo, D.A. Botrel, S.V. Borges, Microencapsulation by spray chilling in the food industry: Opportunities, challenges, and innovations, Trends Food Sci. Technol. 120 (2022) 274–287. https://doi.org/10.1016/j.tifs.2021.12.026.

[6] J. Shield, J. Kuler, A. Gurnani, Regulatory constraints on new product development and approval procedures in the United States, in: Dev. New Funct. Food Nutraceutical Prod., Elsevier, 2017: pp. 123–148. https://doi.org/10.1016/B978-0-12-802780-6.00007-9.

[7] D.J. McClements, H. Xiao, Excipient foods: designing food matrices that improve the oral bioavailability of pharmaceuticals and nutraceuticals, Food Funct. 5 (2014) 1320. https://doi.org/10.1039/c4fo00100a.

[8] D.J. McClements, Y. Li, Structured emulsion-based delivery systems: Controlling the digestion and release of lipophilic food components, Adv. Colloid Interface Sci. 159 (2010) 213–228. https://doi.org/10.1016/j.cis.2010.06.010.

[9] R. Delshadi, A. Bahrami, A.G. Tafti, F.J. Barba, L.L. Williams, Micro and nano-encapsulation of vegetable and essential oils to develop functional food products with improved nutritional profiles, Trends Food Sci. Technol. 104 (2020) 72–83. https://doi.org/10.1016/j.tifs.2020.07.004.

[10] C. Soukoulis, T. Bohn, A comprehensive overview on the micro- and nano-technological encapsulation advances for enhancing the chemical stability and bioavailability of carotenoids, Crit. Rev. Food Sci. Nutr. 58 (2018) 1–36. https://doi.org/10.1080/10408398.2014.971353.

[11] X. Montané, A. Bajek, K. Roszkowski, J.M. Montornés, M. Giamberini, S. Roszkowski, O. Kowalczyk, R. Garcia-Valls, B. Tylkowski, Encapsulation for Cancer Therapy, Molecules. 25 (2020) 1605. https://doi.org/10.3390/molecules25071605.

[12] F. Shahidi, X.Q. Han, Encapsulation of food ingredients, Crit. Rev. Food Sci. Nutr. 33 (1993) 501–547.

[13] E. Assadpour, S.M. Jafari, Advances in Spray-Drying Encapsulation of Food Bioactive Ingredients: From Microcapsules to Nanocapsules, Annu. Rev. Food Sci. Technol. 10 (2019) 103–131. https://doi.org/10.1146/annurev-food-032818-121641.

[14] C.A. Di Battista, D. Constenla, M.V. Ramírez Rigo, J. Piña, Process analysis and global optimization for the microencapsulation of phytosterols by spray drying, Powder Technol. 321 (2017) 55–65. https://doi.org/10.1016/j.powtec.2017.08.008.

[15] M.R.I. Shishir, W. Chen, Trends of spray drying: A critical review on drying of fruit and vegetable juices, Trends Food Sci. Technol. 65 (2017) 49–67. https://doi.org/10.1016/j.tifs.2017.05.006.

[16] C. Arpagaus, A. Collenberg, D. Rütti, E. Assadpour, S.M. Jafari, Nano spray drying for encapsulation of pharmaceuticals, Int. J. Pharm. 546 (2018) 194–214. https://doi.org/10.1016/j.ijpharm.2018.05.037.

[17] A. Gonçalves, B.N. Estevinho, F. Rocha, Formulation approaches for improved retinoids delivery in the treatment of several pathologies, Eur. J. Pharm. Biopharm. 143 (2019) 80–90. https://doi.org/10.1016/j.ejpb.2019.08.014.

[18] E.J. Huang, Y.C. Ye, S.R. Chen, J.R. Chai, J.X. Lu, L. Zhoa, L.J. Gu, Z.Y. Wang, Use of all-trans retinoic acid in the treatment of acute promyelocytic leukemia, Blood. 72 (1988) 567–572.

[19] G. Brown, E. Marcinkowska, Acute Myeloid Leukaemia: New Targets and Therapies, Int. J. Mol. Sci. 18 (2017) 2577. https://doi.org/10.3390/ijms18122577.

[20] F. Lo-Coco, L. Cicconi, M. Breccia, Current standard treatment of adult acute promyelocytic leukaemia, Br. J. Haematol. 172 (2016) 841–854. https://doi.org/10.1111/bjh.13890.

[21] A.P.P. Ng, W.J. Chng, M. Khan, Curcumin sensitizes acute promyelocytic leukemia cells to unfolded protein response-induced apoptosis by blocking the loss of misfolded N-CoR protein, Mol. Cancer Res. 9 (2011) 878–888. https://doi.org/10.1158/1541-7786.MCR-10-0545.

[22] F. Ferrara, M. Molica, M. Bernardi, Drug treatment options for acute promyelocytic leukemia, Expert Opin. Pharmacother. 23 (2022) 117–127. https://doi.org/10.1080/14656566.2021.1961744.

[23] H.M. Kantarjian, N. Jain, G. Garcia-Manero, M.A. Welch, F. Ravandi, W.G. Wierda, E.J. Jabbour, The cure of leukemia through the optimist's prism, Cancer. 128 (2022) 240–259. https://doi.org/10.1002/cncr.33933.

[24] N. Noguera, G. Catalano, C. Banella, M. Divona, I. Faraoni, T. Ottone, W. Arcese, M. Voso, Acute Promyelocytic Leukemia: Update on the Mechanisms of Leukemogenesis, Resistance and on Innovative Treatment Strategies, Cancers (Basel). 11 (2019) 1591. https://doi.org/10.3390/cancers11101591.

[25] C.C. Achkar, J.M. Bentel, J.F. Boylan, H.I. Scher, L.J. Gudas, W.H. Miller, Differences in the pharmacokinetic properties of orally administered all-trans-retinoic acid and 9-cis-retinoic acid in the plasma of nude mice, Drug Metab. Dispos. 22 (1994) 451–458.

[26] T. Hirota, T. Fujimoto, K. Konno, Y. Sakakibara, K. N., M. Tsurusawa, K. Takitani, M. Miyake, Pharmacokinetics studies of all-trans retinoic acid (ATRA) and pilot study of intermittent schedule of ATRA and chemotherapy in childhood acute promyelocytic leukemia. Children's cancer and leukemia study group, Japanese J. Clin. Hematol. 38 (1997) 1170– 1176.

[27] S. Das, A. Chaudhury, Recent advances in lipid nanoparticle formulations with solid matrix for oral drug delivery, AAPS PharmSciTech. 12 (2011) 62–76. https://doi.org/10.1208/s12249-010-9563-0.

[28] C. Errico, M. Gazzarri, F. Chiellini, A novel method for the preparation of retinoic acid-loaded nanoparticles, Int. J. Mol. Sci. 10 (2009) 2336–2347. https://doi.org/10.3390/ijms10052336.

[29] R. Parthasarathy, K. Mehta, Altered metabolism of all-trans-retinoic acid in liposome-encapsulated form, Cancer Lett. 134 (1998) 121–128. https://doi.org/10.1016/S0304-3835(98)00226-2.

[30] B. Ozpolat, K. Mehta, G. Lopez-Berestein, Regulation of a highly specific retinoic acid-4-hydroxylase (CYP26A1) enzyme and all- trans -retinoic acid metabolism in human intestinal, liver, endothelial, and acute promyelocytic leukemia cells, Leuk. Lymphoma. 46 (2005) 1497–1506. https://doi.org/10.1080/10428190500174737.

[31] M.D. Tiwari, S. Mehra, S. Jadhav, J.R. Bellare, All-trans retinoic acid loaded block copolymer nanoparticles efficiently induce cellular differentiation in HL-60 cells, Eur. J. Pharm. Sci. 44 (2011) 643–652. https://doi.org/10.1016/j.ejps.2011.10.014.

[32] E.L. Silva, F.A. Lima, G. Carneiro, J.P. Ramos, D.A. Gomes, E.M. de Souza-Fagundes, L.A. Miranda Ferreira, Improved In Vitro Antileukemic Activity of All-Trans Retinoic Acid Loaded in Cholesteryl Butyrate Solid Lipid Nanoparticles, J. Nanosci. Nanotechnol. 16 (2016) 1291–1300.

[33] F. Nicoletti, L. Hammer, S. Furtado, K. Mangano, E. Mathiowitz, B. Green, D.L. Auci, Oral Delivery of Encapsulated All-Trans Retinoic Acid Ameliorates Disease in Rodent Models of Colitis, Inflamm. Bowel Dis. 28 (2022) 455–465. https://doi.org/10.1093/ibd/izab204.

[34] G. Zuccari, R. Carosio, a. Fini, P.G. Montaldo, I. Orienti, Modified polyvinylalcohol for encapsulation of all-trans-retinoic acid in polymeric micelles, J. Control. Release. 103 (2005) 369–380. https://doi.org/10.1016/j.jconrel.2004.12.016.

[35] A. Gonçalves, B.N. Estevinho, F. Rocha, Microencapsulation of vitamin A: A review, Trends Food Sci. Technol. 51 (2016) 76–87. https://doi.org/10.1016/j.tifs.2016.03.001.

[36] E. V Mccollum, M. Davis, The necessity of certain lipins in the diet during growth, J. Biol. Chem. 15 (1913) 167–175.

[37] S. Mukherjee, A. Date, V. Patravale, H.C. Korting, A. Roeder, G. Weindl, Retinoids in the treatment of skin aging: an overview of clinical efficacy and safety, Clin. Interv. Aging. 1 (2006) 327–348.

[38] S. Khalil, T. Bardawil, C. Stephan, N. Darwiche, O. Abbas, A.G. Kibbi, G. Nemer, M. Kurban, Retinoids: a journey from the molecular structures and mechanisms of action to clinical uses in dermatology and adverse effects, J. Dermatolog. Treat. 28 (2017) 684–696. https://doi.org/10.1080/09546634.2017.1309349.

[39] B.C. Das, P. Thapa, R. Karki, S. Das, S. Mahapatra, T.C. Liu, I. Torregroza, D.P. Wallace, S. Kambhampati, P. Van Veldhuizen, A. Verma, S.K. Ray, T. Evans, Retinoic acid signaling pathways in development and diseases, Bioorganic Med. Chem. 22 (2014) 673–683. https://doi.org/10.1016/j.bmc.2013.11.025.

[40] J. Brtko, Retinoids, rexinoids and their cognate nuclear receptors: character and their role in

chemoprevention of selected malignant diseases, Biomed. Pap. Med. Fac. Univ. Palacky. Olomouc. Czech. Repub. 151 (2007) 187–194. https://doi.org/10.5507/bp.2007.033.

[41] J. Ablain, H. De Thé, Retinoic acid signaling in cancer: The parable of acute promyelocytic leukemia, Int. J. Cancer. 135 (2014) 2262–2272. https://doi.org/10.1002/ijc.29081.

[42] L. Beckenbach, J.M. Baron, H.F. Merk, H. Löffler, P.M. Amann, Retinoid treatment of skin diseases, Eur. J. Dermatology. 25 (2015) 384–391. https://doi.org/10.1684/ejd.2015.2544.

[43] A.O. Huen, E.J. Kim, The role of systemic retinoids in the treatment of cutaneous T-cell lymphoma, Dermatol. Clin. 33 (2015) 715–729. https://doi.org/10.1016/j.det.2015.05.007.

[44] E.H. Heller, N.J. Shiffman, Synthetic retinoids in dermatology, Can. Med. Assoc. J. 132 (1985) 1129–1136.

[45] H. Fritz, D. Kennedy, D. Fergusson, R. Fernandes, S. Doucette, K. Cooley, A. Seely, S. Sagar, R. Wong, D. Seely, Vitamin A and retinoid derivatives for lung cancer: A systematic review and meta analysis, PLoS One. 6 (2011). https://doi.org/10.1371/journal.pone.0021107.

[46] L. Beckenbach, J.M. Baron, H.F. Merk, H. Löffler, P.M. Amann, K.K. Kiningham, A. Silvis, Receptor independent effects of retinoids, in: Nutr. Cancer, from Epidemiol. to Biol., 2012: pp. 50–64. https://doi.org/10.1684/ejd.2015.2544.

[47] C. Peng, S.Q. Zhao, J. Zhang, G.Y. Huang, L.Y. Chen, F.Y. Zhao, Chemical composition, antimicrobial property and microencapsulation of Mustard (Sinapis alba) seed essential oil by complex coacervation, Food Chem. 165 (2014) 560–568. https://doi.org/10.1016/j.foodchem.2014.05.126.

[48] Q. Yang, T. Sakurai, K. Kakudo, Retinoid, retinoic acid receptor β and breast cancer, Breast Cancer Res. Treat. 76 (2002) 167–173. https://doi.org/10.1023/A:1020576606004.

[49] M.J. Young, Y.H. Wu, W.T. Chiu, T.Y. Weng, Y.F. Huang, C.Y. Chou, All-trans retinoic acid downregulates ALDH1-mediated stemness and inhibits tumour formation in ovarian cancer cells, Carcinogenesis. 36 (2015) 498–507. https://doi.org/10.1093/carcin/bgv018.

[50] F. Giannini, R. Maestro, T. Vukosavljevic, F. Pomponi, M. Boiocchi, All-trans, 13-cis and 9-cis retinoic acids induce a fully reversible growth inhibition in HNSCC cell lines: Implications for in vivo retinoic acid use, Int. J. Cancer. 70 (1997) 194–200. https://doi.org/10.1002/(SICI)1097-0215(19970117)70:2<194::AID-IJC10>3.0.CO;2-J.

[51] C. Geisen, C. Denk, J.H. Küpper, E. Schwarz, Growth inhibition of cervical cancer cells by the human retinoic acid receptor β gene, Int. J. Cancer. 85 (2000) 289–295. https://doi.org/10.1002/(SICI)1097-0215(20000115)85:2<289::AID-IJC22>3.0.CO;2-T.

[52] R.S. Quintero Barceinas, A. García-Regalado, E. Aréchaga-Ocampo, N. Villegas-Sepúlveda, C.H. González-De La Rosa, All-Trans Retinoic Acid Induces Proliferation, Survival, and Migration in A549 Lung Cancer Cells by Activating the ERK Signaling Pathway through a Transcription-Independent Mechanism, Biomed Res. Int. 2015 (2015). https://doi.org/10.1155/2015/404368.

[53] E. Messi, M.C. Florian, C. Caccia, M. Zanisi, R. Maggi, Retinoic acid reduces human neuroblastoma cell migration and invasiveness: Effects on DCX, LIS1, neurofilaments-68 and vimentin expression,

BMC Cancer. 8 (2008) 1–12. https://doi.org/10.1186/1471-2407-8-30.

[54] S. Barbus, B. Tews, D. Karra, M. Hahn, B. Radlwimmer, N. Delhomme, C. Hartmann, J. Felsberg, D. Krex, G. Schackert, R. Martinez, G. Reifenberger, P. Lichter, Differential retinoic acid signaling in tumors of long- and short-term glioblastoma survivors, J. Natl. Cancer Inst. 103 (2011) 598–601. https://doi.org/10.1093/jnci/djr036.

[55] C. Liang, L. Yang, S. Guo, All-trans retinoic acid inhibits migration, invasion and proliferation, and promotes apoptosis in glioma cells in vitro, Oncol. Lett. 9 (2015) 2833–2838. https://doi.org/10.3892/ol.2015.3120.

[56] H. Zhang, K. Satyamoorthy, M. Herlyn, I. Rosdahl, All-trans retinoic acid (atRA) differentially induces apoptosis in matched primary and metastatic melanoma cells - A speculation on damage effect of atRA via mitochondrial dysfunction and cell cycle redistribution, Carcinogenesis. 24 (2003) 185–191. https://doi.org/10.1093/carcin/24.2.185.

[57] N. Bushue, Y.-J.Y. Wan, Retinoid pathway and cancer therapeutics, Adv. Drug Deliv. Rev. 62 (2010) 1285–1298. https://doi.org/10.1016/j.addr.2010.07.003.

[58] J. Muindi, S.R. Frankel, W.H. Miller, A. Jakubowski, D. a Scheinberg, C.W. Young, E. Dmitrovsky, R.P. Warrell, R. Frankel, W.H.M. Jr, A. Jakubowski, D. a Scheinberg, C.W. Young, E. Dmitrovsky, R.P.W. Jr, Continuous treatment with all-trans retinoic acid causes a progressive reduction in plasma drug concentrations: implications for relapse and retinoid "resistance" in patients with acute promyelocytic leukemia., Blood. 79 (1992) 299–303.

[59] S.R. Frankel, A. Eardley, G. Lauwers, M. Weiss, R.P.J. Warrell, The "Retinoic Acid Syndrome" in Acute Promyelocytic Leukemia, Ann. Intern. Med. 117 (1992) 292–296.

[60] B.A. Conley, M.J. Egorin, R. Sridhara, R. Finley, R. Hemady, S. Wu, N.S. Tait, E.D.A. Van, Phase I clinical trial of all-trans-retinoic acid with correlation of its pharmacokinetics and pharmacodynamics, Cancer Chemother. Pharmacol. 39 (1997) 291–299.

[61] E. Patatanian, D.F. Thompson, Retinoic acid syndrome: A review, J. Clin. Pharm. Ther. 33 (2008) 331–338. https://doi.org/10.1111/j.1365-2710.2008.00935.x.

[62] L. Baumann, J. Vujevich, M. Halem, L.K. Martin, F. Kerdel, M. Lazarus, H. Pacheco, L. Black, J. Bryde, Open-label pilot study of alitretinoin gel 0.1% in the treatment of photoaging, Cutis. 76 (2005) 69–73. http://www.ncbi.nlm.nih.gov/pubmed/16144296.

[63] A.J. Van Herle, M.L. Agatep, D.N. Padua, T.L. Totanes, D. V. Canlapan, H.M.L. Van Herle, G.J.F. Juillard, Effects of 13 cis-Retinoic Acid on Growth and Differentiation of Human Follicular Carcinoma Cells (UCLA RO 82 W-l) in Vitro, J. Clin. Endocrinol. Metab. 71 (1990) 755–763. https://doi.org/10.1210/jcem-71-3-755.

[64] R. Talpur, S. Ward, N. Apisarnthanarax, J. Breuer-McHam, M. Duvic, Optimizing bexarotene therapy for cutaneous T-cell lymphoma, J. Am. Acad. Dermatol. 47 (2002) 672–684. https://doi.org/10.1067/mjd.2002.124607.

[65] R. Torrisi, A. Decensi, Fenretinide and cancer prevention., Curr. Oncol. Rep. 2 (2000) 263–270.

https://doi.org/10.1007/s11912-000-0077-x.

[66] M.-C. Chen, S.-L. Hsu, H. Lin, T.-Y. Yang, Retinoic acid and cancer treatment, BioMedicine. 4 (2014) 22. https://doi.org/10.7603/s40681-014-0022-1.

[67] S.H. Hong, K.R. Kim, D.K. Oh, Biochemical properties of retinoid-converting enzymes and biotechnological production of retinoids, Appl. Microbiol. Biotechnol. 99 (2015) 7813–7826. https://doi.org/10.1007/s00253-015-6830-8.

[68] B.M. Tashtoush, E.L. Jacobson, M.K. Jacobson, UVA is the major contributor to the photodegradation of tretinoin and isotretinoin: Implications for development of improved pharmaceutical formulations, Int. J. Pharm. 352 (2008) 123–128. https://doi.org/10.1016/j.ijpharm.2007.10.045.

[69] L. Culp, S. Moradi Tuchayi, H. Alinia, S.R. Feldman, Tolerability of topical retinoids: are there clinically meaningful differences among topical retinoids?, J. Cutan. Med. Surg. 19 (2015) 530–538. https://doi.org/10.1177/1203475415591117.

[70] B.A. Hubbard, J.G. Unger, R.J. Rohrich, Reversal of skin aging with topical retinoids, Plast. Reconstr. Surg. 133 (2014) 481–490. https://doi.org/10.1097/PRS.0000000000000043.

[71] H.Y. Kang, L. Valerio, P. Bahadoran, J.P. Ortonne, The role of topical retinoids in the treatment of pigmentary disorders: An evidence-based review, Am. J. Clin. Dermatol. 10 (2009) 251–260. https://doi.org/10.2165/00128071-200910040-00005.

[72] S.M. Bulengo-Ransby, C. Griffiths, C.K. Kimbrough-Green, L.J. Finkel, T.A. Hamilton, C.N. Ellis, J.J. Voorhees, Topical Tretinoin (Retinoic Acid) Therapy for Hyperpigmented Lesions Caused by Inflammation of the Skin in Black Patients, N. Engl. J. Med. 328 (1993) 1438–1443. https://doi.org/10.1056/NEJM199305203282002.

[73] C. Sinico, M. Manconi, M. Peppi, F. Lai, D. Valenti, A.M. Fadda, Liposomes as carriers for dermal delivery of tretinoin: In vitro evaluation of drug permeation and vesicle-skin interaction, J. Control. Release. 103 (2005) 123–136. https://doi.org/10.1016/j.jconrel.2004.11.020.

[74] R.S. Awad, W. Abdelwahed, Y. Bitar, Evaluating the impact of prepatation conditions and formulation on the accelerated stability of tretinoin loaded liposomes prepared by heating method, Int. J. Pharm. Pharm. Sci. 7 (2015) 171–178.

[75] S. Abbas, C. Da Wei, K. Hayat, Z. Xiaoming, Ascorbic Acid: Microencapsulation Techniques and Trends—A Review, Food Rev. Int. 28 (2012) 343–374.

[76] A. Teleki, A. Hitzfeld, M. Eggersdorfer, 100 years of vitamins: the science of formulation is the key to functionality, Kona Powder Part. J. (2013) 144–163.

[77] Microencapsulation Market Estimates & Trend Analysis By Application (Pharmaceutical, Household Product, Agrochemical, Food Additive, Phase Change Material), By Region (North America, Europe, Asia Pacific, RoW), And Segment Forecasts, 2014 - 2025, Gd. View Res. (n.d.). https://www.grandviewresearch.com/industry-analysis/microencapsulation-market (accessed January 5, 2017).

[78] P.D. Fraser, P.M. Bramley, The biosynthesis and nutritional uses of carotenoids, Prog. Lipid Res. 43

(2004) 228–265.

[79] P. Henning, H.H. Conaway, U.H. Lerner, Retinoid receptors in bone and their role in bone remodeling, Front. Endocrinol. (Lausanne). 6 (2015) 1–13. https://doi.org/10.3389/fendo.2015.00031.

[80] D.S. Goodman, H.S. Huang, Biosynthesis of vitamin A with rat intestinal enzymes, Science. 149 (1965) 879–880.

[81] J.A. Olson, O. Hayaishi, The enzymatic cleavage of β-carotene into vitamin A by soluble enzymes of rat liver and intestine, Proc. Natl. Acad. Sci. U. S. A. 54 (1965) 1364–1370.

[82] R. Blomhoff, H.K. Blomhoff, Overview of retinoid metabolism and function, J. Neurobiol. 66 (2006) 606–630.

[83] E. Reboul, Absorption of vitamin A and carotenoids by the enterocyte: Focus on transport proteins, Nutrients. 5 (2013) 3563–3581. https://doi.org/10.3390/nu5093563.

[84] F.M. Herr, D.E. Ong, Differential interaction of lecithin-retinol acyltransferase with cellular retinol binding proteins, Biochemistry. 31 (1992) 6748–6755.

[85] E.H. Harrison, Mechanisms of digestion and absorption of dietary vitamin A., Annu. Rev. Nutr. 25 (2005) 87–103.

[86] R. Blomhoff, P. Helgerud, M. Rasmussen, T. Berg, K.R. Norum, In vivo uptake of chylomicron [3H]retinyl ester by rat liver: evidence for retinol transfer from parenchymal to nonparenchymal cells, Proc. Natl. Acad. Sci. U. S. A. 79 (1982) 7326–7330.

[87] R. Blomhoff, M.H. Green, T. Berg, K.R. Norum, Transport and storage of vitamin A, Science (80-.). 250 (1990) 399–404.

[88] P. Sauvant, M. Cansell, A.H. Sassi, C. Atgié, Vitamin A enrichment: caution with encapsulation strategies used for food applications, Food Res. Int. 46 (2012) 469–479.

[89] J. Paik, S. Vogel, L. Quadro, R. Piantedosi, M. Gottesman, K. Lai, L. Hamberger, M. de M. Vieira, W.S. Blaner, Vitamin A:Overlapping delivery pathways to tissues from the circulation, Am. Soc. Nutr. Sci. (2004) 276S-280S.

[90] D.S. Goodman, H.S. Huang, T. Shiratori, Tissue distribution and metabolism of newly absorbed vitamin A in the rat, J. Lipid Res. 6 (1965) 390–396. https://doi.org/10.1096/fj.11-180935.

[91] H. Ronne, C. Ocklind, K. Wiman, L. Rask, B. Obrink, P. a Peterson, Ligand-dependent regulation of intracellular protein transport: effect of vitamin a on the secretion of the retinol-binding protein., J. Cell Biol. 96 (1983) 907–10. https://doi.org/10.1083/jcb.96.3.907.

[92] P. Bouillet, V. Sapin, C. Chazaud, N. Messaddeq, D. Décimo, P. Dollé, P. Chambon, Developmental expression pattern of Stra6, a retinoic acid-responsive gene encoding a new type of membrane protein, Mech. Dev. 63 (1997) 173–186.

[93] R. Kawaguchi, J. Yu, J. Honda, J. Hu, J. Whitelegge, P. Ping, P. Wiita, D. Bok, H. Sun, A membrane receptor for retinol binding protein mediates cellular uptake of vitamin A, Science. 315 (2007) 820–825.

[94] G. Wolf, Identification of a membrane receptor for retinol-binding protein functioning in the cellular uptake of retinol, Nutr. Rev. 65 (2007) 385–388.

[95] M. Lei, H. De Thé, Retinoids and retinoic acid receptor in cancer, Eur. J. Cancer, Suppl. 1 (2003) 13–18. https://doi.org/10.1016/S1359-6349(03)00010-7.

[96] M. Clagett-Dame, D. Knutson, Vitamin A in reproduction and development, Nutrients. 3 (2011) 385–428.

[97] P. Huang, V. Chandra, F. Rastinejad, Retinoic acid actions through mammalian nuclear receptors, Chem. Rev. 114 (2014) 233–254. https://doi.org/10.1021/cr400161b.

[98] J. Marill, N. Idres, C.C. Capron, E. Nguyen, G.G. Chabot, Retinoic acid metabolism and mechanism of action: a review., Curr. Drug Metab. 4 (2003) 1–10. https://doi.org/10.2174/1389200033336900.

[99] P. Chambon, A decade of molecular biology of retinoic acid receptors., FASEB J. 10 (1996) 940–954. https://doi.org/10.1096/fasebj.10.9.8801176.

[100] L.-N. Wei, Retinoid receptors and their coregulators, Annu. Rev. Pharmacol. Toxicol. 43 (2003) 47–72. https://doi.org/10.1146/annurev.pharmtox.43.100901.140301.

[101] A. Gonçalves, N. Nikmaram, S. Roohinejad, B.N.B.N. Estevinho, F. Rocha, R. Greiner, D.J.D.J. McClements, Production, properties, and applications of solid self-emulsifying delivery systems (S-SEDS) in the food and pharmaceutical industries, Colloids Surfaces A Physicochem. Eng. Asp. 538 (2018) 108–126. https://doi.org/10.1016/j.colsurfa.2017.10.076.

[102] Z. Fang, B. Bhandari, Encapsulation of polyphenols - a review, Trends Food Sci. Technol. 21 (2010) 510–523.

[103] W. Zheng, A water-in-oil-in-oil-in-water (W/O/O/W) method for producing drug-releasing, double-walled microspheres, Int. J. Pharm. 374 (2009) 90–95.

[104] J.-H. Lee, T.G. Park, H.-K. Choi, Effect of formulation and processing variables on the characteristics of microspheres for water-soluble drugs prepared by w/o/o double emulsion solvent diffusion method, Int. J. Pharm. 196 (2000) 75–83.

[105] Q. Gao, C. Wang, H. Liu, Y. Chen, Z. Tong, Dual nanocomposite multihollow polymer microspheres prepared by suspension polymerization based on a multiple pickering emulsion, Polym. Chem. 1 (2010) 75–77.

[106] R. Aveyard, B.P. Binks, J.H. Clint, Emulsions stabilised solely by colloidal particles, Adv. Colloid Interface Sci. 100–102 (2003) 503–546.

[107] D.J. McClements, Edible nanoemulsions: fabrication, properties, and functional performance, Soft Matter. 7 (2011) 2297–2316. https://doi.org/10.1039/C0SM00549E.

[108] D.J. McClements, E.A. Decker, J. Weiss, Emulsion-based delivery systems for lipophilic bioactive components, J. Food Sci. 72 (2007) R109–R124.

[109] H. Yu, Q. Huang, Bioavailability and Delivery of Nutraceuticals and Functional Foods Using Nanotechnology, in: Bio-Nanotechnology A Revolut. Food, Biomed. Heal. Sci., 2013: pp. 593–604. https://doi.org/10.1002/9781118451915.ch35.

[110] A. Gupta, H.B. Eral, T.A. Hatton, P.S. Doyle, Nanoemulsions: formation, properties and applications, Soft Matter. 12 (2016) 2826–2841. https://doi.org/10.1039/C5SM02958A.

[111] M. Üner, G. Yener, Importance of solid lipid nanoparticles (SLN) in various administration routes and future perspective, Int. J. Nanomedicine. 2 (2007) 289–300.

[112] A. Saxena, T. Maity, A. Paliwal, S. Wadhwa, Technological Aspects of Nanoemulsions and Their Applications in the Food Sector, in: Nanotechnol. Appl. Food, Elsevier, 2017: pp. 129–152. https://doi.org/10.1016/B978-0-12-811942-6.00007-8.

[113] S. Jana, A. Gandhi, S. Jana, Nanotechnology in Bioactive Food Ingredients, in: Nanotechnol. Appl. Food, Elsevier, 2017: pp. 21–41. https://doi.org/10.1016/B978-0-12-811942-6.00002-9.

[114] D.J. McClements, Food Emulsions: Principles, Practices, and Techniques, 2nd ed., Boca Raton, Fla.: CRC PressCRC Press, 2005.

[115] W. Mehnert, K. Mäder, Solid lipid nanoparticles: production, characterization and applications, Adv. Drug Deliv. Rev. 47 (2001) 165–96.

[116] C. Li, J. Zhang, Y.J. Zu, S.F. Nie, J. Cao, Q. Wang, S.P. Nie, Z.Y. Deng, M.Y. Xie, S. Wang, Biocompatible and biodegradable nanoparticles for enhancement of anti-cancer activities of phytochemicals, Chin. J. Nat. Med. 13 (2015) 641–652. https://doi.org/10.1016/S1875-5364(15)30061-3.

[117] J.-Y. Fang, C.-L. Fang, C.-H. Liu, Y.-H. Su, Lipid nanoparticles as vehicles for topical psoralen delivery: Solid lipid nanoparticles (SLN) versus nanostructured lipid carriers (NLC), Eur. J. Pharm. Biopharm. 70 (2008) 633–640. https://doi.org/10.1016/j.ejpb.2008.05.008.

[118] A. Behtash, S. Nafisi, H. Maibach, New Generation of Fluconazole: A Review on Existing Researches and Technologies, Curr. Drug Deliv. 14 (2017) 2–15. https://doi.org/10.2174/1567201813666160502125620.

[119] R.H. Müller, M. Radtke, S. a. Wissing, Solid lipid nanoparticles (SLN) and nanostructured lipid carriers (NLC) in cosmetic and dermatological preparations, in: Adv. Drug Deliv. Rev., 2002: pp. 131–155. https://doi.org/10.1016/S0169-409X(02)00118-7.

[120] I. a Aljuffali, C.-H. Huang, J.-Y. Fang, Nanomedical Strategies for Targeting Skin Microbiomes, Curr. Drug Metab. 16 (2015) 255–271. https://doi.org/10.2174/1389200216666150812124923.

[121] S. a. Wissing, O. Kayser, R.H. Müller, Solid lipid nanoparticles for parenteral drug delivery, Adv. Drug Deliv. Rev. 56 (2004) 1257–1272. https://doi.org/10.1016/j.addr.2003.12.002.

[122] R.H. Müller, M. Radtke, S. a. Wissing, Nanostructured lipid matrices for improved microencapsulation of drugs, Int. J. Pharm. 242 (2002) 121–128.

[123] A. Beloqui, M.Á. Solinís, A. Rodríguez-Gascón, A.J. Almeida, V. Préat, Nanostructured lipid carriers: Promising drug delivery systems for future clinics, Nanomedicine Nanotechnology, Biol. Med. 12 (2016) 143–161. https://doi.org/10.1016/j.nano.2015.09.004.

[124] B. Gaba, M. Fazil, A. Ali, S. Baboota, J.K. Sahni, J. Ali, Nanostructured lipid (NLCs) carriers as a bioavailability enhancement tool for oral administration, Drug Deliv. 22 (2015) 691–700. https://doi.org/10.3109/10717544.2014.898110.

[125] G.M. Calixto, J. Bernegossi, L.M. de Freitas, C.R. Fontana, M. Chorilli, Nanotechnology-Based Drug

Delivery Systems for Photodynamic Therapy of Cancer: A Review., Molecules. 21 (2016) 342. https://doi.org/10.3390/molecules21030342.

[126] E.B. Souto, S. a. Wissing, C.M. Barbosa, R.H. Müller, Development of a controlled release formulation based on SLN and NLC for topical clotrimazole delivery, Int. J. Pharm. 278 (2004) 71–77. https://doi.org/10.1016/j.ijpharm.2004.02.032.

[127] J.O. Morales, K. Valdes, J.O. Morales, F. Oyarzun-Ampuero, Lipid nanoparticles for the topical delivery of retinoids and derivatives, Nanomedicine (London, United Kingdom). 10 (2015) 253–269. https://doi.org/10.2217/nnm.14.159.

[128] U. Bulbake, S. Doppalapudi, N. Kommineni, W. Khan, Liposomal formulations in clinical use: An updated review, Pharmaceutics. 9 (2017) 1–33. https://doi.org/10.3390/pharmaceutics9020012.

[129] S.A. Boorjian, M.I. Milowsky, J. Kaplan, M. Albert, M. V Cobham, D.M. Coll, N.P. Mongan, G. Shelton, D. Petrylak, L.J. Gudas, D.M. Nanus, Phase 1/2 clinical trial of interferon alpha2b and weekly liposome-encapsulated all-trans retinoic acid in patients with advanced renal cell carcinoma, J Immunother. 30 (2007) 655–662. https://doi.org/10.1097/CJI.0b013e31805449a8.

[130] L. Sercombe, T. Veerati, F. Moheimani, S.Y. Wu, A.K. Sood, S. Hua, Advances and challenges of liposome assisted drug delivery, Front. Pharmacol. 6 (2015) 1–13. https://doi.org/10.3389/fphar.2015.00286.

[131] B.S. Pattni, V. V. Chupin, V.P. Torchilin, New Developments in Liposomal Drug Delivery, Chem. Rev. 115 (2015) 10938–10966. https://doi.org/10.1021/acs.chemrev.5b00046.

[132] S. Vemuri, C.T. Rhodes, Preparation and characterization of liposomes as therapeutic delivery systems: a review, Pharm. Acta Helv. 70 (1995) 95−111.

[133] K. Taylor, G. Taylor, I. Kellaway, Drug entrapment and release from multilamellar and reverse-phase evaporation liposomes, Int. J. Pharm. 58 (1990) 49−55.

[134] B. de Kruyff, R.A. Demel, L.L. van Deenen, The effect of cholesterol and epicholesterol incorporation on the permeability and on the phase transition of intact Acholeplasma laidlawii cell membranes and derived liposomes, Biochim. Biophys. Acta. (1972) 331−347.

[135] V.P. Torchilin, Recent advances with liposomes as pharmaceutical carriers, Nat. Rev. Drug Discov. 4 (2005) 145–160. https://doi.org/10.1038/nrd1632.

[136] V.P. Chandu, A. Arunachalam, K.Y. S. Jeganath, G.C. K. Tharangini, Niosomes - A novel drug delivery device, Int. J. Nov. Trends Pharm. Sci. 2 (2012) 25–31.

[137] A. Gupta, S. Singh, N.G. Kotla, T.J. Webster, Formulation and evaluation of a topical niosomal gel containing a combination of benzoyl peroxide and tretinoin for antiacne activity, Int. J. Nanomedicine. 10 (2014) 171–182. https://doi.org/10.2147/IJN.S70449.

[138] P. Verma, K. Pathak, Therapeutic and cosmeceutical potential of ethosomes: An overview, J. Adv. Pharm. Technol. Res. 1 (2010) 274. https://doi.org/10.4103/0110-5558.72415.

[139] K. Kumar Mishra, C. Deep Kaur, S. Verma, A. Kumar Sahu, D. Kumar Dash, P. Kashyap, S. Prasad Mishra, Transethosomes and Nanoethosomes: Recent Approach on Transdermal Drug Delivery System,

in: Nanomedicines, IntechOpen, 2019: p. 13. https://doi.org/10.5772/intechopen.81152.

[140] P.L. Honeywell-Nguyen, J.A. Bouwstra, The in vitro transport of pergolide from surfactant-based elastic vesicles through human skin: A suggested mechanism of action, J. Control. Release. 86 (2003) 145–156. https://doi.org/10.1016/S0168-3659(02)00415-7.

[141] M. Trotta, E. Peira, M.E. Carlotti, M. Gallarate, Deformable liposomes for dermal administration of methotrexate, Int. J. Pharm. 270 (2004) 119–125. https://doi.org/10.1016/j.ijpharm.2003.10.006.

[142] C.K. Song, P. Balakrishnan, C.K. Shim, S.J. Chung, S. Chong, D.D. Kim, A novel vesicular carrier, transethosome, for enhanced skin delivery of voriconazole: Characterization and in vitro/in vivo evaluation, Colloids Surfaces B Biointerfaces. 92 (2012) 299–304. https://doi.org/10.1016/j.colsurfb.2011.12.004.

[143] J. Nicolas, S. Mura, D. Brambilla, N. MacKiewicz, P. Couvreur, Design, functionalization strategies and biomedical applications of targeted biodegradable/biocompatible polymer-based nanocarriers for drug delivery, Chem. Soc. Rev. 42 (2013) 1147–1235. https://doi.org/10.1039/c2cs35265f.

[144] S. Lee, Strategic Design of Delivery Systems for Nutraceuticals, in: Nanotechnol. Appl. Food, Elsevier, 2017: pp. 65–86. https://doi.org/10.1016/B978-0-12-811942-6.00004-2.

[145] B.N. Estevinho, F. Rocha, L. Santos, A. Alves, Microencapsulation with chitosan by spray drying for industry applications – a review, Trends Food Sci. Technol. 31 (2013) 138–155.

[146] C. O'Leary, B. Cavanagh, R.E. Unger, C.J. Kirkpatrick, S. O'Dea, F.J. O'Brien, S.A. Cryan, The development of a tissue-engineered tracheobronchial epithelial model using a bilayered collagen-hyaluronate scaffold, Biomaterials. 85 (2016) 111–127. https://doi.org/10.1016/j.biomaterials.2016.01.065.

[147] D.A. Knight, S.T. Holgate, The airway epithelium: Structural and functional properties in health and disease, Respirology. 8 (2003) 432–446. https://doi.org/10.1046/j.1440-1843.2003.00493.x.

[148] J.F. Coelho, P.C. Ferreira, P. Alves, R. Cordeiro, A.C. Fonseca, J.R. Góis, M.H. Gil, Drug delivery systems: Advanced technologies potentially applicable in personalized treatments, EPMA J. 1 (2010) 164–209. https://doi.org/10.1007/s13167-010-0001-x.

[149] F. Danhier, E. Ansorena, J.M. Silva, R. Coco, A. Le Breton, V. Préat, PLGA-based nanoparticles: An overview of biomedical applications, J. Control. Release. 161 (2012) 505–522. https://doi.org/10.1016/j.jconrel.2012.01.043.

[150] S.A. Castleberry, M.A. Quadir, M.A. Sharkh, K.E. Shopsowitz, P.T. Hammond, Polymer Conjugated Retinoids for Controlled Transdermal Delivery, J. Control. Release. 262 (2017) 1–21. https://doi.org/10.1016/j.coviro.2015.09.001.Human.

[151] E. Schultze, A. Ourique, V.C. Yurgel, K.R. Begnini, H. Thurow, P.M.M. De Leon, V.F. Campos, O.A. Dellagostin, S.R. Guterres, A.R. Pohlmann, F.K. Seixas, R.C.R. Beck, T. Collares, Encapsulation in lipid-core nanocapsules overcomes lung cancer cell resistance to tretinoin, Eur. J. Pharm. Biopharm. 87 (2014) 55–63. https://doi.org/10.1016/j.ejpb.2014.02.003.

[152] C. Zea, J. Alcántara, R. Barranco-García, M. Morcillo, D. de la Fuente, Synthesis and Characterization

of Hollow Mesoporous Silica Nanoparticles for Smart Corrosion Protection, Nanomaterials. 8 (2018) 478. https://doi.org/10.3390/nano8070478.

[153] C.L. Winek, M.J. Marks, S.P. Shanor, E.R. Davis, Acute and subacute toxicology and safety evaluation of triphenyl tin hydroxide (vancide KS), Clin. Toxicol. 13 (1978) 281–296. https://doi.org/10.3109/15563657808988238.

[154] S.K. Kim, N. Rajapakse, Enzymatic production and biological activities of chitosan oligosaccharides (COS): A review, Carbohydr. Polym. 62 (2005) 357–368. https://doi.org/10.1016/j.carbpol.2005.08.012.

[155] C.-H. Lin, Y.-P. Fang, S.A. Al-Suwayeh, S.-Y. Yang, J.-Y. Fang, Percutaneous absorption and antibacterial activities of lipid nanocarriers loaded with dual drugs for acne treatment., Biol. Pharm. Bull. 36 (2013) 276–86. https://doi.org/10.1248/bpb.b12-00793.

[156] E. Silva, G. Carneiro, L.; Araujo, M.; Trindade, R. Yoshida, MI ; Orefice, L.; Farias, M.; Carvalho, S.; Santos, G.; Goulart, R.; Alves, L. Ferreira, Solid Lipid Nanoparticles Loaded with Retinoic Acid and Lauric Acid as an Alternative for Topical Treatment of Acne Vulgaris, J. Nanosci. Nanotechnol. 14 (2014) 1–8. https://doi.org/10.1166/jnn.2015.9184.

[157] K. Raza, B. Singh, S. Lohan, G. Sharma, P. Negi, Y. Yachha, O.P. Katare, Nano-lipoidal carriers of tretinoin with enhanced percutaneous absorption, photostability, biocompatibility and anti-psoriatic activity, Int. J. Pharm. 456 (2013) 65–72. https://doi.org/10.1016/j.ijpharm.2013.08.019.

[158] C.F. Hung, W.Y. Chen, C.Y. Hsu, I. a. Aljuffali, H.C. Shih, J.Y. Fang, Cutaneous penetration of soft nanoparticles via photodamaged skin: Lipid-based and polymer-based nanocarriers for drug delivery, Eur. J. Pharm. Biopharm. 94 (2015) 94–105. https://doi.org/10.1016/j.ejpb.2015.05.005.

[159] S. Alireza Mortazavi, S. Pishrochi, Z. Jafari Azar, Formulation and in-vitro evaluation of tretinoin microemulsion as a potential carrier for dermal drug delivery, Iran. J. Pharm. Res. 12 (2013) 599–609.

[160] N. Bavarsad, A. Akhgari, S. Seifmanesh, A. Salimi, A. Rezaie, Statistical optimization of tretinoin-loaded penetration-enhancer vesicles (PEV) for topical delivery, DARU, J. Pharm. Sci. 24 (2016) 1–12. https://doi.org/10.1186/s40199-016-0142-0.

[161] M. Narvekar, H.Y.I. Xue, N.T. Tran, M. Mikhael, H.L.U. Wong, A new nanostructured carrier design including oil to enhance the pharmaceutical properties of retinoid therapy and its therapeutic effects on chemo-resistant ovarian cancer, Eur. J. Pharm. Biopharm. 88 (2014) 226–237. https://doi.org/10.1016/j.ejpb.2014.04.014.

[162] M.H. Akanda, R. Rai, I.J. Slipper, B.Z. Chowdhry, D. Lamprou, G. Getti, D. Douroumis, Delivery of retinoic acid to LNCap human prostate cancer cells using solid lipid nanoparticles, Int. J. Pharm. 493 (2015) 161–171. https://doi.org/10.1016/j.ijpharm.2015.07.042.

[163] R. Sun, Y. Liu, S.Y. Li, S. Shen, X.J. Du, C.F. Xu, Z.T. Cao, Y. Bao, Y.H. Zhu, Y.P. Li, X.Z. Yang, J. Wang, Co-delivery of all-trans-retinoic acid and doxorubicin for cancer therapy with synergistic inhibition of cancer stem cells, Biomaterials. 37 (2015) 405–414. https://doi.org/10.1016/j.biomaterials.2014.10.018.

[164] M. Lei, J. Wang, M. Ma, M. Yu, F. Tan, N. Li, Dual drug encapsulation in a novel nano-vesicular carrier

for the treatment of cutaneous melanoma: characterization and in vitro/in vivo evaluation, RSC Adv. 5 (2015) 20467–20478. https://doi.org/10.1039/C4RA16306K.

[165] M. Kong, J. Tang, Q. Qiao, T. Wu, Y. Qi, S. Tan, X. Gao, Z. Zhang, Biodegradable hollow mesoporous silica nanoparticles for regulating tumor microenvironment and enhancing antitumor efficiency, Theranostics. 7 (2017) 3276–3292. https://doi.org/10.7150/thno.19987.

[166] T. Li, Y. Zhang, Y.-P. Meng, L.-S. Bo, W.-B. Ke, miR-542-3p Appended Sorafenib/All-trans Retinoic Acid (ATRA)-Loaded Lipid Nanoparticles to Enhance the Anticancer Efficacy in Gastric Cancers, Pharm. Res. 34 (2017) 2710–2719. https://doi.org/10.1007/s11095-017-2202-7.

[167] J.L. Liu, J. Li, L.Y. Zhang, P.L. Zhang, J.L. Zhou, B. Liu, Preparation of N, N, N-trimethyl chitosan-functionalized retinoic acid-loaded lipid nanoparticles for enhanced drug delivery to glioblastoma, Trop. J. Pharm. Res. 16 (2017) 1765–1772. https://doi.org/10.4314/tjpr.v16i8.3.

[168] C. O'Leary, F.J. O'Brien, S.A. Cryan, Retinoic Acid-Loaded Collagen-Hyaluronate Scaffolds: A Bioactive Material for Respiratory Tissue Regeneration, ACS Biomater. Sci. Eng. 3 (2017) 1381–1393. https://doi.org/10.1021/acsbiomaterials.6b00561.

[169] S. Yamamoto, Y. Kaneo, H. Maeda, Styrene maleic acid anhydride copolymer (SMA) for the encapsulation of sparingly water-soluble drugs in nanoparticles, J. Drug Deliv. Sci. Technol. 23 (2013) 231–237. https://doi.org/10.1016/S1773-2247(13)50035-9.

[170] E.L. Silva, G. Carneiro, P.A. Caetano, G. Goulart, D. Ferreira Costa, E.M. de Souza-Fagundes, D.A. Gomes, L.A.M. Ferreira, Nanostructured lipid carriers loaded with tributyrin as an alternative to improve anticancer activity of all-trans retinoic acid, Expert Rev. Anticancer Ther. 15 (2015) 247–56. https://doi.org/10.1586/14737140.2015.1000868.

[171] J. Zhang, J. Han, X. Zhang, J. Jiang, M. Xu, D. Zhang, J. Han, Polymeric nanoparticles based on chitooligosaccharide as drug carriers for co-delivery of all-trans-retinoic acid and paclitaxel., Carbohydr. Polym. 129 (2015) 25–34. https://doi.org/10.1016/j.carbpol.2015.04.036.

[172] L. Domínguez Díaz, V. Fernández-Ruiz, M. Cámara, An international regulatory review of food health-related claims in functional food products labeling, J. Funct. Foods. 68 (2020) 103896. https://doi.org/10.1016/j.jff.2020.103896.

[173] B. Kumar, K. Smita, Scope of Nanotechnology in Nutraceuticals, in: Nanotechnol. Appl. Food, Elsevier, 2017: pp. 43–63. https://doi.org/10.1016/B978-0-12-811942-6.00003-0.

[174] L. de S. Simões, D.A. Madalena, A.C. Pinheiro, J.A. Teixeira, A.A. Vicente, Ó.L. Ramos, Micro- and nano bio-based delivery systems for food applications: In vitro behavior, Adv. Colloid Interface Sci. 243 (2017) 23–45. https://doi.org/10.1016/j.cis.2017.02.010.

[175] D. Granato, F.J. Barba, D. Bursać Kovačević, J.M. Lorenzo, A.G. Cruz, P. Putnik, Functional Foods: Product Development, Technological Trends, Efficacy Testing, and Safety, Annu. Rev. Food Sci. Technol. 11 (2020) 93–118. https://doi.org/10.1146/annurev-food-032519-051708.

[176] D.J. McClements, Enhancing nutraceutical bioavailability through food matrix design, Curr. Opin. Food Sci. 4 (2015) 1–6. https://doi.org/10.1016/j.cofs.2014.12.008.

[177] D.I. Santos, J.M.A. Saraiva, A.A. Vicente, M. Moldão-Martins, Methods for determining bioavailability and bioaccessibility of bioactive compounds and nutrients, Elsevier Inc., 2019. https://doi.org/10.1016/B978-0-12-814174-8.00002-0.

[178] S.G. Lee, J. Kim, H. Park, W. Holzapfel, K.W. Lee, Assessment of the effect of cooking on speciation and bioaccessibility/cellular uptake of arsenic in rice, using in vitro digestion and Caco-2 and PSI cells as model, Food Chem. Toxicol. 111 (2018) 597–604. https://doi.org/10.1016/j.fct.2017.11.052.

[179] C. Cardoso, C. Afonso, H. Lourenço, S. Costa, M.L. Nunes, Bioaccessibility assessment methodologies and their consequences for the risk–benefit evaluation of food, Trends Food Sci. Technol. 41 (2015) 5–23. https://doi.org/10.1016/j.tifs.2014.08.008.

[180] A. Gorusupudi, P.S. Bernstein, Macular carotenoids: human health aspects, in: L. John Wiley & Sons (Ed.), Carotenoids Nutr. Ther. Spectrosc. Technol., Chichester, 2016: pp. 59–74.

[181] Q. Ye, N. Georges, C. Selomulya, Microencapsulation of active ingredients in functional foods: From research stage to commercial food products, Trends Food Sci. Technol. 78 (2018) 167–179. https://doi.org/10.1016/j.tifs.2018.05.025.

[182] A. Marisa Ribeiro, B.N. Estevinho, F. Rocha, Microencapsulation of polyphenols - The specific case of the microencapsulation of Sambucus Nigra L. extracts - A review, Trends Food Sci. Technol. 105 (2020) 454–467. https://doi.org/10.1016/j.tifs.2019.03.011.

[183] Dhanjai, A. Sinha, P.K. Kalambate, S.M. Mugo, P. Kamau, J. Chen, R. Jain, Polymer hydrogel interfaces in electrochemical sensing strategies: A review, TrAC - Trends Anal. Chem. 118 (2019) 488–501. https://doi.org/10.1016/j.trac.2019.06.014.

[184] E.M. Ahmed, Hydrogel: Preparation, characterization, and applications: A review, J. Adv. Res. 6 (2015) 105–121. https://doi.org/10.1016/j.jare.2013.07.006.

[185] F. Ullah, M.B.H. Othman, F. Javed, Z. Ahmad, H.M. Akil, Classification, processing and application of hydrogels: A review, Mater. Sci. Eng. C. 57 (2015) 414–433. https://doi.org/10.1016/j.msec.2015.07.053.

[186] K.A. Ishak, M.S. Mohamad Annuar, N. Ahmad, Nano-delivery Systems for Nutraceutical Application, in: Nanotechnol. Appl. Food, Elsevier, 2017: pp. 179–202. https://doi.org/10.1016/B978-0-12-811942-6.00009-1.

[187] M. Pathak, Nanoemulsions and Their Stability for Enhancing Functional Properties of Food Ingredients, in: A.E. Oprea, A.M. Grumezescu (Eds.), Nanotechnol. Appl. Food, Elsevier, 2017: pp. 87–106. https://doi.org/10.1016/B978-0-12-811942-6.00005-4.

[188] M. Geszke-Moritz, M. Moritz, Solid lipid nanoparticles as attractive drug vehicles: Composition, properties and therapeutic strategies, Mater. Sci. Eng. C. 68 (2016) 982–994. https://doi.org/10.1016/j.msec.2016.05.119.

[189] N. Naseri, H. Valizadeh, P. Zakeri-Milani, Solid lipid nanoparticles and nanostructured lipid carriers: Structure preparation and application, Adv. Pharm. Bull. 5 (2015) 305–313. https://doi.org/10.15171/apb.2015.043.

[190] S. Shukla, Y. Haldorai, S.K. Hwang, V.K. Bajpai, Y.S. Huh, Y.K. Han, Current demands for food-approved liposome nanoparticles in food and safety sector, Front. Microbiol. 8 (2017) 1–14. https://doi.org/10.3389/fmicb.2017.02398.

[191] F. Paulo, L. Santos, Deriving valorization of phenolic compounds from olive oil by-products for food applications through microencapsulation approaches: a comprehensive review, Crit. Rev. Food Sci. Nutr. 0 (2020) 1–26. https://doi.org/10.1080/10408398.2020.1748563.

[192] A. Sosnik, K.P. Seremeta, Advantages and challenges of the spray-drying technology for the production of pure drug particles and drug-loaded polymeric carriers, Adv. Colloid Interface Sci. 223 (2015) 40–54. https://doi.org/10.1016/j.cis.2015.05.003.

[193] E. Assadpour, S.M. Jafari, Spray drying of folic acid within nano-emulsions: Optimization by Taguchi approach, Dry. Technol. 35 (2017) 1152–1160. https://doi.org/10.1080/07373937.2016.1242016.

[194] D. Nowak, E. Jakubczyk, The Freeze-Drying of Foods—The Characteristic of the Process Course and the Effect of Its Parameters on the Physical Properties of Food Materials, Foods. 9 (2020) 1488. https://doi.org/10.3390/foods9101488.

[195] S. Ray, U. Raychaudhuri, R. Chakraborty, An overview of encapsulation of active compounds used in food products by drying technology, Food Biosci. 13 (2016) 76–83. https://doi.org/10.1016/j.fbio.2015.12.009.

[196] B. Wang, T.O. Akanbi, D. Agyei, B.J. Holland, C.J. Barrow, Coacervation Technique as an Encapsulation and Delivery Tool for Hydrophobic Biofunctional Compounds, in: Role Mater. Sci. Food Bioeng., Elsevier, 2018: pp. 235–261. https://doi.org/10.1016/B978-0-12-811448-3.00007-3.

[197] B.N. Estevinho, F. Rocha, A Key for the Future of the Flavors in Food Industry, in: Nanotechnol. Appl. Food, Elsevier, 2017: pp. 1–19. https://doi.org/10.1016/B978-0-12-811942-6.00001-7.

[198] C. dos Santos, P. Buera, F. Mazzobre, Novel trends in cyclodextrins encapsulation. Applications in food science, Curr. Opin. Food Sci. 16 (2017) 106–113. https://doi.org/10.1016/j.cofs.2017.09.002.

[199] A.C. Pinheiro, R.F. Gonçalves, D.A. Madalena, A.A. Vicente, Towards the understanding of the behavior of bio-based nanostructures during in vitro digestion, Curr. Opin. Food Sci. 15 (2017) 79–86. https://doi.org/10.1016/j.cofs.2017.06.005.

[200] M. Assad-Bustillos, J. Palier, H. Rabesona, Y. Choiset, G. Della Valle, G. Feron, Role of the bolus degree of structure on the protein digestibility during in vitro digestion of a pea protein-fortified sponge cake chewed by elderly, J. Texture Stud. 51 (2019) jtxs.12486. https://doi.org/10.1111/jtxs.12486.

[201] C. Li, W. Yu, P. Wu, X.D. Chen, Current in vitro digestion systems for understanding food digestion in human upper gastrointestinal tract, Trends Food Sci. Technol. 96 (2020) 114–126. https://doi.org/10.1016/j.tifs.2019.12.015.

[202] R. Lucas-González, M. Viuda-Martos, J.A. Pérez-Alvarez, J. Fernández-López, In vitro digestion models suitable for foods: Opportunities for new fields of application and challenges, Food Res. Int. 107 (2018) 423–436. https://doi.org/10.1016/j.foodres.2018.02.055.

[203] A. Mackie, A.I. Mulet-Cabero, A. Torcello-Gomez, Simulating human digestion: Developing our

knowledge to create healthier and more sustainable foods, Food Funct. 11 (2020) 9397–9431. https://doi.org/10.1039/d0fo01981j.

[204] Q. Guo, J. Su, X. Shu, F. Yuan, L. Mao, J. Liu, Y. Gao, Fabrication, structural characterization and functional attributes of polysaccharide-surfactant-protein ternary complexes for delivery of curcumin, Food Chem. 337 (2021) 128019. https://doi.org/10.1016/j.foodchem.2020.128019.

[205] A. Araiza-Calahorra, A. Sarkar, Designing biopolymer-coated Pickering emulsions to modulate: In vitro gastric digestion: A static model study, Food Funct. 10 (2019) 5498–5509. https://doi.org/10.1039/c9fo01080g.

[206] M. Peanparkdee, R. Yamauchi, S. Iwamoto, Stability of bioactive compounds from Thai Riceberry bran extract encapsulated within gelatin matrix during in vitro gastrointestinal digestion, Colloids Surfaces A Physicochem. Eng. Asp. 546 (2018) 136–142. https://doi.org/10.1016/j.colsurfa.2018.03.021.

[207] T. Bohn, F. Carriere, L. Day, A. Deglaire, L. Egger, D. Freitas, M. Golding, S. Le Feunteun, A. Macierzanka, O. Menard, B. Miralles, A. Moscovici, R. Portmann, I. Recio, D. Rémond, V. Santé-Lhoutelier, T.J. Wooster, U. Lesmes, A.R. Mackie, D. Dupont, Correlation between in vitro and in vivo data on food digestion. What can we predict with static in vitro digestion models?, Crit. Rev. Food Sci. Nutr. 58 (2018) 2239–2261. https://doi.org/10.1080/10408398.2017.1315362.

[208] A. Brodkorb, L. Egger, M. Alminger, P. Alvito, R. Assunção, S. Ballance, T. Bohn, C. Bourlieu-Lacanal, R. Boutrou, F. Carrière, A. Clemente, M. Corredig, D. Dupont, C. Dufour, C. Edwards, M. Golding, S. Karakaya, B. Kirkhus, S. Le Feunteun, U. Lesmes, A. Macierzanka, A.R. Mackie, C. Martins, S. Marze, D.J. McClements, O. Ménard, M. Minekus, R. Portmann, C.N. Santos, I. Souchon, R.P. Singh, G.E. Vegarud, M.S.J. Wickham, W. Weitschies, I. Recio, INFOGEST static in vitro simulation of gastrointestinal food digestion, Nat. Protoc. 14 (2019) 991–1014. https://doi.org/10.1038/s41596-018-0119-1.

[209] J.D. Beltrán, C.E. Sandoval-Cuellar, K. Bauer, M.X. Quintanilla-Carvajal, In-vitro digestion of high-oleic palm oil nanoliposomes prepared with unpurified soy lecithin: Physical stability and nano-liposome digestibility, Colloids Surfaces A Physicochem. Eng. Asp. 578 (2019) 123603. https://doi.org/10.1016/j.colsurfa.2019.123603.

[210] F.F. Visentini, J.B. Ferrado, A.A. Perez, L.G. Santiago, Simulated gastrointestinal digestion of inclusion complexes based on ovalbumin nanoparticles and conjugated linoleic acid, Food Funct. 10 (2019) 2630–2641. https://doi.org/10.1039/c8fo02416b.

[211] B.S. Afonso, A.G. Azevedo, C. Gonçalves, I.R. Amado, E.C. Ferreira, L.M. Pastrana, M.A. Cerqueira, Bio-Based Nanoparticles as a Carrier of β-Carotene: Production, Characterisation and In Vitro Gastrointestinal Digestion, Molecules. 25 (2020) 4497. https://doi.org/10.3390/molecules25194497.

[212] J.B. Ferrado, A.A. Perez, M.C. Ruiz, I.E. León, L.G. Santiago, Chrysin-loaded bovine serum albumin particles as bioactive nanosupplements, Food Funct. 11 (2020) 6007–6019. https://doi.org/10.1039/d0fo00299b.

[213] H. Zhou, T. Dai, J. Liu, Y. Tan, L. Bai, O.J. Rojas, D.J. McClements, Chitin nanocrystals reduce lipid

digestion and β-carotene bioaccessibility: An in-vitro INFOGEST gastrointestinal study, Food Hydrocoll. 113 (2021) 106494. https://doi.org/10.1016/j.foodhyd.2020.106494.

[214] E.C. Thuenemann, Dynamic Digestion Models: General Introduction, in: Impact Food Bioact. Heal., Springer International Publishing, Cham, 2015: pp. 33–36. https://doi.org/10.1007/978-3-319-16104-4_4.

[215] E.C. Thuenemann, G. Mandalari, G.T. Rich, R.M. Faulks, Dynamic Gastric Model (DGM), in: Impact Food Bioact. Heal., Springer International Publishing, Cham, 2015: pp. 47–59. https://doi.org/10.1007/978-3-319-16104-4_6.

[216] L.M. Mason, S. Chessa, H. Huatan, D.E. Storey, P. Gupta, J. Burley, C.D. Melia, Use of the Dynamic Gastric Model as a tool for investigating fed and fasted sensitivities of low polymer content hydrophilic matrix formulations, Int. J. Pharm. 510 (2016) 210–220. https://doi.org/10.1016/j.ijpharm.2016.06.034.

[217] M.J. Ferrua, R.P. Singh, Human Gastric Simulator (Riddet Model), in: Impact Food Bioact. Heal., Springer International Publishing, Cham, 2015: pp. 61–71. https://doi.org/10.1007/978-3-319-16104-4_7.

[218] X. Lu, J. Zhu, Y. Pan, Q. Huang, Assessment of dynamic bioaccessibility of curcumin encapsulated in milled starch particle stabilized Pickering emulsions using TNO's gastrointestinal model, Food Funct. 10 (2019) 2583–2594. https://doi.org/10.1039/c8fo02495b.

[219] T. Van de Wiele, P. Van den Abbeele, W. Ossieur, S. Possemiers, M. Marzorati, The Simulator of the Human Intestinal Microbial Ecosystem (SHIME®), in: Impact Food Bioact. Heal., Springer International Publishing, Cham, 2015: pp. 305–317. https://doi.org/10.1007/978-3-319-16104-4_27.

[220] G. Picariello, P. Ferranti, F. Addeo, Use of brush border membrane vesicles to simulate the human intestinal digestion, Food Res. Int. 88 (2016) 327–335. https://doi.org/10.1016/j.foodres.2015.11.002.

[221] G. Picariello, B. Miralles, G. Mamone, L. Sánchez-Rivera, I. Recio, F. Addeo, P. Ferranti, Role of intestinal brush border peptidases in the simulated digestion of milk proteins, Mol. Nutr. Food Res. 59 (2015) 948–956. https://doi.org/10.1002/mnfr.201400856.

[222] D.C. Murador, L.M. De Souza Mesquita, B. V. Neves, A.R.C. Braga, P.L.G. Martins, L.Q. Zepka, V. V. De Rosso, Bioaccessibility and Cellular Uptake by Caco-2 Cells of Carotenoids and Chlorophylls from Orange Peels: A Comparison Between Conventional and Ionic Liquid Mediated Extractions, Food Chem. (2020) 127818. https://doi.org/10.1016/j.foodchem.2020.127818.

[223] Y. Liu, X. Liang, Y. Zou, Y. Peng, D.J. McClements, K. Hu, Resveratrol-loaded biopolymer core-shell nanoparticles: Bioavailability and anti-inflammatory effects, Food Funct. 11 (2020) 4014–4025. https://doi.org/10.1039/d0fo00195c.

[224] J.R. Costa, M. Xavier, I.R. Amado, C. Gonçalves, P.M. Castro, R. V. Tonon, L.M.C. Cabral, L. Pastrana, M.E. Pintado, Polymeric nanoparticles as oral delivery systems for a grape pomace extract towards the improvement of biological activities, Mater. Sci. Eng. C. 119 (2021) 111551. https://doi.org/10.1016/j.msec.2020.111551.

[225] P. Lundquist, P. Artursson, Oral absorption of peptides and nanoparticles across the human intestine:

Opportunities, limitations and studies in human tissues, Adv. Drug Deliv. Rev. 106 (2016) 256–276. https://doi.org/10.1016/j.addr.2016.07.007.

[226] H. Zheng, W. Wijaya, H. Zhang, K. Feng, Q. Liu, T. Zheng, Z. Yin, Y. Cao, Q. Huang, Improving the bioaccessibility and bioavailability of carnosic acid using a lecithin-based nanoemulsion: Complementary: In vitro and in vivo studies, Food Funct. 11 (2020) 8141–8149. https://doi.org/10.1039/d0fo01098g.

[227] G.P. Kalmekerian, R.K. Jasti, P. Celano, B.D. Nelkin, M. Marby, All-trans-retinoic acid alters myc gene expression Cell, and inhibits in vitro progression in small-cell lung cancer, Cell Growth Differ. 5 (1994) 55–60.

[228] G. Krupitza, W. Hulla, H. Harant, E. Dittrich, E. Kallay, H. Huber, T. Grunt, C. Dittrich, Retinoic acid induced death of ovarian carcinoma cells correlates with c-myc stimulation, Int. J. Cancer. 61 (1995) 649– 657.

[229] Y. Il Jeong, J.G. Song, S.S. Kang, H.H. Ryu, Y.H. Lee, C. Choi, B.A. Shin, K.K. Kim, K.Y. Ahn, S. Jung, Preparation of poly(DL-lactide-co-glycolide) microspheres encapsulating all-trans retinoic acid, Int. J. Pharm. 259 (2003) 79–91. https://doi.org/10.1016/S0378-5173(03)00207-2.

[230] B. Ozpolat, G. Lopez-Berestein, P. Adamson, C.H.J. Fu, A.H. Williams, Pharmacokinetics of intravenously administered liposomal all-trans-retinoic acid (atra) and orally administered atra in healthy volunteers, J. Pharm. Pharm. Sci. 6 (2003) 292–301.

[231] E.H. Estey, F.J. Giles, H. Kantarjian, S. O'Brien, J. Cortes, E.J. Freireich, G. Lopez-Berestein, M. Keating, Molecular remissions induced by liposomal-encapsulated all-trans retinoic acid in newly diagnosed acute promyelocytic leukemia, Blood. 94 (1999) 2230–5. https://doi.org/10.1182/blood.v99.3.759.

[232] G. Carneiro, E.L. Silva, L.A. Pacheco, E.M. de Souza-Fagundes, N.C.R. Corrêa, A.M. de Goes, M.C. de Oliveira, L.A.M. Ferreira, Formation of ion pairing as an alternative to improve encapsulation and anticancer activity of all-trans retinoic acid loaded in solid lipid nanoparticles, Int. J. Nanomedicine. 7 (2012) 6011–6020. https://doi.org/10.2147/IJN.S38953.

[233] D. Cosco, R. Molinaro, V.M. Morittu, F. Cilurzo, N. Costa, M. Fresta, Anticancer activity of 9-cis-retinoic acid encapsulated in PEG-coated PLGA-nanoparticles, J. Drug Deliv. Sci. Technol. 21 (2011) 395–400. https://doi.org/10.1016/S1773-2247(11)50064-4.

[234] A. Gharsallaoui, G. Roudaut, O. Chambin, A. Voilley, R. Saurel, Applications of spray-drying in microencapsulation of food ingredients: an overview, Food Res. Int. 40 (2007) 1107–1121.

[235] K. Letchford, H. Burt, A review of the formation and classification of amphiphilic block copolymer nanoparticulate structures: micelles, nanospheres, nanocapsules and polymersomes, Eur. J. Pharm. Biopharm. 65 (2007) 259–269. https://doi.org/10.1016/j.ejpb.2006.11.009.

[236] S.K. Nitta, K. Numata, Biopolymer-based nanoparticles for drug/gene delivery and tissue engineering, Int. J. Mol. Sci. 14 (2013) 1629–1654. https://doi.org/10.3390/ijms14011629.

[237] F. Mohanty, S.K. Swain, Bionanocomposites for Food Packaging Applications, in: Nanotechnol. Appl.

Food, Elsevier, 2017: pp. 363–379. https://doi.org/10.1016/B978-0-12-811942-6.00018-2.

[238] A.C. Bertolini, A.G. Siani, C.R.F. Grosso, Stability of monoterpenes encapsulated in gum arabic by spray-drying, J. Agric. Food Chem. 49 (2001) 780–785.

[239] H.M.C. de Azeredo, Encapsulação: aplicação à tecnologia de alimentos, Aliment. e Nutr. 16 (2005) 89–97.

[240] N.Z. Othman, N.H. Shadan, S. Ramli, M.R. Sarmidi, Study on the effects of carbohydrate-protein-coconut oil on the viability of lactobacillus bulgaricus during spray drying, simulated gastrointestinal conditions and unrefrigerated storage by simplex-lattice mixture design, Chem. Eng. Trans. 63 (2018) 553–558. https://doi.org/10.3303/CET1863093.

[241] V. Reyes, A. Chotiko, A. Chouljenko, S. Sathivel, Viability of Lactobacillus acidophilus NRRL B-4495 encapsulated with high maize starch, maltodextrin, and gum arabic, Lwt. 96 (2018) 642–647. https://doi.org/10.1016/j.lwt.2018.06.017.

[242] N.T. Annan, A.D. Borza, L.T. Hansen, Encapsulation in alginate-coated gelatin microspheres improves survival of the probiotic Bifidobacterium adolescentis 15703T during exposure to simulated gastro-intestinal conditions, Food Res. Int. 41 (2008) 184–193. https://doi.org/10.1016/j.foodres.2007.11.001.

[243] T.K. Giri, A. Thakur, A. Alexander, H. Badwaik, D.K. Tripathi, Modified chitosan hydrogels as drug delivery and tissue engineering systems: present status and applications, Acta Pharm. Sin. B. 2 (2012) 439–449. https://doi.org/10.1016/j.apsb.2012.07.004.

[244] M.R. Corbo, A. Bevilacqua, B. Speranza, B. Di Maggio, M. Gallo, M. Sinigaglia, Use of alginate beads as carriers for lactic acid bacteria in a structured system and preliminary validation in a meat product, Meat Sci. 111 (2016) 198–203. https://doi.org/10.1016/j.meatsci.2015.10.005.

[245] A. Gonçalves, B.N. Estevinho, F. Rocha, Design and characterization of controlled-release vitamin A microparticles prepared by a spray-drying process, Powder Technol. 305 (2017) 411–417. https://doi.org/10.1016/j.powtec.2016.10.010.

[246] A.A. Santana, R.A. de Oliveira, L.E. Kurozawa, K.J. Park, Microencapsulation of pequi pulp by spray drying: use of modified starches as encapsulating agent, Eng. Agrícola. 34 (2014) 980–991.

[247] T.C. Kha, M.H. Nguyen, P.D. Roach, C.E. Stathopoulos, Microencapsulation of gac oil: optimisation of spray drying conditions using response surface methodology, Dry. Technol. 32 (2014) 385–397.

[248] Y. Xie, A. Wang, Q. Lu, M. Hui, The effects of rheological properties of wall materials on morphology and particle size distribution of microcapsule, Czech J. Food Sci. 28 (2010) 433–439.

[249] B.N. Estevinho, I. Carlan, A. Blaga, F. Rocha, Soluble vitamins (vitamin B12 and vitamin C) microencapsulated with different biopolymers by a spray drying process, Powder Technol. 289 (2016) 71–78.

[250] B.N. Estevinho, A.R. Lopes, V. Sousa, F. Rocha, O.C. Nunes, Microencapsulation of Gulosibacter molinativorax ON4Tcells by a spray-drying process using different biopolymers, J. Hazard. Mater. 338 (2017) 85–92. https://doi.org/10.1016/j.jhazmat.2017.05.018.

[251] B.M.A.N. Estevinho, F.A.N. Rocha, L.M. da S. Santos, M.A.C. Alves, Using water-soluble chitosan for

flavour microencapsulation in food industry, J. Microencapsul. 30 (2013) 571–579.

[252] B.N. Estevinho, A.M. Damas, P. Martins, F. Rocha, The Influence of Microencapsulation with a Modified Chitosan (Water Soluble) on β-Galactosidase Activity, Dry. Technol. 32 (2014) 1575–1586.

[253] I.C. Carlan, B.N. Estevinho, F. Rocha, Study of microencapsulation and controlled release of modified chitosan microparticles containing vitamin B12, Powder Technol. 318 (2017) 162–169. https://doi.org/10.1016/j.powtec.2017.05.041.

[254] B.N. Estevinho, I. Ramos, F. Rocha, Effect of the pH in the formation of β-galactosidase microparticles produced by a spray-drying process, Int. J. Biol. Macromol. 78 (2015) 238–242.

[255] B. Gonçalves, M. Moeenfard, F. Rocha, A. Alves, B.N. Estevinho, L. Santos, Microencapsulation of a Natural Antioxidant from Coffee—Chlorogenic Acid (3-Caffeoylquinic Acid), Food Bioprocess Technol. 10 (2017) 1521–1530. https://doi.org/10.1007/s11947-017-1919-y.

[256] B.N. Estevinho, A.M. Damas, P. Martins, F. Rocha, Microencapsulation of β-galactosidase with different biopolymers by a spray-drying process, Food Res. Int. 64 (2014) 134–140.

[257] B.N. Estevinho, A. Ferraz, F. Rocha, L. Santos, A. Alves, Uncertainty in the determination of glucose in aqueous solutions by high-performance liquid chromatography with evaporative light scattering detection, J. Sep. Sci. 32 (2009) 3116–3125. https://doi.org/10.1002/jssc.200900205.

[258] C. Siontorou, G.-P. Nikoleli, D. Nikolelis, S. Karapetis, Artificial Lipid Membranes: Past, Present, and Future, Membranes (Basel). 7 (2017) 1–24. https://doi.org/10.3390/membranes7030038.

[259] G. Klopman, H. Zhu, Recent Methodologies for the Estimation of N-Octanol / Water Partition Coefficients and their Use in the Prediction of Membrane Transport Properties of Drugs, Mini-Reviews Med. Chem. 5 (2005) 127–133.

[260] S. Dash, P.N. Murthy, L. Nath, P. Chowdhury, Kinetic modeling on drug release from controlled drug delivery systems, Acta Pol. Pharm. 67 (2010) 217–23. https://doi.org/10.1016/S0928-0987(01)00095-1.

[261] C. Liu, K.G. Desai, X. Tang, X. Chen, Drug Release Kinetics of Spray-Dried Chitosan Microspheres, Dry. Technol. 24 (2006) 769–776.

[262] B.N. Estevinho, F. Rocha, Kinetic models applied to soluble vitamins delivery systems prepared by spray drying, Dry. Technol. 35 (2017) 1249–1257.

[263] U.R. Pothakamury, G. V Barbosa-Cánovas, Fundamental aspects of controlled release in foods, Trends Food Sci. Technol. 6 (1995) 397–406.

[264] M.G. Sankalia, R.C. Mashru, J.M. Sankalia, V.B. Sutariya, Reversed chitosan-alginate polyelectrolyte complex for stability improvement of alpha-amylase: Optimization and physicochemical characterization, Eur. J. Pharm. Biopharm. 65 (2007) 215–232. https://doi.org/10.1016/j.ejpb.2006.07.014.

[265] X.C. Fu, G.P. Wang, W.Q. Liang, M.S.S. Chow, Prediction of drug release from HPMC matrices: Effect of physicochemical properties of drug and polymer concentration, J. Control. Release. 95 (2004) 209–216. https://doi.org/10.1016/j.jconrel.2003.11.007.

[266] K.G.H. Desai, H.J. Park, Recent developments in microencapsulation of food ingredients, Dry. Technol.

23 (2005) 1361–1394.

[267] I. Antal, R. Zelkó, N. Röczey, J. Plachy, I. Rácz, Dissolution and diffuse reflectance characteristics of coated theophylline particles, Int. J. Pharm. 155 (1997) 83–89. https://doi.org/10.1016/S0378-5173(97)00161-0.

[268] Y.-I. Jeong, M.-K. Kang, H.-S. Sun, S.-S. Kang, H.-W. Kim, K.-S. Moon, K.-J. Lee, S.-H. Kim, S. Jung, All-trans-retinoic acid release from core-shell type nanoparticles of poly(epsilon-caprolactone)/poly(ethylene glycol) diblock copolymer., Int. J. Pharm. 273 (2004) 95–107. https://doi.org/10.1016/j.ijpharm.2003.12.012.

[269] R. Dinarvand, E. Rahmani, E. Farbod, Gelatin Microspheres for the Controlled Release of All-trans-Retinoic Acid Topical Formulation and Drug Delivery Evaluation, Iran. J. Pharm. Res. (2003) 47–50.

[270] H. Bouterfa, T. Picht, D. Keß, C. Herbold, E. Noll, P.M.L. Black, K. Roosen, J.C. Tonn, Retinoids inhibit human glioma cell proliferation and migration in primary cell cultures but not in established cell lines, Neurosurgery. 46 (2000) 419–430. https://doi.org/10.1097/00006123-200002000-00029.

[271] Y. Il Jeong, K.D. Chung, D.H. Kim, Y.H. Kim, Y.S. Lee, K.C. Choi, All-trans retinoic acid-incorporated nanoparticles of deoxycholic acid-conjugated dextran for treatment of CT26 colorectal carcinoma cells, Int. J. Nanomedicine. 8 (2013) 485–493. https://doi.org/10.2147/IJN.S40580.

[272] Siddikuzzaman, C. Guruvayoorappan, V.M. Berlin Grace, All trans retinoic acid and cancer, Immunopharmacol. Immunotoxicol. 33 (2011) 241–249. https://doi.org/10.3109/08923973.2010.521507.

[273] R. Lotan, Retinoids as modulators of tumor cell invasion and metastasis, Semin. Cancer Biol. (1991) 197–208.

[274] M.A. Sanz, P. Fenaux, M.S. Tallman, E.H. Estey, B. Löwenberg, T. Naoe, E. Lengfelder, H. Döhner, A.K. Burnett, S.J. Chen, V. Mathews, H. Iland, E. Rego, H. Kantarjian, L. Adès, G. Avvisati, P. Montesinos, U. Platzbecker, F. Ravandi, N.H. Russell, F. Lo-Coco, Management of acute promyelocytic leukemia: Updated recommendations from an expert panel of the European LeukemiaNet, Blood. 133 (2019) 1630–1643. https://doi.org/10.1182/blood-2019-01-894980.

[275] K.D. Chung, Y. Il Jeong, C.W. Chung, D.H. Kim, D.H. Kang, Anti-tumor activity of all-trans retinoic acid-incorporated glycol chitosan nanoparticles against HuCC-T1 human cholangiocarcinoma cells, Int. J. Pharm. 422 (2012) 454–461. https://doi.org/10.1016/j.ijpharm.2011.10.057.

[276] J.R.F. Muindi, S.R. Frankel, C. Huselton, F. DeGrazia, W.A. Garland, C.W. Young, R.P. Warrell, Clinical Pharmacology of Oral All-trans Retinoic Acid in Patients with Acute Promyelocytic Leukemia, Cancer Res. 52 (1992) 2138–2142.

[277] Y.-R. Byun, S.-Y. Kim, S.-H. Kim, Y.-D. Choi, I.-S. Han, K.-S. Lee, C.-H. Kim, Controlled drug release system of retinoic acid, 2004.

[278] A. Gonçalves, B.N. Estevinho, F. Rocha, Characterization of biopolymer-based systems obtained by spray-drying for retinoic acid controlled delivery, Powder Technol. 345 (2019) 758–765. https://doi.org/10.1016/j.powtec.2019.01.062.

[279] J. Imagi, R. Matsuno, T. Yamanouchi, K. Okada, M. Tanimoto, Properties of Agents that Effectively Entrap Liquid Lipids, Biosci. Biotechnol. Biochem. 56 (1992) 477–480. https://doi.org/10.1271/bbb.56.477.

[280] A. Sharma, S. Gautam, S. Wadhawan, Xanthomonas, in: Encycl. Food Microbiol., Elsevier, 2014: pp. 811–817. https://doi.org/10.1016/B978-0-12-384730-0.00359-1.

[281] Y.M. Lo, S. Argin-Soysal, C.H. Hsu, Bioconversion of Whey Lactose into Microbial Exopolysaccharides, Bioprocess. Value-Added Prod. from Renew. Resour. (2007) 559–583. https://doi.org/10.1016/B978-044452114-9/50023-2.

[282] L.C. Corrêa-Filho, M.M. Lourenço, M. Moldão-Martins, V.D. Alves, Microencapsulation of β -Carotene by Spray Drying: Effect of Wall Material Concentration and Drying Inlet Temperature, Int. J. Food Sci. 2019 (2019) 1–12. https://doi.org/10.1155/2019/8914852.

[283] A. Bahmani, S. Saaidpour, A. Rostami, A Simple, Robust and Efficient Computational Method for n-Octanol/Water Partition Coefficients of Substituted Aromatic Drugs, Sci. Rep. 7 (2017) 1–12. https://doi.org/10.1038/s41598-017-05964-z.

[284] X. Liu, B. Testa, A. Fahr, Lipophilicity and Its Relationship with Passive Drug Permeation, Pharm. Res. 28 (2011) 962–977. https://doi.org/10.1007/s11095-010-0303-7.

[285] A.M. Bakry, Z. Fang, Y. Ni, H. Cheng, Y.Q. Chen, L. Liang, Stability of tuna oil and tuna oil/peppermint oil blend microencapsulated using whey protein isolate in combination with carboxymethyl cellulose or pullulan, Food Hydrocoll. 60 (2016) 559–571. https://doi.org/10.1016/j.foodhyd.2016.04.026.

[286] P.H. Campelo, E.L. do Carmo, R.D. Zacarias, M.I. Yoshida, V.P. Ferraz, R.V. de Barros Fernandes, D.A. Botrel, S.V. Borges, Effect of dextrose equivalent on physical and chemical properties of lime essential oil microparticles, Ind. Crops Prod. 102 (2017) 105–114. https://doi.org/10.1016/j.indcrop.2017.03.021.

[287] V.M. Shapovalov, On the Applicability of the Ostwald–De Waele Model in Solving Applied Problems, J. Eng. Phys. Thermophys. 90 (2017) 1213–1218. https://doi.org/10.1007/s10891-017-1676-9.

[288] D.A. Botrel, S.V. Borges, R.V. de B. Fernandes, R. Antoniassi, A.F. de Faria-Machado, J.P. de A. Feitosa, R.C.M. de Paula, Application of cashew tree gum on the production and stability of spray-dried fish oil, Food Chem. 221 (2017) 1522–1529. https://doi.org/10.1016/j.foodchem.2016.10.141.

[289] G. Schramm, A Practical Approach to Rheology and Rheometry, 2 nd, Thermo Electron, Karlsruhe, 2004. http://www.polymer.cn/bbs/File/UserFiles/UpLoad/200904010309415s.pdf.

[290] V. Goëlo, M. Chaumun, A. Gonçalves, B.N. Estevinho, F. Rocha, Polysaccharide-based delivery systems for curcumin and turmeric powder encapsulation using a spray-drying process, Powder Technol. 370 (2020) 137–146. https://doi.org/10.1016/j.powtec.2020.05.016.

[291] B.E. Rapp, Fluids, in: Microfluid. Model. Mech. Math., Elsevier, 2017: pp. 243–263. https://doi.org/10.1016/B978-1-4557-3141-1.50009-5.

[292] H.C.F. Carneiro, R. V. Tonon, C.R.F. Grosso, M.D. Hubinger, Encapsulation efficiency and oxidative stability of flaxseed oil microencapsulated by spray drying using different combinations of wall

materials, J. Food Eng. 115 (2013) 443–451. https://doi.org/10.1016/j.jfoodeng.2012.03.033.

[293] E. Drozłowska, A. Bartkowiak, P. Trocer, M. Kostek, A. Tarnowiecka-Kuca, Ł. Łopusiewicz, Formulation and evaluation of spray-dried reconstituted flaxseed oil-in-water emulsions based on flaxseed oil cake extract as emulsifying and stabilizing agent, Foods. 10 (2021). https://doi.org/10.3390/foods10020256.

[294] U.M.S.P. Perera, N. Rajapakse, Chitosan Nanoparticles: Preparation, Characterization, and Applications, in: Seaf. Process. By-Products, Springer New York, New York, NY, 2014: pp. 371–387. https://doi.org/10.1007/978-1-4614-9590-1_18.

[295] a Soottitantawat, H. Yoshii, T. Furuta, M. Ohkawara, P. Linko, Microencapsulation by Spray Drying : Influence of Emulsion Size on the retention of volatile compounds, Food Eng. Phys. Prop. 68 (2003) 2256–2262.

[296] C. Bustos-Garza, J. Yáñez-Fernández, B.E. Barragán-Huerta, Thermal and pH stability of spray-dried encapsulated astaxanthin oleoresin from Haematococcus pluvialis using several encapsulation wall materials, Food Res. Int. 54 (2013) 641–649.

[297] N. Phisut, Spray drying technique of fruit juice powder: some factors influencing the properties of product, Int. Food. 19 (2012) 1297–1306.

[298] S.Y. Quek, N.K. Chok, P. Swedlund, The physicochemical properties of spray-dried watermelon powders, Chem. Eng. Process. Process Intensif. 46 (2007) 386–392.

[299] S. Santhalakshmy, S.J. Don Bosco, S. Francis, M. Sabeena, Effect of inlet temperature on physicochemical properties of spray-dried jamun fruit juice powder, Powder Technol. 274 (2015) 37–43. https://doi.org/10.1016/j.powtec.2015.01.016.

[300] R. Jog, D.J. Burgess, Comprehensive quality by design approach for stable nanocrystalline drug products, Int. J. Pharm. 564 (2019) 426–460. https://doi.org/10.1016/j.ijpharm.2019.04.050.

[301] M. Aghbashlo, H. Mobli, A. Madadlou, S. Rafiee, Influence of Wall Material and Inlet Drying Air Temperature on the Microencapsulation of Fish Oil by Spray Drying, Food Bioprocess Technol. 6 (2013) 1561–1569. https://doi.org/10.1007/s11947-012-0796-7.

[302] J.A. Zakarian, C.J. King, Volatiles loss in the nozzle zone during spray drying of emulsions, Ind. Eng. Chem. Process Des. Dev. 21 (1982) 107–113. https://doi.org/10.1021/i200016a019.

[303] J. Lucas, M. Ralaivao, B.N. Estevinho, F. Rocha, A new approach for the microencapsulation of curcumin by a spray drying method, in order to value food products, Powder Technol. 362 (2020) 428–435. https://doi.org/10.1016/j.powtec.2019.11.095.

[304] R. Santiago-Adame, L. Medina-Torres, J.A. Gallegos-Infante, F. Calderas, R.F. González-Laredo, N.E. Rocha-Guzmán, L.A. Ochoa-Martínez, M.J. Bernad-Bernad, Spray drying-microencapsulation of cinnamon infusions (Cinnamomum zeylanicum) with maltodextrin, LWT - Food Sci. Technol. 64 (2015) 571–577. https://doi.org/10.1016/j.lwt.2015.06.020.

[305] D. Zare, A. Salehi, M. Niakousari, Determination of physical properties of sour orange juice powder produced by a spray dryer, Am. Soc. Agric. Biol. Eng. Annu. Int. Meet. 2012, ASABE 2012. 5 (2012)

4240–4253. https://doi.org/10.13031/2013.41947.

[306] M. Chaumun, V. Goëlo, A.M. Ribeiro, F. Rocha, B.N. Estevinho, In vitro evaluation of microparticles with Laurus nobilis L. extract prepared by spray-drying for application in food and pharmaceutical products, Food Bioprod. Process. 122 (2020) 124–135. https://doi.org/10.1016/j.fbp.2020.04.011.

[307] C.A. Di Battista, D. Constenla, M.V. Ramírez-Rigo, J. Piña, The use of Arabic gum, maltodextrin and surfactants in the microencapsulation of phytosterols by spray drying, Powder Technol. 286 (2015) 193–201. https://doi.org/10.1016/j.powtec.2015.08.016.

[308] B.N. Estevinho, R. Lazar, A. Blaga, F. Rocha, Preliminary evaluation and studies on the preparation, characterization and in vitro release studies of different biopolymer microparticles for controlled release of folic acid, Powder Technol. 369 (2020) 279–288. https://doi.org/10.1016/j.powtec.2020.05.048.

[309] D.X. Li, Y.K. Oh, S.J. Lim, J.O. Kim, H.J. Yang, J.H. Sung, C.S. Yong, H.G. Choi, Novel gelatin microcapsule with bioavailability enhancement of ibuprofen using spray-drying technique, Int. J. Pharm. 355 (2008) 277–284. https://doi.org/10.1016/j.ijpharm.2007.12.020.

[310] L.G. Gómez-Mascaraque, M.J. Fabra, J.L. Castro-Mayorga, G. Sánchez, M. Martínez-Sanz, A. López-Rubio, Nanostructuring Biopolymers for Improved Food Quality and Safety, in: Biopolym. Food Des., Elsevier, 2018: pp. 33–64. https://doi.org/10.1016/B978-0-12-811449-0.00002-5.

[311] I.C. Carlan, B.N. Estevinho, F. Rocha, Production of vitamin B1 microparticles by a spray drying process using different biopolymers as wall materials, Can. J. Chem. Eng. 98 (2020) 1682–1695. https://doi.org/10.1002/cjce.23735.

[312] M.C.S. Aguiar, M.F. das Graças Fernandes da Silva, J.B. Fernandes, M.R. Forim, Evaluation of the microencapsulation of orange essential oil in biopolymers by using a spray-drying process, Sci. Rep. 10 (2020) 1–11. https://doi.org/10.1038/s41598-020-68823-4.

[313] A.M. Ribeiro, B.N. Estevinho, F. Rocha, Spray Drying Encapsulation of Elderberry Extract and Evaluating the Release and Stability of Phenolic Compounds in Encapsulated Powders, Food Bioprocess Technol. (2019) 1381–1394. https://doi.org/10.1007/s11947-019-02304-z.

[314] A. Gonçalves, B.N. Estevinho, F. Rocha, Spray-drying of oil-in-water emulsions for encapsulation of retinoic acid: Polysaccharide- and protein-based microparticles characterization and controlled release studies, Food Hydrocoll. 124 (2022) 107193. https://doi.org/10.1016/j.foodhyd.2021.107193.

[315] T. Cardoso, A. Gonçalves, B.N. Estevinho, F. Rocha, Potential food application of resveratrol microparticles: Characterization and controlled release studies, Powder Technol. 355 (2019) 593–601. https://doi.org/10.1016/j.powtec.2019.07.079.

[316] A.M. Ribeiro, M. Shahgol, B.N. Estevinho, F. Rocha, Microencapsulation of Vitamin A by spray-drying, using binary and ternary blends of gum arabic, starch and maltodextrin, Food Hydrocoll. 108 (2020) 106029. https://doi.org/10.1016/j.foodhyd.2020.106029.

[317] P.C. Adamson, All- Trans -Retinoic Acid Pharmacology and Its Impact on the Treatment of Acute Promyelocytic Leukemia , Oncologist. 1 (1996) 305–314. https://doi.org/10.1634/theoncologist.1-5-305.

[318] L. Lu, Y. Du, M. Ismail, L. Ling, C. Yao, Z. Fu, X. Li, Liposomes assembled from dimeric retinoic acid phospholipid with improved pharmacokinetic properties, Eur. J. Pharm. Sci. 112 (2018) 186–194. https://doi.org/10.1016/j.ejps.2017.11.017.

[319] A. Gonçalves, B.N. Estevinho, F. Rocha, Microencapsulation of retinoic acid by atomization into biopolymeric matrices: Binary and ternary blends of alginic acid sodium, xanthan gum and modified chitosan, Food Hydrocoll. 124 (2022) 107310. https://doi.org/10.1016/j.foodhyd.2021.107310.

[320] K. Wasilewska, K. Winnicka, Ethylcellulose-a pharmaceutical excipient with multidirectional application in drug dosage forms development, Materials (Basel). 12 (2019). https://doi.org/10.3390/ma12203386.

[321] S. Prasertmanakit, N. Praphairaksit, W. Chiangthong, N. Muangsin, Ethyl cellulose microcapsules for protecting and controlled release of folic acid, AAPS PharmSciTech. 10 (2009) 1104–1112. https://doi.org/10.1208/s12249-009-9305-3.

[322] V.R. Malipeddi, R. Awasthi, K. Dua, Formulation and evaluation of controlled release ethylcellulose and polyethylene glycol microspheres containing metoprolol tartrate, Interv. Med. Appl. Sci. 8 (2016) 60–67. https://doi.org/10.1556/1646.8.2016.2.6.

[323] S.C. Coelho, S. Laget, P. Benaut, F. Rocha, B.N. Estevinho, A new approach to the production of zein microstructures with vitamin B12, by electrospinning and spray drying techniques, Powder Technol. 392 (2021) 47–57. https://doi.org/10.1016/j.powtec.2021.06.056.

[324] A. Belščak-Cvitanović, S. Lević, A. Kalušević, I. Špoljarić, V. Đorđević, D. Komes, G. Mršić, V. Nedović, Efficiency Assessment of Natural Biopolymers as Encapsulants of Green Tea (Camellia sinensis L.) Bioactive Compounds by Spray Drying, Food Bioprocess Technol. 8 (2015) 2444–2460. https://doi.org/10.1007/s11947-015-1592-y.

[325] L. Corrêa-Filho, S. Lourenço, D. Duarte, M. Moldão-Martins, V. Alves, Microencapsulation of Tomato (Solanum lycopersicum L.) Pomace Ethanolic Extract by Spray Drying: Optimization of Process Conditions, Appl. Sci. 9 (2019) 612. https://doi.org/10.3390/app9030612.

[326] M. Waghulde, J. Naik, Comparative study of encapsulated vildagliptin microparticles produced by spray drying and solvent evaporation technique, Dry. Technol. 35 (2017) 1645–1655. https://doi.org/10.1080/07373937.2016.1273230.

[327] M.W. Stocker, A.M. Healy, S. Ferguson, Spray Encapsulation as a Formulation Strategy for Drug-Based Room Temperature Ionic Liquids: Exploiting Drug-Polymer Immiscibility to Enable Processing for Solid Dosage Forms, Mol. Pharm. 17 (2020) 3412–3424. https://doi.org/10.1021/acs.molpharmaceut.0c00467.

[328] E. Tsolaki, M.W. Stocker, A.M. Healy, S. Ferguson, Formulation of ionic liquid APIs via spray drying processes to enable conversion into single and two-phase solid forms, Int. J. Pharm. 603 (2021) 120669. https://doi.org/10.1016/j.ijpharm.2021.120669.

[329] P. Wagh, A. Mujumdar, J.B. Naik, Preparation and characterization of ketorolac tromethamine-loaded ethyl cellulose micro-/nanospheres using different techniques, Part. Sci. Technol. 37 (2019) 347–357.

https://doi.org/10.1080/02726351.2017.1383330.

[330] L.M.B. De Francisco, J.A. Cerquetani, M.L. Bruschi, Development and characterization of gelatin and ethylcellulose microparticles designed as platforms to delivery fluoride, Drug Dev. Ind. Pharm. 39 (2013) 1644–1650. https://doi.org/10.3109/03639045.2012.728610.

[331] B. Thompson, N. Katsanis, N. Apostolopoulos, D.C. Thompson, D.W. Nebert, V. Vasiliou, Genetics and functions of the retinoic acid pathway, with special emphasis on the eye, Hum. Genomics. 13 (2019) 1–15. https://doi.org/10.1186/s40246-019-0248-9.

[332] M.R. Abdelaal, S.H. Soror, M.R. Elnagar, H. Haffez, Revealing the Potential Application of EC-Synthetic Retinoid Analogues in Anticancer Therapy, Molecules. 26 (2021) 506. https://doi.org/10.3390/molecules26020506.

[333] M.I. Flamini, G.V. Gauna, M.L. Sottile, B.S. Nadin, A.M. Sanchez, L.M. Vargas-Roig, Retinoic acid reduces migration of human breast cancer cells: role of retinoic acid receptor beta, J. Cell. Mol. Med. 18 (2014) 1113–1123. https://doi.org/10.1111/jcmm.12256.

[334] J. Cui, M. Gong, Y. He, Q. Li, T. He, Y. Bi, All-trans retinoic acid inhibits proliferation, migration, invasion and induces differentiation of hepa1-6 cells through reversing EMT in vitro, Int. J. Oncol. 48 (2016) 349–357. https://doi.org/10.3892/ijo.2015.3235.

[335] N. Li, Y. Lu, D. Li, X. Zheng, J. Lian, S. Li, H. Cui, L. Zhang, L. Sang, Y. Wang, J.J. Yu, T. Lu, All-trans retinoic acid suppresses the angiopoietin-Tie2 pathway and inhibits angiogenesis and metastasis in esophageal squamous cell carcinoma, PLoS One. 12 (2017) 1–15. https://doi.org/10.1371/journal.pone.0174555.

[336] A. Gonçalves, F. Rocha, B.N. Estevinho, Application of ethyl cellulose and ethyl cellulose + polyethylene glycol for the development of polymer based formulations by spray-drying technology for retinoic acid encapsulation, Submitt. Pap. (n.d.).

[337] A. Gonçalves, B.N. Estevinho, F. Rocha, Methodologies for simulation of gastrointestinal digestion of different controlled delivery systems and further uptake of encapsulated bioactive compounds, Trends Food Sci. Technol. 114 (2021) 510–520. https://doi.org/10.1016/j.tifs.2021.06.007.

[338] M.M.C. Sobral, M.A. Faria, S.C. Cunha, B. Miladinovic, I.M. Ferreira, Transport of mycotoxins across human gastric NCI–N87 and intestinal Caco-2 cell models, Food Chem. Toxicol. 131 (2019) 110595. https://doi.org/10.1016/j.fct.2019.110595.

[339] M.A. Faria, A. Araújo, E. Pinto, C. Oliveira, M.T. Oliva-Teles, A. Almeida, C. Delerue-Matos, I.M.P.L.V.O. Ferreira, Bioaccessibility and intestinal uptake of minerals from different types of home-cooked and ready-to-eat beans, J. Funct. Foods. 50 (2018) 201–209. https://doi.org/10.1016/j.jff.2018.10.001.

[340] M. Silva, M. Ribeiro, O. Viegas, Z.E. Martins, M. Faria, S. Casal, E. Pinto, A. Almeida, O. Pinho, I.M.P.L.V.O. Ferreira, Exploring two food composition databases to estimate nutritional components of whole meals, J. Food Compos. Anal. 102 (2021) 104070. https://doi.org/10.1016/j.jfca.2021.104070.

[341] M. Silva, M. Ribeiro, O. Viegas, Z.E. Martins, M. Faria, S. Casal, E. Pinto, A. Almeida, O. Pinho,

I.M.P.L.V.O. Ferreira, DIETImpact - Nutritional composition database of model meals, Zenodo. (2022). https://doi.org/10.5281/zenodo.6772838.

[342] I. Hubatsch, E.G.E. Ragnarsson, P. Artursson, Determination of drug permeability and prediction of drug absorption in Caco-2 monolayers, Nat. Protoc. 2 (2007) 2111–2119. https://doi.org/10.1038/nprot.2007.303.

[343] D.A. Garrett, M.L. Failla, R.J. Sarama, Development of an in Vitro Digestion Method To Assess Carotenoid Bioavailability from Meals, J. Agric. Food Chem. 47 (1999) 4301–4309. https://doi.org/10.1021/jf9903298.

[344] M. Zelenková, T. Zima, M. Kalousová, Determination of retinoic acid in human serum and plasma by high-performance liquid chromatography, Monatshefte Fur Chemie. 150 (2019) 1731–1735. https://doi.org/10.1007/s00706-019-02489-1.

[345] N.V.N. Jyothi, P.M. Prasanna, S.N. Sakarkar, K.S. Prabha, P.S. Ramaiah, G.Y. Srawan, Microencapsulation techniques, factors influencing encapsulation efficiency, J. Microencapsul. 27 (2010) 187–197. https://doi.org/10.3109/02652040903131301.

[346] M.M.C. Sobral, R. Romero-Gonzalez, M.A. Faria, S.C. Cunha, I.M.P.L.V.O. Ferreira, A. Garrido-Frenich, Stability of antibacterial and coccidiostat drugs on chicken meat burgers upon cooking and in vitro digestion, Food Chem. 316 (2020) 126367. https://doi.org/10.1016/j.foodchem.2020.126367.

[347] M.A. Faria, A. Melo, I.I.M.P.L.V.O. Ferreira, Influence of dietary patterns on contaminants bioaccessibility and intestinal transport by in vitro assays, Food Res. Int. 137 (2020) 109358. https://doi.org/10.1016/j.foodres.2020.109358.

[348] G. Chen, J. Zhu, X. Shi, J. Ni, H. Zhong, G. Si, X. Jin, W. Tang, X. Li, S. Xong, Z. Shen, G. Sun, J. Ma, P. Zhang, T. Zhang, C. Gazin, T. Naoe, S. Chen, Z. Wang, Z. Chen, In vitro studies on cellular and molecular mechanisms of arsenic trioxide (As2O3) in the treatment of acute promyelocytic leukemia: As2O3 induces NB4 cell apoptosis with downregulation of Bcl-2 expression and modulation of PML-RAR alpha/PML proteins, Blood. 88 (1996) 1052–1061. https://doi.org/10.1182/blood.V88.3.1052.1052.

[349] A.E.G. Osman, J. Anderson, J.E. Churpek, T.N. Christ, E. Curran, L.A. Godley, H. Liu, M.J. Thirman, T. Odenike, W. Stock, R.A. Larson, Treatment of Acute Promyelocytic Leukemia in Adults, J. Oncol. Pract. 14 (2018) 649–657. https://doi.org/10.1200/JOP.18.00328.

[350] M. Alcalay, D. Zangrilli, P.P. Pandolfi, L. Longo, A. Mencarelli, A. Giacomucci, M. Rocchi, A. Biondi, A. Rambaldi, F. Lo Coco, D. Diverio, E. Donti, F. Grignani, P.G. Pelicci, Translocation breakpoint of acute promyelocytic leukemia lies within the retinoic acid receptor α locus, Proc. Natl. Acad. Sci. U. S. A. 88 (1991) 1977–1981. https://doi.org/10.1073/pnas.88.5.1977.

[351] H. De Thé, C. Chomienne, M. Lanotte, L. Degos, A. Dejean, The t(15;17) translocation of acute promyelocytic leukaemia fuses the retinoic acid receptor α gene to a novel transcribed locus, Nature. 347 (1990) 558–561. https://doi.org/10.1038/347558a0.

[352] F. Grignani, P.F. Ferrucci, U. Testa, G. Talamo, M. Fagioli, M. Alcalay, A. Mencarelli, F. Grignani, C.

Peschle, I. Nicoletti, P.G. Pelicci, The acute promyelocytic leukemia-specific PML-RARα fusion protein inhibits differentiation and promotes survival of myeloid precursor cells, Cell. 74 (1993) 423–431. https://doi.org/10.1016/0092-8674(93)80044-F.

[353] O. Naksuriya, S. Okonogi, R.M. Schiffelers, W.E. Hennink, Curcumin nanoformulations: A review of pharmaceutical properties and preclinical studies and clinical data related to cancer treatment, Biomaterials. 35 (2014) 3365–3383. https://doi.org/10.1016/j.biomaterials.2013.12.090.

[354] M. Kelkel, C. Jacob, M. Dicato, M. Diederich, Potential of the dietary antioxidants resveratrol and curcumin in prevention and treatment of hematologic malignancies, 2010. https://doi.org/10.3390/molecules15107035.

[355] K. Jepsen, O. Hermanson, T.M. Onami, A.S. Gleiberman, V. Lunyak, R.J. McEvilly, R. Kurokawa, V. Kumar, F. Liu, E. Seto, S.M. Hedrick, G. Mandel, C.K. Glass, D.W. Rose, M.G. Rosenfeld, Combinatorial roles of the nuclear receptor corepressor in transcription and development, Cell. 102 (2000) 753–763. https://doi.org/10.1016/S0092-8674(00)00064-7.

[356] S. Battaglia, O. Maguire, M.J. Campbell, Transcription factor co-repressors in cancer biology: Roles and targeting, Int. J. Cancer. 126 (2010) 2511–2519. https://doi.org/10.1002/ijc.25181.

[357] R.J. Lin, L. Nagy, S. Inoue, W. Shao, W.H. Miller, R.M. Evans, Role of the histone deacetylase complex in acute promyelocytic leukaemia, Nature. 391 (1998) 811–814. https://doi.org/10.1038/35895.

[358] F. Grignani, S. De Matteis, C. Nervi, L. Tomassoni, V. Gelmetti, M. Cioce, M. Fanelli, M. Ruthardt, F.F. Ferrara, I. Zamir, C. Seiser, F. Grignani, M.A. Lazar, S. Minucci, P.G. Pelicci, Fusion proteins of the retinoic acid receptor-α recruit histone deacetylase in promyelocytic leukaemia, Nature. 391 (1998) 815–818. https://doi.org/10.1038/35901.

[359] M.M. Khan, T. Nomura, T. Chiba, K. Tanaka, H. Yoshida, K. Mori, S. Ishii, The Fusion Oncoprotein PML-RARα Induces Endoplasmic Reticulum (ER)-associated Degradation of N-CoR and ER Stress, J. Biol. Chem. 279 (2004) 11814–11824. https://doi.org/10.1074/jbc.M312121200.

[360] M. Khan, Interplay of protein misfolding pathway and unfolded-protein response in acute promyelocytic leukemia, Expert Rev. Proteomics. 7 (2010) 591–600. https://doi.org/10.1586/epr.10.38.

[361] T.W. Tan, H.R. Tsai, H.F. Lu, H.L. Lin, M.F. Tsou, Y.T. Lin, H.Y. Tsai, Y.F. Chen, J.G. Chung, Curcumin-induced cell cycle arrest and apoptosis in human acute promyelocytic leukemia HL-60 cells via MMP changes and caspase-3 activation, Anticancer Res. 26 (2006) 4361–4371.

[362] K.L. Tan, S.B. Koh, R.P.L. Ee, M. Khan, M.L. Go, Curcumin Analogues with Potent and Selective Anti-proliferative Activity on Acute Promyelocytic Leukemia: Involvement of Accumulated Misfolded Nuclear Receptor Co-repressor (N-CoR) Protein as a Basis for Selective Activity, ChemMedChem. 7 (2012) 1567–1579. https://doi.org/10.1002/cmdc.201200293.

[363] A.R. Kini, M. Nagabhushan, M.S. Tallman, S. Roychowdhury, Curcumin Enhances Differentiation of All-Trans Retinoic Acid (ATRA)-Sensitive and ATRA-Resistant Acute Promyelocytic (APL) Cells., Blood. 106 (2005) 4456–4456. https://doi.org/10.1182/blood.v106.11.4456.4456.

[364] M. Czop, A. Bogucka-Kocka, T. Kubrak, K. Knap-Czop, A. Makuch-Kocka, D. Galkowski, J. Wawer,

T. Kocki, J. Kocki, Imaging Flow Cytometric Analysis of Stilbene-Dependent Apoptosis in Drug Resistant Human Leukemic Cell Lines, Molecules. 24 (2019) 1896. https://doi.org/10.3390/molecules24101896.

[365] E.M. Varoni, A.F. Lo Faro, J. Sharifi-Rad, M. Iriti, Anticancer Molecular Mechanisms of Resveratrol, Front. Nutr. 3 (2016). https://doi.org/10.3389/fnut.2016.00008.

[366] Z. Estrov, S. Shishodia, S. Faderl, D. Harris, Q. Van, H.M. Kantarjian, M. Talpaz, B.B. Aggarwal, Resveratrol blocks interleukin-1β–induced activation of the nuclear transcription factor NF-κB, inhibits proliferation, causes S-phase arrest, and induces apoptosis of acute myeloid leukemia cells, Blood. 102 (2003) 987–995. https://doi.org/10.1182/blood-2002-11-3550.

[367] C.K. Singh, M.A. Ndiaye, N. Ahmad, Resveratrol and cancer: Challenges for clinical translation, Biochim. Biophys. Acta - Mol. Basis Dis. 1852 (2015) 1178–1185. https://doi.org/10.1016/j.bbadis.2014.11.004.

[368] J. Meng, G.J. Liu, J.Y. Song, L. Chen, A.H. Wang, X.X. Gao, Z.J. Wang, Preliminary results indicate resveratrol affects proliferation and apoptosis of leukemia cells by regulating PTEN/PI3K/AKT pathway, Eur. Rev. Med. Pharmacol. Sci. 23 (2019) 4285–4292. https://doi.org/10.26355/eurrev_201905_17933.

[369] Y. Cao, L. Huang, J. Chen, J. Liang, S. Long, Y. Lu, Development of a controlled release formulation based on a starch matrix system, Int. J. Pharm. 298 (2005) 108–116.

[370] Y. Fan, M. Chen, J. Meng, L. Yu, Y. Tu, L. Wan, K. Fang, W. Zhu, Arsenic trioxide and resveratrol show synergistic anti-leukemia activity and neutralized cardiotoxicity, PLoS One. 9 (2014) 1–9. https://doi.org/10.1371/journal.pone.0105890.

[371] W. Zhang, J. Xue, M. Ge, M. Yu, L. Liu, Z. Zhang, Resveratrol attenuates hepatotoxicity of rats exposed to arsenic trioxide, Food Chem. Toxicol. 51 (2013) 87–92. https://doi.org/10.1016/j.fct.2012.09.023.

[372] A. Gonçalves, O. Viegas, M. Faria, I. Ferreira, F. Rocha, B.N. Estevinho, In vitro bioaccessibility and intestinal transport of retinoic acid in ethyl cellulose-based microparticles and impact of meal co-ingestion, Submitt. Pap. (n.d.).

[373] J. Bajac, B. Nikolovski, I. Lončarević, J. Petrović, B. Bajac, S. Đurović, L. Petrović, Microencapsulation of juniper berry essential oil (Juniperus communis L.) by spray drying: microcapsule characterization and release kinetics of the oil, Food Hydrocoll. 125 (2022) 107430. https://doi.org/10.1016/j.foodhyd.2021.107430.

[374] L. Han, Y. Fu, A.J. Cole, J. Liu, J. Wang, Co-encapsulation and sustained-release of four components in ginkgo terpenes from injectable PELGE nanoparticles, Fitoterapia. 83 (2012) 721–731. https://doi.org/10.1016/j.fitote.2012.02.014.